Residual ultimate strength of seamless metallic pipelines with structural damage

Cai, Jie

DOI
10.4233/uuid:998e0f8b-11d4-40b7-b803-0df865044631

Publication date
2018

Document Version
Final published version

Citation (APA)
Cai, J. (2018). *Residual ultimate strength of seamless metallic pipelines with structural damage*. [Dissertation (TU Delft), Delft University of Technology]. https://doi.org/10.4233/uuid:998e0f8b-11d4-40b7-b803-0df865044631

Residual Ultimate Strength of Seamless Metallic Pipelines with Structural Damage

Jie Cai

Residual Ultimate Strength of Seamless Metallic Pipelines with Structural Damage

Proefschrift

ter verkrijging van de graad van doctor
aan de Technische Universiteit Delft,
op gezag van de Rector Magnificus prof. dr. ir. T.H.J.J. van der Hagen,
voorzitter van het College voor Promoties,
in het openbaar te verdedigen op dinsdag 4 september 2018 om 10:00 uur

door

Jie CAI

Master of Science in Design and Construction
of Naval Architecture and Ocean Engineering,
Shanghai Jiao Tong University, Shanghai, P. R. China
geboren te Yiyang, Hunan, P. R. China.

Dit proefschrift is goedgekeurd door de promotoren:
Promotor: Prof. dr. ir. G. Lodewijks
Copromotor: Dr. X. Jiang

Samenstelling promotiecommissie bestaat uit:

Rector Magnificus,	voorzitter
Prof. dr. ir. G. Lodewijks	Technische Universiteit Delft, promotor
Dr. X. Jiang	Technische Universiteit Delft, copromotor

Onafhankelijke leden:

Prof. ir. J. J. Hopman	Technische Universiteit Delft
Prof. dr. M. Veljkovic	Technische Universiteit Delft
Prof. ir. F. S. K. Bijlaard	Technische Universiteit Delft
Prof. dr. L. Zhu	Wuhan University of Technology
Prof. dr. C. G. Soares	Universidade de Lisboa

This thesis is the result from a project funded by the China Scholarship Council [Grant number 201406 230001], the section of Transport Engineering and Logistics in Department of Maritime and Transport Technology, Delft University of Technology in the Netherlands, and the School of Transportation of Wuhan University of Technology in P. R. China.

TRAIL Thesis Series T2018/5, the Netherlands TRAIL Research School
P.O.Box 5017
2600 GA Delft, the Netherlands
Email: info@rstrail.nl

Published and distributed by: Jie Cai
E-mail: cj26765811@gmail.com

ISBN 978-90-5584-236-0

Keywords: Residual ultimate strength, Metallic pipelines, Pipe tests, Nonlinear FEM, Dent, Metal loss, Combined dent and notch.

Printed in the Netherlands

Preface

Working on a Ph.D. research project is a pleasant but challenging journey. At the end of this journey, there are so many people I would like to thank. Not only because I have been inspired by these talented and diligent people, but also because of the happiness, joy and exciting moments I have experienced during the past four years in the Netherlands. I sincerely want to thank them for their contributions to my research work in different ways and to my life living in an exotic country. Particularly, I would like to mention some of them in the preface.

First of all, I would like to thank my promotor Prof. Gabriel Lodewijks, for your great support, trust and commitment to my research project. Without your professional suggestions in this research, especially for the experiments, I would not have obtained so many meaningful research results. It is my great honor to join your group as a Ph.D. student. I was also amazed at your enthusiasm and expertise in the Chinese culture and the cuisine. I still remember that, during your visiting to the structural laboratory for my test in Wuhan, we have shared a lot of interesting views about the culture differences. In addition, I have also learned a lot from you on the collaboration with people from different countries, the professional attitudes on your students, the sense of humor and the scientific writing skills.

I also want to express my appreciation to my daily supervisor Dr. Xiaoli Jiang, for the great contributions and guidance on this research. You acted as a tutor as well as a friend of mine. I am very grateful for all the discussions and communications we had for the research in our weekly meetings. Meanwhile, all the feedback from you for the papers we have published is appreciated. If somehow I let you feel uncomfortable and being offended due to my silly jokes, please accept my humble apologies. I always show a huge respect to you in my heart. Besides, I would like to thank you for your constant encouragement when I was in a bad mood and deeply frustrated by the things whatever academically or personally. You pushed me to update myself constantly, for instance the presentation skills and the writing skills, which is also greatly appreciated.

I want to acknowledge Prof. Mirek Kaminski. Although I only spent a couple of months in your group, your kindness, considerateness and humorous personality impress me a lot. I remember clearly that every time after seven o'clock in the evening, you pushed us go back home and enjoy the life. I am grateful for such moving consideration. Thanks to my mentor Dr. Dick Plettenburg for your listening to my complains. Besides, I would like to express my warmly gratitude to Prof. Yunxiang You in Shanghai Jiao Tong University. Thanks for your fatherly care and helping me make struggling decisions.

I would like to thank all my friends and colleagues in the Netherlands, for making my life here colorful and much easier, and for the unforgettable experience you shared with me. Particularly, I would like to mention some of them: Special thanks to Minchang, Yazhou,

and Wenhua, we are roommates as well as close friends living together. Thank you for the support and the enjoyable time when cooking, drinking and hanging out together. I cannot imagine how boring the life would be without you guys. Lindert and Johan, you are so nice and helpful as my office mates. Thank you for your sharing of personal stories and interesting life in the Netherlands, and your patience to answer my silly questions on my poor Dutch. Chenguang, thanks to you for your accompanying during your visiting in Delft, especially for the exciting sailing time on an inflated boat with many other friends in the canal, although it was too dangerous. Congbiao, thanks for the cycling together, even at midnight on the Afsluitdijk. Yaya, thank you for the happy time we have been together. Emanuele, thanks for your precious influence in my mindset to the fitness, and now I go to the gym very often. Mr. Dick Mensch, thanks for your time and kindness for the translation work of my thesis Summary. I would further like to thank in random order: Xiao, Wenbin, Gannis, Hui, Fan, Dr. Pang, Linying, Qingsong, Wenjing, Xiaojie, Hamid, Javad, Mark, Lode, Patty, Monique, Dineke, Josephina, Pauline, Anouk, Huarong, Guangming, Daijie, Xiangwei, Qinqin, Breno, Qu, Arthur, Ali, Kai, Xiao, Zongchen, Xing, Xiaobo, Tao, Xiuhan, Meng, Hai, Shuai, Zhi and all the other people who made my life here a memorable experience.

Further greatly gratitude has been expressed to all the guys from my Dutch courses in Mondriaan, including Cancan, Gil, Hasim, Alaaeddin, Arvind, Mohammed, Cathy, John, Ventsislav, Sofia, de docenten Ellen and Annette. We spent so much enjoyable time in the evenings of weekdays for learning, chatting, and parties together, which made me totally refreshed in my leisure time.

For the experimental test in my Ph.D. research, I am very grateful for the support from Prof. Zhiyong Pei, Prof. Ling Zhu and Prof. Weiguo Wu from Wuhan University of Technology. Meanwhile, I would like to thank Jianqiang, and the other six master students who were involved in the test preparation, measurement, data recording, and the dealing with test exceptions together. Besides, I really appreciate the help from the director of the structural laboratory, Mr. Weiguo Tang, and all the other engineers/staffs in this laboratory. We finally made it out of these heavy workload days and nights during the three months' testing because of the contributions from these diligent and intelligent people.

Thanks to the China Scholarship Council, the financial support for living abroad is greatly appreciated.

I am very grateful to all my old friends in China, especially Bin, Xun, Xiao, Jiaqiang, Jiangbo, Wei and Chao, for being there when I need you. Having you guys is one of my greatest luck in my life. I also really appreciate for what I have learned from my former colleagues in China Ship Development and Design Center, for not only the expertise on the challenged work, but also being a mature man. Here I only list some of the names: Qijian, Liming, Lianjiang, Junkai, Wei, and Peng.

Except for my research, I was also a big fan of sports, especially for the basketball. Specially, I would like to thank LeBron James, a role model in my generation in NBA, for your games and stories which inspired me every time when I was frustrated during my growing up. Being your fan for more than fifteen years since high school before your draft, I really appreciate the motivation and joy I have obtained from you.

Last but not least, I would like to thank my family. Firstly, my dear parents, without you I would not be on this beautiful world. You often supported me unconditionally. But I poured out too much negative energy on you because of my immaturity. I want to express

my deepest apologies, and I will not let you down anymore. I am also very grateful to my grandmother, for your great contribution to my family. My little brother, we grew up together, thank you for your company. I sincerely hope you grow into the man with strong shoulders soon. For my very cute, little boy, I love you so much. You are my greatest motivation in these years. I will do everything I can to protect and support you whatever happens in the future as long as you are happy. Many thanks also to the mother of my son, we have experienced so many ups and downs together. You made me the man I am today, being selfless, humble, mature and peaceful. I really appreciate that.

In the end, completing this Ph.D. research means a start of another journey in my life. No matter how tortuous the road to the future is, the only things I know are to face the music and keep my nose to the grindstone. Millions of thanks to everyone.

Jie Cai,
Delft, September 2018.

Contents

Chapter 1

Introduction

1.1 Research motivation

The petroleum industry has proven that pipelines are one of the most economical ways to transport crude oil and natural gas across extensive regions [27]. Figure 1.1 shows the typical use of pipelines underwater. Such pipes can be classified as flowlines transporting oil and/or gas from wells to manifolds, flowlines transporting oil and/or gas from manifolds to platforms, infield flowlines between different platforms, and export pipelines between platforms and bases onshore.

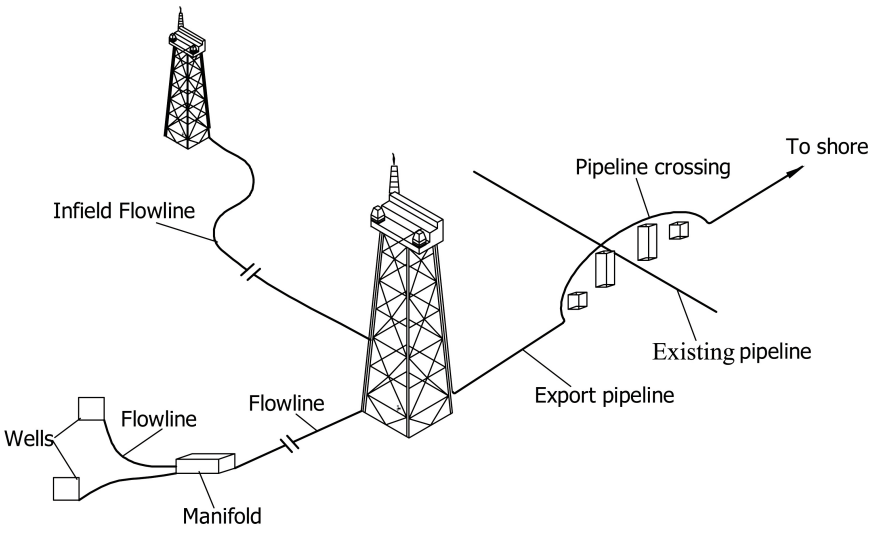

Figure 1.1: A typical use of offshore pipelines [72].

Structure damage, such as scratches, dents, cracks or even cavities, occurs commonly on both onshore and offshore fluid transmission pipelines. In the broadest definition, structural damage could be tiny defects, voids, notches or cracks of structure induced by material

welding, machining processes or other secondary treatments. Usually, they cannot be visually detected and exist with little effect on the integrity of structures. However, in a narrow definition, structural damage can also be large defects in terms of corrosion, dents, metal loss or large cracks due to factors such as mechanical interference, and natural forces (earthquakes, etc.) during different phases of pipelines including manufacturing, installation, commissioning and operation.

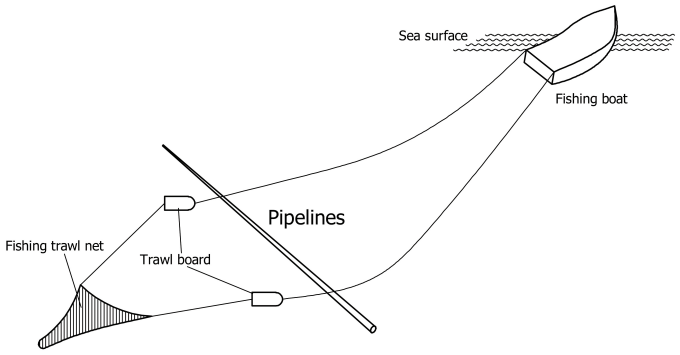

Figure 1.2: A typical mechanical interference between fishing equipment and pipelines underwater [46].

The occurrence of damage on metallic pipes indicates a degradation of their performance. It can merely have an aesthetic effect such as the discoloring of the pipe coating. However, the damage can also have severe consequences in terms of local and/or global buckling, overall failure, and oil/gas leaking, etc. Incidents in pipelines with such severe consequences can be categorized as so-called significant incidents which will produce a considerable loss of assets and cause a fatality. According to the reported data from PHMSA (Pipeline and Hazardous Materials Safety Administration) [103], within all the 11459 reported pipe incidents on liquids transmission pipelines (both onshore and offshore) with structural damage, the number of these significant incidents is between 41% and 53 %.

Mechanical interference such as collision and excavation plays an important role on the introduction of pipe structural damage. Approximately, 23% of all the reported structural damage on pipelines in the past 20 years is caused by mechanical interference [103]. Specifically, mechanical interference may be scenarios such as dropped foreign objects [25], dragging anchors, excavations, operation of underwater fishing equipment [46], sinking vessels and even mudslides on the sea bottom [65]. Figure 1.2 shows a typical mechanical interference between otter trawl and pipelines underwater. The trawl board is used to hold the trawl net open through hydrodynamic forces. During fishing operation, such boards are dragged along the seabed, which may represent a hazard to pipelines. Unlike the widely investigated corrosion damage in pipe structures [87], the type of structural damage caused by mechanical interference is still rarely studied. As stated in DNV-RP-F101 [45] and DNV-OS-F101 [48], for instance, the metal loss caused by mechanical interference has not been generally taken into account,

Actual loading conditions that the structure is undergoing play a critical role on the structural behavior when damage occurs. The types of dominant loads are complex and

vary with pipeline phases. In general, the life phases of pipelines consist of manufacturing, installation, commissioning and the operational stage [74, 84]. As an important type of loading conditions encountered by a pipe, bending moments exist extensively during the entire life cycle of pipelines. For instance, pipes are exposed to a considerable large bending moment during a typical reeling installation: reeling-on, reeling-off, bending over the aligner and bending through the straightening [68, 74, 88, 89, 96, 125]. For a pipe on the rough seabed during the operational stage [46], a large bending will be introduced when the contact between pipelines and the seabed is lost over an appreciable distance. Under these circumstances, the failure of pipelines caused by bending could be easily initiated. As a result, the structure of damaged or defected pipelines must be still able to withstand the anticipated bending loads.

For intact pipelines, analytical solutions and empirical prediction models for strength prediction do exist [12, 13]. However, few effective models are proposed for pipelines with damage due to factors such as the geometrical complexity of damage. Correction parameters are used to take into account the effect of different types of damage, generally providing a very conservative prediction result. To date, there is still a lack of common agreement on how to account for the severity of the damage on metallic pipes under bending. For instance, the upper limit of accepted dents (a typical structural damage) in terms of depth proportion is $8\%D$ (D is the outer diameter of pipes) from gas industry in UK [76, 77], $10\%D$ in PDAM (Pipeline Defect Assessment Manual) [42, 92], and $6\%D$ from ASME B31.8 and DNV-RP-F111 [8, 46]. Meanwhile, in the standard of DNV-OS-F101 [48], the maximum acceptable dent size in terms of the permanent depth is $5\%D$ due to the mechanical interference such as collision on pipes. Such lacking of consensus, to some extent, reflects the reality that the effects of structural damage to date have not been fully quantified.

Therefore, the occurrence of the structural damage raises questions on its consequences subjected to a specific bending load and on the necessities for intervention. These questions correspond to the level of residual performance that a pipe is expected to meet: is the damage only visually unpleasant? Or to which extent will the damage weaken the ultimate strength and then the use of the pipes? Is it still safe to continue the use of this pipe in the short term? Except for the regular engineering ways such as rigorous inspections, better monitoring and proper maintenance, what could be a better solution to answer these questions when damage happens? In many cases, it is not easy to provide a clear answer since there is no common agreement on how to quantitatively assess the severity of the damage on metallic pipes under bending. The identification of the residual strength can play an important role in addressing these questions related to damaged pipes after mechanical interference. An effective prediction model accounting for the on-site measurement, such as the real geometrical dimension or the loss volume of damage, could be a better solution to solve these problems.

1.2 Definition of residual ultimate strength

When there is no artificial damage on pipes, the corresponding load carrying capacity of pipes subjected to a load such as a bending moment due to the lack of strength or stability is the so-called ultimate strength. In this thesis, the residual ultimate strength (or residual strength) is defined as the residual load carrying capacity of the pipe structures with certain

types of structural damage. Details of these concepts and the relevant strength theory will be further addressed in Section 2.1 in Chapter 2.

1.3 Research objectives and related research questions

The main objective of this study is to develop an effective prediction model of residual ultimate strength for damaged metallic pipes under bending moment based on the existing information of structural damage. In order to fulfill this goal in the research, both main question and key questions that are needed to be solved are listed as follows.

The main question that addressed in this research project is:

- To what extent does structural damage induced by mechanical interference affect the residual ultimate strength of seamless metallic pipelines subjected to a bending moment?

The main question leads to the following key questions:

1. What are the influential parameters that affect the structural behavior of metallic pipelines ?

2. How do these influential parameters affect the structural behavior of pipelines?

3. What kind of structural damage normally occurs in metallic pipes due to mechanical interference?

4. How do the different types of structural damage and the relevant damage parameters affect the structural behavior of pipelines?

5. To what extent does the dent damage affect the structure ultimate strength in terms of bending moment and critical curvature?

6. To what extent does the metal loss damage affect the structure ultimate strength in terms of bending moment and critical curvature?

7. To what extent does the combined dent and metal loss damage affect the structure ultimate strength in terms of bending moment and critical curvature?

8. What is the effect of existing cracks on the residual strength of metallic pipes?

1.4 Research methods

Three parallel approaches (Finite Element Method (FEM), Experimental test and Analytical method) are used in this thesis, as seen from the flowchart in Figure 1.3. In order to answer these key questions in Section 1.3 and develop an effective solution, the FEM is particularly well suited due to its accessibility, reliable predictions, and wide use in engineering practice. It will be used for the numerical investigation of both general parameters of pipes and specific parameters of damage. Numerical models accounting for damage will then be developed and used for further analysis. Experimental tests for both intact and damaged pipes will be used to reveal the real physical phenomena and to gain the pipe strength in terms of residual ultimate strength. All possible structural damage induced by mechanical interference will be well produced on pipelines in a laboratory. The real test conditions will be taken into account, and the test results are used for the validation of numerical models. After completion of these investigations, an effective prediction model accounting for the on-site measured damage parameters will be proposed based on statistical methods, which can be applied for strength prediction in practice.

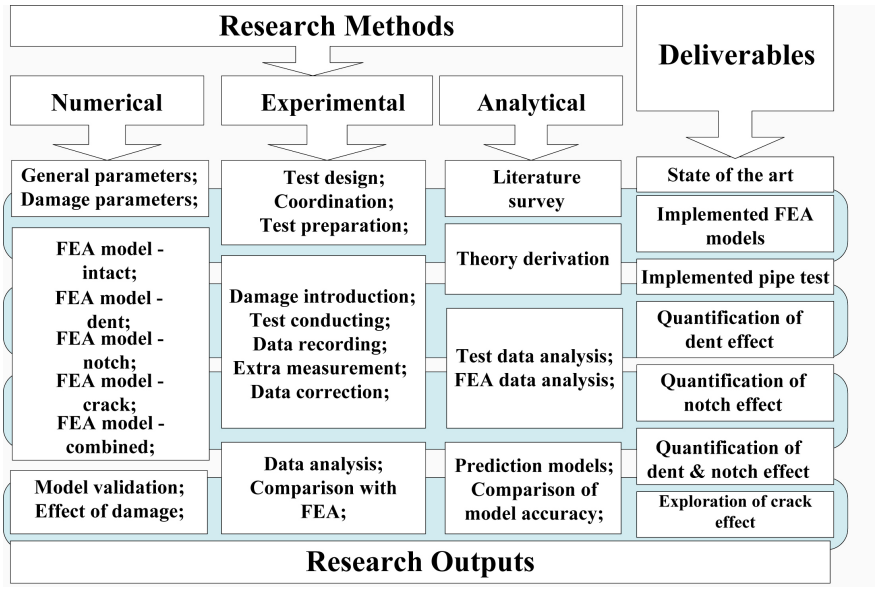

Figure 1.3: Research methods in this thesis.

1.5 Scope

As indicated from Section 1.1, the types of pipelines vary with the factors such as pipe functions and pipe installation locations. This research does not cover every type of the pipelines. Instead, only metallic pipes suffering from specific types of mechanical interference are accounted for. It is expected that the final results obtained from this research can be easily applied to the relevant industry region. Once the residual strength of structures is readily predictable after mechanical interference, the decision-making process, for instance,

pipe maintenance or replacement, by stakeholders such as classification societies, offshore companies and engineers, will be facilitated as well.

The research of residual ultimate strength in this dissertation specifically focuses on the seamless metallic pipelines with a low diameter-to-thickness ratio (D/t around 21). A standard generic pipe (D=168.3 mm, t=8.0 mm) according to API 5L [9] is selected for both the experiments and the numerical investigation in this thesis. There is a practical reason for this selection: Despite the new occurrence of pipelines made of composite material, seamless metallic pipes are still widely deployed in industry. The majority of old pipelines around the world are made of seamless metal, which are sensitive to the occurrence of structural damage. Furthermore, with the exploitation of the oil and gas into deep water, the use of the transmission pipes with a relative low diameter-to-thickness (D/t) increases because of the high requirements of load carrying capacity. Therefore, by focusing on this typical type of pipelines, it is expected that the outcomes of this research can be deployed effectively for practical purposes.

As indicated in Section 1.1, the actual loading conditions that structures are undergoing determine the distributions of stress and their relevant structural response. A bending moment, as one of the dominant loading cases, is mainly considered in this research. Large bending moments occur in pipelines during procedures such as the reeling procedure of pipe installation. How to effectively predict the ultimate strength of damaged pipes under a bending still remains a problem. Therefore, solving the strength problem of pipelines under a bending is the main issue in this thesis .

Steel material Q345 is majorly adopted in this thesis, which is a typical material with the specified minimum yield stress of 345 MPa [61]. There is a practical reason for this selection. In the pipeline domain, this material is widely used due to its relatively low price and relative high strength. In spite of the increasingly use of new metallic materials with high strength such as X70 [9] in pipes industry, the material Q345 is still widely used in pipelines. Therefore, the obtained research results can still have an extensive application.

There are two basic inputs, including damage type and damage dimensions, to determine the damage severity and to assess the damage consequences. Typical types of damage accounting for, in this thesis, are dents, metal loss, cracks and the combinations thereof. The size of damage is also critical for the following investigation. From the strength point of view, tiny damage has insignificant influence on structures. Normally, their effects can be taken into account through factors such as initial imperfections. From the fracture point of view, tiny damage produces significant stress concentration which will undermine the fatigue behavior of structures in the long term. However, such fatigue effect is out of the research domain of this thesis, which will not account for in this thesis. Meanwhile, the extra large size of damage that would produce rapid structural failure or immediate gas leaking has not been taken into account from the practice point of view. Therefore, the structural damage investigated in this thesis will have a moderate dimension and should be visible and easily measurable by regular engineering methods.

1.6 Thesis outline

The content of this dissertation is arranged as follows, as shown from the flowchart in Figure 1.4.

The purpose of **Chapter 2** is to review the recent research on the ultimate strength and the residual strength of metallic pipelines, to explore the influential parameters and their relevant effects on pipe strength, as well as to survey the typical structural damage due to mechanical interference. By doing so, the research gap on pipe residual strength can be explicitly revealed, paving the way for both the experimental and numerical investigations on the metallic pipelines with structural damage in the following chapters. The key questions 1, 2, and 3 will be, partially, answered in this chapter.

Chapter 3 provides a fundamental experimental investigation on damaged pipes. Test design and measurement methods are described in detail. Different types of structural damage are properly introduced. Residual strength of damaged specimens are presented and discussed. Discussions on experimental errors are also presented. The key question 4 will be partially answered in this chapter. Moreover, the test data presented in this chapter provide a solid foundation for the following chapters to quantify the effects of structural damage.

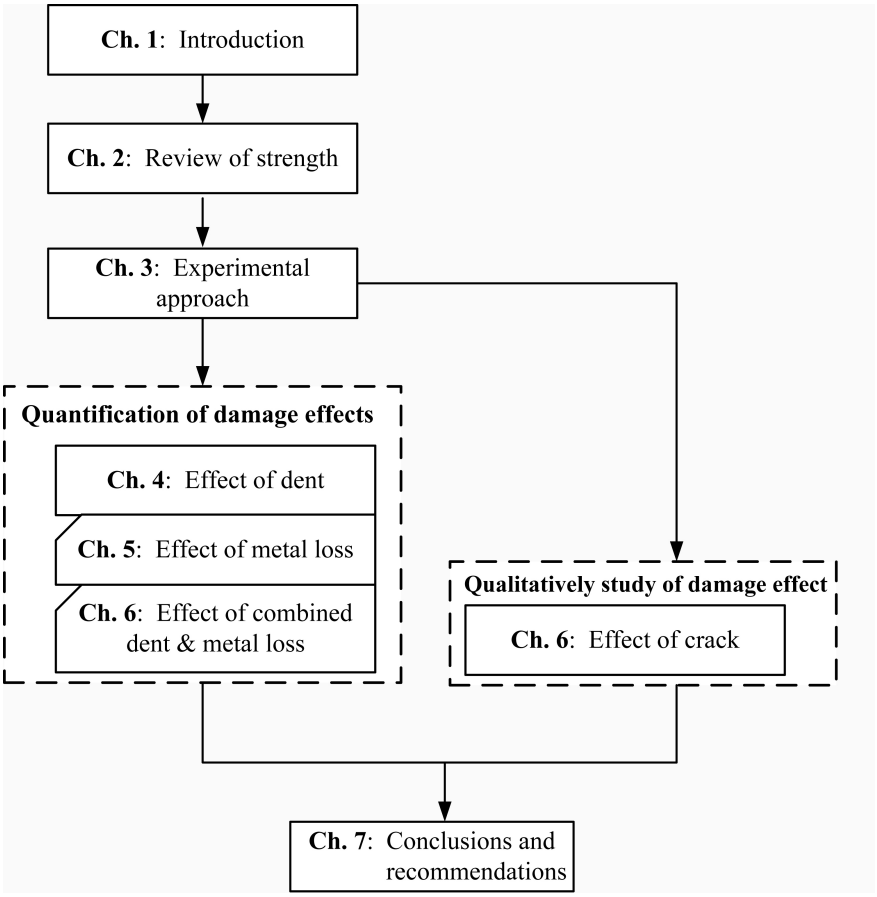

Figure 1.4: Outline of the thesis.

Chapter 4 quantifies the effect of a dent on the pipe residual ultimate strength. Numerical models are developed accounting for the dent parameters such as dent angle (θ_d), depth (d_d), length (l_d), and width (w_d), capable of predicting the pipe residual strength in terms of bending moment and critical curvature. Model validation is carried out based on the tests. Influential parameters including the anisotropy of materials, initial imperfections, test boundary conditions, and diameter-to-thickness ratios, are clarified. The dent parameters including dent orientation, dent location, dent depth, dent length and dent width are clarified through simulations. Empirical models based on statistical methods in the function of dent parameters are proposed for both strength and curvature prediction. Therefore, the key question of "to what extent does the dent damage affect the residual ultimate strength of metallic pipes" (key question 5 in Section 1.3) will be answered.

Chapter 5 quantifies the effect of metal loss in terms of a notch on the pipe residual ultimate strength. The notch simplification is first presented for further study. Numerical models are developed accounting for the notch parameters, which are validated through the test results in Chapter 3. Analytical solutions of damaged pipes with a notch is derived. Simulations on the effects of the metal loss parameters including depth (d_m), length (l_m), and width (w_m), are carried out. Through the simulation results, empirical models based on statistical methods in the function of the notch parameters and the volume loss due to the notch are proposed for both strength and curvature prediction. Therefore, the key question of "to what extent does the metal loss damage affect the residual ultimate strength of metallic pipes" (key question 6 in Section 1.3) will be answered in this chapter.

On the basis of the previous chapters, investigation and quantification of the effect of a combination of a dent and a metal loss on the residual ultimate strength is presented in **Chapter 6**. Meanwhile, the fracture failure due to damage that affects the residual strength of metallic pipes is also studied in this chapter. The simplifications of these types of damage are detailed described. Validated numerical models are developed for pipes with the combined dent and notch damage. Case studies on residual stress, combined damage and the interaction effect between fracture failure and the residual strength are carried out. XFEM (Extended Finite Element Method) is used for the numerical simulation of the pipes with possible fracture failure. The physical phenomena of metallic pipes with a crack are studied. Implementing the proposed prediction models for each type of single damage as well as the simulations, a new empirical model is developed. As a consequence, the key question of "to what extent does the combined damage affect the residual ultimate strength of metallic pipes" (key question 7 in Section 1.3) will be answered in this chapter. The key question 8 on the effect of existing cracks is initial explored.

Finally, **Chapter 7** concludes this thesis and recommends the future work.

Chapter 2

Literature review of the strength of metallic pipelines*

The strength of intact structures has been widely studied in the past few decades. However, research on residual strength of metallic pipes suffering from structural damage is relatively rare. The occurrence of structural damage on pipes may cause significant differences on their residual strength and relevant strength behavior compared with intact ones. In order to have a better understanding of the strength of metallic pipes, a literature review on metallic pipes with and/or without structural damage is carried out in this chapter. Through this chapter, the key questions on the influential parameters of pipes and their relevant effects are initially identified. The typical pipe damage induced by mechanical interference is clarified.

To investigate the residual strength of pipes, fundamental theories of pipe structures are first explained in Section 2.1. Then Section 2.2 categorizes the structural damage in pipes. Section 2.3 summarizes the typical production methods of damage on pipe surface and the relevant damage effects. The strength of pipes is affected by parameters including, but not limited to, diameter-to-thickness ratios of pipes (D/t), initial imperfections, residual stresses, material properties, and load conditions. Such influential parameters are discussed in Section 2.4.

After the clarification of these influential parameters on pipes, the following three sections (2.5, 2.6 and 2.7) focus on the methods of obtaining pipe ultimate and/or residual strength under different dominant loads. Among these methods, the experimental test is the most reliable means for strength evaluation, which is discussed in Section 2.5. In order to overcome drawbacks from a test such as high cost, the most economical method - nonlinear Finite Element Method (FEM) - is applied for the investigation of pipe strength, which is discussed in Section 2.6. Fundamental factors in the numerical modeling of metallic pipes are described and discussed. In Section 2.7, empirical prediction models on pipe strength are presented and discussed, which provides a foundation for the investigation of residual strength of pipes. In the end, conclusions of this chapter are drawn in Section 2.8.

*This chapter is based on the paper Jie Cai, Xiaoli Jiang, and Gabriel Lodewijks. Residual ultimate strength of offshore metallic pipelines with structural damage - a literature review. Ships and Offshore Structures. 2017: 1-19 [34].

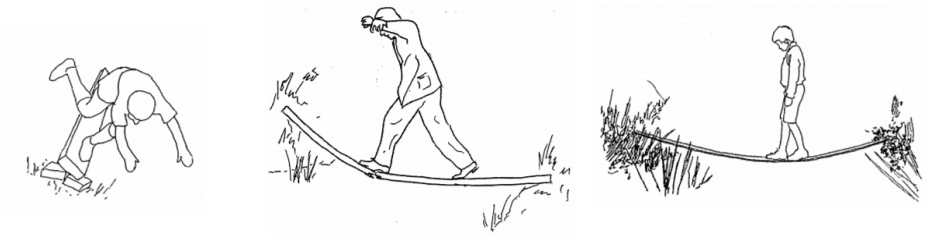

Figure 2.1: Three basic scenarios on structures [22].

2.1 Theory of pipe structures

A pipe structure is a typical cylindrical shell, which has a constant curvature in only one direction. The classical elastic theory of the strength of cylindrical shells has been extensively developed during the last century [121, 122], in spite of the large discrepancies compared with experiments. Generally, a structure in practice should satisfy three basic demands, as listed below:

- It should have sufficient stability;
- It should have sufficient strength; and
- It should have sufficient stiffness.

In a word, these three features compose the load carrying capacity of a structure. If a structure can not, or no longer, satisfy these demands, it fails. Figure 2.1 illustrates the corresponding scenarios when a normal structure lacks any of the types of the load carrying capacity. Likewise, the structure of pipes also concentrates on the problems of a lack of strength, a lack of stability and/or a lack of stiffness. The following Sections 2.1.1 and 2.1.2 explain the stability and strength of pipes, respectively. The pipe stiffness is always associated with either stability or pipe strength. Thus, no separate discussions will be conducted on it.

2.1.1 Stability of pipes

When the load on structures has reached a certain level, and if it continues to increase by a tiny increment, the equilibrium configuration of structures will have a large sudden change. This phenomenon is called “buckling” or the loss of stability. The corresponding load is the buckling load (or critical load).

For thin-walled pipe shells, there are two basic types of buckling/instability: bifurcation buckling and snap-through buckling. As seen from the example of a load-displacement diagram in Figure 2.2 (a), there is no obvious bifurcation point, instead, a limit load point exists. When external load has reached this value, displacement will increase rapidly, whereas

the load will decrease. Such ultimate type normally happens in the pipes under bending moment. When shells are subjected to external pressure or axial compression force, the snap-through buckling will happen, as shown in Figure 2.2 (b). OA and BC phases in the diagram are stable, however, AB phase is unstable. Therefore, there is an obvious snap between the two equilibrium configurations, which means that a snap-through buckling happens. Pre-buckling (OA) and post-buckling equilibrium configuration (BC) is therefore categorized.

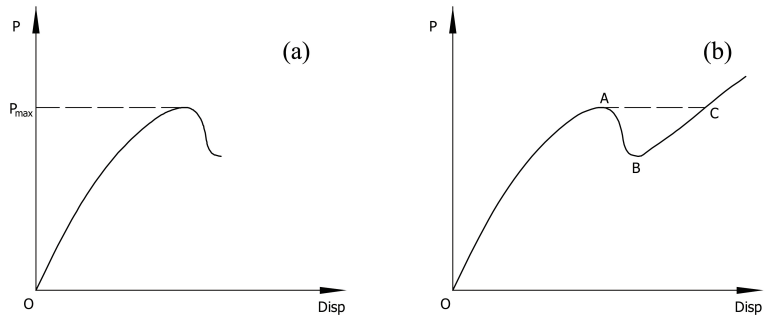

Figure 2.2: Two basic buckling type in pipes: (a) bifurcation buckling (with a limit point); (b) snap-through buckling.

Many researchers have contributed to the classical stability theory for cylindrical shells. Karman [79] proposed a nonlinear large deflection theory based on classical linear structure stability theory. Koiter [83] clarified the relationship between structures' initial imperfection sensitivity and the initial post-buckling features based on energy criterion. His theory was a high order theory which can confirm both the slope and the curvature of secondary path (equilibrium path after buckling) at the structures' bifurcation points. Stein [118] proposed the pre-buckling consistent theory, he abandoned the nonmomental assumption in pre-buckling stage, but deployed the nonlinear equilibrium equations accounting for bending. Under this situation, the deformation shape in pre-buckling stage was not constant any more and satisfied the geometry boundary condition.

For thin-walled cylindrical shell structures, the orthogonal curvilinear coordinate system is deployed in theory derivation due to its convenience. The transformation with Cartesian coordinate system is through the Lame parameter which is used for the correction of the arc-length. Meanwhile, Kirchhoff assumptions [122] are adopted for thin-walled shell structures including:

- straight lines normal to the mid-surface remain straight after deformation;
- straight lines normal to the mid-surface remain normal to the mid-surface after deformation; and
- the thickness of the plate does not change during a deformation.

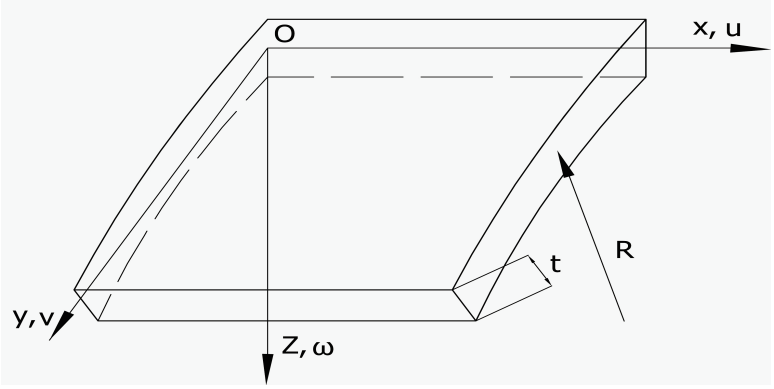

Figure 2.3: Shell element from cylindrical pipes under Cartesian coordinate system.

Based on these assumptions, the mid-surface of pipe shell can be used to represent a three-dimensional plate in two-dimensional form [122]. For thin-walled cylindrical shells in Cartesian coordinate system (transformed from orthogonal curvilinear coordinate system), as seen in Figure 2.3, any shell element should satisfy both the differential equilibrium equation (Equation (2.1)) and the differential deformation compatibility equation (Equation (2.2)) [50].

$$D \bigtriangledown^4 \omega - \frac{N_y}{R} = (N_x \frac{\partial^2 \omega}{\partial x^2} + N_y \frac{\partial^2 \omega}{\partial y^2} - 2N_{xy} \frac{\partial^2 \omega}{\partial x \partial y}) + q \tag{2.1}$$

$$\frac{\partial^2 \varepsilon_x}{\partial y^2} + \frac{\partial^2 \varepsilon_y}{\partial x^2} - \frac{\partial^2 \gamma_{xy}}{\partial x \partial y} = -\frac{1}{R} \frac{\partial^2 \omega}{\partial x^2} + (\frac{\partial^2 \omega}{\partial x \partial y})^2 - \frac{\partial^2 \omega}{\partial x^2} \frac{\partial^2 \omega}{\partial y^2} \tag{2.2}$$

Where D is the bending stiffness and can be expressed as $D = \frac{Et^3}{12(1-\nu^2)}$. $\bigtriangledown^2$ is the Laplace operator. For two dimensional problem, it can be expressed as $\bigtriangledown^2 = \frac{\partial^2}{\partial x^2} + \frac{\partial^2}{\partial y^2}$. R is the radius of the mid-surface of the cylindrical shell. N_x, N_y and N_{xy} are the unit internal forces on the mid-surface of shell element. q is the external force exerted on the shell element. ω is the shell deflection. ε_x, ε_y and γ_{xy} are the strain in the corresponding coordinate direction, respectively.

To investigate the stability problems of a shell, two neighboring equilibrium positions are given, as shown in Equation (2.3).

$$\begin{aligned} u &\to u_0 + u_1 \\ v &\to v_0 + v_1 \\ \omega &\to \omega_0 + \omega_1 \end{aligned} \tag{2.3}$$

Where (u, v, ω) and (u_0, v_0, ω_0) are the two neighboring equilibrium configurations corresponding to the same load. (u_1, v_1, ω_1) is the infinitesimal increment of displacement. Likewise, the internal force in the two neighboring equilibrium positions can be also expressed as Equation (2.4).

$$\begin{aligned} N_x &\to N_{x0} + N_{x1} \\ N_y &\to N_{y0} + N_{y1} \\ N_{xy} &\to N_{xy0} + N_{xy1} \end{aligned} \tag{2.4}$$

Substituting Equation (2.3) and (2.4) into the corresponding equilibrium equations Equations (2.1) and (2.2), and accounting for the geometry relationship between strain and displacement, the physical relationship between strain and stress of shell element can be obtained. In addition, all the terms including u_0, v_0 and ω_0 and the external force q can be removed from the derivation equations because of the equilibrium state they have already satisfied. Thus, the differential stability equation of a shell element with a perfect shape in three directions can be written as Equation (2.5):

$$\begin{aligned} \bigtriangledown^4 u_1 &= \frac{1}{R}\left(\frac{\partial^3 \omega_1}{\partial x \partial y^2} - \nu \frac{\partial^3 \omega_1}{\partial x^3}\right) \\ \bigtriangledown^4 v_1 &= -\frac{1}{R}\left((2+\nu)\frac{\partial^3 \omega_1}{\partial x^2 \partial y} + \frac{\partial^3 \omega_1}{\partial y^3}\right) \\ D \bigtriangledown^8 \omega_1 &+ \frac{Et}{R^2}\frac{\partial^4 \omega_1}{\partial x^4} - \bigtriangledown^4 \left(N_{x0}\frac{\partial^2 \omega_1}{\partial x^2} + 2N_{xy0}\frac{\partial^2 \omega_1}{\partial x \partial y} + N_{y0}\frac{\partial^2 \omega_1}{\partial y^2}\right) = 0 \end{aligned} \tag{2.5}$$

In the stability equations, (u_0, v_0, ω_0) is also called the pre-buckling deformation, while the displacements (u_1, v_1, ω_1) are considered as buckling mode. It should be emphasized that assumptions such as the nonmomental assumption, the small deflection of shell, the ignoring of nonlinear items, and the ignoring of pre-buckling rotational angle have been made during the theoretical derivation. In order to satisfy the nonmomental assumption, the mid-surface of a pipe shell should be smooth enough, and there should be no abrupt variation of the curvature along surface. When structural damage is produced, local curvature has been inevitably changed, which indicates that the nonmomental assumption is no longer satisfied. Therefore, it is very difficult to have a theoretical derivation for cylindrical shells with damage.

Based on these basic stability equations, some analytical solutions can be derived. For instance, the critical stress of pipes under a bending moment with a simply supported boundary condition can be expressed as Equation (2.6). A specific buckling mode (Equation (2.7)) with an axisymmetric instability shape is prescribed, where m is the number of half-wave along shell axis, A_m is the parameter of buckling shape. Detail derivation is not presented here for clarity reason. This equation can be used as the reference value of the further strength research.

$$\sigma_{cr} = \frac{Et}{R\sqrt{3(1-\nu^2)}} \tag{2.6}$$

$$\omega(x) = \sum_{m=1} A_m sin\frac{m\pi x}{L} \tag{2.7}$$

2.1.2 Strength of pipes

With the decrease of pipe diameter-to-thickness ratios, the failure of cylindrical shells will gradually turn to the pattern of elastic-plastic failure. The sudden buckling/instability, as

descried in Section 2.1.1, will not occur any more. Instead, the strength of pipes is dominant by the plasticity of materials and its relevant distribution. Therefore, the ultimate strength of intact pipes under this circumstance is derived in this section.

Providing the bending stress in the entire pipe cross-section is uniform and the pipe material is elasto-perfectly plastic, the analytical solution of pipe strength is firstly derived when it is subjected to a combination of bending and axial force, as shown in Figure 2.4. It illustrates an intact pipe with a simplify-supported boundary condition, and its stress distribution of a specific pipe cross-section when failure happens. The ultimate bending strength has reached when the stresses σ_{comp} and σ_{ten} in the pipe cross-section increase to the material yield stress σ_y.

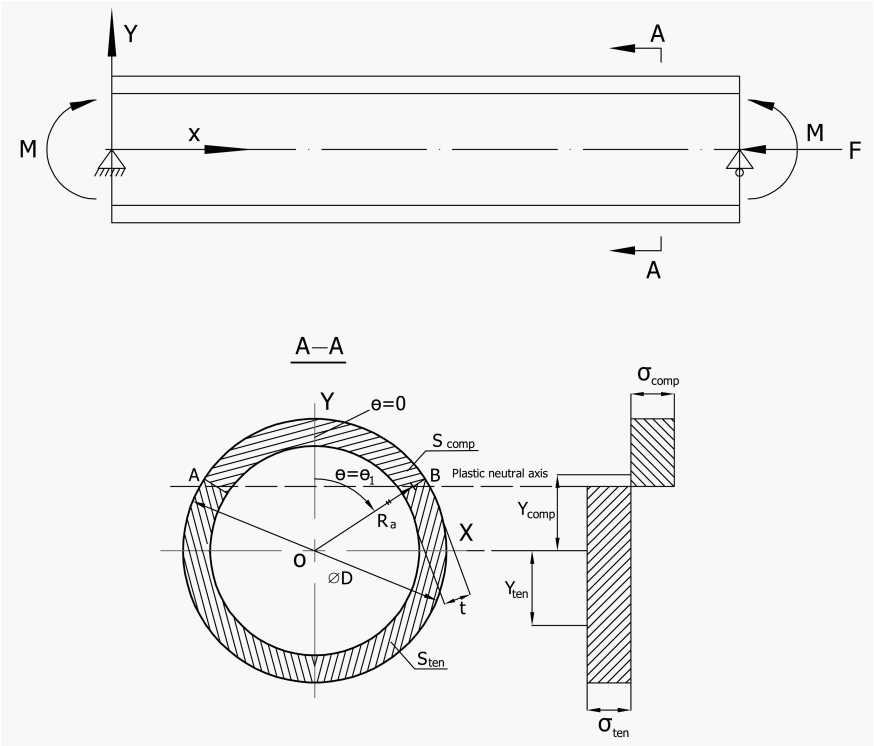

Figure 2.4: Sketch of a pipe subjected to bending and the stress distribution on a pipe cross-section.

In order to derive the expression of ultimate strength, we first need to obtain the location of plastic neutral axis *AB*, as shown in Figure 2.4.

Integrating all the stresses on the pipe cross-section, the axial force F can be expressed as:

$$\begin{aligned} F &= 2\int_0^{\theta_1} -\sigma_y t R_a d\theta + 2\int_{\theta_1}^{\pi} \sigma_y t R_a d\theta \\ &= 2R_a t\sigma_y(\pi - 2\theta_1) \end{aligned} \tag{2.8}$$

Where θ_1 is the plastic neutral axis angle, θ is between 0 and θ_1. Hence, θ_1 can be denoted as :

$$\theta_1 = \frac{F - 2\pi R_a t \sigma_y}{4 R_a t(\sigma_y)} \tag{2.9}$$

Meanwhile, the bending arm y_{comp} and y_{ten} can be expressed as Equation (2.10).

$$\begin{aligned} y_{comp} = \frac{R_a^2 t \int_0^{\theta_1} \cos\theta d\theta}{R_a t \theta_1} &= R_a \frac{\sin\theta_1}{\theta_1} \\ y_{ten} &= R_a \frac{\sin\theta_1}{\pi - \theta_1} \end{aligned} \tag{2.10}$$

Hence, the ultimate bending strength can be expressed as:

$$\begin{aligned} M_c = 2\int_0^{\theta_1} -\sigma_y t R_a^2 \cos\theta d\theta + 2\int_{\theta_1}^{\pi} \sigma_y t R_a^2 \cos\theta d\theta \\ = 4 R_a^2 t \sigma_y \sin\theta_1 \end{aligned} \tag{2.11}$$

If there is no axial force, then, $\theta_1 = \pi/2$. Hence, the bending strength of intact pipes is expressed as Equation (2.12), which is also called plastic bending moment.

$$M_y = 4 R_a^2 t \sigma_y \tag{2.12}$$

If the hardening effect is taken into account, the bending strength of metallic pipe under pure bending can be expressed as Equation (2.13) [12, 126]:

$$M_{yh} = 4 R_a^2 t \sigma_y + R_a^2 t \pi (\sigma_u - \sigma_y) \tag{2.13}$$

Therefore, the analytical solution of the ultimate bending strength of an intact pipe is derived.

2.1.3 Residual ultimate strength of pipes

As discussed in the former sections, pipe strength is a complex problem, and the classical theory cannot fully take into account all the factors due to simplifications and assumptions. Depending on the ratios of D/t, pipe strength is determined by either its stability or its strength related to material plasticity. Under any of these situations, the load carrying capacity of pipes has been reached. The corresponding structural behavior is determined. Therefore, in this thesis, residual ultimate strength (or residual strength) is defined as the residual load carrying capacity of pipe structures with certain types of structural damage due to either a lack of stability or a lack of strength related to material plasticity. When there is no artificial damage on pipes, the corresponding concept is the so-called ultimate strength.

2.2 Structural damage

In this section, the concept of structural damage on pipes is first presented. Then, typical structural damage that normally occurs in metallic pipes due to mechanical interference is identified. Existing research related to pipe damage is surveyed.

2.2.1 What is damage?

In a broad definition, structural damage can be defined as any unexpected and/or expected defects on structures, which could affect their performance. However, controversy on a common definition of structural damage still exists due to its complexity, as seen in existing standards such as ASME B31G [11] and DNV-RP-F108 [49]. Therefore, the concept of structural damage on pipelines is, at least partially, subjective during the assessment of residual strength.

The subjective perspective comes from the variation of damage causes, damage dimensions or conventionality in practice. Generally, structural damage on pipes could be permanent deformations, voids, notches, corrosion or cracks induced by material welding, fabrication, machining processes, environment or other secondary treatment. Due to its subjective characteristic, the definition of damage is not always explicitly clear, leaving space for different interpretation. For instance, permanent deformation could be categorized as either structure's initial imperfection or individual dent damage, depending on its dimensions and causes. Therefore, the evaluation method of the actual residual ultimate strength could be disputable openly. In this thesis, the structure damage refers to the damage with a moderate size induced by mechanical interference. Specific description of each type of damage is presented in the following sections.

2.2.2 Typical structural damage

One of the main causes of structural damage is mechanical interference. It has been estimated that the failure of oil and gas transmission pipelines resulting from mechanical damage ranges from 55 percent in the USA to around 70 percent in Europe[65]. The mechanical interference includes, but not limited to, dropped foreign objects [25], dragging anchors, excavations, operation of underwater fishing equipment [32, 46], sinking vessels and even mudslides on the sea bottom [2, 65].

After mechanical interference, the main types of damage on metallic pipelines are a dent, metal loss, a crack and combinations thereof. In the past twenty years, considerable amount of studies have been conducted on different types of pipe damage. Park and Kyriakides [102] experimentally studied the resistance capacity of cylinders with a single dent under external pressure. Starnes and Rose [116, 117] investigated the nonlinear buckling behavior of thin-walled cylinders with a longitudinal crack subjected to combined loads. Macdonald [92] conducted a detailed literature review on the effect of dent and gouge damage on pipeline structures. Vaziri and Estekanchi [124] numerically studied the buckling behavior of a cracked cylinder subjected to combined internal pressure and axial force in a linear domain. Ghaednia et al. [64, 65] investigated the effect of dent and crack damage on the burst capacity of a pipeline. Lee et al. [87] carried out numerical simulations on the burst capacity of pipeline elbow with metal loss.

As listed above, many studies have focused on the pipe damage under different load conditions. In order to better investigate and quantify the damage effect in this thesis, a specific definition of each damage is given in the following sections, and each type of damage is addressed in detail.

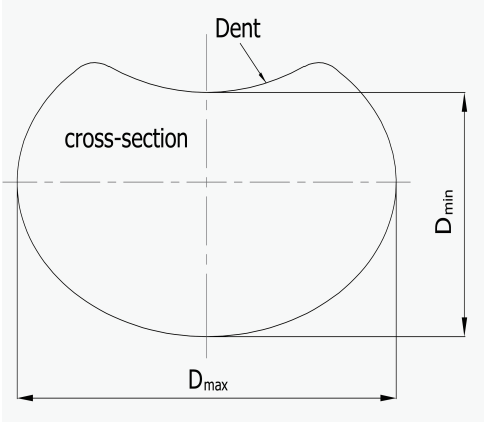

Figure 2.5: Sketch of an impact induced dent on metallic pipes.

Dent

A dent is a permanent plastic deformation on a pipe wall that produces a gross distortion of the pipe cross-section [42, 92], as seen in Figure 2.5. The dents on pipelines can be categorized into two basic types:

- Plain dent: A dent with smooth curvature variation but without wall thickness reduction and other defects.
- Kinked dent: A dent that causes an abrupt curvature variation of a pipe wall.

There are two ways to express the severity of a dent. The ovalization parameter δ is used in some standards [3, 48]. As shown in Equation (2.14), D_{max}, D_{min} and D_{ave} are the maximum, minimum and average outer diameter of the pipe cross-sections, respectively. Another equal method is the use of the dent depth ratio (d_d/D). For instance, the upper limits of an accepted dent depth under internal pressure is 8%D in British Gas [76, 77], 10%D in PDAM [42, 92], and 6%D in ASME B31.8 [8] and DNV [46, 48].

$$\delta = \frac{D_{max} - D_{min}}{D_{ave}} \tag{2.14}$$

Therefore, the dent depth (or ovalization parameter) is considered a significant influential factor. As Park and Kyriakides [102] stated for pipes subjected to external pressure, the "collapse capacity of pipes was relatively insensitive to the detailed geometry of a dent such as shape and size but to be critically dependent on the maximum ovalization of its most deformed cross-section". When the ovalization parameter of dented pipes is small, the effect of a dent on collapse performance of pipeline subjected to external pressure is quite benign [13]. Normally, the minimum initial ovalization ($\delta_0 = 0.005$) is introduced to any structures during calculation in order to account for its effect as specified in the standard DNV-OS-F101 [48]. The profile of a dent is not as critical as dent depth as long as the dent is a plain type [19, 85, 86, 98, 112] .

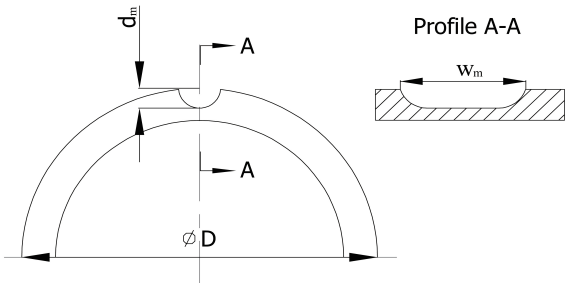

Figure 2.6: Sketch of a type of metal loss on metallic pipes.

Metal loss

The second type of structure damage is metal loss. It is a generalized kind of structural damage that involves partial loss of material in the form of gouges or notches, etc. A gouge or a notch is a typical metal loss pattern [85, 92], which has a regular profile but will not change the shape of pipe cross-section, as seen in Figure 2.6. Corrosion is generally considered the major cause of metal loss in offshore pipelines [60, 88, 127]. Meanwhile, contact with sharp foreign objects such as anchors and fishing boards that have scraped partial material out of the pipe is another common scenario for pipe metal loss.

Metal loss reduces the bursting and fatigue strength of the pipe. A longitudinally orientated gouge is considered the most severe condition for pipes subjected to internal pressure [92]. Normally, parameters such as metal loss shape, length, width and depth, are used to express a metal loss. In the design standard from DNV-RP-F101 [45], metal loss profiles are normally idealized as parabolic, rectangular or exponential type. The metal loss depth is a critical parameter, as stated in the bursting strength research from [87]. Fracture failure might be initiated in the metal loss region, which can be denoted by a so called "notch stress-intensity concept" [105].

Crack

The third important pipe damage is a crack. A crack, as shown in Figure 2.7, is a kind of structure damage that is easily initiated on a pipe surface. Except for the typical mechanical interference, other causes such as corrosive environment and/or cyclic loading arising from the pressure fluctuations and geologic movements [41, 64, 65] can introduce surface crack on pipes. Some chemical contents such as hydrogen gas, can even speed up the occurrence of cracks at corrosion sites [56].

Generally, two types of crack can be categorized in practice: one is a through-crack, while the other is a surface crack. From the engineering perspective, surface cracks on pipe structures are strictly inspected and prohibited during the fabrication stage, let alone through-cracks.

Cracks in pipelines may significantly compromise the buckling behavior, jeopardize the structural integrity, and induce detrimental structure failure [18, 52, 124]. From the perspective of fracture mechanics, a general scheme of safety assessment on cracked structures is illustrated in Figure 2.8. It has clearly illustrated the relationship between different critical

states in terms of the critical loads, the critical crack size, the required minimum fracture toughness and the residual lifetime due to crack propagation. In the linear elastic domain, the stress intensity factor (K) can be well used to denote the crack characteristics [7, 109]. In elastic-plastic domain, the $CTOD$ (crack tip opening displacement) or J integral has been widely accepted to denote the cracks, although they have not been strictly proved by theorems [7]. The so-called *CDF* (crack driving force) and *FAD* (failure assessment diagram) [10, 31] approaches have been used for fracture assessment. In *FAD* method, a failure curve is used to assess the failure zone, safe zone, and the security and safety factors [105].

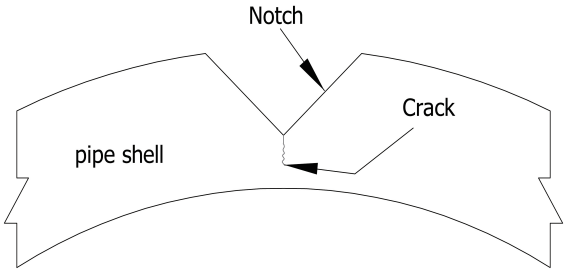

Figure 2.7: Sketch of crack at a notch tip on a metallic pipe.

A typical parameter of surface crack is the crack depth, which will largely compromise the structural capacity. Studies [64] have shown that once the crack depth exceeds a certain limitation - for example, a 4 *mm* crack depth in a pipe with 8.5 *mm* thickness - the bursting capacity of pipes subjected to internal pressure can be reduced by 38 percent. However, a shallow surface crack might not affect the pipe strength as demonstrated by [63, 65]: when a crack depth is less than 2 *mm* in a pipe with 8.5 *mm* wall thickness, it did not affect the bursting capacity at all. When the depth of pipe surface crack is less than 12.5%D, the crack can be physically removed by grinding in advance so that its effect on structural strength can be eliminated [25, 43, 85]. Few studies have been found to address the buckling strength of a cracked pipe subjected to bending moment. Therefore, the effect of a crack on pipe residual ultimate strength should be continued to investigate.

In sum, three basic types of structural damage exist in the surface of metallic pipes. Mechanical interference is one of the main causes of such damage. In reality, the combinations thereof are more likely to happen due to the complexity of damage introduce environment. It is widely accepted that the combined damage, such as combined dent and metal loss, is more detrimental than single damage [25, 51]. Therefore, studies are also required in order to investigate the effect of such combined damage.

2.3 Produce of pipe damage

In the strength research of pipes with structural damage, how to produce a proper damage on pipe surface is an essential problem. Thus, typical methods to introduce damage in a laboratory are presented in this section.

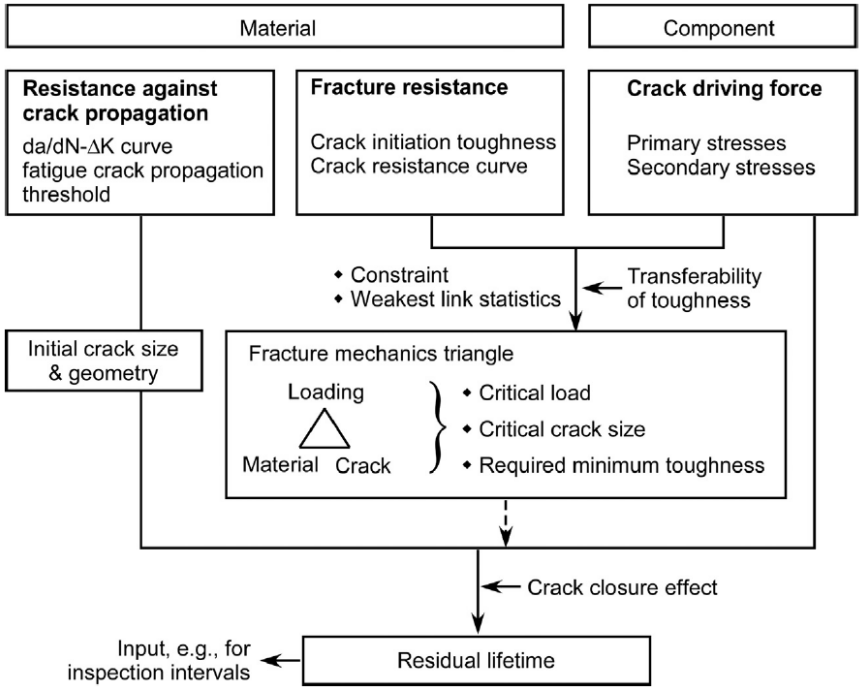

Figure 2.8: Schematic principle of fracture mechanics analysis [128].

2.3.1 Production of a dent

Before introduce a dent in a laboratory environment, two different scenarios should be first considered: produce damage without internal pipe pressure, or produce damage with internal pipe pressure. The majority of dents are introduced into pipe without prescribed internal pressure [4, 48, 58, 85, 106]. A few are introduced with prescribed internal pressure [65, 85, 106, 125], which is more close to reality. According to the research in [70], the presence of internal pressure has a large effect on the indentation procedure and will largely increase the indentation force to develop the same dent size.

There are two ways to introduce a dent on pipe walls. One is the quasi-static way, in which an indenter is loaded with a low speed in order to eliminate the dynamic effect. The other is the dynamic way, which requires a high-speed indenter to impact specimens. The initial impact energy should be well designed so that artificial cracks are not produced.

2.3.2 Production of metal loss

In order to introduce metal loss in a laboratory environment, the electro-discharging machining method [65, 88] is generally deployed with specified types of electrodes. Alternatively, machining method through customized cutting tools is used to fabricate metal loss with a different size, angle, shape and location. After the introduction of metal loss on a pipe surface, a grinding process should be used to eliminate the effect of a possible existing crack [25, 85].

2.3.3 Production of a crack

Under laboratory environments, there are basically two ways to introduce a prescribed crack in pipe walls. One is the cyclic loading method, which can introduce a fatigue crack in a region with prescribed metal loss and/or dent. Preliminary work has been conducted to clarify the required number of loading cycles for a single fatigue crack, showing that approximately 50,000 loading cycles on the region with metal loss (V-notch) could introduce a 0.3 *mm* (pipe thickness is 8.5 *mm*) depth crack at the tip of the notch [65, 114]. However, a disadvantage of this method is that it is not easy to pre-control the initiation place of crack and crack size. Therefore, alternative methods such as machining method and laser cutting technique are used so that the size and location of a tiny crack on pipe walls can be precisely controlled. Besten [23] successfully introduced 2D artificial edge cracks by laser to mimic welding-induced defects in his fatigue research. It should be noted that the HAZ (heat affected zone) generated by laser cutting may lead to undesirable effects on the strength of structures, as shown from the laser test in [94].

2.3.4 Production of combined damage

For the introduction of a combined damage, special attention should be paid to the sequence of every single piece of damage, since the existing type and size of damage could be affected by new processes and new damage. Delicate design is needed in order to avoid such adverse interaction. For instance, in order to produce a combined dent and metal loss, a special indenter has been designed with a protruding tiny wedge that is coordinated with the existing V-notch in the studies in [25] and [65]. Thus, the combined dent and notch was then well produced.

2.4 Influential parameters on pipe strength

Except for the structural damage, the pipe strength is affected by many other influential parameters. In order to quantify the effect of structural damage, the effect of these influential parameters should be first identified. In this section, influential parameters that include diameter-to-thickness ratios (D/t), length-to-diameter ratios (L/D), manufacture methods, residual stress, and pipe loads, are summarized and discussed.

2.4.1 Diameter-to-thickness ratio

The internal mechanism of pipe residual strength is largely determined by the D/t ratio of pipes. In other words, whether pipes fail due to a lack of stability or a lack of strength depends on the D/t ratio as well as the type of pipes. From the standpoint of application, the common transmission pipes in deep water have D/t ratios between 25 and 30, while much larger D/t ratios are employed in shallow water. Among these pipes, the buckling/instability failure pattern generally happens when the D/t is larger than 40, while elastic-plastic failure normally occurs when the D/t is less than 20. A combined failure mode would occur on the structures with ratios between 20 and 40 [72].

In addition, the length-to-diameter (L/D) ratio also affects the behavior of the structure strength under certain situations, such as pipes subjected to pure axial load [131]. Thus, the L/D ratio should not be neglected during the strength investigation of pipes.

2.4.2 Manufacture methods

The manufacture method is another factor that has a considerable effect on pipe strength. Two typical types of pipelines exist based on manufacture methods: seamless pipes and pipes with a longitudinal or spiral-welded seam. The former type is produced by metal forming method (hot-rolling or cold-rolling) without a seam. Thus, the material properties of pipes haven't been significantly affected. The latter is generally produced by the UOE (U-ing, O-ing, and expanding) process [68, 69], which is a common manufacture method for large-diameter pipelines. During such process, the prepared plate is first formed into a U-shape by a special press. Then, through an Oing-press, it is formed into a circular shape. The "Bauschinger effect", therefore, could be activated, which decreases the material yield stress when the loading direction has been changed [29, 47, 69, 106, 125]. The reduction ratio of the compression yield stress of material can reach up to 30 percent of the un-processed material [29, 47, 119]. Therefore, materials are no longer isotropic and will cause large discrepancies in the prediction of pipe strength.

2.4.3 Residual stress

Residual stress is the auto-balancing stress that is locked into material when it is free from external forces. Factors such as fabrication processes, pipe joining processes, thermal processing, welding, heat treatment, mechanical forming and long term service conditions are the most common sources of residual stresses [5, 104, 113]. They are presented in every manufacture component and assembled structures. For seamless pipes, it is generally coming from the fabrication process including the hot-rolling or cold-drawing process.

Residual stress can be estimated through numerical modeling of forming processes and welding processes, or through experimental methods. Shadley and Rybicki [113] carried out a test to determine the residual hoop stresses in seamless thin-walled pipes. By a through thickness axial cutting, the strain changes on pipe surface are measured using strain gauges. Amirat et al. [5] used BRSL method (block removal splitting and layering method) to obtain the residual hoop strain distribution along pipe thickness. Crampton [91] has developed an equation for the estimation of circumferential residual stresses based on test information. By slitting the longitudinal length of pipes and measuring the diameter change, the residual stress can be written as Equation (2.15).

$$\sigma_c = E't\left(\frac{1}{D_0} - \frac{1}{D_1}\right) \tag{2.15}$$

Where t is wall thickness, D_0 is the original diameter and D_1 is the final diameter after slitting. E' is expressed as $E' = E/(1-\nu^2)$. This method is based on the assumptions of elasticity theory, invariant of stress along the pipe length and material being homogeneous during layer removal.

The distribution of residual stress in pipes varies with their manufacture methods. For instance, the spiral-welded pipes, developed by the cold bending manufacture process [53],

has a tensile residual stress on the inner surface and a compression stress on the outer surface in pipe hoop direction. The largest stress component has reached the value of $0.65\sigma_y$. Due to the occurrence of weld seam, the stress component in hoop direction has several turning points between compression and tension along the pipe thickness. The maximum stress component in the axial direction is much smaller (about $0.3\sigma_y$).

For seamless pipes produced by hot-rolling, the residual stress component in the hoop direction presents a monotonical increase/decrease state. In the test from [5] on a typical API X60 seamless steel pipe, it is measured that there is a compression stress component in the hoop direction on the outside layer of seamless pipe, monotonical decreasing until the largest tensile stress on the inside layer of pipes has been reached. The maximum residual stress is approximately 10% of the material yield stress. However, in the seamless pipe test from [113], an opposite conclusion on the stress distribution in hoop direction is observed, with compression on the inner layer and tension stress on the outer layer of pipes. For the stress component in axial direction, it is generally assumed to be invariant due to its slight change based on test observation.

For seamless pipes produced by cold-drawing, residual stress also presents a monotonical state. As shown from the test in [104] on a copper pipes, the residual stress component in the hoop direction changes from compression on the inner surface to tensile on the outer surface. The axial component changes from a strong compression on the inner surface to tensile on the outer surface. The residual stress in the radial direction is slight, varying from 0 in the inner surface to slight compression on the outside of pipe.

2.4.4 Pipe loads

Load conditions on pipelines are complex, varying with installation methods (S-lay, J-lay, or Reel lay [74, 84]) and pipe phases (installation, test and operation, etc.). A summary of typical load conditions for offshore pipelines is presented in Table 2.1, which indicates that bending moment is a widely existing load in pipes. However, the dominant load is changable and could induce different types of structural failure. For instance, external pressure becomes dominant during a dry installation in deep water [72]. Another example is that, during the hydrotest phase before operation, pipe structures suffer from high internal pressure up to 1.25 times of the design internal pressure [48], which is used to check the structural integrity. As a result, internal pressure becomes dominant. Meanwhile, with the variation of ocean environments such as uneven sea bottoms, mudslides and collision with foreign objects such as anchors and fishing boats, the dominant load changes as well. Therefore, it makes sense that investigations of pipe strength should be accompanied by careful checks of load conditions.

2.5 Experimental methods for pipe strength evaluation

There are many ways to investigate the residual strength of metallic pipes. Among them, an experimental test is the most traditional and reliable way to evaluate strength. A successful test is often contributed by the joint efforts of personnel including engineers, technicians, researchers and workers. Significant endeavor should be involved for test including test design, specimen fabrication, facility installation, data collection, data processing and even

project management. Figure 2.9 shows some typical experimental set-ups for the evaluation of pipe strength. Therefore, in this section, existing experiments for strength evaluation of pipes under different loads are presented and discussed.

Table 2.1: A summary of load condition for offshore pipelines.

Load type	Installation phase		Test phase		Operation phase	
	Shallow water	Deep water	Shallow water	Deep water	Shallow water	Deep water
Bending moment	++++*	+++	/	/	++	++
Axial force	++	++	+	+	+	+
Internal pressure	+	+	+++	+++	+	+
External pressure	+	+++	+	+	+	++
Others(Lateral force)	/	/	/	/	+++	+++

* The number of "+" denotes the significance of specific load.

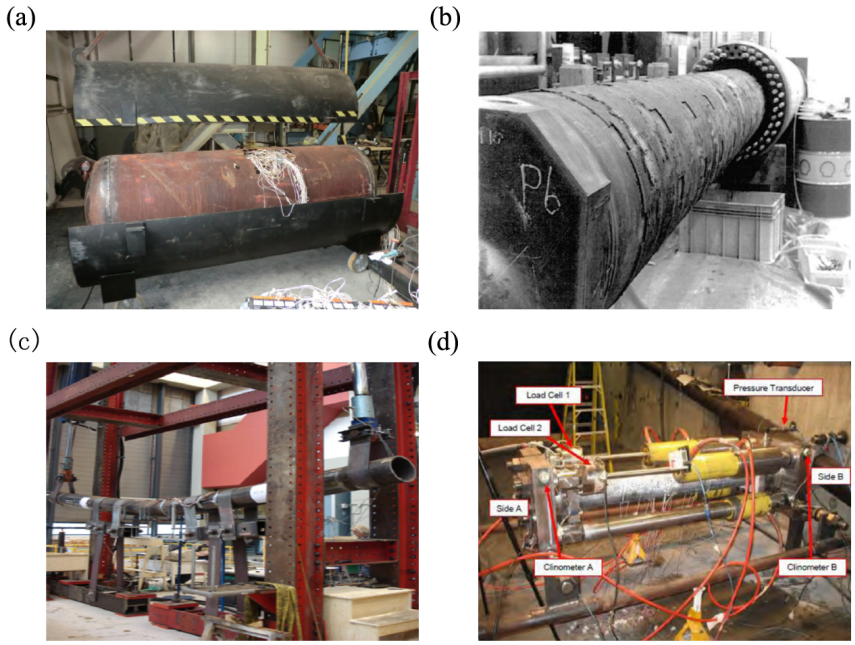

Figure 2.9: The typical test set-ups: (a) a set-up for bursting test [65]; (b) a set-up for pipe under external pressure [69]; (c) a four-point bending test set-up [74]; (d) a set-up for pure bending test [88].

Table 2.2: A summary of critical parameters in existing bursting tests.

S.N	Parameters	Domain
1	Outer diameter D(mm)	100-810
2	Wall thickness t(mm)	1-20
3	D/t	27-54
4	L/D	3-6.5
5	Materials	Steel,Al
6	Dent direction	Longitudinal, Hoop(rare)
7	d_d/D (%)	5-28
8	d_m(mm)	2-10
9	d_m/t (%)	9-70
10	l_m/D(%)	15-76
11	Failure location	Damaged region

2.5.1 Bursting test

The bursting capacity of pipes subjected to internal pressure has attracted considerable interest from researchers such as [21, 59, 82, 85, 90]. A brief summary of critical parameters from existing bursting tests can be seen in Table 2.2.

A typical bursting set-up of a pipe is shown in Figure 2.9(a). An end cap is introduced in order to fashion a space for pressurization in a pipe segment. A pressure meter is deployed to detect the bursting pressure, which is a critical factor in such a test. An alternative way to seal pipe segments is by using end flanges and flat rubber [85], which can eliminate the welding effect. But it is only suitable for pipes with a small diameter.

2.5.2 External pressure test

Buckling-induced failure can occur when pipelines are subject to external pressure. Considerable studies on such test such as [29, 51, 69, 96, 102] have been done on pipelines. A brief summary of critical parameters from existing tests under external pressure can be seen in Table 2.3. A typical set-up for pipe external pressure test can be seen in Figure 2.9(b). In this case, the pressure vessel was a cylindrical pressure chamber made of high-strength steel with large pressurization capacity. The test specimen was sealed at the ends with solid plugs. A volume-controlled strategy was deployed based on a high-power pump for pressurization. The pumping speed was quite slow to maintain a quasi-static loading procedure.

2.5.3 Bending test

A typical set-up to investigate the bending capacity of pipes is a four-point bending configuration, as illustrated in Figure 2.9(c). A brief summary of concerned parameters from existing bending tests can be seen in Table 2.4. In the set-up of a four-point bending test, a pure bending moment is provided in the central part of specimen between two vertical load (or support) points.

There are several points that should be highlighted in a successful four-point bending test. Firstly, the specimen length should be long enough in order to eliminate the end effect (both supports and loading points). For the central pipe segment under pure bending, the

minimal length should be at least 4D (D is the pipe outer diameter) according to existing literature [53, 74, 81, 95, 123]. The minimum length of bending arm is determined by both the loading capacity and the bending capacity of specimens. In addition, extra length for loading heads and support bases is required from a practical perspective. According to this review, the selection of entire specimen length for a pipe test is generally between 9D and 24D.

Table 2.3: A summary of critical parameters in existing tests under external pressure.

S.N	Parameters	Domain
1	Outer diameter D(mm)	30-510
2	Wall thickness t(mm)	0.9-24
3	D/t	18-45
4	L/D	20-30
5	Materials	Steel,Al
6	Dent direction	Longitudinal
7	d_d/D (%)	0.4-1.6
8	Dent ovalization δ(%)	0.04-24

Table 2.4: A summary of critical parameters in existing bending tests.

S.N	Parameters	Domain
1	Outer diameter D(mm)	168-559
2	Wall thickness t(mm)	6-24
3	D/t	20-45
4	L/D	9-24
5	Materials	Steel
6	δ_0(%)	0.078-0.3
6	d_m/t(%)	30-50
7	Prescribed internal pressure(MPa)	18-22
8	Failure location	Damaged region/section

The loading strategy is also important in bending test. Loads can either be exerted on the pipe end [74] or on the middle span [125], depending on the specific laboratory conditions. In order to avoid artificial pipe failure induced by a high concentration force, wide strips [53] are generally adopted for loading heads. In addition, the support bases should be carefully designed so that the pipe ovalization cannot be restricted. As shown by the tests from [71], ovalization could cause the maximum discrepancy of 1.59 times between the longitudinal compression strain on the pipe's top location and the tensile strain in the bottom location. The structure should be reinforced if the unconcerned regions are prone to fail in advance. For instance, extra sleeves were used on the side segments of pipes to avoid artificial failure [125]. Apart from the four-point bending set-up, other customized facilities can also be used, as illustrated in Figure 2.9(d).

Table 2.5: A summary of numerical models in existing research.

S.N	D(mm)	D/t	Material	Damage	Load (dominant load)	Mesh	Software
1 Levold et al. (2013)	168	26.5	X70	Metal loss	Combined bending, internal pressure & axial force(bending)	C3D8R (solid)	ABAQUS
2 Park et al.(1996)	31.8	18-33	Stainless steel	Dent	External pressure	S4R (shell)	ABAQUS
3 Vitali et al.(2005)	559	26.5, 34.2	X65	Intact	Combined bending, internal pressure & axial force(bending)	Shell	ABAQUS
4 Bartolini(2004)	813	39, 74	X65	Intact	Combined bending, & axial force	Solid	ABAQUS
5 Lee et al.(2015)	168.3	9.5	X42	Metal loss	Internal pressure	Solid	ANSYS
6 Vasilikis et al.(2015)	1068	65-120	X70, X60	Intact	Bending	S4R (Shell)	ABAQUS

2.6 Numerical methods for pipe strength evaluation

The numerical method is an alternative to an experimental method in pipe strength research. A brief summary of existing numerical research on metallic pipes is shown in Table 2.5. In this section, influential parameters in FEA related to pipelines such as mesh, material property, boundary conditions and initial imperfections are discussed. Details on how to introduce, simplify and simulate structural damage are presented.

2.6.1 General requirements in pipe simulation

Choosing a suitable software is important for numerical simulation on pipes. To investigate the ultimate strength of pipeline structures, a static solver generally suffices. In case the dynamic effect should be accounted for, an explicit solver that does not require matrix iterations is much better than the implicit static solver in order to obtain a reasonable result [24]. Newton-Raphson's iterative criterion is generally deployed for strength investigation. A disadvantage of the traditional Newton method is that the load-displacement path beyond a limit point cannot be well traced once the limit solution has been reached. In order to make up for such a limitation, Riks [110, 111] proposed an updated arc length method, which can easily capture the post-buckling behaviors of a structure.

2.6.2 Mesh

Mesh is a key factor during numerical research of pipes. It includes the selection of element type and the selection of mesh density.

The selection of element type strongly depends on the investigated problems. For instances, the deployed element type is normally a shell element such as S4R and S8R in Abaqus [1], or Shell181 and Shell93 in Ansys [57] for the investigation of intact pipes. In contrast, for damaged pipes with a surface crack or metal loss, solid elements such as C3D8R (an eight-node linear brick element), C3D10R (a ten-node quadratic tetrahedron element), or C3D20R can be also selected in order to capture detailed structure behaviors and

crack front features. Generally speaking, the solid element can provide a better prediction than a shell element, but it will be more time-consuming.

The element integration rule, which affects the accuracy of output results, should be selected carefully. For instance, the reduced integration rule can not only reduce simulation time, but also avoids the self-locking effect. However, it is prone to be affected by hourglass phenomenon, which largely reduces the accuracy of simulation. A practical technique to detect the severity of hourglass during simulation is to check the hourglass energy, which should be less than 5 percent of the system internal energy [47]. Another aspect involved in the element type selection is the order of the element. A high-order element can provide a better stress and strain prediction, but results in more simulation time.

For a pipe with a dent or metal loss on its surface, the mesh density should be largely refined so that the artificial local bending stress and stress concentration will not be introduced. The shape of a dent or metal loss should therefore be accurately modeled. A quantitative criterion for determining mesh size is to employ the critical half-wave length λ_{cl}, as seen in Equation (2.16), where R is the pipe radius and t is the pipe wall thickness. It is related to the buckling of a cylindrical shell [107, 115]. The mesh size deployed in the interested areas should be less than the critical half-wave length, for example, 3-6 elements within one half-wave length [47]. An alternative approach to determine mesh density is to carry out a mesh sensitivity study. When reducing the mesh size to half scale, the variation of concerned structure response is less than 1 percent. Under this situation, the mesh density could therefore be considered good enough for numerical research of the pipe strength.

$$\lambda_{cl} = 1.728\sqrt{Rt} \tag{2.16}$$

For a pipe with a crack on its surface, the mesh should be carefully arranged. Crack characteristics such as tip singularity should be expressed through special mesh strategies. However, in the study of pipe ultimate strength accounting for crack singularity, more simulation time is required and numerical convergence is more difficult. A practical method to realize crack tip singularity is the collapse technique, which has been integrated into simulation software such as Abaqus and Ansys. Based on this method, all the side nodes of the crack tip elements collapse into a single node, as illustrated in Figure 2.10. Point A is the crack tip, while element E is the special collapsed element with six nodes. According to this method, element E is formed by an eight-node quadrilateral shell element, as illustrated in Figure 2.10(c). This method is deployed in the research of [54] and [124]. In order to introduce a crack during numerical simulation, both a solid element and a shell element can be used [124]. Mesh density around the cracked tip is important and should be refined. It has been demonstrated that four layers of elements at the crack tip region, as illustrated in Figure 2.10 (a), are capable of capturing the main crack characteristics.

2.6.3 Material properties

The material property is another key factor during numerical research. Three typical material models, including the linear elastic model, the elastic-perfectly plastic model and the elastic-plastic model, are deployed in numerical research. The elastic-perfectly plastic model can provide a conservative prediction, as shown in the numerical research of [100]. However, a convergence problem is easily produced by using this model from a practice

point of view. A method to conquer this drawback, according to experience, is to deploy the elastic-plastic model accounting for material hardening.

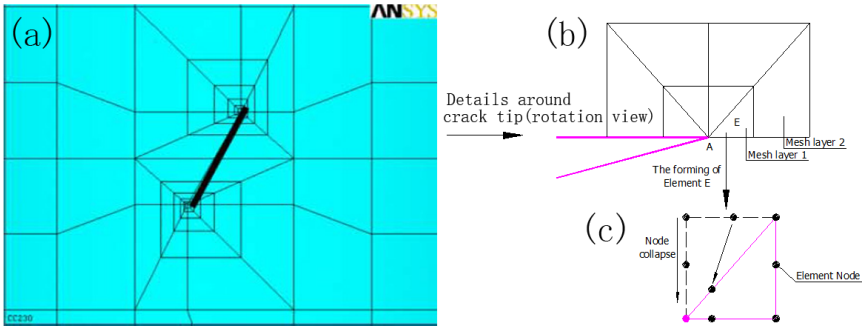

Figure 2.10: The mesh strategy accounting for crack tip singularity [124]:(a) FE mesh; (b) mesh details around crack tip; (c) element collapse.

Approximate empirical equations based on basic material inputs are usually deployed for material stress-strain curve. A typical example is the formulation from Ramberg and Osgood [108], as seen in Equation (2.17) with 0.002 plastic strain at yield point. Nevertheless, it is not accurate enough to denote the stress-strain relation after the occurrence of material necking. Due to the stress triaxiality in the necking zone [129], the engineering stress cannot be accurately calculated by the original cross-section of material samples. Accordingly, corrections are needed. For instance, Pakiding [101] deployed a parabolic relation to express the relation of a metallic material. Based on the transformation of Equations (2.18) and (2.19), the true stress and strain can then be obtained, which can be directly used for FEA.

$$\varepsilon_{eng} = \sigma_{eng}/E + 0.002(\sigma_{eng}/\sigma_y)^n \tag{2.17}$$

$$\sigma_{true} = \sigma_{eng}(1+\varepsilon_{eng}) \tag{2.18}$$

$$\varepsilon_{true} = ln(1+\varepsilon_{eng}) \tag{2.19}$$

In spite of the commonly used isotropic feature in the material of metallic pipes, anisotropy is sometimes very prominent due to manufacture methods. For instance, the UOE manufacture method induces the " Bauschinger effect" on pipes, which produces an unequal yield stress when material is under two different scenarios: compression and tenstion [29, 69, 125, 126]. As Bruschi et al. [29] pointed out: "the bending capacity of pipelines could be reduced by 16% when the compression yield stress of material in the hoop direction reduced to 85% of the longitudinal yield stress during simulation". For seamless pipe without a seam or weld, the anisotropy is not as obvious as the one with welding. Generally, the Hill48 yield criterion [75] is deployed to account for such anisotropy characteristic in numerical research.

2.6.4 Boundary conditions

Boundary conditions largely affect the accuracy of numerical research. A basic criterion for the selection of boundary conditions in numerical simulations is that any simplification or idealization should conform to the real situations. Therefore, a trade-off between calculation accuracy and calculation time must be accounted for.

For metallic pipes subjected to internal or external pressure, extra pipe segments are often introduced to make sure that the boundary is far enough from the concerned pipe segments. With this regard, the effect of boundary condition will be neglected. When the studied pipes have no structural damage, symmetric boundary condition such as half model or one quarter of the model can be used. However, such boundary conditions should be carefully deployed for damaged pipes. It is because that the failure patterns may be affected as well.

When pipes are subjected to a pure bending moment, whether or not to constrain the ovalization of pipe ends is a critical point. The reason is that such boundaries affect the stress distributions and failure modes of pipes. There are two ways to set a free ovalization boundary at the pipe ends in numerical simulations. One is by introducing an extra sliding plane near the pipe end. By forcing the pipe ends to contact with the sliding plane, a local boundary restriction is formed and, therefore, the radial motion is set to free [71]. However, because of the contact analysis, the entire model calculation time increases greatly. A simple alternative is to use a kinematic coupling constraint for all the nodes at pipe end, which can easily release the radial motion. In that case, the calculation time is largely saved with a good accuracy. In case it is difficult to define boundary conditions, a sensitivity study could be carried out so that the insignificant degrees of freedom can be excluded and a suitable boundary condition will be then selected.

2.6.5 Initial imperfections

Initial imperfection of pipe structures needs to be considered in a numerical research. The initial imperfection is generally introduced during the pipe manufacture process, which typically has an oval, lobed shape or wave-type [17, 123]. The effect of an initial imperfection largely depends on the exertion of dominant loads on pipes. For instance, the effect is insignificant for pipes subjected to pure bending since the disturbances of loading and asymmetrical deformation are large enough to cause structure failure. In contrast, for pipes under uni-axial force, the initial imperfection could reduce pipe buckling strength by as much as 50 percent [115]. In numerical simulation, there are basically two ways to introduce initial imperfections. One is to deploy a single or a combined structure eigenvalue modes and the other is to deploy the measurement geometrical data from tests.

2.7 Empirical models for pipe strength evaluation

Section 2.1 has explained the classical theory of pipe ultimate strength. However, the classical theory generally overestimates the capacity of metallic pipes. For instance, the real buckling strength of thin-walled pipes under uniaxial compression is considerably smaller than theoretical predictions [121]. Accordingly, researchers developed a number of empirical or semi-empirical equations for the supplement of strength predictions based on existing theory, experiments and numerical simulations. In this section, empirical solutions on metallic pipes are summarized and discussed.

2.7.1 Pipes under external pressure

When pipes are subjected to external pressure, buckling failure is the dominant failure pattern. Two solutions of the pipe buckling pressure based on theory are first listed in Equations (2.20) and (2.21), where P_{ee} is the elastic buckling pressure, and P_{ye} is the yield pressure of pipes.

$$P_{ee} = \frac{2E}{(1-\nu^2)}(\frac{t}{D})^3 \tag{2.20}$$

$$P_{ye} = \frac{2\sigma_y t}{D} \tag{2.21}$$

Accounting for the effect of initial imperfection, Timoshenko and Gere [121] proposed a linear relationship (Equation (2.22)) to predict the buckling capacity of pipes (P_{ce}) accounting for the initial ovalization of pipe cross-section (δ_0). Both elastic buckling pressure (P_{ee}) and yield pressure (P_{ye}) were integrated together. Meanwhile, a modification equation was deployed by some rules [30, 48], as seen in Equation (2.23). As demonstrated by the research from [69], Eqution (2.23) can provide a better prediction to the collapse pressure of metallic pipes.

$$(P_{ce}-P_{ee})(P_{ce}-P_{ye}) = P_{ce}P_{ee}(\frac{3\delta_0 D}{t}) \tag{2.22}$$

$$(P_{ce}-P_{ee})(P_{ce}^2-P_{ye}^2) = P_{ce}P_{ee}P_{ye}(\frac{2\delta_0 D}{t}) \tag{2.23}$$

For a pipe with metal loss, Equation (2.24) is deployed by [14, 16] to predict the collapse pressure. It should be noted that only the depth of metal loss (d_m) is accounted for in this equation, where R_a is the average pipe radius, P_{ee} is the elastic buckling pressure calculated from Equation (2.20), h is the pipe wall thickness subtracting the depth of metal loss d_m, δ_{max} is the maximum ovalization of pipe cross-section.

$$(P_{ce})^2 - (\frac{\sigma_y h}{R_a} + (1+\frac{6\delta_{max}}{h})P_{ee})P_{ce} + \frac{\sigma_y h}{R_a}P_{ee} = 0 \tag{2.24}$$

2.7.2 Bursting capacity of pipes

Bursting capacity is a critical feature of metallic pipes subjected to internal pressure. Equations (2.25) and (2.26) denote the analytical solutions of hoop membrane stress (σ_θ) and longitudinal stress (σ_l) respectively, when pipes are subjected to internal pressure (p_i) [122]. They demonstrate that the failure of an intact pipe will first initiate in its longitudinal direction.

$$\sigma_\theta = \frac{p_i D}{2t} \tag{2.25}$$

$$\sigma_l = \frac{p_i D}{4t} \tag{2.26}$$

For a dented metallic pipe, Orynyak et al. [99] developed a simple equation to predict the bursting strength with respect to dimensionless length of dent ($\lambda_d = l_d/\sqrt{Rt}$). However, only a single dimension of dent was taken into account. The dent is assumed to be infinite in pipe longitudinal direction. The equation is shown as follows:

$$p_b = \frac{\sigma_u t}{R_a}(\sqrt{\lambda_d^4 + 1} - \lambda_d^2) \tag{2.27}$$

For the metallic pipe with metal loss, there are considerable number of empirical equations to denote its bursting capacity. Kiefner [80] and Lancaster and Palmer [85] deployed Equation (2.28) to calculate the bursting capacity of pipes. In this equation, the metal loss depth (d_m) and axial length (l_m) are taken into account. $\bar{\sigma}$ is the flow stress of the material that generally lies between the material yield stress and the ultimate tensile stress, M_f is the bulging parameter relating to axial length (w_m) of metal loss. In addition, Equation (2.29) is another widely deployed expression for bursting capacity of damaged pipes [26, 31, 45], where Q is the correction factor based on the length of metal loss in pipe longitudinal direction, which can be expressed as $Q = \sqrt{1 + 0.31(\frac{w_m}{\sqrt{Dt}})^2}$.

$$\sigma_{cb} = \bar{\sigma}\frac{1 - d_m/t}{1 - d_m/(M_f t)} \tag{2.28}$$

$$P_b = \frac{2t}{(D-t)}\sigma_u \frac{1 - d_m/t}{1 - d_m/(tQ)} \tag{2.29}$$

2.7.3 Bending capacity of pipes

When pipes are subjected to a bending moment, the empirical equation such as Equation (2.30) is generally deployed to express the ultimate strength of pipes, taking into account different influential parameters in engineering practice.

$$M_c = M_y(c_{11} - c_{22}\frac{D}{t}) \tag{2.30}$$

Where M_y is the plastic bending moment of pipe, c_{11} and c_{22} are correction coefficients that were proposed through tests. Such coefficients varied a little bit within different research. For instance, c_{11} and c_{22} are 1.05 and 0.0015, respectively, from the research of [13]. But in the British standard [30], the adopted values are 1 and 0.0024, respectively.

When there is a dent on the pipe surface, the effect of the dent should be considered from the strength of an intact metallic pipe (M_c). The influential term of a dent can be simply expressed as $F(\eta_c\theta_d)$ [13], where θ_d is the dent angle on pipe surface, and η_c is a correction factor based on dent locations and safety class, etc. For the cracked pipe, fracture failure could occur when the crack is on the tensile side of pipes. With the stable growth of crack on metallic pipes, "leak-before break" phenomenon may happen [105]. When metal loss is introduced, an effective thickness $f(w_m/\sqrt{Rt})t$ was generally used to correct the so called "neighbor response" caused by finite width (w_m) in pipe longitudinal direction [14, 130].

2.7.4 Pipes under uniaxial loading

For metallic pipes subjected to uniaxial compression, either elastic buckling or elastic-plastic strength failure can happen. When pipes are subjected to a pure tensile load, the pipe wall will become thinning until the material yielding has reached. For these two load conditions, the maximum axial force can be calculated using Equation (2.31). For damaged pipes, no specific research on empirical solutions was found, although a considerable amount of numerical research has focused on this subject.

$$T_{ya} = \pi D \sigma_y \tag{2.31}$$

2.7.5 Pipes under combined loading

When metallic pipes are subjected to combined loading, interactive behaviors between each force (or corresponding stress) exist. Bai et al. [15] proposed a bending moment (M) - tension (T) interaction relation, as expressed in Equation (2.32). The applicable domain of pipe D/t ratio is between 10 and 40. Where M_c and T_c are the ultimate bending moment and ultimate tension force subjected to respective load.

$$(\frac{M}{M_c})^2 + (\frac{T}{T_c})^{2.4} = 1.0 \tag{2.32}$$

For metallic pipes subjected to combined loads including axial force, bending moment, internal and external pressure, Equation (2.33) is deployed for design purpose based on the load-controlled condition [48]. The exerted forces (M,T) should satisfy this criterion at all pipe cross-sections, which is applicable for D/t between 15 and 45, where a_{11}, a_{22} and a_{33} are correction parameters according to numerical simulations and tests, M_y, T_{ya} and P_b are the plastic bending moment, plastic axial force and bursting pressure of pipes under respective load, p_i and p_e are the internal pressure and the external pressure, respectively.

$$(a_{11}\frac{M}{M_y} + (a_{22}\frac{T}{T_{ya}})^2)^2 + (a_{33}\frac{p_i - p_e}{P_b})^2 \leq 1 \tag{2.33}$$

A similar equation (Equation (2.34)) in terms of pipe longitudinal and hoop stress is deployed in [12] to denote the strength of metallic pipes subjected to combined loading.

$$(\frac{\sigma_l}{\sigma_{long}})^2 + (\frac{\sigma_\theta}{\sigma_h})^2 - 2a_{44}\frac{\sigma_l\sigma_\theta}{\sigma_{long}\sigma_h} = 1.0 \tag{2.34}$$

Where σ_{long} and σ_h are the ultimate stress of metallic pipe in their respective directions, a_{44} is correction factor depending on specific conditions such as compression or tensile.

2.8 Conclusions

This chapter has reviewed the literature on the research of ultimate strength and residual ultimate strength of metallic pipelines. The key questions on the influential parameters of pipe strength and their relevant effects are initially clarified. Three typical structural damage and their combinations thereof induced by mechanical interference are identified. Furthermore, research methods on pipe residual strength in terms of experimental tests, numerical simulations and empirical predictions are summarized and discussed. Based on the research in this chapter, conclusions are drawn as follows:

(1) Empirical predictions on metallic pipelines with a dent is rare, especially for the pipes subjected to a bending moment. Specific damage parameters such as dent depth, angle, shape and length should be taken into account. Numerical simulations and experiments are required in order to propose empirical formulas. Quantification of the dent effect will be conducted in Chapters 3 and 4.

(2) For metal loss on the pipe surface, its length in the pipe longitudinal direction (w_m) is generally ignored in both theoretical derivation and empirical predictions. Not many studies have been found on the residual strength of pipes under a bending moment. Numerical simulations or experiments are needed to take into account such effect and hence to further quantify the effect of metal loss on pipes under a bending moment. Quantification of the metal loss effect will be conducted in Chapter 5.

(3) It is widely accepted that the combined damage is more detrimental than single damage. However, the strength investigation of combined damage on pipes has not been found. Therefore, studies are also required in order to identify its effect. Relevant research has been carried out in Chapter 6.

(4) Fracture failure is a critical issue and probably happens on metallic pipelines under a bending. In spite of the difficulties in the study of residual strength accounting for crack, the interactions between fracture and residual strength are still necessary. Fracture mechanism should be taken into account during the research of residual strength on metallic pipes. Relevant research and case studies will be carried out in Chapter 6.

(5) For residual strength research of metallic pipelines, the investigations on damaged pipes subjected to dynamic loads and their relevant structural behavior are rare. The impact effect from mechanical interference, such as the residual stress and the variation of material properties, has not been accounted for in the vast majority of research. The ultimate strength may be also affected due to such factors. The effect of residual stress is carried out in Chapter 6.

In the following chapters of this thesis, the quantification of each type of structural damage on metallic pipes (both onshore and offshore) under bending is primarily studied. The major cause of structural damage is considered from mechanical interference so that corresponding simplifications and assumptions of damage are made in the following studies. In the following Chapter 3, each type of structural damage as mentioned in this chapter is produced in laboratory, and experimental tests on residual strength are designed and carried out.

Chapter 3

Experimental investigation of residual strength of damaged metallic pipelines*

As discussed in Chapter 2, there is still a lack of quantification of the residual ultimate strength of damaged metallic pipes subjected to a bending moment. Therefore, a pipe strength test accounting for structural damage has been designed. The test results will be discussed in this chapter to enhance the understanding of the strength of the damaged pipes and the corresponding structural behaviors, as well as to aid the validation of numerical models and the proposal of prediction equations in the following chapters.

Section 3.1 provides an overview of the pipe tests including pipe specimens, test set-ups and damage introduce. Material properties of pipes are obtained from tensile tests, which are discussed in Section 3.2. In Section 3.3, the measurement approaches of test parameters are presented. In addition, preliminary measurement results are given and discussed. The correction methods of measured bending arm and curvature are described in Section 3.4. The results of four-point bending tests are summarized in Section 3.5. Comparison between the results from intact pipes and analytical solutions are also conducted. Section 3.6 deals with the analysis of the effects of structural damage based on test results, while Section 3.7 discusses the experimental errors due to design and laboratory conditions. Conclusions of this chapter are drawn in Section 3.8.

3.1 Outline of test

The aim of the test is to investigate the residual ultimate strength of seamless metallic pipes with artificial damage under a pure bending. Structural damage normally occurs after mechanical interference is properly produced on the surface of pipes. As a joint project for pipe

*This chapter is based on the paper Jie Cai, Xiaoli Jiang, Gabriel Lodewijks, Zhiyong Pei, and Ling Zhu. Experimental investigation of residual ultimate strength of damaged metallic pipelines (accepted). Journal of Offshore Mechanicis and Arctic engineering. 2017 [40].

residual strength, all the experiments were carried out in the Structural Engineering Laboratory and Impact Laboratory, School of Transportation, Wuhan University of Technology, P.R. China. In this section, overview of specimens from the test is provided in Section 3.1.1. The description of the four-point bending set-up and its relevant accessories are presented in Section 3.1.2. The produced structural damage and its rigs are described in Section 3.1.3.

Table 3.1: The principal dimension of specimens in four-point bending test.

Parameters	Value
Full length of specimen (L) (mm)	2200
Half length under pure bending ($L1$) (mm)	400
Length of loading\support strip ($L2\backslash\ L4$) (mm)	100
Original bending arm ($L3$) (mm)	300
Side length ($L5$) (mm)	200
Specimen type	Seamless (hot-rolled)
Specimen material	Q345B [61]
Nominal diameter	168.3 (mm)
Nominal thickness	8.0 (mm)

3.1.1 Test specimens

The entire test project consists of 39 successfully conducted seamless metallic specimens with nominal diameter-to-thickness ratio (D/t) of 21.04, as shown in Figure 3.1. All specimens have a nominal diameter D of 168.3 mm, and a length of 2200 mm. The real diameter-to-thickness ratios (D/t) of specimens varied from 20.41 to 23.75 due to manufacture deviation. Relevant principal dimensions of the specimens based on the design of the bending test are listed in Table 3.1, detailed description of the bending test configuration is presented in Section 3.1.2.

Among all these completed specimens, four specimens were intact with no structural damage, whereas thirty-five were damaged specimens with different types of structural damage. Among the damaged ones, there were seven specimens with a dent introduced by quasi-static indentation, four specimens with a dent introduced by impact, five specimens with metal loss introduced by machining method, fourteen specimens with surface crack introduced by either machining or laser methods, another five specimens with combined damage. The structural damage was introduced properly on each specimen before the strength test, locating on either its compression side or on its tensile side. The cetner of damage locates at the mid-span of each specimen. All the specimens were acquired through the same production batch from the same provider at the same time, which makes sure that every specimen has a similar material property. Each specimen was cut from an original pipe product with an overall length of 12 m in the structural laboratory.

An overview of the intact specimens without structural damage is shown in Table 3.2, while an overview of the damaged specimens is shown in Tables 3.3 to 3.6. For clarity reason, specimens were named and divided in different groups as follows: The intact specimens were put into the first group, naming from S1N1 to S1N4. The series number of specimens

(S.N.) with a dent from quasi-static indentation was from S2N1 to S2N7, while specimens with impact induced dent damage were from S2N8 to S2N11 in the second group. The third group consisted of specimens with metal loss, while the specimens with a single crack were put into the fourth group. Besides, the fifth group contained specimens with combined damage. Before the introduction of structural damage, every intact specimen was visually inspected for the integrity checking.

Table 3.2: Overview of intact specimens (Dimension unit: mm).

S.N.	D	t	D/t	M_{cr}[1] (kNm)	κ_{cr}[2] (1/m)
S1N1	168.09	7.90	21.28	104.37	0.422
S1N2	167.36	7.87	21.27	103.65	0.439
S1N3	167.55	7.92	21.16	103.21	0.441
S1N4	167.01	7.84	21.30	102.71	0.401

[1] M_{cr} denotes the bending capacity of specimen, the same in the following tables.
[2] κ_{cr} denotes the global curvature measured from test, the same in the following tables.

Figure 3.1: A photo of seamless pipe specimens in the test.

Table 3.3: Overview of specimens with dent damage (Dimension unit: mm; Angle unit: degree).

S.N.	D	t	D/t	Dent ($l_d \times w_d \times d_d$)	Dent angle	Location (kNm)	M_{cr}	κ_{cr} (1/m)
S2N1	169.21	8.25	20.51	$89 \times 68 \times 10.3$	90	C	92.57	0.154
S2N2	168.23	8.13	20.69	$100 \times 75 \times 10.3$	90	C	93.55	0.109
S2N3	169.38	7.90	21.44	$130 \times 60 \times 10.3$	45	C	91.65	0.158
S2N4	169.26	7.42	22.81	$150 \times 30 \times 10.3$	0	C	91.36	0.154
S2N5	168.74	8.15	20.70	$110 \times 85 \times 10.3$	90	C	90.97	0.164
S2N6	169.31	7.39	22.91	$80 \times 60 \times 10.3$	90	C	92.58	0.139
S2N7	168.52	7.66	22.00	$95 \times 60 \times 10.3$	90	T	102.34	0.458
S2N8	167.19	7.57	22.09	$43 \times 40 \times 10$	90	C	94.11	0.325
S2N9	168.54	7.80	21.61	$60 \times 40 \times 8$	90	C	95.96	0.260
S2N10	168.25	7.37	22.83	$60 \times 80 \times 9.6$	90	C	95.88	0.187
S2N11	168.42	7.50	22.46	$60 \times 40 \times 12$	90	C	92.03	0.211

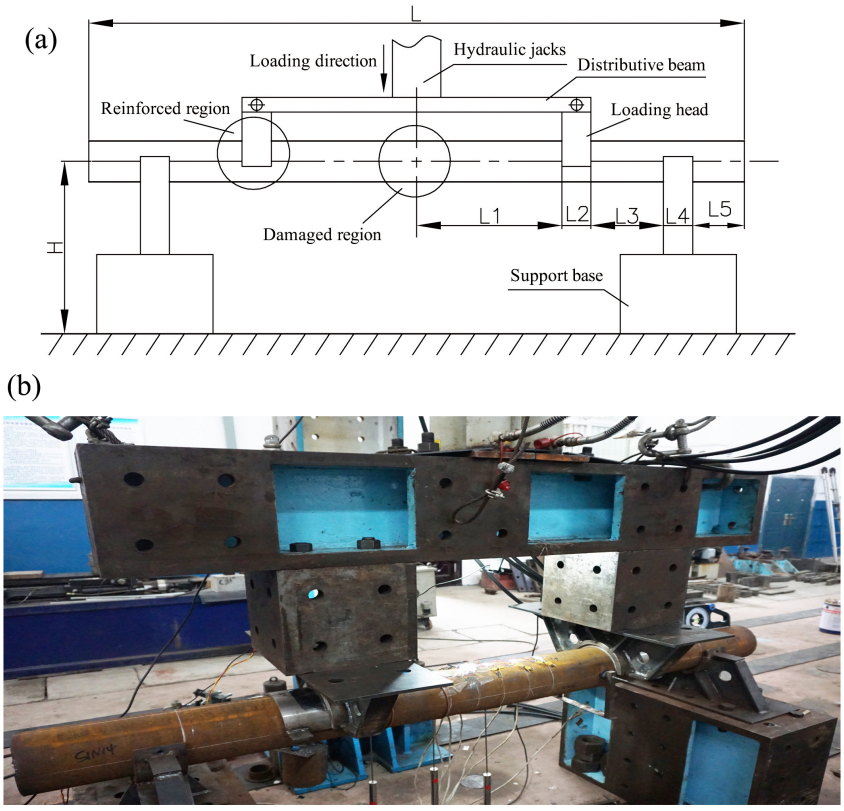

Figure 3.2: Configuration of four-point bending test: (a) the design of bending test set-up; (b) the real test set-up in the laboratory.

Table 3.4: Overview of specimens with metal loss damage (Dimension unit: mm; Angle unit: degree).

S.N.	D	t	D/t	Notch ($l_m \times w_m \times d_m$)	Notch angle	Location	M_{cr} (kNm)	κ_{cr} (1/m)
S3N1	167.03	7.40	22.57	$44 \times 10 \times 3$	90	C	106.34	0.327
S3N2	167.31	7.54	22.19	$45 \times 10 \times 3$	90	C	95.10	0.412
S3N3	166.89	7.90	21.13	$45 \times 10 \times 3$	90	C	92.89	0.268
S3N4	168.30	7.90	21.30	$45 \times 10 \times 3$	90	T	100.00	0.393
S3N5	167.96	8.23	20.41	$45 \times 10 \times 3$	90	T	105.96	0.321

Table 3.5: Overview of specimens with crack damage (Dimension unit: mm; Angle unit: degree; Damage size: $l_c \times w_c \times d_c$).

S.N.	D	t	D/t	Crack	Angle	Location	M_{cr} (kNm)	κ_{cr} (1/m)
S4N1	167.01	7.10	23.52	$10 \times 0.5 \times 0.70$	90	T	107.76	0.691
S4N2	168.42	7.58	22.22	$10.5 \times 0.52 \times 0.75$	90	T	104.65	0.785
S4N3	167.70	7.30	22.97	$10.5 \times 0.54 \times 0.70$	90	C	100.34	0.259
S4N4	168.08	8.23	20.42	$10.5 \times 0.5 \times 0.70$	0	C	116.29	0.219
S4N5	167.80	8.08	20.77	$10.5 \times 0.5 \times 0.70$	0	T	106.09	0.698
S4N6	168.19	8.03	20.95	$10.5 \times 0.5 \times 0.70$	0	T	109.55	0.332
S4N7	168.3	7.50	22.44	$10.00 \times 0.35 \times 2.10$	90	T	108.60	0.729
S4N8	168.20	7.66	21.96	$10.00 \times 0.22 \times 2.50$	90	T	100.69	0.717
S4N9	168.38	7.09	23.75	$10.00 \times 0.31 \times 3.00$	90	T	101.89	0.714
S4N10	168.69	7.34	22.98	$10.00 \times 0.40 \times 3.00$	90	T	104.16	0.617
S4N11	168.18	7.60	22.13	$10.00 \times 0.40 \times 2.50$	90	C	101.38	0.227
S4N12	168.35	7.24	23.25	$20.00 \times 0.50 \times 2.20$	0	T	104.63	0.740
S4N13	168.24	7.43	22.64	$22.00 \times 0.25 \times 3.40$	0	C	96.38	0.250
S4N14	168.55	7.22	23.34	$20.00 \times 0.35 \times 1.50$	0	C	100.45	0.403

Table 3.6: Overview of specimens with combined damage (Dimension unit: mm; Damage size: $l_{(i)} \times w_{(i)} \times d_{(i)}$).

S.N.	D	t	D/t	Crack	Dent	Notch	Location	M_{cr} (kNm)	κ_{cr} (1/m)
S5N1	168.25	8.33	20.20	$44 \times 0.31 \times 0.70$	$110 \times 80 \times 10$	$44 \times 9.5 \times 3.0$	C	97.17	0.163
S5N2	168.80	7.60	22.21	$44 \times 0.31 \times 0.70$	$110 \times 80 \times 10$	$44 \times 10 \times 3.0$	C	85.72	0.153
S5N3	167.65	7.38	22.72	$45 \times 0.50 \times 0.70$	-	$45 \times 9.5 \times 3.0$	T	87.68	0.170
S5N4	167.37	7.15	23.41	$45 \times 0.53 \times 0.70$	-	$45 \times 10 \times 3.0$	T	85.98	0.224
S5N5	169.52	7.72	21.96	$37.5 \times 0.28 \times 0.70$	$78 \times 96 \times 8.5$	$44 \times 9.5 \times 3.5$	T	90.38	0.300

3.1.2 Four-point bending test

To determine bending capacity, the specimens were loaded in a four-point bending way. An overview of the test set-up is shown in Figure 3.2, while Table 3.1 lists the principal dimension of specimens. Boundary conditions have a strong effect on the accuracy of bending capacity and the distribution of stresses in a bending test. In this test, the design of boundary is to mimic the simply-supported boundary so that a pure bending can be accurately obtained. Hence, the translations of vertical and lateral direction have been fully constrained through loading heads and supports (Figure 3.3), whereas the axial translation was partially restrained through the friction force between the supports and the specimens. The support bases were fully fixed on the ground. The test set-up has been designed to deliver the maximum force of 1200 *kN* through a distributive beam and hydraulic jacks. Therefore, sufficient loads can be guaranteed in order to collapse specimens. Four hydraulic jacks were fixed at the center of distributive beam (Figure 3.4) so that a symmetrical loading pattern was introduced, having a force capacity of 300 *kN* and a stroke of 300 *mm* for each. The dead weight of the distributive beam was 1.0 *t*, which has been accounted for during bending moment calculation. A load-controlled strategy was deployed in the bending test. Specimens were loaded in fixed intervals in a consecutive way. During each loading interval, test situation was carefully inspected and extra data were recorded.

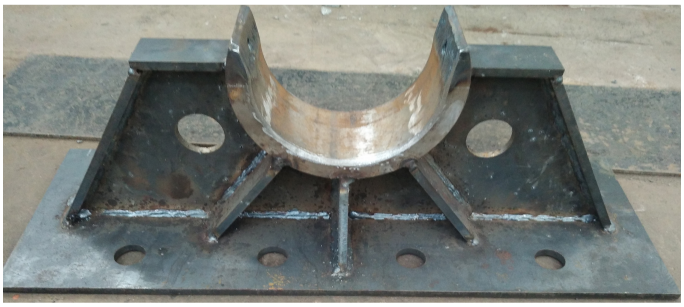

(Support of bending set-up)

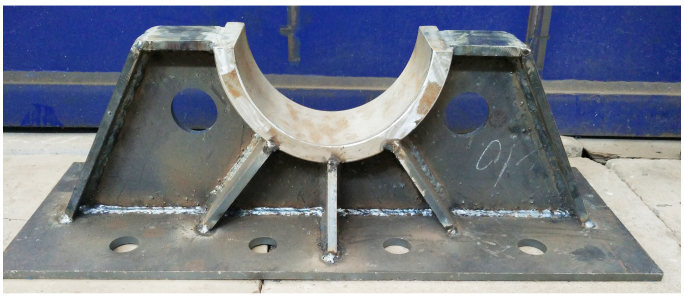

(Loading head of bending set-up)

Figure 3.3: Front view of the support and loading head of bending test set-up.

The configuration of pipe specimens was carefully designed. For instance, the overall length (L) was set to 2200 *mm* ($L/D = 13.07$), while the length under pure bending was designed to 800 *mm* ($L_0/D = 4.75$). There are practical reasons for such design: according to the literature review [34] in Chapter 2 on existing bending test of intact pipes, a widely selection of overall length-to-diameter ratio of pipes is between 9-24. Considering the specific laboratory condition and the sufficient space for the test operation, therefore, a medium length ratio within this range was selected. Meanwhile, the minimum length of specimen under pure bending should be no less than four times of its outer diameter. In this way, the effect of loading head on pure bending would be effectively reduced. Reinforcements were also introduced so that local deformation and artificial failure of specimens can be avoided due to loading. A half-sleeve with a length of 200 *mm* and a thickness of 20 *mm* was therefore designed, as shown in Figure 3.5 (a). Extra heat-treatment was used on the half-sleeve in order to increase its hardness. However, load deformation of the sleeve was unavoidable (see Figure 3.5 (b)) so that it has been replaced by a new one every three or four times of strength test.

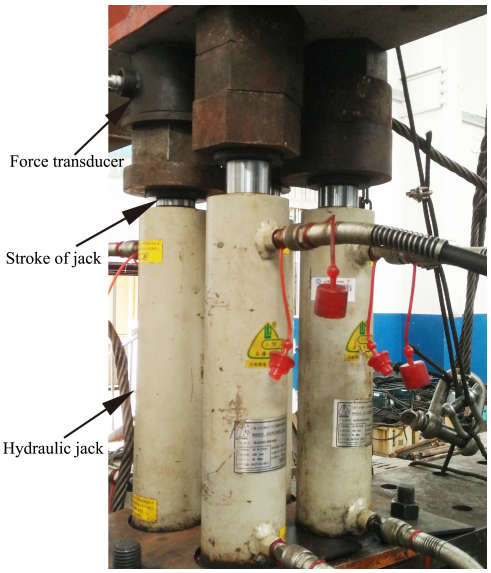

Figure 3.4: Hydraulic jacks used for loading, fixed at the center of distributive beam.

In such a four-point bending test, the friction force between specimen and its supports and loading heads played an important role. During loading, an equivalent axial compression force (P_{11}) through loading heads has been introduced with the increase of the rotational angle of the specimen, as seen in Figure 3.6. Under a certain range, the axial force was small and can be counterbalanced by a friction force. As a result, the structure stays stable. The friction force helped to maintain such stability to some extent. However, when the rotational angle of specimen was sufficient large, such structural stability cannot be maintained by friction any more. As a consequence, a sudden sliding of a specimen appeared which indicated that boundary condition and force arm have been changed significantly. Hence, this phenomenon in the four-point bending test was used as the sign of test termination.

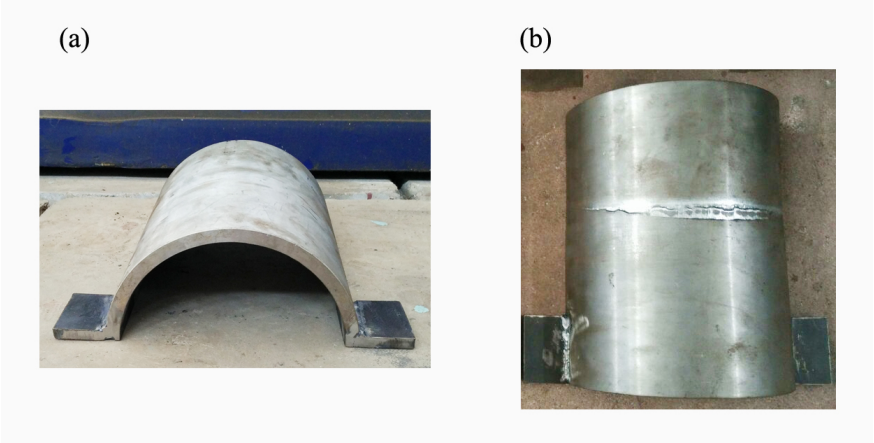

Figure 3.5: Photos of half sleeves used for reinforcement in bending test: (a) front view of intact sleeve; (b) vertical view of deformed sleeve.

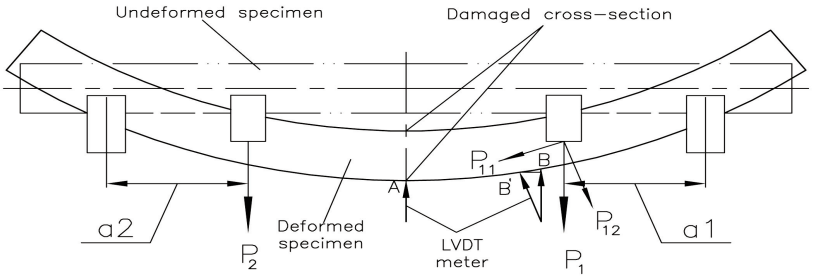

(Sketch of deformed pipe)

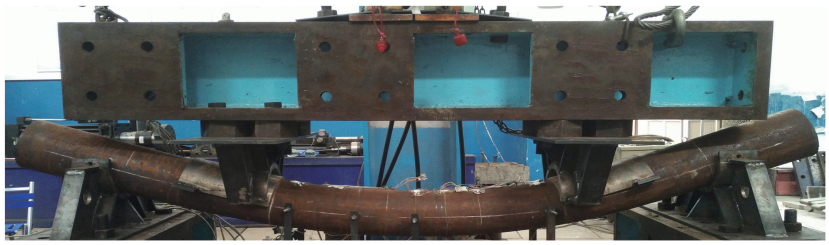

(Deformed specimen in test)

Figure 3.6: Scheme of deformed specimen in four-point bending test.

3.1.3 Production of structural damage

In order to introduce proper structural damage on specimens, different methods were deployed. A dent was produced through indentation by a customized indentor, while the metal

loss in terms of a notch was produced by mechanical machining method. The laser cutting technique was used to introduce a proper surface crack with a deep depth. For the combined damage, the introduction sequence of each single damage was crucial. Otherwise, the original size and shape of damage would be readily changed. In this test, a notch has been firstly fabricated, then a crack was produced at the notch tip, and a dent was introduced in the final step from indentation. A customized indentor with a bulge which matched the notch shape has been also fabricated to produce the dent for combined damage.

Each damage was denoted by its length ($l_{(i)}$), width ($w_{(i)}$), depth ($d_{(i)}$) and rotation angle ($\theta_{(i)}$), as illustrated in Figures 3.7, and 3.8, where i denotes the damage type, varying with different types by d, m and c, respectively. The rotational angle of damage was defined as the angle between damage length and the axis of specimen. The depth of dent is the depth between the lowest point of a dent in radial direction and the original pipe surface before deformation. It should be noted that Figure 3.8 only contains the schema of dent parameters for clarity reason. Furthermore, the structural damage was intentionally introduced at the center of each specimen, either on the compression side (C) or on the tensile side (T) of the specimen (under a bending moment).

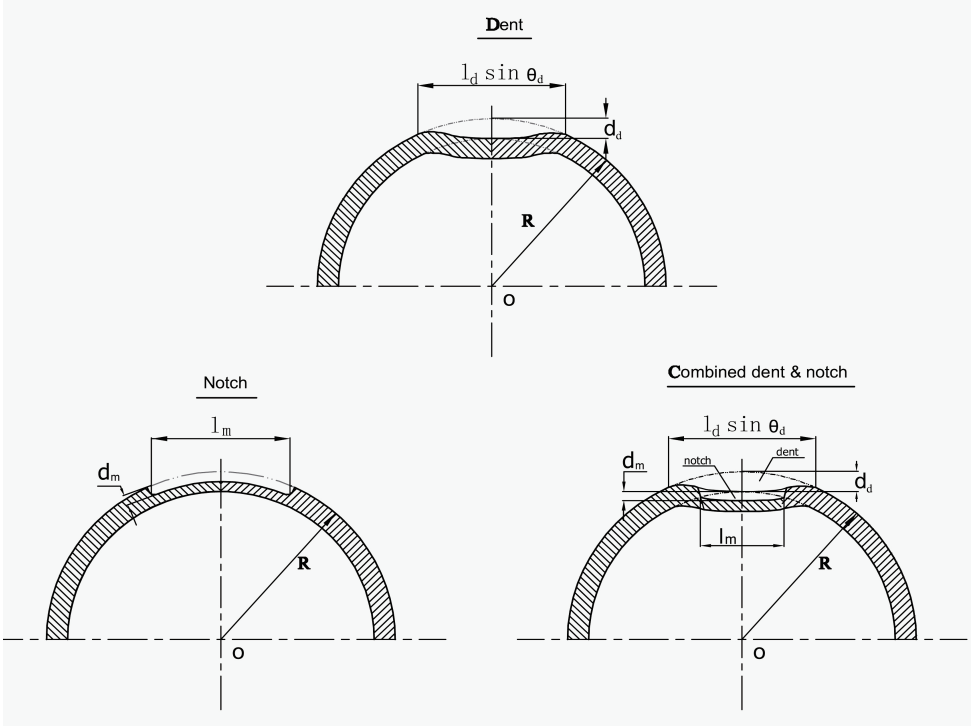

Figure 3.7: Sketches of three different types of damage on the external surface of specimens (a dent, a notch and combined dent and notch).

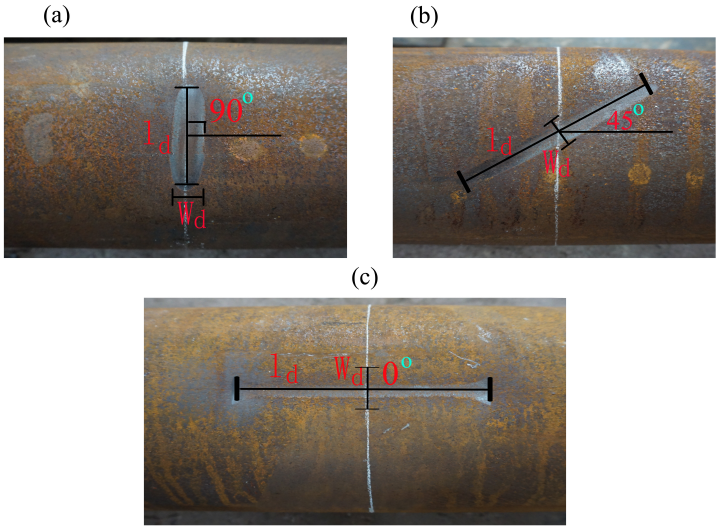

Figure 3.8: A dent damage produced on the pipe surface: (a) the dent on S2N2 (90^o); (b) the dent on S2N3 (45^o); (c) the dent on S2N4 (0^o).

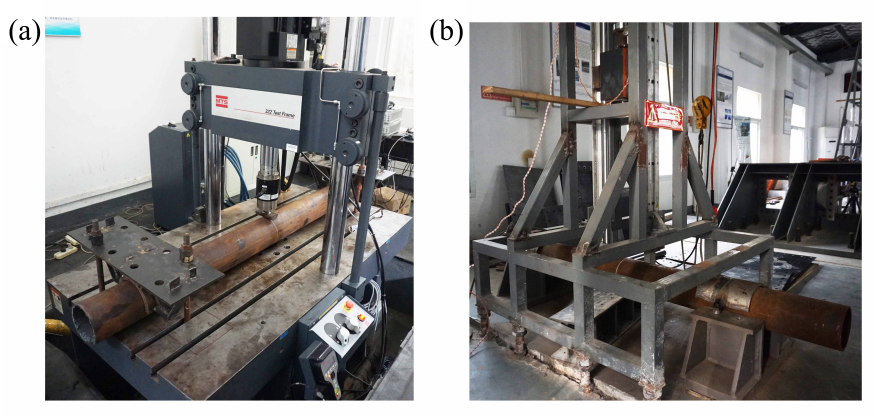

Figure 3.9: Configuration of set-ups for produce of a dent: (a) quasi-static indentation; (b) impact indentation.

Dent

The dent on a specimen surface was produced through two methods: quasi-static indentation and impact, as seen in Figure 3.9. The aim of impact is to study the dynamic effect produced by real mechanical interference. Different types of indentors were designed and fabricated to produce dents with varied shapes and rotational angles such as 90^o, 45^o and 0^o, as seen in Figure 3.10. The indentor with bulge, as shown in Figure 3.10 (d), was deployed for

the introduction of a dent in combined damage. An example of such dent in combined damage is shown in Figure 3.11 (d). In this way, the existing damage can largely maintain its original size and shape after test. After the introduction of a dent, the size, location and angle of damage were manually remeasured and documented.

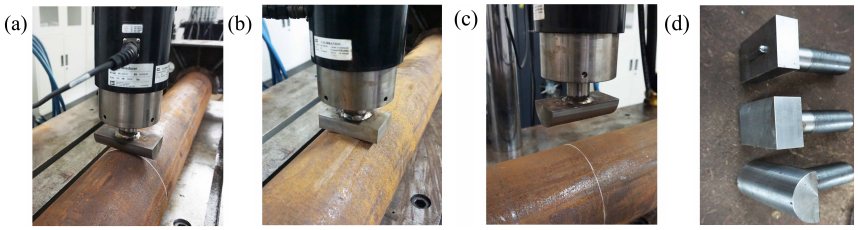

Figure 3.10: Variation of indentor angle and shape in the indentation: (a) 90^o, cylindercal shape; (b) 90^o, rectangular shape; (c) 0^o, cylindrical shape; (d) different types of indentors.

The quasi-static indentation test was conducted on a MTS machine with a capacity of 25 *ton* (250 *kN*). Specimens lay on a solid platform with both ends fully fixed so that only local damage was introduced. The loading speed was set to 0.083 mm/s, which was slow enough to eliminate the possible dynamic effect during test. A displacement-controlled strategy has been deployed to produce the required dent with a designated depth. The amount of springback has been subtracted after test.

For the impact test, a customized indentor with a weight of 54 *kg* was hoisted to an initial height of 2.45 *m*, and then released in order to produce the structural damage, as seen in Figure 3.9 (b). The pipe ends were fixed, and the vertical displacement of the pipe central segment was constrained through a box girder. It should be noted that the bases cannot be fully fixed on the ground due to the limit laboratory condition, which dissipated the impact energy a little. Additionally, the repetitive impact due to bouncing back cannot be fully restrained, which leaded to some scatters for the real geometrical size of the dent between the test and the original design. Despite the difference, the following bending tests of specimens will not be affected, since the damage dimensions were further measured before each strength test.

Metal Loss

The metal loss in the form of a notch was produced by the machining method. As shown in Figure 3.11 (a), the orientation of the notch in each specimen was constant with a rotational angle of 90^o. A chamfer with radius of 1.5 *mm* was made at the notch tip in order to eliminate the random crack due to fabrication. Figures 3.11 (c) and (d) show the combined damage which have been properly introduced. The notch depth was fabricated in parallel with the arc-length in hoop direction. However, the fabricated depth was not strictly constant due to the surface roughness of the specimen. The notch ends were filleted into a steep slope.

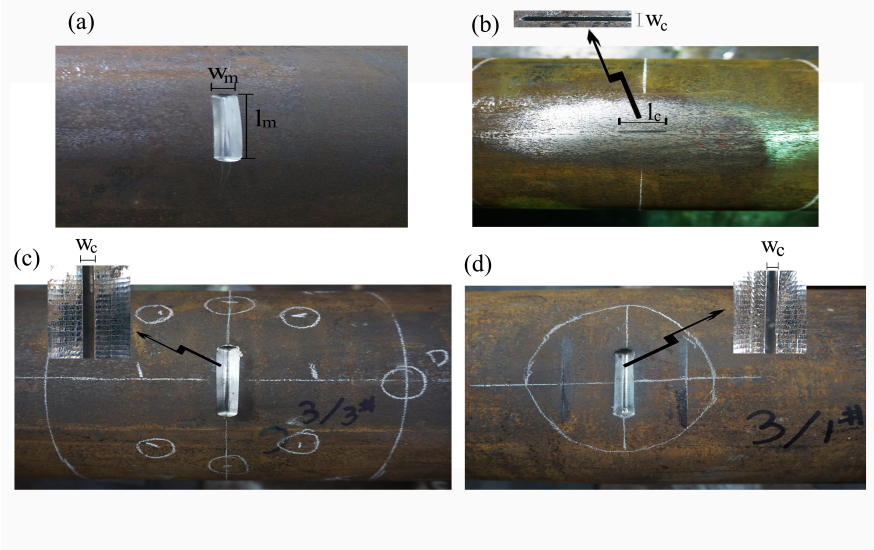

Figure 3.11: Photos of notch and crack damage on pipe surface: (a) single notch; (b) single crack (the crack can be seen from the zooming in area); (c) combined notch and crack (the crack can be seen from the zooming in area); (d) combined dent, notch and crack.

Crack

As shown in Figure 3.11 (b), the surface crack has been properly introduced on the surface of the specimen. The detection of the variation of crack dimension was carried out through a portable crack detector. Two types of crack (shallow crack and deep crack) were fabricated in order to obtain the interaction effect between fracture failure and bending strength. The definition of a shallow crack in this thesis is a crack with crack depth smaller than 1 *mm* and crack width no less than 0.5 *mm*, which was fabricated by machining method (S4N1-S4N6). With the increase of crack depth, this method was not suitable due to the limitation of workmanship. Hence, the laser method has been deployed for a deep crack (a crack depth larger than 1 *mm* and a width less than 0.5 *mm*). Different crack locations and directions were used for each specimen, for instance, the tensile side and hoop direction in S4N1. There are two basic aims for the introduction of such surface cracks. For the crack on the tensile side and in the hoop direction, the fracture failure in terms of the opening type (Mode I) was supposed to occur. In addition, in real impact scenarios, crack along the pipe longitudinal direction was possible. Therefore, different types of crack were produced here.

The crack depth-to-half crack length ratios (d_c/a) were 0.14, 0.42, 0.5 and 0.6 in the test, respectively. In addition, the surface of the cracked region was carefully ground in advance to eliminate the effect of surface roughness on crack depth. For the crack profile, it was impossible to make a specific shape such as the half-elliptical shape or the circular shape on structural surface under the current laboratory conditions. Therefore, a simple rectangular profile was made for all the cracks.

For combined damage, as shown in Figure 3.11 (c) and (d), the crack was introduced

after the introduction of the notch. At the notch tip along its length, a tiny crack was cut by the machining method.

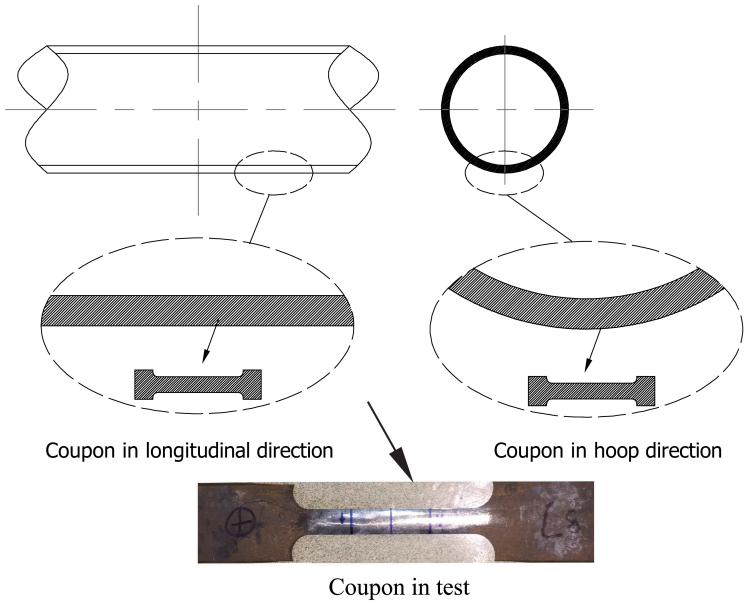

Figure 3.12: Tensile coupons of material extracted from the pipe wall.

3.2 Material test

The deployed pipe material in this test was $Q345B$ [61], which is a typical material for transmission pipes with the specified minimum yield stress (σ_y) of 345 MPa. In order to investigate the specific mechanical behavior of this material, as well as to facilitate the following numerical studies, a tensile test of materials has been deployed for the same batch of pipes. However, it should be noted that the pipes used for material test were selected by random in the batch before four-point bending test due to the laboratory limitation.

Dog-bone type of coupons was cut from both pipe longitudinal and hoop direction, as illustrated in Figure 3.12. The material coupons cut from pipe longitudinal direction keeped its original arc-shape, while the coupons cut from pipe hoop direction were flattened by a hydraulic machine with a low pressing speed (15 mm/s) according to the material test standard [62]. Therefore, the hoop coupons had a higher yield strength and low ductility due to the flattening corrections.

3.2.1 Test results and analysis

A summary of the material properties from different coupons in terms of yield stress (σ_y), ultimate tensile stress (σ_u) and the maximum elongation (e_u) is presented in Table 3.7. In total, seven coupons (L1 to L7) were cut from the longitudinal direction of specimens, while

the other four coupons (H1 to H4) were from the hoop direction of specimens. Material yield stress is obtained directly from the diagrams in Figure 3.13. Normally, the value of 0.002 plastic strain is used to obtained the yield stress of coupons without yield plateau.

Table 3.7: Summary of material properties of coupons measured from the tensile test ("-" denotes the missing data in test).

S.N.	Yield strength (Mpa)	Ultimate tensile strength (Mpa)	Elongation (%)
L1	392	532	-
L2	388	548	-
L3	388	552	-
L4	400	583	22.6
L5	378	532	20.2
L6	380	563	21.6
L7	378	542	24.6
H1	404	506	-
H2	388	522	-
H3	402	545	16.0
H4	408	548	16.3

Figure 3.13 shows the engineering stress-strain relationship of different coupons. A yield plateau occurs in coupons from the longitudinal direction, as seen in Figure 3.13 (a) and (b). The plateau disappears in the coupons from the pipe hoop direction due to the flattening effect in coupons manufacture. The stress-strain relationship in each coupon matches well in each direction of specimens. However, It should be noted that the stress-strain relationship has not been accurately recorded after the post-necking of coupons due to the stress triaxiality in necking zone [129]. Further measurements of real cross-section of coupons after necking should be carried out, which has not been done in this test. Therefore, it can be found from the diagrams that the largest strain which has been successfully measured in the material test has only reached 10%. Equivalent fitting method [33] will be used to get the further stress-strain relation for large strain, which is explained in Chapter 4.

The manufacture method of seamless pipes is hot-rolled without mechanical treatments. However, a slight anisotropy of pipe material has been ovserved. The yield stresses of coupons in the hoop direction (H1 to H4) are slightly larger than ($\backsim$ 3.68%) the ones (L1 to L7) in the longitudinal direction. The ultimate tensile stresses of coupons in the hoop direction are slightly smaller than ($\backsim$ 3.64%) the ones in the longitudinal direction. As mentioned above, the flattening effect in the manufacture of coupons is the major cause of these discrepancies.

3.3 Data measurements

There are three types of measurements during the test: geometrical measurements that were conducted before test, continuous measurements during test, and discrete measurement. In

Section 3.3.1, the geometrical measurements are described, while the continuous measurement and the discrete measurement are described in Section 3.3.2 and 3.3.3, respectively.

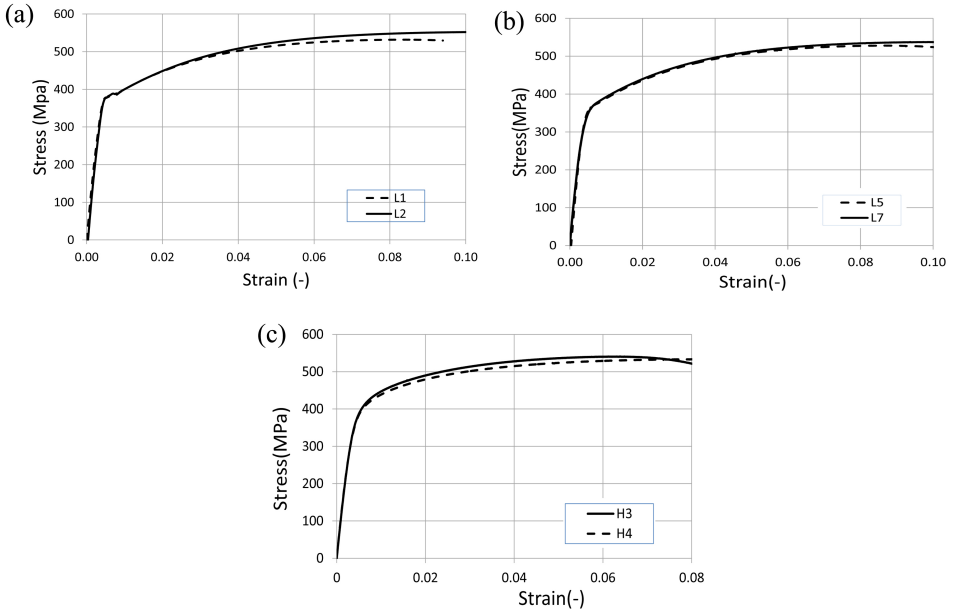

Figure 3.13: Material stress-strain relationship from tensile tests: (a) coupons L1 and L2; (b) coupons L5 and L7; (c) coupons H3 and H4.

3.3.1 Measurement of pipe geometry

Before the start of each bending test, the geometrical information of specimens including outer diameter (D) and wall thickness (t) is measured. The outer diameter has been measured by the vernier callipers in different pipe cross-sections, while the pipe thickness has been measured by an ultrasonic thickness gauge. Due to the limitation of laboratory conditions, the initial imperfection of specimen has not been measured. Instead, only visual checking was performed. However, this has not affected the further investigation of damaged pipes. According to the former research from [13], initial imperfection has insignificant effect on the bending capacity of pipes with low diameter-to-thickness ratio due to the large disturbance caused by bending moment. Further investigation in Chapter 4 will demonstrate this point.

The pipe thickness (t) and outer diameter (D) of each specimen were manually measured before the bending test, as listed in Tables 3.2 - 3.6. Followed by a strict surface preparation, i.e. polishing, and surface cleaning (as shown in Figure 3.14), the pipe thickness was measured by an ultrasonic thickness gauge. The general measured points are illustrated in Figure 3.15. The pipe outer diameter was measured in each cross-section for at least three times to obtain an average value. The measured locations were generally the cross-sections in $0D$, $\pm 05D$ and $\pm 1D$.

Additionally, an extra full measurement was performed in several specimens in order to

obtain the real distribution of pipe geometry, providing an acceptance level of the measured data. Such measurement of diameter was carried out in every cross-section with an increment of 50 *mm* along the specimen axis. In each cross-section, four points were selected for further thickness measurement. Therefore, there are at least 44 diameter data and 176 thickness data available in each specimen, which can be used for a statistical analysis. Four specimens were selected by random in the pipe batch for refined measurement, i.e. S4N4 (Three other specimens (S1N5, S1N6 and S1N7) were not further used for bending tests). It is expected that these data may reflect the accuracy and variation tendency of the pipe population (all specimens) in this test.

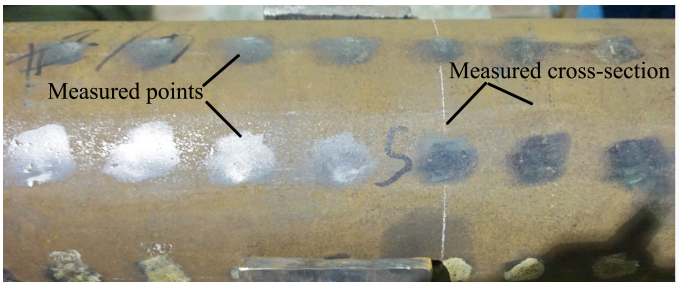

Figure 3.14: A photo of measured points with treated surface (S4N4).

Table 3.8: Summary of average thickness and outer diameter of specimens in refined measurement.

S.N.	Outer diameter(D) avearage(mm)	Thickness(t) average(mm)
S1N5	168.38	8.21
S4N4	168.08	8.23
S1N6	168.32	7.67
S1N7	167.94	7.49

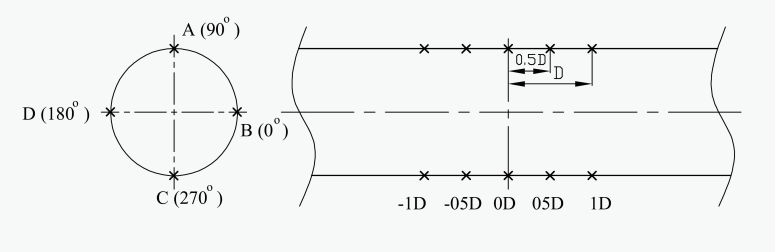

Figure 3.15: Sketch of general measurement points for thickness on a pipe surface.

Assuming a normal distribution of measured data, the variation ranges of pipe diameter

and thickness with a 95% confidence interval are presented in Figure 3.16 (the mean value and standard deviation calculated from the finite coupons can be used as the true parameters). The average values from the specimens are summarized in Table 3.8. Results show that the spread of the wall thickness and the outer diameter within each specimen is small, whereas the variation of mean thickness is relative large between different specimens. For instance, the mean thickness of S1N7 is 7.49 *mm*, whereas the thickness of S1N5 is 8.21 *mm*. Another real distribution of measured data along the pipe axis is presented in Figure 3.17, where Line 0^o and Line 90^o are two respective parallel lines on the specimen surface along the longitudinal axis, as shown in Figure 3.15.

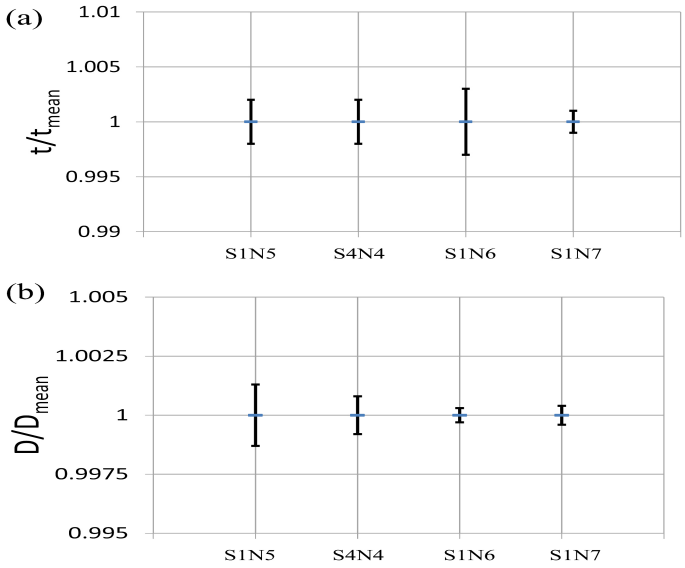

Figure 3.16: The 95% confidence interval of wall thickness and outer diameter of specimens (S1N5,S1N6 and S1N7 were not further used for bending test): (a) wall thickness; (b) outer diameter.

3.3.2 Continuous measurements

Critical parameters such as loading force, and vertical displacement were measured continuously in the test. The loading forces (P_1 and P_2) were measured through a force transducer, as shown in Figure 3.4. The vertical displacements used for curvature calculation were measured through LVDT meter with a measurement range of ± 200 *mm*, as seen in Figure 3.18 (c). Critical pipe cross-sections such as 0D (central cross-section), 05D (half pipe diameter offset from central cross-section), 1D (one pipe diameter offset from central cross-section) and End-50 (50 *mm* offset from loading head) were selected for the deployment of LVDT meter. These meters were located at the lowest point of each selected pipe cross-section.

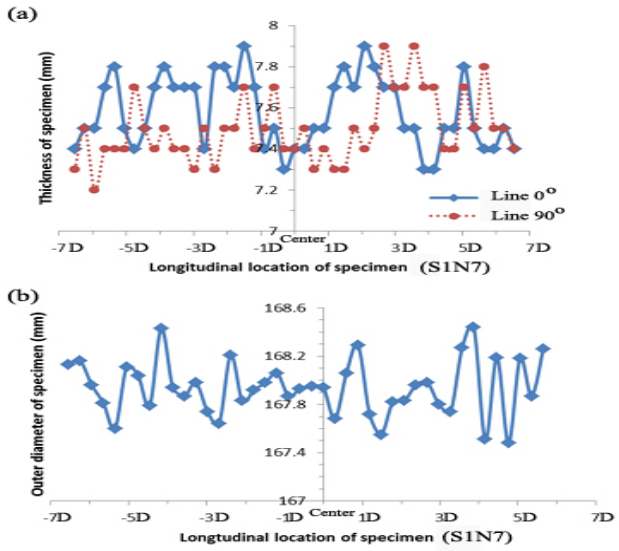

Figure 3.17: Variations of pipe thickness and outer diameter on measured points along the pipe axis: (a) wall thickness; (b) outer diameter.

The global bending moment (M) is calculated by Equation (3.1), where $a1$ and $a2$ are the real bending arms, as shown in Figure 3.6. As observed in test, the bending arm is not constant during the loading procedure due to test design, varying between 300 *mm* and 400 *mm*. As a result, corrections are needed, which is discussed in Section 3.4.

Equation (3.2) is deployed to calculate bending curvature through the measured vertical displacements, where d_r is the relative vertical displacement between two measured points and l_{curv} is two times of the corresponding longitudinal distance. Both local curvature (κ_1, κ_2) and global curvature (κ) are calculated based on the measured data. The local curvature was acquired between cross-sections 0D and 1D or 1D and End-50 in some cases, while the global curvature was obtained between the cross-sections 0D and End-50. However, the data of so-called "local curvature" have been removed due to large discrepancy caused by system error of the test, which will be discussed in Section 3.7.

$$\begin{aligned} M_1 &= P_1 \times a1 \\ M_2 &= P_2 \times a2 \\ M_{ave} &= (M_1 + M_2)/2 \end{aligned} \tag{3.1}$$

$$\kappa = 8d_r/l_{curv}^2 \tag{3.2}$$

3.3.3 Discrete measurements

Discrete measurements were performed in the test due to some limitations in both test design and laboratory. Data were manually recorded during every loading interval, for instance, the strain. Strains in terms of hoop and longitudinal components at critical locations were

measured by strain gauges (range of $\pm 3\%$). The measured locations varied with the types of structural damage. For instance, the used cross-sections for intact specimens were 0D, 05D, 1D and End-50, as illustrated in Figure 3.19, where the Arabic numerals indicate the direction of each strain gauge with its corresponding channel from data recording device. Therefore, strain components in two directions (ε_{22} and ε_{11}) were obtained. Only part of the measured strains list in the following chapters for comparison with numerical results due to the discrete measurements.

The strains in critical locations were measured by a common type of electrical-resistance strain gauge with a measure range of $\pm 3\%$ in room temperature. In order to obtain an accurate strain measurement, surface treatments of each selected location, including polishing and cleaning, were necessary. The gauge was then carefully glued to the treated surface with a mild pressure so that a compact contact between the gauge and the specimen surface would be obtained. In the end, silica gel was used for gauge protection.

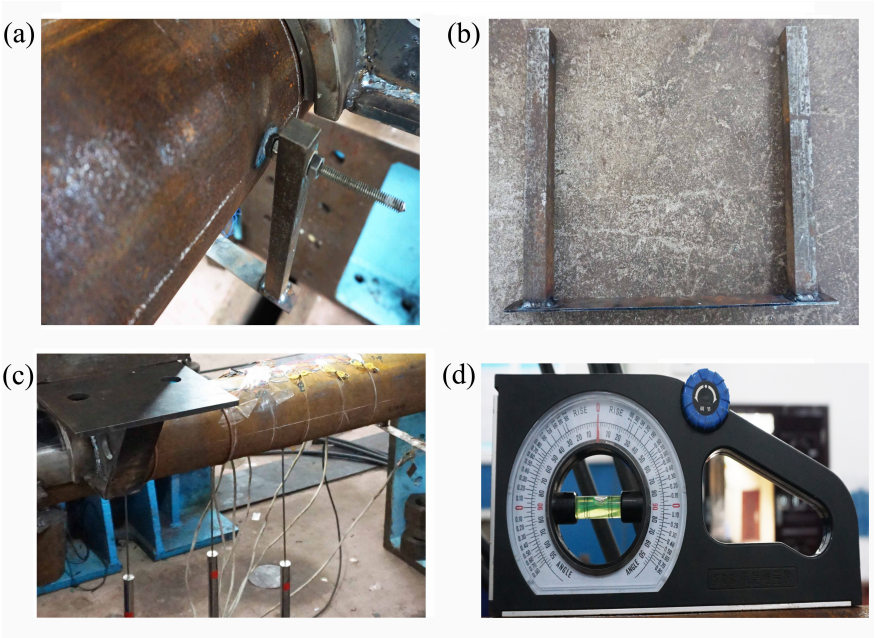

Figure 3.18: Measurement tools in bending test: (a) configuration of ovalization meter on a specimen; (b) customized ovalization meter; (c) LVDT for measurement of vertical displacement and its configuration; (d) magnetic angle meter.

In addition, the horizontal ovalizations in critical cross-sections in the form of lateral displacement were measured by customized displacement meters, as seen in Figures 3.18 (a) and (b). The customized displacement meter was made of two steel bars with large stiffness and a flexible flat steel with small stiffness, attaching to the neutral axis of the specimen cross-section when using. Strain gauges located at the center of flat steel were used to measure the variations of the bending strain. The lateral displacement can then be reflected based on such strain information. A calibration before measurement was necessary in order to obtain an accuracy result. However, discrete data are not presented here since it

is impossible to have a reasonable comparison in the further study due to its asynchronism. It has only been used as a qualitative checking for the test.

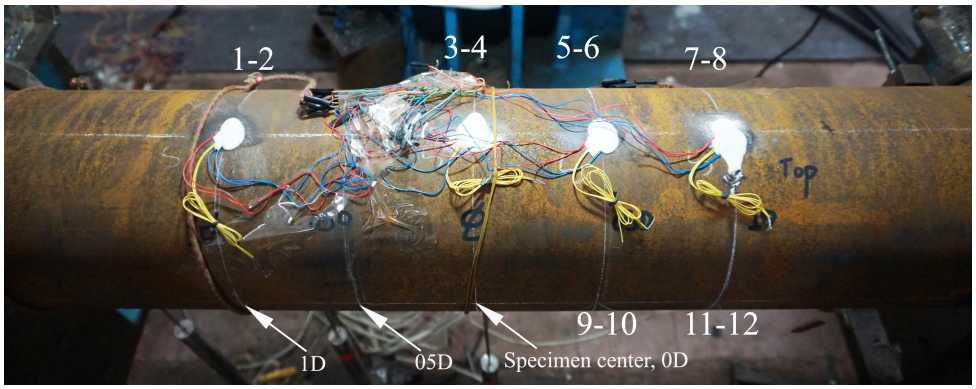

Figure 3.19: Strain gauge distribution on intact specimen (Cross-section End-50 is not shown in this figure).

3.4 Correction of bending arm and curvature

As described in Section 3.3, some experimental errors due to the test design, are unavoidable and should be corrected afterwards. Strictly speaking, the real bending arm cannot keep constant during loading. Instead, it varies gradually with the increase of loading loads. Such discrepancy is minor and can be neglected when the bending arms of specimens are very long, like the tests in [53] and [74]. However, extra measurement is needed in this test due to the relative short length of the bending arm. Another discrepancy needed to correct is the curvature due to the displacement measurement method through LVDT (Linear Variable Differential Transformer) in this thesis. Therefore, extra data are measured and used for corrections. The correction methods in this test are described in this section.

3.4.1 Bending arm

As we have already discussed, the real bending arm cannot keep constant during loading in a bending test, decreasing with the increase of loading load as well as the bending angle of specimens. Theoretically, it varies from full bending arm 400 *mm* to the original bending arm 300 *mm*, as seen in Figure 3.6. Practically, the final bending arm could be slightly less than 300 *mm* due to factors in the test such as asymmetrical configuration of set-up or slight sliding.

Therefore, an extra variation relation between bending arm and loading time is required for the correction. In order to trace such relationship, extra measurements were added for each group of specimens. The practical operational procedure for data measurements and correction is listed as follows: At the end of each loading interval of a bending test, the real bending arm was manually measured. Since the loading time in each loading stage was automatically recorded, we can then obtain the corresponding loading time for each bending arm. Provided that the variation of bending arm within each loading interval was uniform,

the real relationship between the bending arm and the loading time was then fitted in terms of a polynomial diagram, as shown in Figure 3.20. Therefore, the real bending moment has been corrected through such relationship in each time increment.

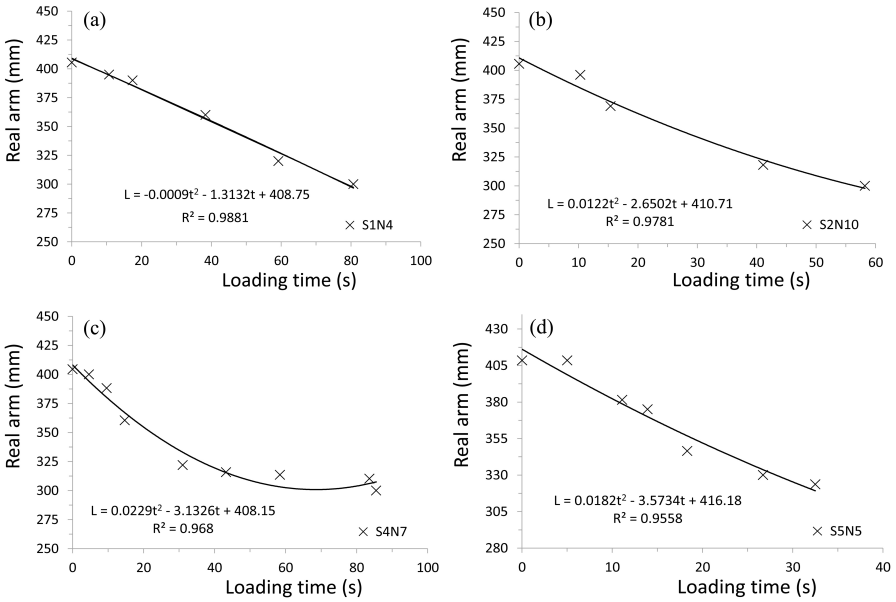

Figure 3.20: Variation relationship between bending arm and loading time: (a) specimen S1N4; (b) specimen S2N10; (c) specimen S4N4; (d) specimen S5N5.

3.4.2 Bending curvature

As will be discussed in Section 3.7, the measurement method through LVDT provided an overestimation of specimen's curvature. Therefore, extra measurements were used to correct such experimental discrepancy.

It is easily derived that the curvature of a long beam during bending can be also written as Equation (3.3), which is the function of the tangential angle (θ_{arc}) of a given arc and the chord length of the arc (l_{curve}). The measurement of each tangential angle was through a magnetic angle meter with dual scale and an accuracy of ± 1 degree, as shown in Figure 3.18 (d). The measured location was the same with cross-section End-50.

$$\kappa = \frac{2sin(\theta_{arc})}{l_{curve}} \tag{3.3}$$

Therefore, through the measured tangential angles at the end of each loading interval, the corresponding curvature can be obtained through both Equation (3.2) and Equation (3.3). After a careful comparison between the two calculation methods, a correction coefficient is proposed for the curvature of each group of specimen, as shown in Table 3.9. By using this coefficient, a reasonable final curvature value is obtained.

Table 3.9: Correction coefficients of curvature.

Series	ξ		Series	ξ	
	C[3]	T[4]		C	T
S1	1.645	-	S2	1.445	1.645
S3	1.445	1.645	S4	1.645	1.645
S5	-	1.645	-	-	-

[3] C denotes the specimen with damage on its compression side, the same in the following tables.
[4] T denotes the specimen with damage on its tensile side, the same in the following tables.

3.5 Results of four-point bending test

In this section, results in terms of structural failure mode, bending moment-curvature diagram, and the comparison of strength capacity are presented and discussed. It should be noted that the series number of each specimen in this thesis has been renumbered for the sake of clarity in further numerical research. Hence, the numbers marked on some specimens do not necessarily match with the real series numbers in this thesis, for instance, the mark on the specimen S4N13 in Figure 3.21 (d).

3.5.1 Reference values

For the bending moment-curvature diagrams in this thesis, the bending is normalized by the plastic bending moment M_y ($M_y = 4R_a^2 t\sigma_y$), while the curvature κ is normalized by the curvature-like expression $\kappa_0 = t/4R_a^2$. For the residual ultimate strength of damaged specimens, results from the average value of intact specimens are used for reference values. The reduction ratio of pipe ultimate strength can be expressed by $1 - M_{cr}/M_i$.

3.5.2 Structural failure modes

For pipes with low diameter-to-thickness ratio subjected to bending, they fail as a result of the increase of structural deformation in the form of ovalization in pipe cross-sections. Under a certain extent, such ovalization can be counterbalanced by the material yielding and further material hardening so that the structure stays stable. When the ovalization cannot be compensated for, the structure reaches its bending capacity with the largest ovalization in a specific pipe cross-section. Hence, the structure fails with a certain failure mode.

The failure modes of different types of specimens are presented in Figures 3.21 and 3.22. It is observed that an outward bulge is first formed on the compression side of the intact specimen (S1N4) at the offset position of 25 *mm* from the loading edge. With the increase of loading, a recession region is then fashioned in the adjacent surface of the outward bulge. In the same cross-section with outward bulge, an extra large ovalization appears.

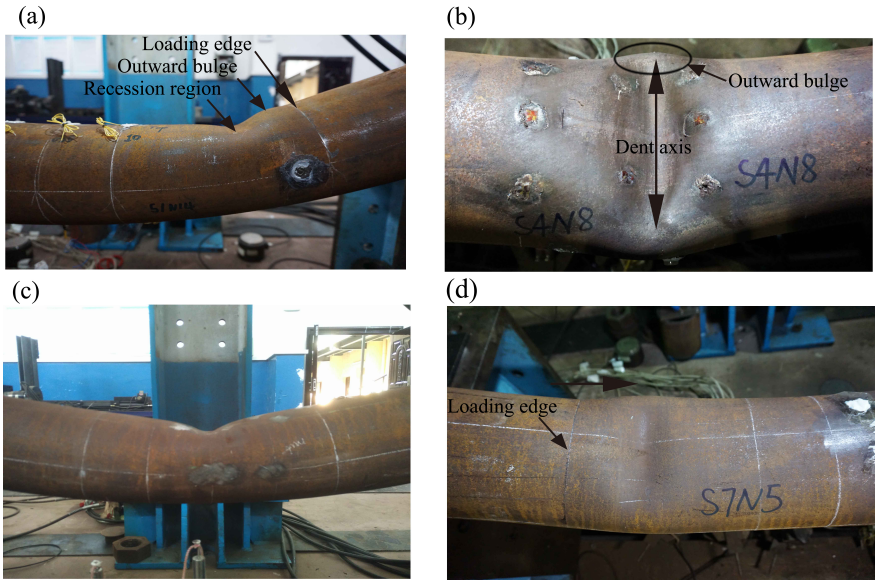

Figure 3.21: Failure modes of specimens with damage on the compression side: (a) intact specimen (S1N4); (b) dented specimen (S2N4); (c) specimen with metal loss (S3N1); (d) specimen with single crack (S4N13).

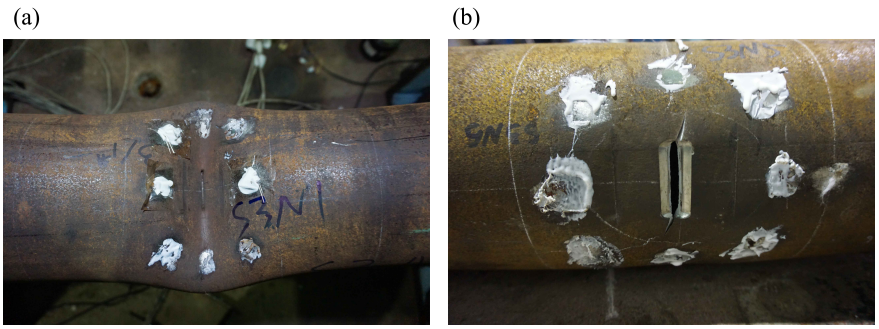

Figure 3.22: Failure modes of specimens with combined damage: (a) specimen with combined damage on the compression side (S5N1); (b) specimen with combined damage on the tensile side (S5N5).

The failure mode in dented specimen is different with the intact one. As seen from the specimen S2N4 in Figure 3.21 (b), an inward, depressed region is rapidly developed in the dented area. Two outward bulges along the dent axis are then fashioned. An extra large ovalization appears in the cross-section with the dent. For a dent on the tensile side (S2N7), a recovery of the existing dent occurs firstly, and then it fails in the same mode as the intact specimen. Compared with a dent on the compression side, a similar failure pattern has also been observed on both the specimen with metal loss (Figure 3.21 (c)) and on the specimen with combined damage (Figure 3.22 (a)) on the compression side.

The fracture failure has been induced at a low loading force on specimens (as seen from S5N5 in Figure 3.22 (b)) with combined notch and crack on its tensile side. The propagation direction of fracture is about 30 degree along the notch axis. No variation of pipe ovalization in the damaged pipe cross-section occurs in this case. However, for specimens with a single crack either on the compression side or on the tensile side, no fracture failure has been observed. Instead, the same failure mode as the intact specimens occurs, as seen in Figure 3.21 (d). The phenomenon will be further discussed in Section 3.7.

3.5.3 Moment-curvature diagrams

The bending moment-curvature diagram is one of the most important features of the strength of pipelines, which can reveal the variations of structural behavior in an explicit way. The calculation methods of bending moment and curvature have been described in Section 3.3.2.

The typical moment-curvature diagrams of both intact specimens and damaged specimens are presented in Figures 3.23-3.29. It is observed from Figure 3.23 that the diagrams in the listed four intact specimens have a very similar variation tendency. The intact specimens have a gradual and stable failure procedure. The vibration on the curve of case S1N1 is due to the external disturbance of data acquisition device during loading process. The occurrence of structural damage on the compression side of structures accelerates the failure in different ways due to the rapid localization of the damaged region, as seen from the diagrams for dented specimens in Figure 3.24 and the notched specimens in Figure 3.26. Detailed discussions of damage effects will be presented in Section 3.6.

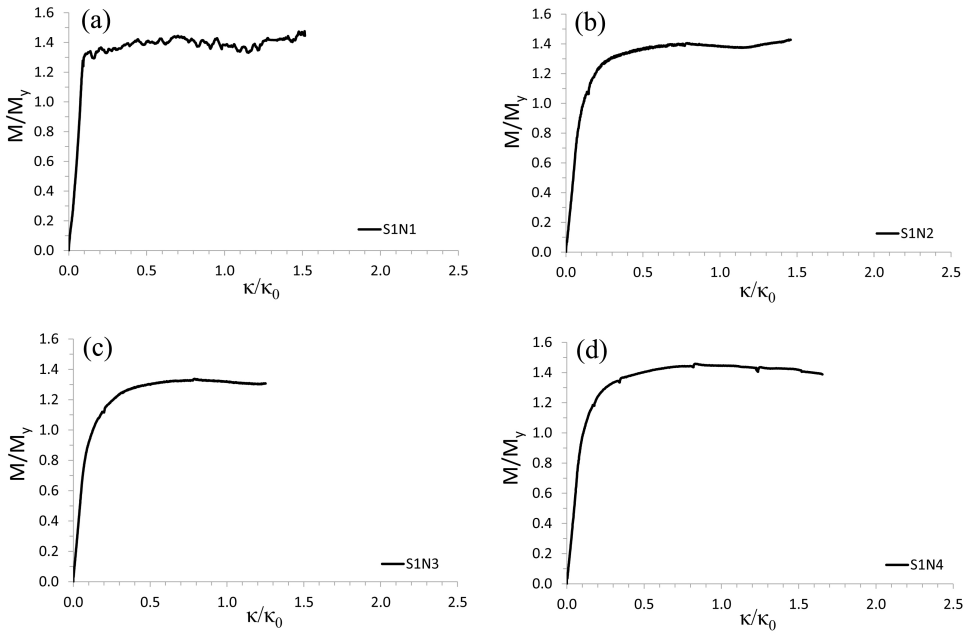

Figure 3.23: Moment-curvature diagrams of intact specimens: (a) S1N1; (b) S1N2; (c) S1N3; (d) S1N4.

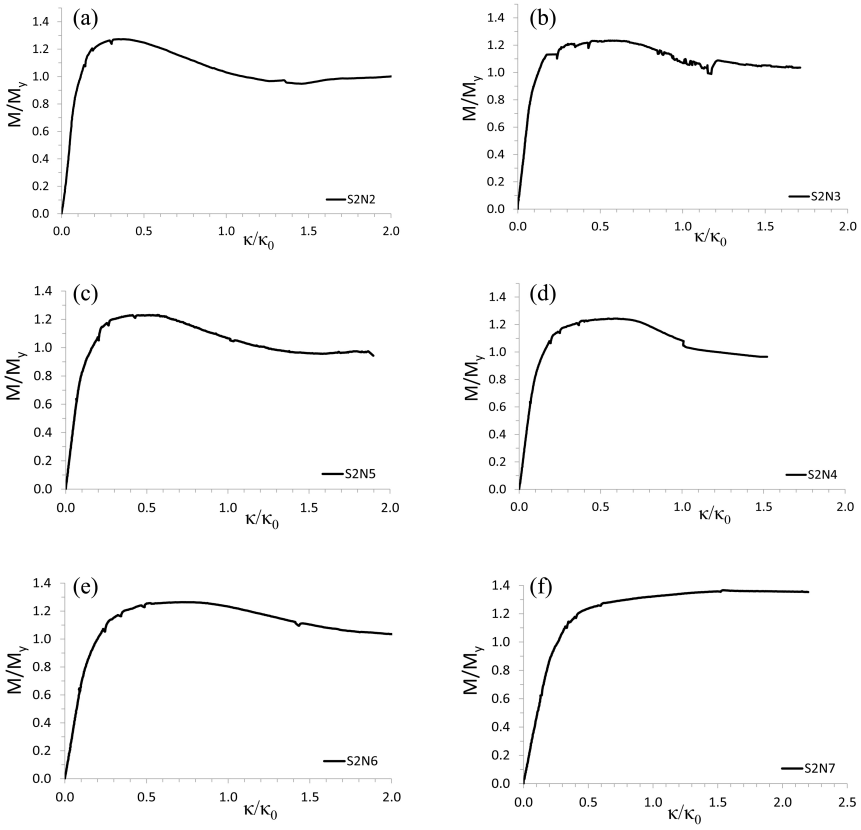

Figure 3.24: Moment-curvature diagrams of dented specimens: (a) S2N2 with a 90^o *dent; (b) S2N3 with a* 45^o *dent; (c) S2N4 with a* 0^o *dent; (d) S2N5 with a* 90^o *dent; (e) S2N6 with a* 90^o *dent; (f) S2N7 with a* 90^o *dent on the tensile side.*

3.5.4 Comparison between test results and empirical solutions

In this section, the comparison between test results and existing analytical and/or empirical solutions on intact metallic pipes is carried out. The aim of this section is to verify the accuracy of the test results. Due to the lack of formulas in damaged pipes, such comparisons are only for specimens without damage (S1N1 to S1N4).

Figure 3.30 shows the comparison results of normalized ultimate bending strength (M_{ref} is from the analytical formulas) between intact specimens and analytical formulas. These formulas are listed in Equation (3.4) [120], Equation (3.5) [73], Equation (3.6) [66] and Equation (3.7) [44] from former researchers. Where $X_1 = \sigma_y D/Et$. Plastic bending moment is expressed as $M_y = 4R^2 t\sigma_y$. The outer diameter D and outer radius R of pipe are used in these formulas.

Comparison results show a good agreement between intact specimens and the analytical formulas. As expected, all formulas provide a conservative prediction for test specimens. The minimum discrepancy of ultimate bending moment between the test and the formulas is 13.75% in Equation (3.6), while the maximum one is 23.75% in Equation (3.7). The results

are quite consistent due to the uncertainties such as the test methods [66]. Therefore, it demonstrates a relative high accuracy of the test results after reasonable corrections. In the following sections, damage effect will be analyzed through the comparison with the results from these intact specimens.

$$M_c = 3\sigma_u t R^2 \tag{3.4}$$

$$M_c = (1.05 - 0.0015\frac{D}{t})\sigma_y D^2 t \tag{3.5}$$

$$M_c = 1.13 M_y e^{-X_1} \tag{3.6}$$

$$M_c = \frac{4}{3}\sigma_y((R+\frac{t}{2})^3 - (R-\frac{t}{2})^3) \tag{3.7}$$

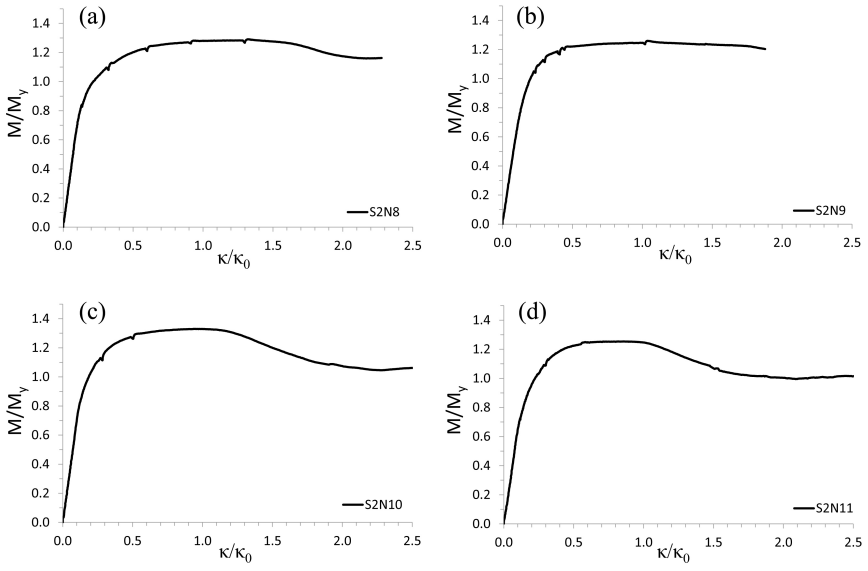

Figure 3.25: Moment-curvature diagrams of specimens with impact-induced dent (all on the compression side): (a) S2N8 with a 90^o dent; (b) S2N9 with a 90^o Dent; (c) S2N10 with a 90^o dent; (d) S2N11 with a 90^o dent.

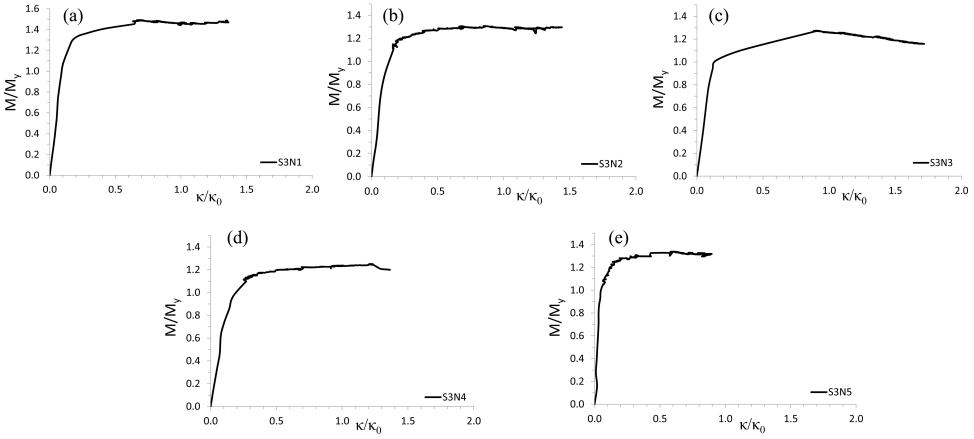

Figure 3.26: Moment-curvature diagrams of specimens with metal loss damage: (a) S3N1 with metal loss on the compression side; (b) S3N2 with metal loss on the compression side; (c) S3N3 with metal loss on the compression side; (d) S3N4 with metal loss on the tensile side; (e) S3N5 with metal loss on the tensile side.

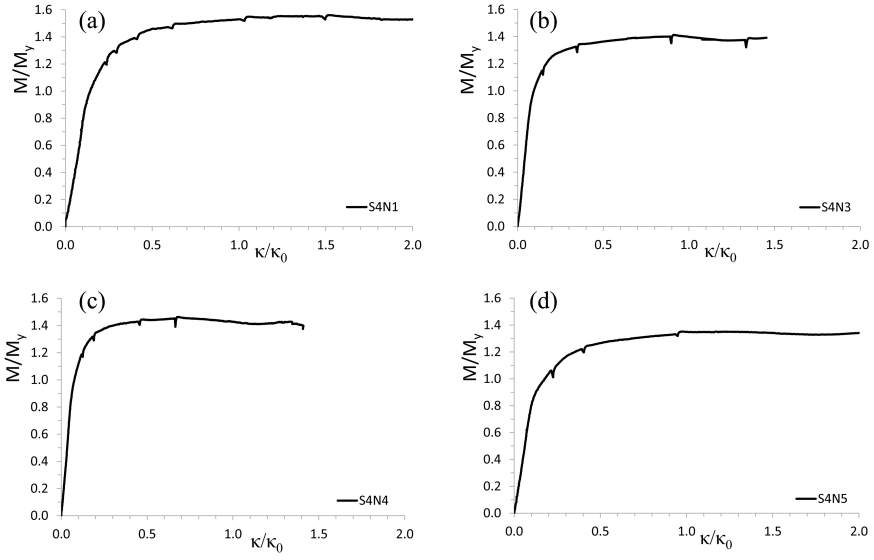

Figure 3.27: Moment-curvature diagrams of specimens with shallow crack: (a) S4N1 with a crack in hoop direction on the tensile side; (b) S4N3 with a crack in hoop direction on the compression side; (c) S4N4 with a crack in longitudinal direction on the compression side; (d) S4N5 with a longitudinal direction on the tensile side.

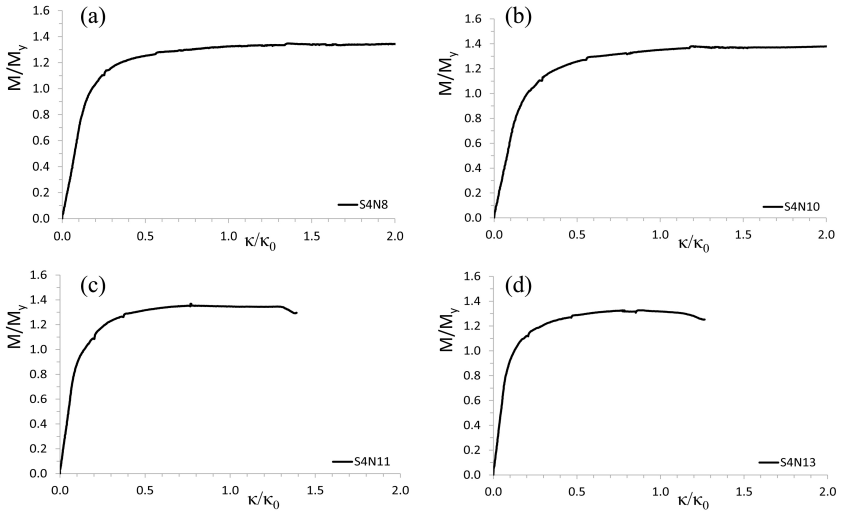

Figure 3.28: Moment-curvature diagrams of specimens with deep crack: (a) S4N8 with a crack in hoop direction on the tensile side; (b) S4N10 with a crack in hoop direction on the compression side; (c) S4N11 with a crack in hoop direction on the compression side; (d) S4N13 with a crack in longitudinal direction on the compression side.

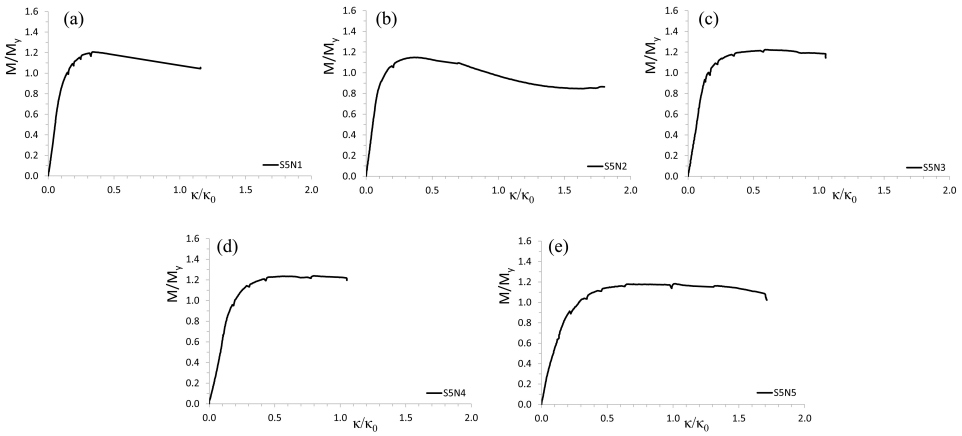

Figure 3.29: Moment-curvature diagrams of specimens with combined damage: (a) S5N1 with combined dent, notch and crack on the compression side; (b) S5N2 with combined dent, notch and crack on the compression side; (c) S5N3 with combined notch and crack on the tensile side; (d) S5N4 with combined notch and crack on the tensile side; (e) S5N5 with combined notch and crack on the tensile side.

3.6 Analysis of structural damage

In order to identify the effect of each structural damage, a detailed comparison is carried out in this section. Results in terms of the residual ultimate bending moment, the critical curvature and the structural stable range are compared. Tables 3.2-3.6 list all the relevant results from the specimens. In the following comparisons, the average values from intact specimens are used as references.

A general comparison of bending features in terms of M_{cr} and κ_{cr} is shown in Figure 3.31. The horizontal axis is the cross-sectional slenderness ($D/(t\varepsilon^2)$) of pipes, expressing as the function of the geometric slenderness (D/t) and material's yield stress, where ε^2 is equal to $235/\sigma_y$ based on the rule [55]. It should be noted that results from cracked specimen are intentionally removed due to their abnormal large values. Discussions are conducted in Section 3.7. A boundary line is also produced based on the average value of intact results in order to have an explicit comparison. In addition, the surface strain ($\varepsilon = \kappa D/2$) is calculated in order to compare the stable range before collapse of each specimen. For instance, the average stable strain range for intact specimens is between 1.02% and 3.91%, as seen in Figure 3.23.

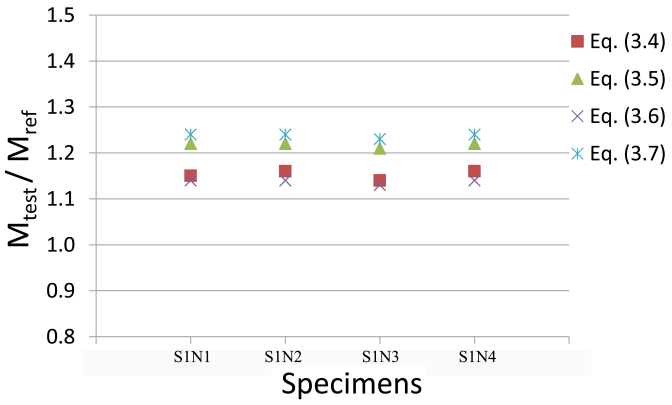

Figure 3.30: Comparison of ultimate bending strength between intact specimens and existing analytical solutions.

Results from Figure 3.31 show that structural damage including a dent, a notch and combined damage on the compression side of the specimens has a considerable large effect on their bending strength. For the damage on the tensile side of specimens, ultimate strength mainly depends on the happening of fracture failure. For the case with a dent on its tensile side (S2N7), only a slight reduction of bending capacity occurs. However, a larger critical curvature is produced due to the recovery of the existing dent, as mentioned in Section 3.5.2.

3.6.1 Effect of dent

A more specific comparison is presented in this section to obtain the effect of a dent. As seen in Figure 3.32, a comparison of dent effect on residual strength under different scenarios is carried out. Five different scenarios are compared here, categorized according to the

introduce method of a dent and the dent rotational angle. The average values of specimens with similar dent depth are used as the same category, in spite of the existing discrepancies between each specimen. For instance, the "Quasi-C-90" scenario consists of specimens S2N1, S2N2, S2N5 and S2N6 with the same dent depth (10.3 *mm*), and with the dent on the compression side in pipe hoop direction produced by the quasi-static indentation. The "Impact-C-90" consists of specimens from S2N8 to S2N11 with a similar dent depth, and with the dent on the compression side in pipe hoop direction produced by the impact indentation (Figure 3.9 (b)). The quantification of damage effects are presented in the following Chapters 4, 5 and 6.

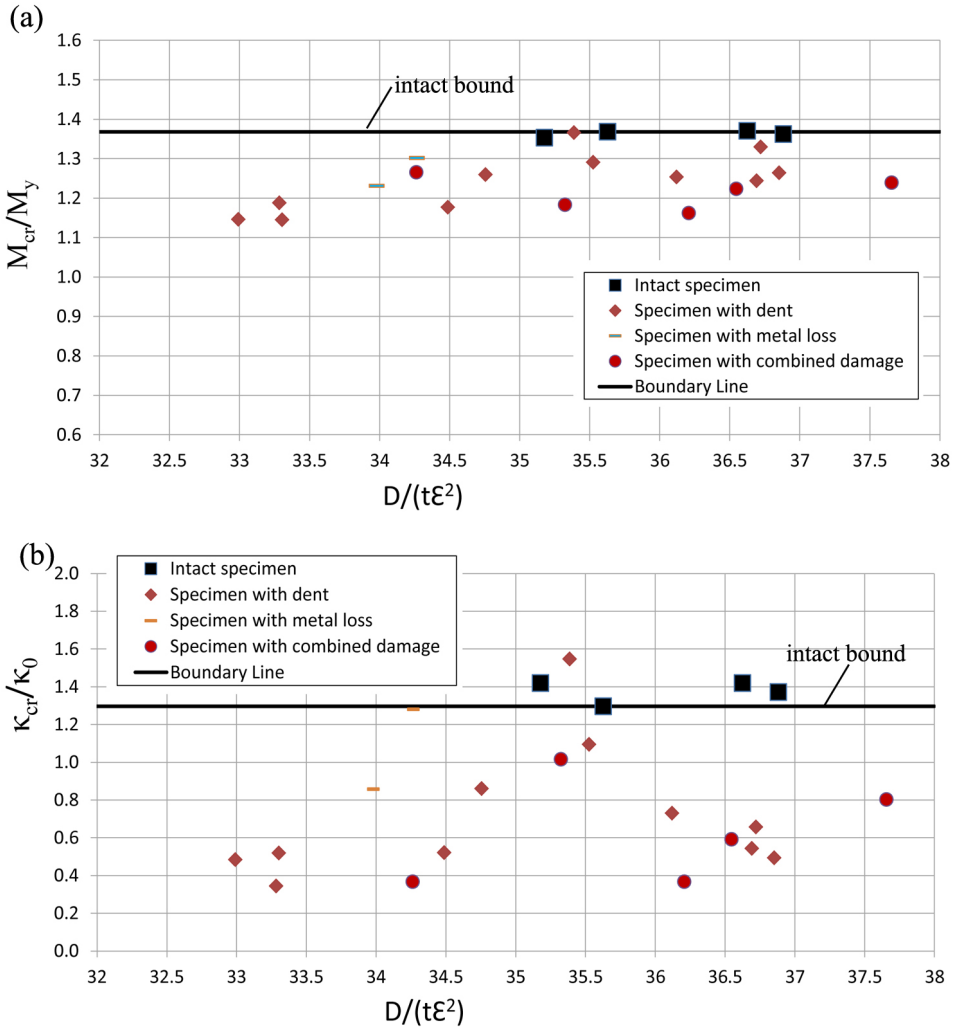

Figure 3.31: Relationship between bending features in terms of M_{cr} and κ_{cr}, and pipe slenderness: (a) normalized bending capacity (M_{cr}/M_y); (b) normalized critical curvature (κ_{cr}/κ_0).

Results from Figure 3.32 show that the dent on the compression side has a large negative effect on pipe strength. For instance, the largest reduction ratio of ultimate bending has reached 11.72%, while the largest reduction of critical curvature is 66.67%. A rapid failure occurs due to such dent, as seen in Figure 3.24.

Compared to the scenarios with a dent introduced by quasi-static indentation, the impact effect has not produced obvious difference. The reduction ratio of ultimate bending is 8.68%, while the reduction ratio of critical curvature is 42.25%. In addition, there is a similar negative effect of dent with different rotational angle, as seen from scenarios "Quasi-C-90", "Quasi-C-45" and "Quasi-C-0". Therefore, a further quantification of both dent angle and the impact effect is still needed to be done.

It is observed that there is only a slight effect on ultimate strength for the specimen (S2N7) with a dent on its tensile side. For instance, the reduction ratio of ultimate bending is 1.11%. Due to the recovery of a dent on the tensile side, as described in Section 3.5.2, the critical curvature has increased a little (7.5%). However, the bending moment is, at any situation, reduced due to the occurrence of the dent.

For the stable range of strain before specimen failure, it has been largely reduced for the specimens with a dent on the compression side (from 0.54% to 1.67%), as calculated from Figure 3.24, whereas it is pretty close to the intact specimens for the specimens with a dent on the tensile side (from 1.74% to 5.08%).

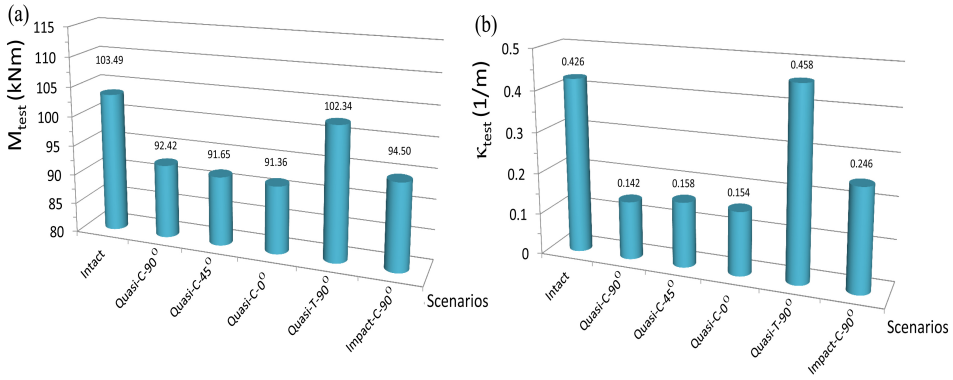

Figure 3.32: Dent effect on residual strength of specimens in different scenarios: (a) ultimate bending moment; (b) critical curvature.

3.6.2 Effect of metal loss

The metal loss in terms of a notch has been properly introduced on pipe specimens. All the notches are put at the center of specimen with the angle of 90^0 degree. The notch on specimens including S3N1, S3N2 and S3N3 is on the compression side, while the notch on specimens S3N4 and S3N5 is on the tensile side. Exceptions appeared on specimens S3N1, S3N2 and S3N5 due to pre-failure of loading region caused by the insufficient reinforcement, as mentioned in Section 3.1.2. Failures of these specimens initiate in the region close to the loading head instead of the damaged region. However, all the moment-curvature diagrams of notched specimens are still presented for comparison, as seen in Figure 3.26.

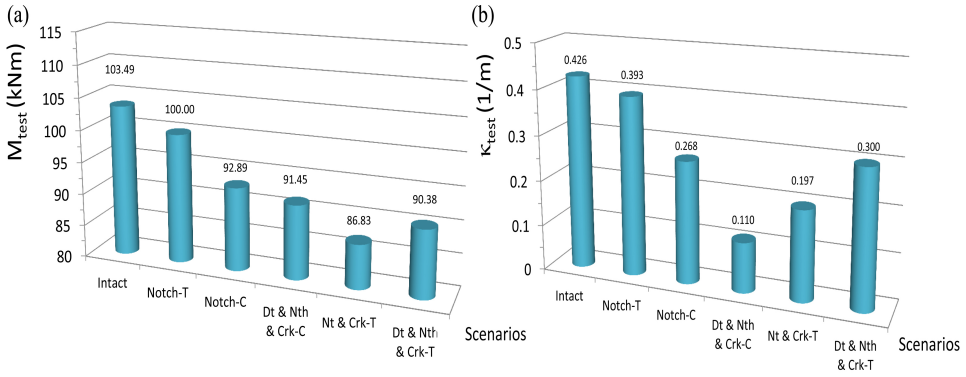

Figure 3.33: Notch and combined damage effects on residual strength of specimens in different scenarios: (a) ultimate bending moment; (b) critical curvature.

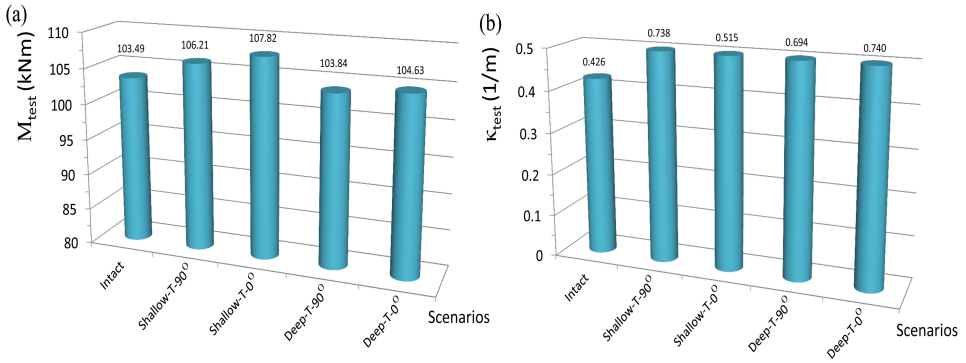

Figure 3.34: Crack effect on residual strength of specimens in different scenarios: (a) ultimate bending moment; (b) critical curvature.

For clarity reason, the effects of both notch and combined damage are presented together in Figure 3.33. Different scenarios are also used for comparison. "Notch-T" means the scenario of a notch putting on the tensile side of specimen. A negative effect has been introduced for a notch on the compression side. For instance, the reduction ratio of bending is 10.24%, while the reduction ratio of critical curvature is 37.09%.

Fracture failure happens on the specimen (S3N4) with notch on its tensile side. Its bending capacity majorly depends on when and where the fracture starts to propagate. It is observed that, in this case, fracture starts to initiate and propagates at the bending moment of 100 kNm and the critical curvature of 0.393 $1/m$, as shown in Figure 3.33. In addition, such fracture failure has not changed the variation of moment-curvature diagram, as shown in Figure 3.26 (d). The stable range of strain has been largely reduced (from 0.54% to 0.93% for notch on the compression side), as seen in Figure 3.26.

3.6.3 Effect of crack

In order to investigate the crack effect, a single crack has been introduced to the pipe surface by machining methods. The single crack in each specimen is set at different locations and directions. For instance, specimen S4N1 has a crack on its tensile side and in the hoop direction, while specimen S4N4 has a crack on its compression side and in the longitudinal direction. The so-called shallow crack in Figure 3.27 in this thesis is a crack with a depth less than 1 *mm* (measured by feeler gauge), while the deep crack in Figure 3.28 is a crack with a depth larger than 1 *mm*.

Figure 3.34 shows the comparison results of crack effect on pipe bending strength. "Shallow-T-90" scenario means the specimen with a shallow crack on its tensile side and in the hoop direction. It is observed that there is an occurrence of positive effect for all the specimens with a crack on the tensile side, which obviously violates the common sense. For instance, an increase of 4.18% in ultimate bending moment at a larger curvature (0.515 $1/m$) occurs in the scenario of "Shallow-T-0^o". No fracture has been initiated, and the bending moment-curvature diagrams in all these cracked specimens are very close to the intact specimens, as shown in Figure 3.27 and Figure 3.28.

Accounting for the laser cutting method to produce crack in this test, it is possible that a strengthened region in specimen has been produced due to the HAZ (heat affected zone). Noticed in the research of [94], the HAZ generated by the laser cutting introduces a high hardness to a maximum depth of 0.5 *mm*. Hence, such strengthened region shields the initiation and propagation of the crack and produce a higher ultimate strength in the material of these specimens. However, it is impossible to quantify its effect due to the lack of measured data, which would be a part of future research. Discussions will be further made in Section 3.7.

3.6.4 Effect of combined damage

The combined damage is more prone to happen on the pipe surface in reality. Two types of combined damage are therefore introduced and presented here. One is the combination of metal loss and crack, the other is the combination of metal loss, dent and crack. As shown in Figure 3.33, three different scenarios of combined damage are compared. "Dt & Nth & Crk-C" means the scenario of combined dent, notch and crack on the compression side of specimen.

Results show that the combined damage has the most severe effect on pipe ultimate strength. For combined damage on the compression side, the reduction ratio of ultimate bending moment is 11.63%, while the reduction ratio of critical curvature is 74.18%. The results indicate that a rapid failure occurs at the lowest curvature. Figures 3.29 (a) and (b) also demonstrate this phenomenon according to the variation of bending moment-curvature diagram. In addition, for combined damage on the tensile side, fracture failure in terms of Mode I has occurred in a very early time during loading. As shown in the combined notch and crack scenario in Figure 3.33, the initiation and propagation of crack happened at the bending moment of 86.83 *kNm* and the curvature of 0.197 $1/m$.

3.7 Discussions on experimental uncertainty

In this section, the possible causes for the introduction of experimental errors in this test are discussed in order to have a better understanding of the real physical mechanism of pipe strength.

As mentioned in Section 3.6.3, a strengthening phenomenon has been observed for the specimens with a single crack. The major cause of such abnormal phenomenon is the strengthened region induced by laser cutting technique. The laser cutting technique was used for the introduction of a surface crack. Compared to conventional cutting, it has more advantages such as accurate cutting, non-contact processing, and short time of processing. Therefore, the designated crack dimensions are properly fabricated in this test. However, the HAZ (heat affected zone) generated by this technique may lead to undesirable effects on the structure. The HAZ is the zone of the base material which has not melted but whose micro-structure and mechanical properties are affected by the heat generated during laser cutting. Hence, a much higher hardness of the material in the vicinity of the surface crack region is induced. As a consequence, the induced martensite around the crack creates a high-strengthen region, effectively strengthening the pipe structure and shielding the effect of crack. Further research is required in order to quantify its effect so that the real interaction between fracture and residual ultimate strength could be revealed.

A shear force exists due to the use of loading heads in the four-point bending test. The strain distribution of the pure bending segment ($2L1$) has been affected as a consequence. Pre-failure of structure will be introduced in the region adjacent to the loading heads due to the change of such strain distribution. One of the methods to alleviate the effect is to extend the segment length of specimen under pure bending ($2L1$). Thus, the affected-region of shear force will be restricted in a very limited area. In addition, a reinforcement in the loading region is necessary in order to avoid the pre-failure of specimens due to shear force. A special designed half-sleeve is used in this test. By using half-sleeve, its own stiffness should be carefully checked after each test in order to guarantee the accurate behavior of pipe behavior. For instance, exceptions happened on specimen S3N1, S3N2 and S3N5 due to the softening of the half-sleeve, as seen from Figure 3.5 (b). The effect of damage has been shielded by the pre-failure of structure in the regions adjacent to the loading head.

The variation of the real bending arm in four-point bending test and its correction method may introduce experimental errors. With the gradually increased rotational angle of specimen during loading, the contact area between the loading heads and the specimen is decreasing. This phenomenon indicates that the bending arm change. Therefore, the real bending arms ($a1$ and $a2$) cannot stay constant any more, varying between 300 *mm* to 400 *mm* in this test. A reasonable correction on the bending arm of each specimen is descried in Section 3.4.1, with the assumption of uniform variation of bending arm within each loading interval. Thus, experimental errors are introduced.

Another major cause of experimental errors is the measured method of the pipe curvature through LVDT displacement meter. The LVDT meter is used to measure the vertical displacement in specific points. The installation of LVDT meter is realized by the use of a glue and cotton, fashioning a so called “elastic-connection” between specimens and meters. The base of the meter is fixed to the ground. Such connections are supposed to be stable and can resist the variation of large deformation. The problem is that the meter will incline inward and slide slightly (from point B to B’) due to such design, as seen in Figure 3.6. Un-

der this situation, the measured vertical displacement (point B' in Figure 3.6) is larger than the true value. As a consequence, the calculated vertical displacement d_r becomes larger, which means an overestimation of the curvature in this test. Furthermore, the error induced by this method would be more significant with the decrease of the longitudinal span (l_{curv}), as expressed in Equation (3.2). Therefore, only the so-called global curvature with a long span (l_{curv}) is finally adopted in this thesis. In order to correct such effect, extra data such as rotational angles in each loading interval have been measured by a magnetic angle meter, as described in Section 3.4.2.

Other causes in this test may also induce discrepancies as well, such as the slightly coarse inner surface of specimens which may affect the measurement accuracy of pipe thickness, the strengthening effect due to unloading, the accuracy of the material property due to the stress triaxiality after coupon necking, and the restriction of ovalization by loading heads. As stated in the research from [71], the ovalization restriction of pipe specimen will introduce discrepancy in strain distribution.

3.8 Conclusions

This chapter presents an extensive experimental investigation on the residual strength of damaged metallic pipes. Thirty-nine seamless pipe specimens with nominal diameter-to-thickness ratio of 21.04 have been successfully completed. The conclusions of this chapter can be drawn as follows:

(1) Different failure modes have been observed in this test. Intact pipe fails on its compression side close to the loading head in the form of an outward bulge. For a pipe with damage (a dent, a notch and the combined dent and notch) on its compression side, structure fails rapidly in the form of an inward, depressed region in the damaged place. Additional outward bulges along the damage axis also appear.

(2) For a pipe with a dent on its tensile side, a recovery of the existing dent appears in the beginning, and then it fails in the same mode as intact specimens. The fracture failure has been induced at a low loading force on the specimen with combined notch and crack on its tensile side.

(3) The ultimate strength of the intact specimen has a good agreement with the empirical formulas from former researcher, which demonstrates the accuracy of the strength test.

(4) Structural damage including a dent, a notch and combined damage on the compression side of pipe specimens has a large effect on their bending strength. The residual strength of damaged pipes on the tensile side mainly depends on the happening of fracture failure.

(5) A considerable reduction of bending strength is induced by a dent on the compression side of pipes, whereas only a light effect is observed for a dent on the tensile side due to damage recovery. The effects of impact and dent parameters such as rotational angle have not been quantitatively obtained due to the lack of sufficient data in this chapter.

(6) A considerable reduction of bending strength is induced by the metal loss on the compression side of specimens. Fracture failure dominates the specimen behavior when the metal loss is on its tensile side.

(7) The interaction effect between a single crack and the strength has been shielded by the strengthening effect of a heat affected region. A high hardness region is induced by the introduction of a crack through laser cutting technique.

(8) The combined damage has the most severe effect on the pipe residual strength. The largest reduction ratio of bending capacity has reached 11.63%, while the reduction ratio of critical curvature is 74.18%. Further research in Chapter 6 is going to quantify the effect of combined damage.

In summary, the initial comparison results of damaged specimens in this chapter have provided a general insight of the damage effects. The test data have built a solid foundation on the further quantification of damage effects on the residual strength of seamless metallic pipes. Combined with numerical simulations and regression analyses, the effects of damage on the structural strength in terms of bending moment and critical curvature will be identified in Chapters 4, 5 and 6.

Chapter 4

Quantification of a dent effect on the residual strength of metallic pipes*

In Chapter 3, an experimental investigation on the bending capacity of damaged seamless metallic pipelines has been completed. Artificial damage such as a dent, metal loss in terms of a notch, a crack and their combinations thereof is properly introduced. Meaningful phenomena on damaged metallic pipes are observed. Due to the limited number of specimens, however, there is a necessity to further quantify damage effects.

Therefore, in this chapter, numerical investigations on dented metallic pipes are performed. Structural damage in terms of a dent is accounted for, and the effects of pipe influential parameters and the relevant dent parameters are identified. The 4^{th} key question of this thesis in terms of dent damage and the 5^{th} key question " To what extent does the dent damage affect the structure residual ultimate strength in terms of bending moment and critical curvature? " have been solved.

In Section 4.1, the developed numerical models accounting for different parameters, capable of predicting of pipe residual strength, are described. Then, simulations of the tests on both intact specimens and dented specimens are carried out in Sections 4.2 and Section 4.3 respectively in order to validate the numerical models. Section 4.4 performs a study on the effects of different pipe influential parameters. Subsequently, in Section 4.5, parametric investigations on dent parameters are carried out based on the validated numerical models. Combined all these numerical data and existing test results, empirical formulas for residual strength of metallic pipes are proposed in Section 4.6. The chapter comes to conclusions in Section 4.7.

*This chapter is based on the papers Jie Cai, Xiaoli Jiang, and Gabriel Lodewijks. Numerical investigation of residual ultimate strength of dented metallic pipes subjected to pure bending. Ships and Offshore Structures. 13(5):519-531, 2018 [36], and Jie Cai, Xiaoli Jiang, Gabriel Lodewijks, Zhiyong Pei, and Weiguo Wu. Residual ultimate strength of seamless metallic pipelines under a bending moment - a numerical investigation. Ocean Engineering. 164:148-159, 2018 [38].

4.1 Description of numerical models

In this section, numerical models on both intact pipes (Section 4.1.2) and dented pipes (Section 4.1.4) are described. Fitting method of material relation is explained in Section 4.1.1 based on existing material parameters. Furthermore, the simplification of dent damage is performed in Section 4.1.3, which will facilitate the following research.

The numerical models have been developed in ABAQUS/Standard [1] through Python for the simulation of test specimens and the following investigation of dent parameters. For intact pipes, symmetry has been introduced for the sake of simulation efficiency. For dented pipes, symmetry has not been taken into account any more due to the occurrence of damage at the pipe center. Meanwhile, two types of models for dented pipes are used to clarify the possible boundary effect on simulation: full model with the same configuration as the test (Figure 4.1) and simplified model only accounting for central segment under pure bending (Figure 4.2). Comparison results are presented in Section 4.3.1.

A strip is introduced to mimic both the loading and the supports of the specimens in numerical predictions, as illustrated in Figure 4.1. A friction coefficient of 0.26, as estimated in engineering practice for steel [67], is deployed for the contact between specimen and strips. Moreover, a surface-to-surface contact strategy with finite sliding is used during simulation. In this way, the bending moment has been produced through the two vertical downward forces, leading to the same four-point bending pattern as used in the physical test.

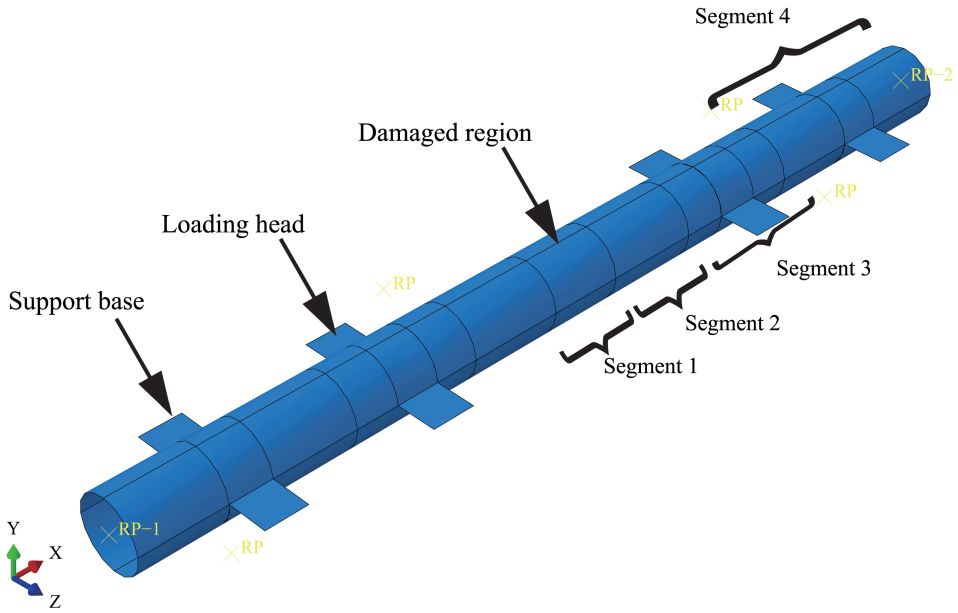

Figure 4.1: Full pipe model based on the real test configuration (Symmetry is only used for intact specimens).

In order to avoid the pre-failure that is caused by the loading heads, the side structures (Segment 4, as seen in Figure 4.1) are reinforced by an increase of the wall thickness which represents the function of half-sleeves in the physical tests. Furthermore, the initial imperfection in terms of a wave-type is introduced for all the models in the form of the combination of the first two orders of the eigenvalue buckling modes. Since the initial imperfection has not been measured during the test, the imperfection amplitude in simulation (as seen in Figure 4.3) is set to $3\%t$ (normally between $1\%t$ and $12\%t$, t is pipe thickness) based on the recommendation from [53]. The impact induced residual stress has not accounted for due to the lack of real test data.

An elastic-plastic material with von Mises yield criterion and isotropic hardening is deployed. When the anisotropy characteristic in terms of different material yield stress is accounted for in the following parameter investigation in this chapter, the Hill48 criterion [75] is deployed. For both intact and dented models, the cylindrical shells are modeled with a curved three-dimensional shell element (S8R5). It is a 8-node, quadrilateral element with reduced integration and five degrees of freedom in each node (three displacement components and two in-surface rotation components), providing both an accurate and economical simulation. The discrete rigid element R3D4 [1] is employed for the strips.

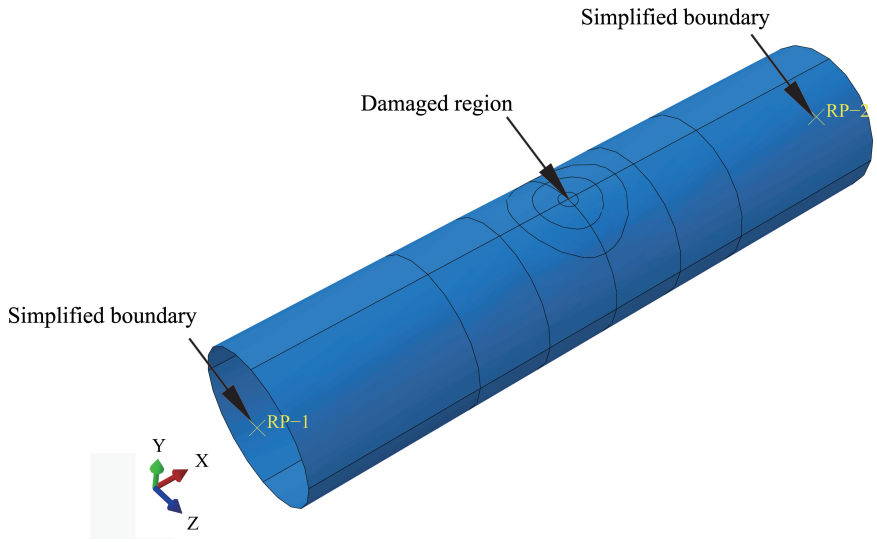

Figure 4.2: Simplified pipe model.

4.1.1 Material properties

A typical pipe material Q345B [61] is deployed in the pipe test, which is a type of pipe structural steel with high strength and large ductility. An elastic-plastic property with von Mises yield criterion and isotropic hardening is deployed. The strain-hardening effect of material is developed by the Ramberg-Osgood equation [108] based on measured material parameters from the test, as seen in Equation (4.1). Where n is the material constant, ε_{eng} and σ_{eng} are the engineering strain and stress, respectively. It should be noted that an assumption of

0.002 plastic strain for ductile material at yield point is made in this equation.

$$\varepsilon_{eng} = \sigma_{eng}/E + 0.002(\sigma_{eng}/\sigma_y)^n \tag{4.1}$$

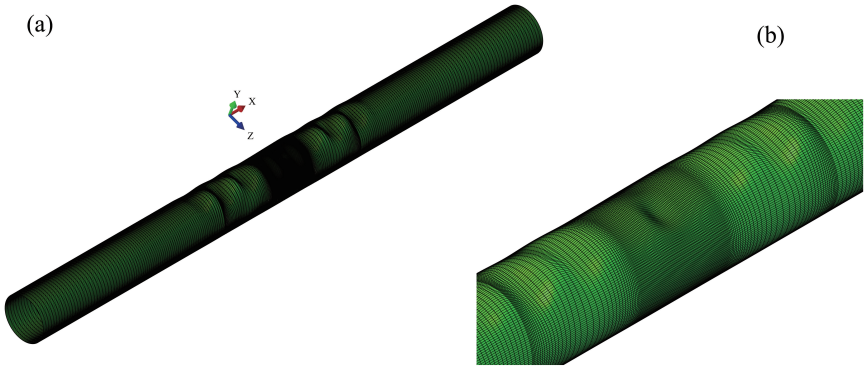

Figure 4.3: (a) intial imperfection in terms of wave-type on the pipe specimens (deformation scale factor is set to 20 for the sake of clarity); (b) details of imperfection.

In order to circumvent the stress triaxiality in necking zone during material coupon test (Section 3.2.1 in Chapter 3), an equivalent fitting method is used. Thus, the true stress/strain curve with large strain can be obtained and used for simulation, as shown in Figure 4.4. In this method, basic material parameters including the material yield stress (σ_y), ultimate tensile stress (σ_u) and the maximum elongation (e_u) with an assumption that σ_y, σ_u and material failure appears on the strain of 0.002, $e_u/3$ and e_u, respectively [33, 101].

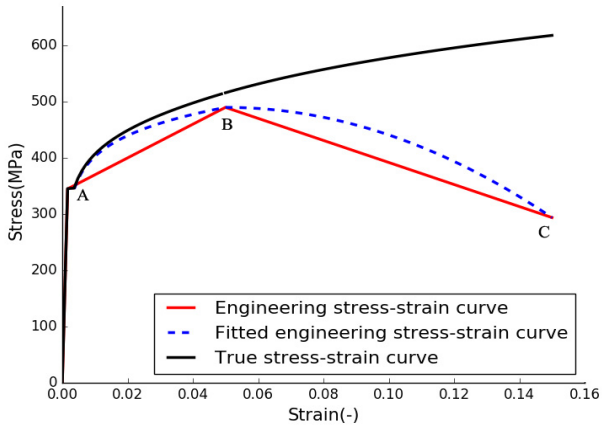

Figure 4.4: The fitted stress-strain curve of material.

This equivalent fitting method for true stress/strain relation is simply summarized as follows. A Python script is developed based on this method, as seen in Appendix A.

- Three reference points (A, B, C) based on the material parameters are first introduced, as seen in Figure 4.4. Where Point A is the yield point, Point B is the ultimate tensile stress point with the corresponding strain of $e_u/3$, Point C is the material failure point. The failure stress of material is assumed as $0.6R_m$ at the maximum elongation of e_u. Thus, the original reference curve is obtained, as seem from the red line.
- Then, the upward curve AB is fitted by Ramberg-Osgood equation (Equation (4.1)). The downward curve BC is approximated by a parabolic relation, as show in Equation (4.2), where $\alpha_s = \frac{\sigma_u(1-\beta_m)}{e_u^2(1-\alpha_m)^2}$, $\beta_m = 0.6$, $\alpha_m = 0.33$, σ_u is the ultimate tensile stress. The fitted engineering relation of material is shown from the blue broken curve.
- After obtaining the fitted engineering stress/strain relation, the true stress/strain relation is then easily developed, as seen from the black curve. Where the upward part of curve is approximated based on the theoretic relations in Equations (4.3) and (4.4), and the downward part of curve is approximated based on Equation (4.5). Where ε_{true} and σ_{true} are the true strain and stress of material in upward part respectively, ε_{true1} and σ_{true1} are the true strain and stress of material in downward part respectively, K_1 and $n1$ are material constants. The values of parameter K_1 and $n1$ can be easily derived from the known upward relation.

$$\sigma_{eng} = \sigma_u - \alpha_s(\varepsilon_{eng} - \frac{e_u}{3})^2 \tag{4.2}$$

$$\sigma_{true} = \sigma_{eng}(1+\varepsilon_{eng}) \tag{4.3}$$

$$\varepsilon_{true} = ln(1+\varepsilon_{eng}) \tag{4.4}$$

$$\sigma_{true1} = K_1\varepsilon_{true1}^{n1} \tag{4.5}$$

4.1.2 Intact numerical model

For the intact model that does not contain any artificial damage, the symmetry and shell element are deployed as mentioned above. The entire model has been partitioned into four basic segments for different mesh strategy, as shown in Figure 4.1. In Segments 1 and 3, a relative dense mesh is assigned with the size of 4 *mm* in the hoop direction and 3 *mm* in the logitudinal direction, while a coarse mesh is assigned to Segments 2 and 4 with the largest size of 12 *mm* in their center locations through a double-bias strategy. In other words, there are at least twenty-one elements within a half-wave length (expressed as $\lambda_{cl} = 1.728\sqrt{Rt}$ [107]) of refined regions, while there are at least five elements within a half-wave length of the coarse regions. An overall of 100000 elements for each model is therefore produced. A displacement-control strategy with a maximum of 0.001 *mm* downward displacement in each increment is deployed for loading so that every detailed variation of the structural behavior of specimens can be traced. A central reference point that is coupled with the corresponding cross-section has been employed for the symmetrical boundary condition through a kinematic coupling method. A slight anisotropy in terms of yield stress ($\sigma_{hy}/\sigma_y = 1.063$) is set in the intact model due to the observation from material tensile test.

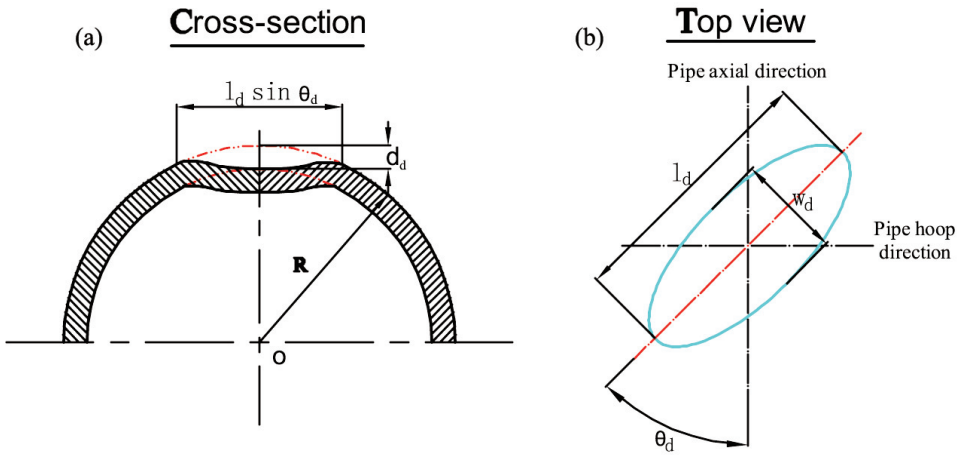

Figure 4.5: Sketch of a plain dent on pipe surface: (a) dented cross-section; (b) top view.

4.1.3 Dent simplification

A dent is a permanent plastic deformation on pipe wall that produces a gross distortion of the pipe cross-section. In this thesis, only a plain dent with a smooth curvature variation is accounted for, expressing as a function of dent length (l_d), dent width (w_d), dent depth (d_d), dent angle (θ_d) and dent location, as illustrated in Figure 4.5. The dent shape is postulated as a cosinusoidal shape, as expressed in Equation (4.6), where ω is the depth variation of the dent. In addition, the dent angle is defined as the angle between the dent axis in its length direction and the pipe axial direction, increasing along the clockwise direction, as seen in Figure 4.5 (b). Hence, a dent with the angle of 0^o runs in the pipe's longitudinal direction. In this definition, the l_d should be always larger than w_d in order to avoid ambiguity. A Python script of a dent on the pipe surface is presented in Appendix B.

$$\omega_d = d_d \cdot (1+\cos(2\pi x/l_d)) \cdot (1+\cos(2\pi y/w_d))/4 \tag{4.6}$$

4.1.4 Dented numerical models

In this section, two types of numerical models for dented pipes are developed. One is a full model [38], which is the same with the test configuration, the other is a simplified model only accounting for the central segment of the specimen under pure bending [36]. The location of the dent is the center of pipe cross-section on either the compression side or the tensile side of pipe surface.

Full dented model

On the basis of the intact numerical model, the full model of specimen with dent is developed, accounting for the variation of dent angle and size. The mesh is largely refined in the damaged region (Segment 1 in Figure 4.1) in order to avoid the artificial bending moment, with the minimum mesh equal to 2 *mm*, i.e. less than 3.2% of the half-wave length

($\lambda_{cl} = 1.728\sqrt{Rt}$) of cylindrical shells. The symmetry strategy has not be deployed any more due to the introduce of structural damage. An overall of 170000 elements for each full dented model is therefore produced.

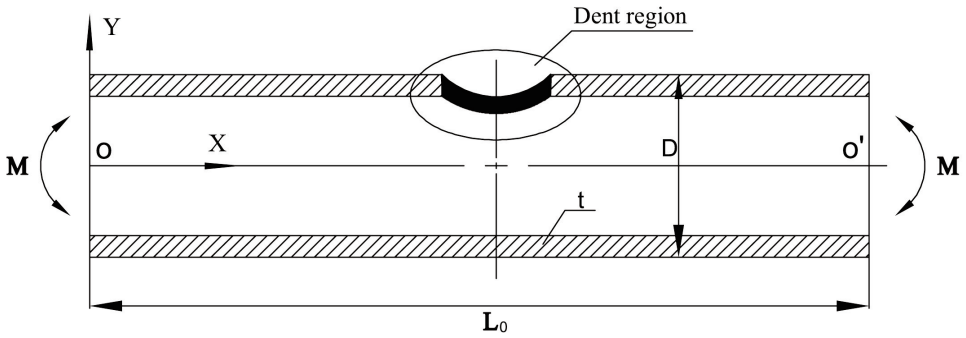

Figure 4.6: Sketch of simplified dented pipe subjected to pure bending moment.

Simplified dented model

In order to save simulation sources and identify the boundary effect, a simplified dented model is also developed through reasonable simplifications, as seen in Figure 4.6. A simply-supported boundary condition is deployed. Rotations along X and Y axis at both pipe ends are restricted so that no torsion would be induced during simulation. All the translations are restricted in the pipe end O, while the axial translation is set to free in the other end O' such that no extra axial force would be induced. The symmetry of model has not been introduced due to the occurrence of a dent.

The mesh strategy of the FEA model is shown in Figure 4.7, partitioning the entire model into three different segments. The length of central segment (segment 1) is set to $1D$ (D is the outer diameter of pipe) with a maximum element size in pipe longitudinal and hoop direction of 3 *mm* and 4 *mm*, respectively, i.e. less than 9% of the critical half-wave length ($\lambda_{cl} = 1.728\sqrt{Rt}$). Segment 2 is a mesh transition region with a length of $0.5D$, arranging with a biased mesh, while segment 3 has a coarse distribution of mesh with the maximum element size of 12 *mm*.

In the damaged region, as illustrated in Figure 4.7(b), mesh is largely refined. The geometry of this region is further partitioned into three concentric circular regions, with the radius of $0.1l_d, 0.35l_d$, and $0.6l_d$, respectively. The aim of such mesh strategy is to fashion a well-organized mesh distribution so that the possible artificial local bending stress and stress concentration would be avoided. The maximum mesh size of inner circle is strictly limited within 2 *mm* with a structured mesh strategy, i.e. less than 4% of one half-wave length λ_{cl} of cylindrical shells. The maximum mesh size of outer regions is limited within 3 *mm* with a sweep mesh strategy, i.e. more than 14 elements in one critical-half wavelength.

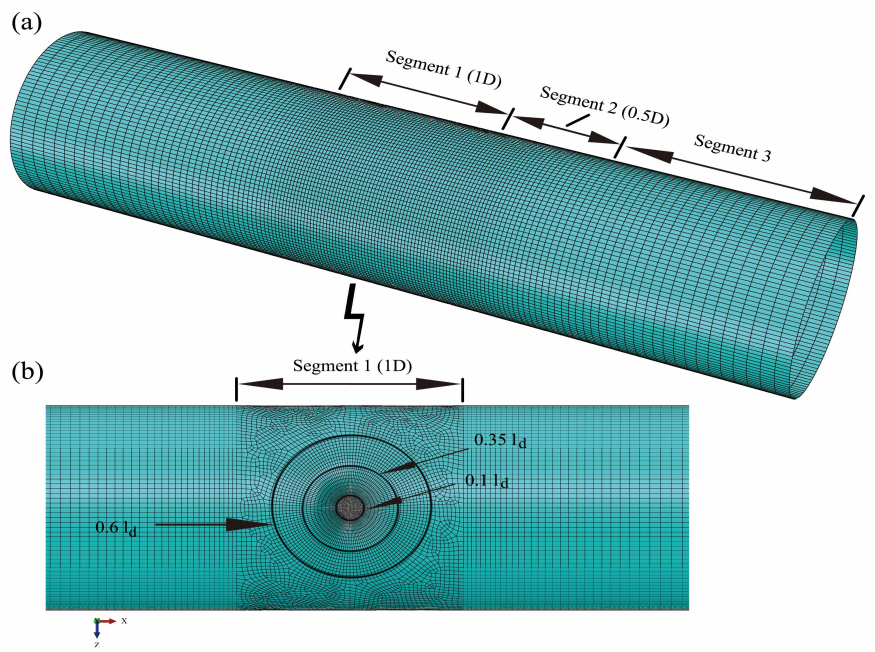

Figure 4.7: FEA model of simplfied dented pipe: (a) general mesh distribution; (b) refined dent region.

4.2 Simulations of intact specimens from tests

In this section, the intact specimens from tests are simulated based on the developed numerical models in the previous section. The simulation results in terms of structural failure modes, strain distributions and bending moment-curvature diagrams have been compared and discussed.

In this chapter, bending moment is normalized by the plastic bending moment $M_y = 4R_a^2 t\sigma_y$; Meanwhile, bending curvature κ is normalized by the curvature-like expression $\kappa_0 = t/4R_a^2$. It should be noted that only global curvature as discussed in Chapter 3 is selected for comparison between test and numerical simulation for the sake of accuracy. The selected locations for calculation of the global curvature in simulation are exactly the same with tests, while the bending moment is the resultant of all the node forces multiplying their corresponding force arms in the central cross-section of the specimen. For the proposed formulas of damaged pipes in Section 4.6, the results from intact pipes (M_i and κ_i) are used as reference values.

4.2.1 Structural failure modes and strain distribution

The comparison results of structural failure modes of specimens between numerical prediction and test are illustrated in Figure 4.8. As a result of the increase of the structural deformation in the form of ovalization in the pipe cross-sections, the specimens fail due to

the increase of bending moment. The initiation of failure for an intact specimen appears on the top region far from the center of the specimen with an extra large ovalization in the same cross-section. The failure mode and failure location between the test and the simulation have a good agreement with each other.

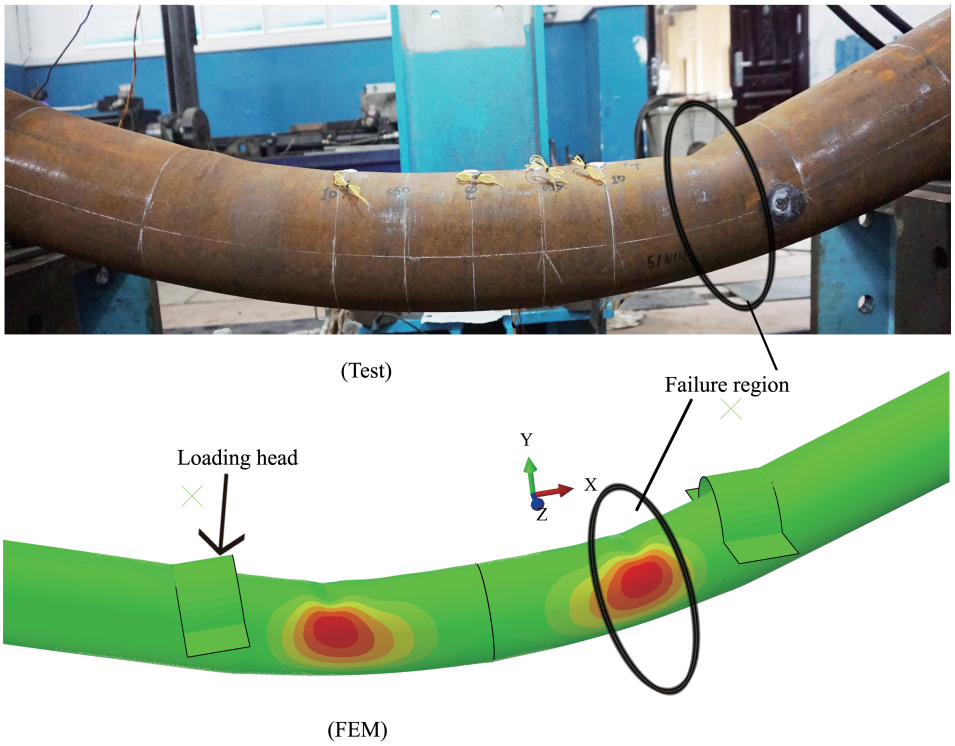

Figure 4.8: Comparison of failure mode of intact specimen (S1N4).

Figure 4.9 shows the evolution of axial strain (ε_{11}) along the pipe longitudinal path (AB) and the hoop strain (ε_{22}) along the pipe hoop path (CD) in four different loading stages of specimen S1N4, respectively. The test results from the measurement of strain gauges in specific points and corresponding stages (such as stage1, stage2 and stage3) are also presented. The corresponding locations for strain measurement on the intact specimen are illustrated in Figure 3.19. Along the longitudinal direction of the specimen, including Point A (pipe center), 05D ($\backsim 0.21AB$), and 1D ($\backsim 0.42AB$), the strain gauges are put on the top side (compression side) of the pipe. Only axial strains are presented due to the lack of data. The numbers in this figure indicate the measured directions of the strain gauges. It is observed that ε_{11} in the beginning stages is quite benign with a uniform distribution, whereas a large increase and localization of strain happen in the critical region that initiates structural failure (Figure 4.9 (c)). The critical region that has the largest variation along the pipe axis is between $0.6L_{AB}$ and $0.8L_{AB}$ (L_{AB} is the half length of pipes under pure bending), matching well with the location of outward bulge in the test. Most of the strains that were measured from test lie on or close to the predictions curves, as seen in Figure 4.9

(c). However, an exception of strain distribution happened in point A, which locates in the central cross-section of the pipe. Such discrepancy may be introduced by the use of the symmetrical boundary condition during simulation. For the hoop strain ε_{22}, as shown in Figure 4.9 (d), it starts with a small tension value on point *C* in the beginning stages, and then turns to a large compression value from the lateral region ($0.2L_{CD}$) all the way to the bottom ($0.5L_{CD}$), where L_{CD} is the circumference length of the pipe cross-section. This phenomenon demonstrates that the ovalization largely increases in these regions.

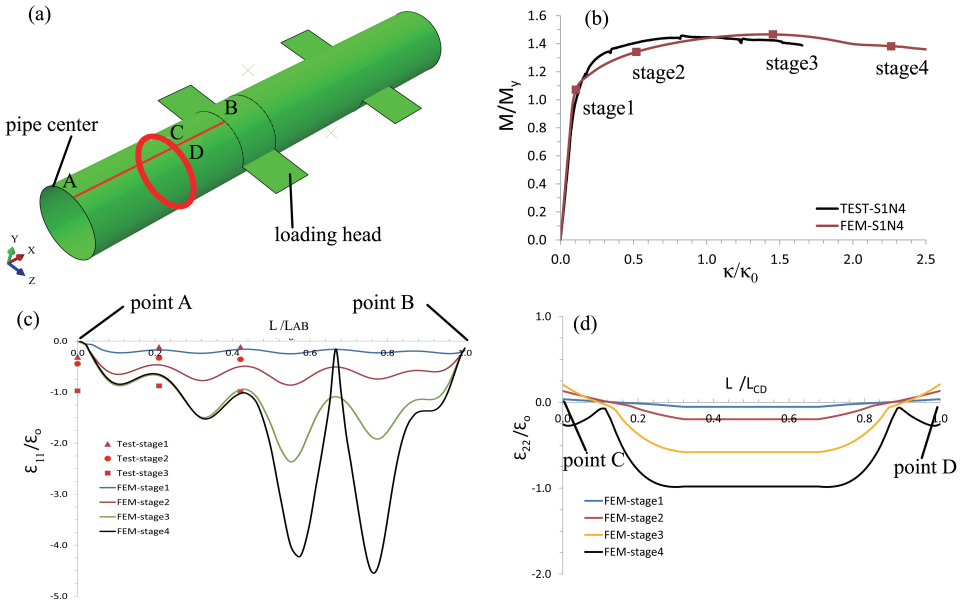

Figure 4.9: (a) sketch of representative paths on specimen surface; (b) four stages during the loading of specimen S1N4; (c) strain along longitudinal path of pipe specimen (AB, S1N4); (d) strain along hoop path of specimen (CD,S1N4).

4.2.2 Moment-curvature diagrams

The comparisons of bending moment-curvature diagrams between test data and numerical predictions are presented in Figure 4.10, which shows a good agreement. Only small scatters happen in the hardening and post-buckling stages. As observed in Figure 4.10, there is a slight recovery in terms of the bending moment in the test. This is due to the instability of the real support boundary conditions when the specimen suffers from large curvature. Instead, there is no such recovery in the simulation results due to its boundary stability.

Table 4.1 lists the comparison results on intact specimens. For the prediction result of M_{cr}, less than 2.25% discrepancy has been obtained for the intact specimen. The discrepancy of κ_{cr} is less than 2.95% for intact specimen. The discrepancies may be introduced by the measurement of material properties and the selection of friction parameter, as discussed in Chapter 3. The elastic-plastic failure pattern is dominant with a smooth failure procedure. For an intact specimen, M_{cr} is larger than 1.32 times of M_y.

Table 4.1: Comparison results on intact specimens (Dimension unit: mm).

S.N.	D	t	D/t	M_{cr}(Test) (kNm)	M_{cr}(FEA) (kNm)	κ_{cr} (Test) (1/m)	κ_{cr}(FEA) (1/m)
S1N1	168.09	7.90	21.28	104.37	103.39	0.422	0.421
S1N2	167.36	7.87	21.27	103.65	102.43	0.439	0.428
S1N3	167.55	7.92	21.16	103.21	101.35	0.441	0.428
S1N4	167.01	7.84	21.30	102.71	100.40	0.401	0.412

4.3 Simulations of dented specimens from tests

In this section, simulations for dented specimens are preformed based on the developed numerical models in Section 4.1.4. A photo of the dent damage in both test specimen and numerical model is shown in Figure 4.11. A comparison between results from the full and simplified dented models has been carried out to identify the effect of boundary.

4.3.1 A comparison of numerical models

In order to identify the discrepancies between the developed full dented model and the simplified dented model (in Section 4.1.4), simulations on the test specimens are first carried out. Tables 4.2 and 4.3 show the prediction results of dented specimens in terms of critical bending moment (M_{cr}) and curvature (κ_{cr}). "S" denotes the results obtained by the simplified dented model, while "F" denotes the results obtained by the full dented model. "dis-ST-M" denotes the discrepancies of critical bending moment between simplified numerical models and test results, while "dis-FT-M" denotes the discrepancies between full numerical models and test result. "dis-SF-M" denotes the discrepancies of critical bending moment between simplified models and full models. The same definition is for the critical curvature.

It is found that both models can provide a good prediction for pipe results in terms of bending moment and curvature. As seen in Table 4.3, the full model overestimates the pipe results in terms of moment slightly. The maximum discrepancy on bending moment between full model and test is 3.47%, while the value between simplified model and test is -6.44%. A relative large discrepancy exists for critical curvature. The maximum discrepancy on curvature between full model and test is -34.76%, while the value between simplified model and test is -38.41%. However, both simulations provide an underestimation prediction on the test results, which is on the safe side. Considering the uncertainties for curvature measurement in test, it is still well acceptable. It is found that the improvement of the accuracy by using full model is not significant. The simplified model can also provide predictions as accurate as the full model. Hence, results from the two models will not be intentionally distinguished in the following research.

Table 4.2: Comparison results on dented specimens through two types of FEM models (Dimension unit: mm; Angle unit: degree; Dents are on the compression side of specimens).

S.N.	D	t	D/t	Dent ($l_d \times w_d \times d_d$)	Dent angle	BM(test) (kNm)	BM(FEA) (kNm)	κ(test) (1/m)	κ(FEA) (1/m)
S2N1	169.21	8.25	20.51	$89 \times 68 \times 10.3$	90	92.57	91.75 (S)	0.154	0.124 (S)
							93.86 (F)		0.143 (F)
S2N2	168.23	8.13	20.69	$100 \times 75 \times 10.3$	90	93.55	87.53 (S)	0.109	0.108 (S)
							90.04 (F)		0.124 (F)
S2N3	169.38	7.90	21.44	$130 \times 60 \times 10.3$	45	91.65	92.25 (S)	0.158	0.122 (S)
							94.83 (F)		0.157 (F)
S2N5	168.74	8.15	20.70	$110 \times 85 \times 10.3$	90	90.97	87.00 (S)	0.164	0.101 (S)
							89.18 (F)		0.107 (F)

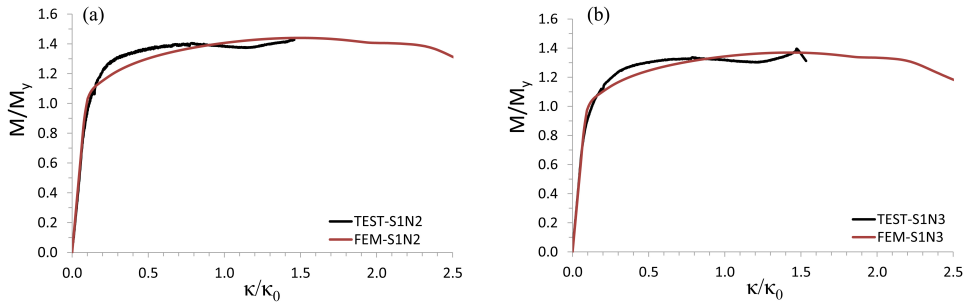

Figure 4.10: Comparison between numerical and test results in terms of bending moment-curvature diagram for intact specimens: (a) specimen S1N2; (b) specimen S1N3.

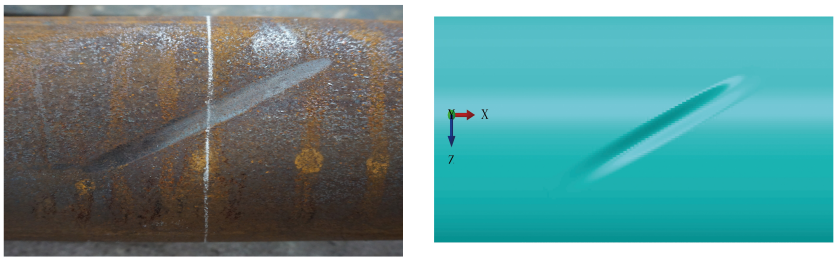

(dent in test) (dent in FEM)

Figure 4.11: A photo of dent damage in both test specimen and numerical model (θ_d=45^o).

Table 4.3: Discrepancies between simplified dented models and full dented models.

S.N.	dis-ST-M (%)	dis-FT-M (%)	dis-SF-M (%)	dis-ST-κ (%)	dis-FT-κ (%)	dis-SF-κ (%)
S2N1	-0.89	1.20	2.06	-19.48	-7.14	13.29
S2N2	-6.44	-3.75	2.79	-0.92	13.76	12.90
S2N3	0.65	3.47	2.72	-22.78	-0.63	22.29
S2N5	-4.36	-1.97	2.44	-38.41	-34.76	5.61

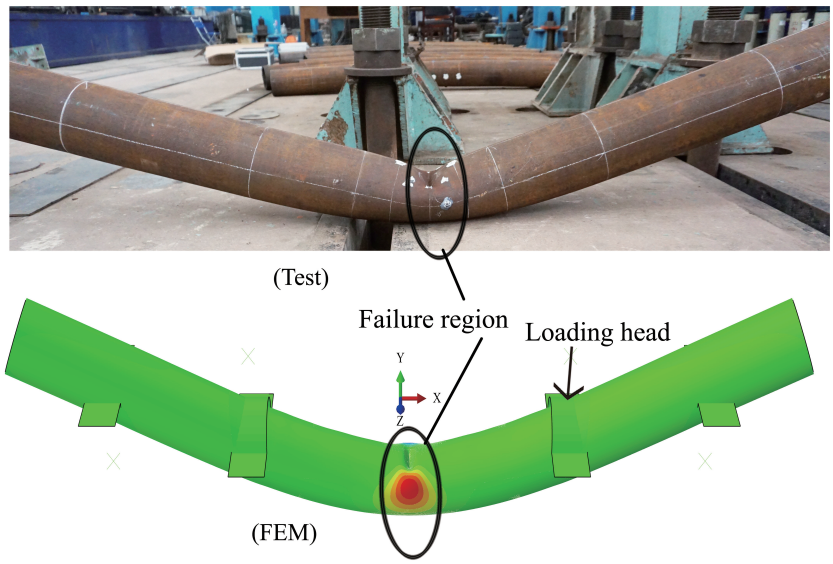

Figure 4.12: Comparison of failure mode of the specimen with dent damage (S2N2, full model).

4.3.2 Structural failure modes

The comparison of the structural failure mode of dented specimens is illustrated in Figures 4.12 and 4.13. The result shows that a similar failure mode has been simulated in the local dented region. For the pipe with a dent, the failure initiates and propagates in the dent region in the form of an inward bulge.

The failure of the structure is also reflected by the variation of strain, as illustrated in Figure 4.14. The test results from the measurement of strain gauges in specific points and corresponding stages are presented, accompanied by the simulation results. It shows the evolution of both axial strain (ε_{11}) and hoop strain (ε_{22}) along the pipe longitudinal path and the hoop path across the dent center (the chord length of CD is 120 mm), respectively. The strain here is normalized by ε_0, which can be expressed as $\varepsilon_0 = \kappa_0 D/2$. It is observed that the occurrence of a dent has changed the strain distribution from the first beginning, and a localization of strain appears in the dented region, concentrating on both the dent center

and the dent edge (Figures 4.14 (c) and (d)).

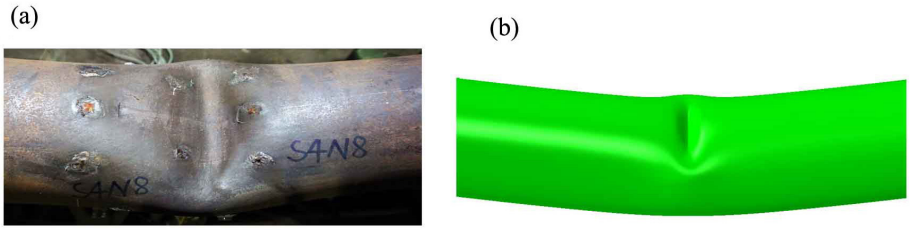

Figure 4.13: Comparison of failure mode of the specimen with dent damage (S2N1 in Chapter 3, simplified model).

Most of the strains measured from test lie on or close to the predictions curves. However, discrepancy exists due to the limit measurement range of stain gauges ($\pm 3\%$), workmanship of gauge and the possible shear force effect that was introduced by loading heads. For the hoop strain ε_{22}, as shown in Figure 4.14 (d), it starts with a small compression value on point *C* in the beginning stage in the outside dent region, and then turns to a large tensile value inside the dent region, decreasing all the way to the dent center. This phenomenon implies the fashion of the inward bulge and the increasing tendency of the ovalization in the dented cross-section.

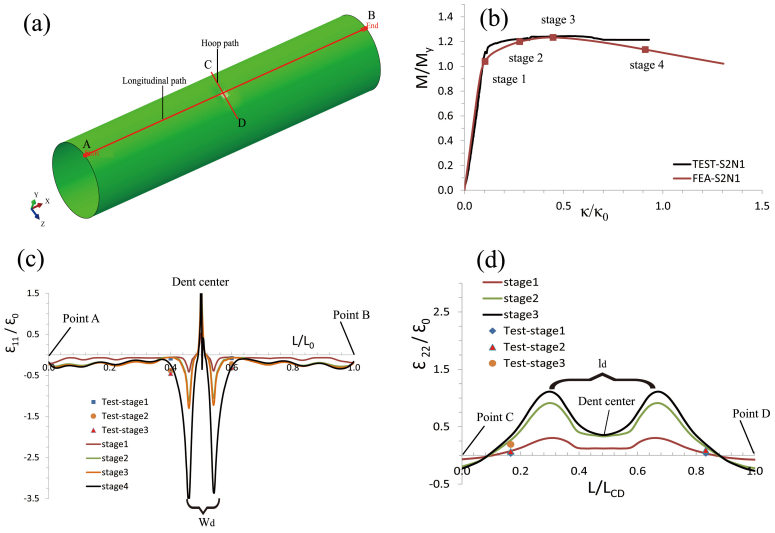

Figure 4.14: (a) sketch of representative paths on specimen surface (S2N1); (b) four stages during the loading procedure; (c) strain along the longitudinal path AB; (d) strain along the hoop path CD.

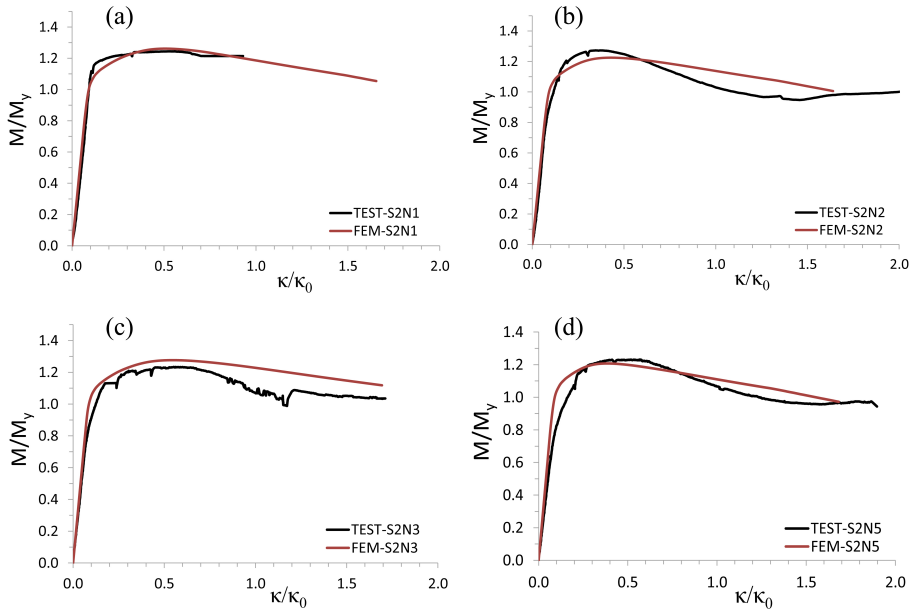

Figure 4.15: Comparison between numerical and test results in terms of bending moment-curvature diagram for specimens with a dent: (a) specimen S2N2 with 90^0 *dent on compression side; (b) specimen S2N3 with* 45^0 *dent on compression side; (c) specimen S2N5 with* 90^0 *dent on compression side.*

4.3.3 Moment-curvature diagrams

The representative bending moment-curvature diagrams for the comparison between test data and numerical predictions are presented in Figure 4.15. Table 4.2 lists all the comparison results in terms of bending moment and critical curvature.

Three specimens (S2N1, S2N2 and S2N5) contain dent in 90^o on the compression side, while the specimen S2N3 contains dent in 45^o on the compression side. The occurrence of a dent has changed the variation tendency of the bending moment-curvature diagram, initiating a rapid failure of specimen and considerably reducing the critical bending curvature. It is found that, compared with the intact specimens in test, M_{cr} was decreased by 6.5%-11.5% due to the occurrence of a dent.

The diagrams from Figure 4.15 show a satisfying prediction in terms of failure tendency and the maximum bending moment, i.e. less than 6.5% discrepancy compared with the test (Table 4.3). Meanwhile, the simulation of the critical curvature provides a little underestimation for the test specimens, which is on the safe side. The reason of some discrepancies between predictions and tests, such as case S2N2 and S2N5, is mainly because of the material discrepancy, which has been discussed in the Chapter 3.

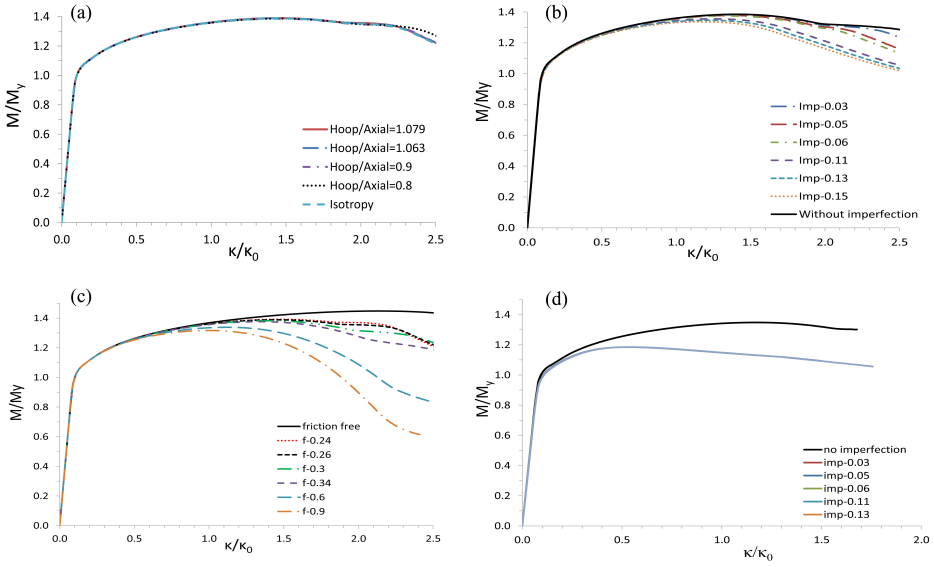

Figure 4.16: Normalized bending moment-curvature diagram with the changing of different parameters: (a) varying of material anisotropy (based on specimen S1N4); (b) varying of initial imperfection (based on specimen S1N4); (c) varying of friction coefficient (based on specimen S1N4); (d) varying of intial imperfection (based on specimen S2N1).

4.4 Investigation of pipe influential parameters

Based on the simulation of test specimens in the previous section, sufficient confidence has been gained to use the developed numerical models for further investigation. Thus, in this section, the effects of pipe influential parameters that could affect the structural behavior of metallic pipes are investigated through simulations.

4.4.1 Anisotropy effect

As indicated from the material tensile tests from Section 3.2 in Chapter, anisotropy in terms of different material yield stress has been observed, in spite of a slight anisotropy of seamless pipe compared with welded-pipes. Its effect on strength is investigated in this section. The Hill48 yield criterion [75] is deployed to take into account the anisotropy feature in numerical simulation. In this place, the material yield stress in the pipe hoop direction varies when the yield stress keeps constant in the pipe longitudinal direction. As seen in Figure 4.16 (a), the effect of anisotropy on pipes with relative thick D/t is insignificant. The results imply that the yielding stress in the pipe longitudinal direction dominates the pipe residual strength.

4.4.2 Initial imperfection effect

The initial imperfection in terms of a wave-type is investigated, as seen in Figure 4.16 (b) and (d). Six types of initial imperfection with different imperfection amplitude-to-thickness ratios are accounted for. The variation of amplitude lies between 3%t-15%t (t is pipe thickness), while the specific shape of imperfection is from the eigenvalue buckling analysis with a combination of the first two-order eigenvalue shape. Both the intact specimen S1N4 and dented specimen S2N1 are adopted with the same friction coefficient and material property (L7 in Table 3.7 in Chapter 3) in each case. A very interesting phenomenon has been observed from the simulation results. It can be seen that the initial imperfection has a negative effect on both bending strength and curvature of a pipe without damage, whereas it can hardly affect the structural strength of a dented pipe. Moreover, such effect is still small for an intact specimen, when the imperfection is no larger than 0.06t. A much larger effect happens when the imperfection is larger than 0.11t. For instance, for the case with imperfection of 0.15t, the decrease of critical curvature reaches by 17% compared with the perfect case. Therefore, it can be briefly concluded that the effect of manufacturing induced initial imperfection is insignificant and can be neglected in the FEM simulation for the pipe with a considerable dent size. The shielding effect of a dent appears.

4.4.3 Friction effect on test set-up

In the four point bending test in reality, the boundary condition of pipe specimen is affected by the friction between the specimen and the strips. Therefore, such friction may affect the strength behavior and corresponding curvature variation. An investigation of the friction effect has been carried out with the variation of friction coefficient between 0 and 0.9. As seen in Figure 4.16 (c), the introduce of friction results in a considerable variation of the moment-curvature diagram compared with the friction-free case. However, the effect is small when the friction coefficient lies in the normal engineering domain, say 0.2-0.4. Then, a significant effect has been observed with the further increase of friction coefficients. For instance, compared with the case with friction of 0.26, the decrease of critical curvature in the case with friction of 0.9 reaches as large as 30.33%. The reason can be explained as follows: an equivalent axial compression force has been introduced by the loading heads with the increase of rotational angle of the specimen during the quasi-static loading procedure. Under a center range, the axial force is small and can be counterbalanced by the friction force. Hence, the structure stays stable. The friction force helps to maintain such stable to some extent. The larger the friction force is, the larger the introduced equivalent axial force the test set-up can counterbalance. As a consequence, a lower bending capacity of the specimen is produced due to the effect of such equivalent compression force. It can be concluded that the structural response is quite sensitive to the frictions that have been introduced by the test configuration.

4.4.4 Diameter-to-thickness ratio

As one of the critical parameters, the pipe diameter-to-thickness ratio (D/t) affects the residual ultimate strength and corresponding failure mode of metallic pipes. With the decrease of D/t ratio, the failure mode of structures will gradually change from an elastic buckling to

an elastic-plastic failure or even fracture failure. Figure 4.17 presents the variation of normalized bending capacity with respect to D/t between 20 and 50. A plain dent is postulated in the pipe center on the compression side of the pipe surface. All the dent angles are set to 90^o (the pipe hoop direction). It is found that, with the increase of D/t, the residual strength of a dented pipe decreases approximately in a linear way.

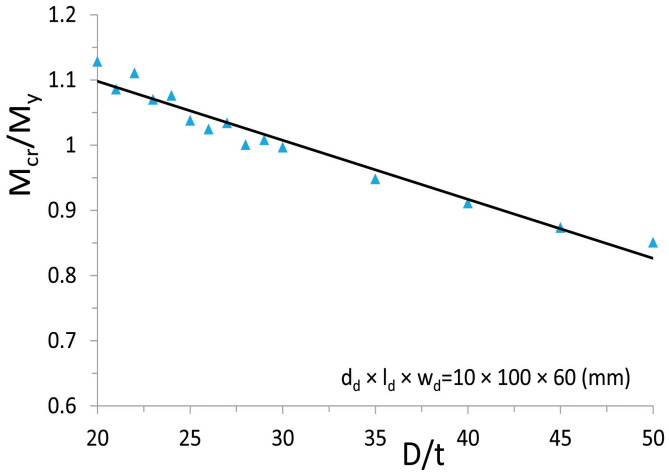

Figure 4.17: Bending capacity of a dented pipe with varying of D/t.

Figure 4.18 denotes the normalized bending moment-curvature diagram of dented pipes with varying of D/t ratio. The curvatures here are calculated from the longitudinal strain (ε_{11}) on the bottom of pipe central cross-section ($\kappa = 2\varepsilon_{11}/D$). It implies that different failure modes have happened. For instance, for a pipe with D/t of 21, the elastic-plastic failure happens with $M_{cr} = 1.09M_y$, whereas for pipe with $D/t = 50$, elastic buckling happens with a small ultimate bending moment, equal to $0.77M_y$. The structure fails smoothly with the increase of bending moment for pipes with $D/t = 21$. Structure first reaches the linear limit point, as see from Point A. Then, the plastic deformation starts to occur and expanding until Point B due to the material hardening effect. When the bending energy is keeping accumulation, the limit point C has been reached. Afterwards, the strength capacity of pipes does not increase anymore, but gradually decreases with the rapid increase of plastic deformation until the critical collapse point D has been reached. In contrast, for pipes with large D/t, as seen in the dotted curve of $D/t = 50$. A sudden collapse happens once the limit point has been reached.

4.5 Investigation of dent parameters

By changing different dent parameters, the effect of each dent parameter is identified through developed numerical models in this section. Both simplified numerical model (for dent orientation and location) and full numerical model (for other dent parameters) have been used for simulation due to their similarity in simulation results. The principal dimension of pipes from Table 4.4 is used for the following research with simplified model, while the principal

dimension from specimen S2N1 in Table 4.2 is used for full dented model. The material relation is obtained by the method from Section 4.1.1, using the measured parameters from material test.

A moderate size of dents is selected, as explained from the research scope of this thesis in Chapter 1. The selected d_d/t in the following research of this chapter is between 0.13 and 2.0, and the normalized dent length $l'_d/\sqrt{Rt}$ is between 0.4 and 5.0 (l'_d is the dent length in pipe hoop direction).

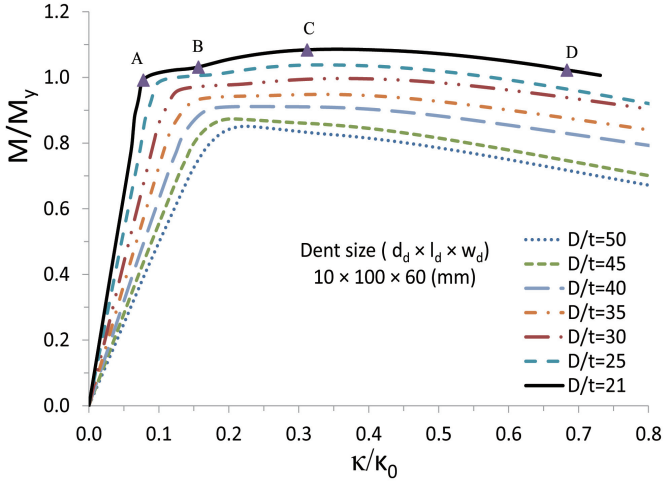

Figure 4.18: Bending moment-curvature diagrams with varying of D/t.

Table 4.4: Principal dimension of pipes for the simulation of dent parameters.

Pipe type	Diameter D(mm)	Thickness t(mm)	Length L_0(mm)	D/t	L_0/D
Seamless	168.3	7.9	720	21.3	4.28

4.5.1 Effect of dent orientation

The dent orientation affects the load carrying capacity of damaged pipes. Figure 4.19 shows the diagram with respect to the critical bending moment and dent angle. A moderate dent ($d_d \times l_d \times w_d$=$10 \times 100 \times 60$ mm) is postulated in pipe surface on the compression side. As demonstrated by the simulation results, the larger the dent rotation angle (θ_d) is, the smaller the residual ultimate strength will be. In other words, a pipe with a hoop dent on its compression side is the most critical scenario for the bending condition.

Figure 4.20 shows the membrane stress distribution of a dented pipe with the varying of the dent rotation angle. Only two angles are presented here for clarity reason. The highest stress happens inside the dent. There is a low compression stress region in terms of σ_{11} along the pipe longitudinal direction, whereas a large tensile stress in terms of σ_{22} occurs at the dent tips. With the increase of the dent rotation angle, the compression region is increasing and the distribution of both stress components become uniform.

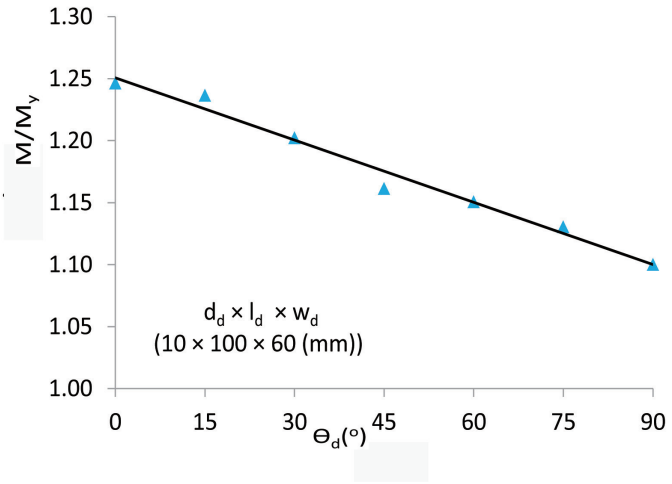

Figure 4.19: Bending capacity of a dented pipe with varying of dent rotation angle.

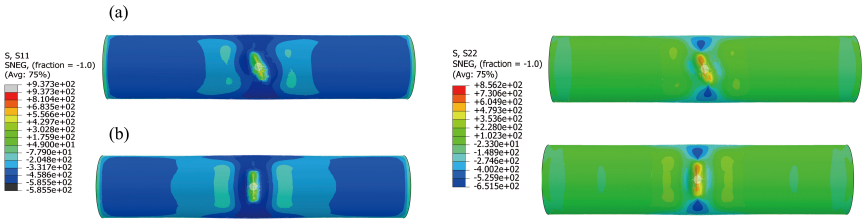

Figure 4.20: (a) membrane stress distribution of a dented pipe with dent rotation angle $\theta_d = 45^o$ at the ultimate bending point; (b) membrane stress distribution of a dented pipe with dent rotation angle $\theta_d = 90^o$ at the ultimate bending point.

Figure 4.21 illustrates the variation of the equivalent plastic strain region of a dented pipe with varied θ_d at the ultimate limit point. The PEEQ, as a function of the plastic strain, is a scalar measurement of the accumulated plastic strain, which is equivalent to the von Mises stress. The range of the legend for PEEQ here is between 0 and 6.5%. It is found that, with the increase of dent angle, the plastic region gradually concentrates, fashioning four regular lobes adjacent to the dent. Structure fails as a consequence of the extra large and concentrated plastic strain.

4.5.2 Effect of dent location

Figure 4.22 is the normalized bending moment-curvature diagram of pipes with varying of the dent location. The dent angle is set to 90^o (pipe hoop direction) with a dent length of 100 *mm* and a width of 60 *mm*. It demonstrates that a dent on the compression side has produced a significant negative effect on the critical bending moment and critical curvature, while a dent on the tensile side only has a slight negative effect on the bending moment compared with the intact pipes. The critical curvature has been enlarged a little due to the recovery of

the dent on the tensile side, which conforms to the observation from tests in Chapter 3.

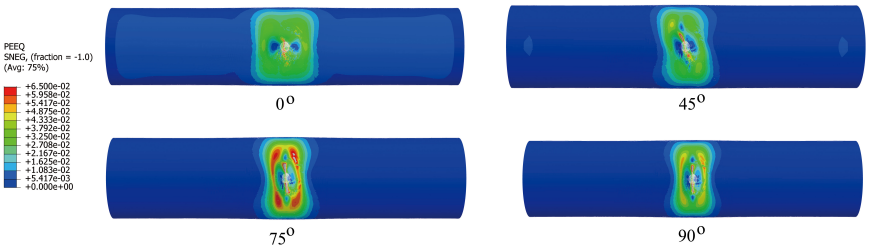

Figure 4.21: Equivalent plastic strain (PEEQ) of a dented pipe with varying of dent rotation angle (θ_d) at the ultimate bending point.

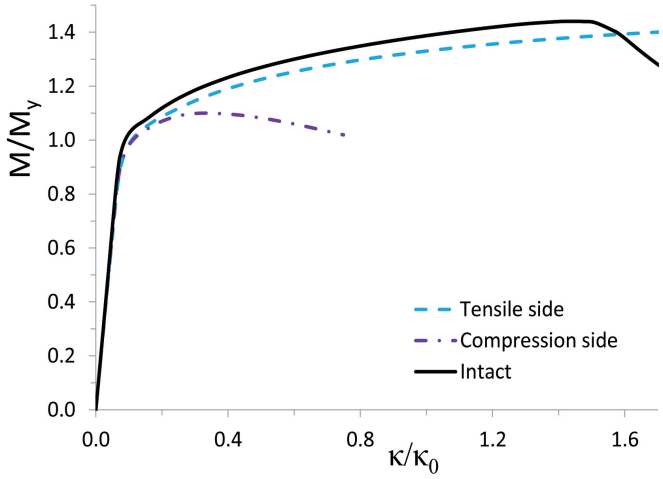

Figure 4.22: Bending moment-curvature diagram of pipes with varying of the dent location (l_d=100 mm,w_d=60 mm).

4.5.3 Effect of dent depth

By changing the dent parameters, a series of numerical simulations on dented pipes are carried out to clarify their effects. Tables 4.5 to 4.8 list all these simulation data from full dented model. All the dents are put on the compression side with a rotation angle of 90^0 so that we can get the most severe effect based on the research in previous sections. The reference values M_i and κ_i are 108.9 kNm and 0.367 based on the intact FEM model, respectively. The value of d_d is normalized by the pipe thickness t, while l_d and w_d are normalized by $\sqrt{Rt}$, expressed as $\lambda_l = l_d/\sqrt{Rt}$ and $\lambda_w = w_d/\sqrt{Rt}$, respectively.

Figure 4.23 shows the normalized bending moment-curvature diagrams with the variation of the dent depth, length and width. Results indicate that the residual strength decreases rapidly with the increase of d_d/t, and the ovalization in terms of the largest lateral displacement has an increasing tendency with the increase of d_d/t, as shown in Figure 4.24. A dent

depth equal to 0.73 times of the pipe thickness can reduce the M_{cr} and κ_{cr} by more than 9% and 50%, respectively. The larger the dent depth, the larger the ovalization will be. For instance, the lateral displacement reaches the largest value of 4.273 *mm* at the residual strength limit point at $d_d = 15$ *mm*. In contrast, the lateral displacement is only 1.38 *mm* at $d_d = 2$ *mm*. It is also observed that, with the increase of the dent depth, the location with the largest lateral displacement is gradually moving to the dent tip region.

Table 4.5: Residual ultimate strength of pipes with varying of dent depth.

Capacity	l_d=89 mm, w_d=68 mm d_d/t											
	0.12	0.36	0.48	0.61	0.73	0.85	0.97	1.25	1.33	1.45	1.58	1.70
M_{cr}/M_i	0.998	0.968	0.943	0.922	0.905	0.891	0.880	0.862	0.856	0.852	0.848	0.844
κ_{cr}/κ_i	1.001	0.736	0.586	0.510	0.452	0.431	0.398	0.390	0.381	0.379	0.387	0.368
	1.82	1.94	2.06	2.18								
M_{cr}/M_i	0.843	0.841	0.840	0.839								
κ_{cr}/κ_i	0.384	0.392	0.395	0.392								

Table 4.6: Residual ultimate strength of pipes with varying of dent length.

Capacity	d_d=5.3 mm, w_d=68 mm $\lambda_l = l_d/\sqrt{Rt}$										
	0.8	1.5	2.0	2.3	2.5	3.4	4.2	4.5	4.7	5.0	5.2
M_{cr}/M_i	0.998	0.992	0.975	0.961	0.952	0.916	0.890	0.879	0.875	0.869	0.864
κ_{cr}/κ_i	1.011	0.978	0.771	0.689	0.638	0.488	0.401	0.381	0.354	0.349	0.360

Table 4.7: Residual ultimate strength of pipes with varying of dent length.

Capacity	d_d=10.3 mm, w_d=68 mm $\lambda_l = l_d/\sqrt{Rt}$											
	0.80	1.51	1.60	1.70	1.80	1.90	2.00	2.20	2.30	2.40	2.50	2.90
M_{cr}/M_i	0.997	0.980	0.975	0.969	0.962	0.956	0.949	0.935	0.928	0.921	0.914	0.888
κ_{cr}/κ_i	0.980	0.888	0.845	0.785	0.741	0.703	0.670	0.586	0.567	0.520	0.501	0.436
	3.37	3.79	4.16	4.54	4.70	4.80	5.00	5.10	5.20			
M_{cr}/M_i	0.862	0.838	0.81	0.803	0.797	0.793	0.785	0.783	0.780			
κ_{cr}/κ_i	0.390	0.338	0.302	0.286	0.270	0.264	0.253	0.251	0.267			

Table 4.8: Residual ultimate strength of pipes with varying of dent width.

Capacity	d_d=10.3 mm, l_d=89 mm $\lambda_w = w_d/\sqrt{Rt}$								
	1.06	1.44	1.89	2.04	2.20	2.35	2.95	3.33	3.71
M_{cr}/M_i	0.856	0.853	0.855	0.855	0.857	0.858	0.865	0.870	0.875
κ_{cr}/κ_i	0.395	0.381	0.376	0.371	0.379	0.384	0.390	0.395	0.403

4.5.4 Effect of dent length

The dent length significantly influences the pipe residual strength, as shown in Figure 4.23(b) and Figure 4.25 (a). The bending capacity decreases with the increase of dent length. For instance, a dent length equal to 3.37 times of $\sqrt{Rt}$ can reduce the M_{cr} and κ_{cr} by more than 14% and 61%, respectively.

4.5.5 Effect of dent width

The dent width in the pipe longitudinal direction has an small effect on the pipe residual strength subjected to pure bending. Figure 4.23(c) and 4.25(c) show the effect of dent width with varying of w_d. Results from the cases with the variation of dent width in a large domain show that the variation values are less than 3% and 1% for M_{cr} and κ_{cr}, respectively. It is plausible to neglect the dent width effect on the predictions of residual strength of metallic pipes.

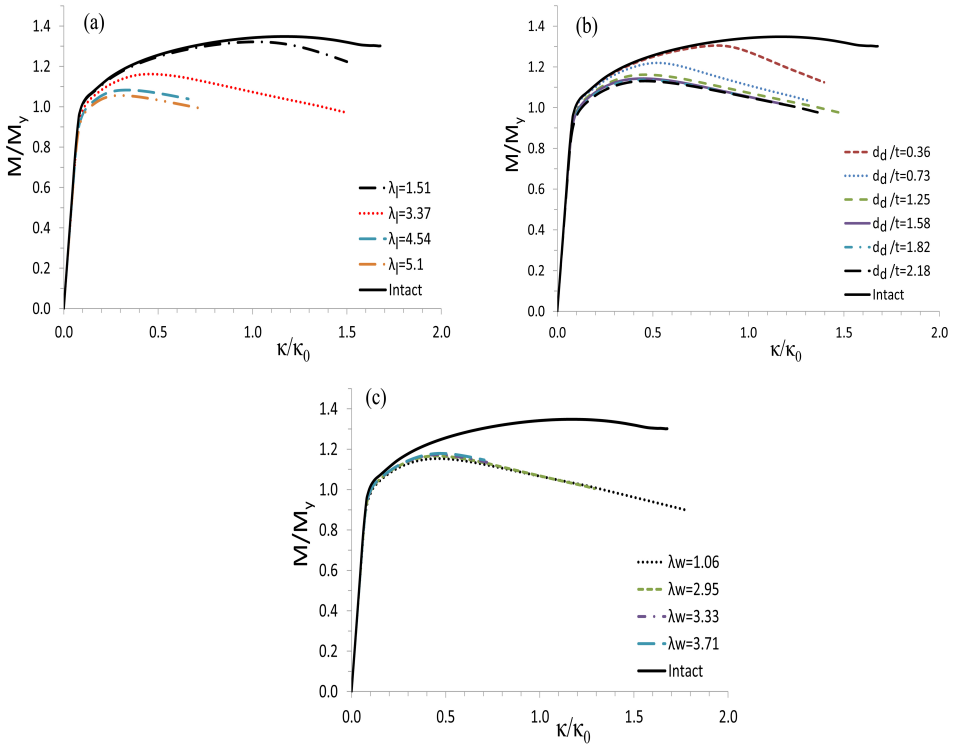

Figure 4.23: Normalized bending moment-curvature diagrams with varing of dent parameters (S2N1, 90^o): (a) diagrams with variation of normalized dent length (λ_l, d_d=10.3 mm, w_d=68 mm); (b) diagrams with variation of normalized dent depth (d_d/t, l_d=89 mm, w_d=68 mm); (c) diagrams with variation of normalized dent width (λ_w, l_d=89 mm, d_d=10.3 mm).

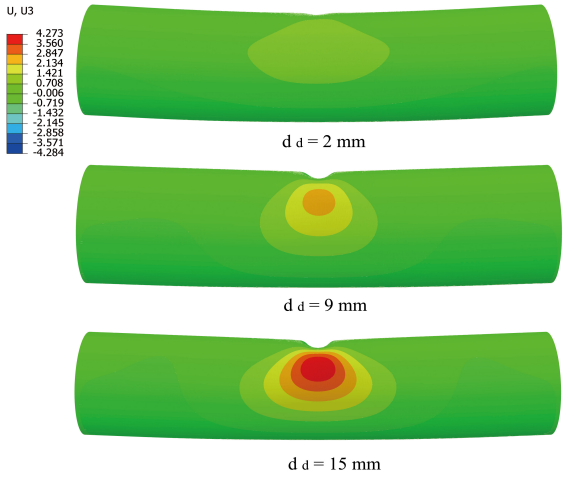

Figure 4.24: Lateral displacement distribution of a dented pipe with the varied dent depth d_d at the residual limit point.

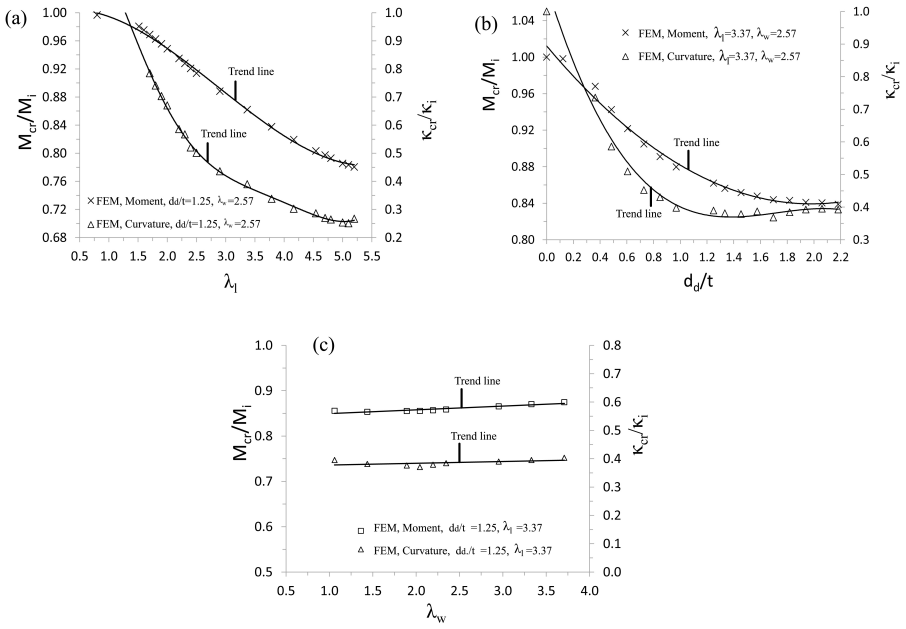

Figure 4.25: Effect of dent parameters: (a) dent length; (b) dent depth; (c) dent width.

4.6 Empirical formulas for residual strength prediction

As investigated in the previous section, it is reasonable to propose prediction formulas as the function of critical dent parameters (l_d and d_d). The formulas are first constructed as follows:

Table 4.9: Model uncertainties of the proposed formulas.

X	Moment, Equation (4.8)		Curvature, Equation (4.9)	
	Mean (Bias)	COV	Mean (Bias)	COV
FEM	1.0014	0.0124	1.024	0.1541
Test	1.0068	0.0459	0.892	0.2563

$$M_{cr}/M_i(\kappa_{cr}/\kappa_i) = 1 - f(\lambda_l, d_d/t) \tag{4.7}$$

where λ_l is the normalized dent length in the pipe hoop direction, M_i and κ_i are the ultimate bending moment and the critical curvature from intact pipes, respectively.

A regression analysis on the FEM results from Section 4.5 is undertook to build up the relationship between the prediction values and the significant dent parameters. Therefore, the empirical formulas for residual strength are listed as follows:

$$M_{cr}/M_i = 1 - a_1(d_d/t)^{b_1}(\lambda_l)^{c_1} \tag{4.8}$$

$$\kappa_{cr}/\kappa_i = 1 - (a_2 + b_2 t/d_d)(\lambda_l)^{c_2} \tag{4.9}$$

Where a_1, b_1 and c_1 is 0.017, 0.696 and 1.48, respectively; a_2, b_2 and c_2 is 0.192, -0.026 and 0.955, respectively.

In order to validate the accuracy of the proposed formulas, the prediction results are compared with both the test and simulation results, as shown in Figure 4.26. It shows that the two proposed equations have a satisfying comparison with the simulation results. Compared with the test results, the formula has a little pessimistic estimation for some cases, which is probably due to the discrepancies in test such as material, and geometry measurement. Furthermore, following the definition from [15], the model uncertainty parameter can be written as:

$$X = X_{true}/X_{predict} \tag{4.10}$$

Where X_{true} is the data from either experimental test or numerical simulation, and $X_{predict}$ is the prediction values due to the proposed equations. It is assumed that both X_{true} and $X_{predict}$ are from the same cases with the same material properties and geometry. Hence, the mean value (bias), standard error of X, and the coefficient of variation (COV) are statistically calculated, as shown in Table 4.9.

The model uncertainties of the proposed equations indicate that the extent of variability (COV) for the prediction of residual bending moment is smaller than 5% in relation to the mean bias value. For the critical curvature, the equation provides a prediction with a relative

large scatter, as seen from the mean bias value of 0.892 and the COV of 0.2563 from the comparison with test data.

Figure 4.27 shows the prediction results of dented metallic pipes with the changing of dent parameters. Two different dent depth including $d_d/t = 1.25$ and $d_d/t = 0.64$ are used when the normalized dent length is varying (Figure 4.27 (a)). In Figure 4.27 (b), the normalized dent length is fixed to $\lambda_l = 3.37$ when the dent depth is varying. The FEM results are also presented in these figures. The R square of the fitted equation (R^2) are 0.971 and 0.903, respectively, which reflects a high precision of prediction.

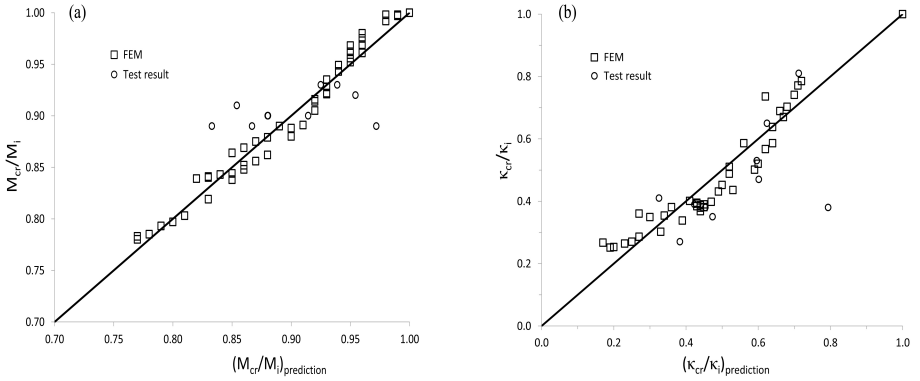

Figure 4.26: Comparison between prediction of proposed equations and both experimental and numerical results: (a) Normalized residual ultimate moment (M_{cr}/M_i); (b) Normalized critical curvature (κ_{cr}/κ_i).

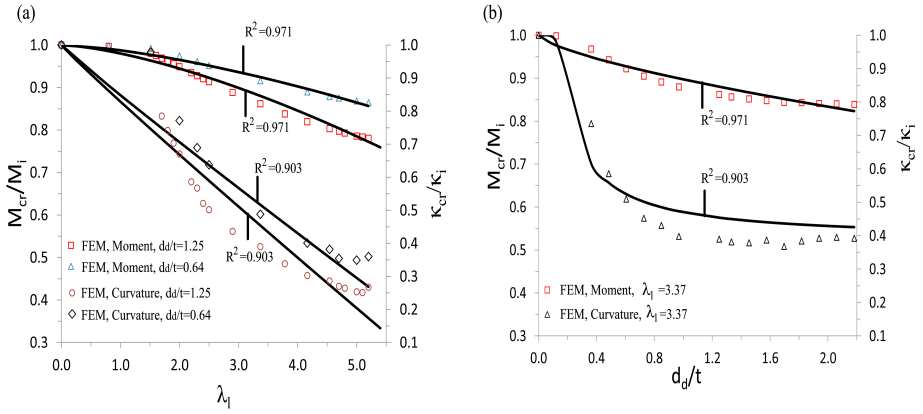

Figure 4.27: Prediction of dented metallic pipes with the changing of dent parameters: (a) variation of normalized dent length (λ_l=$l_d/\sqrt{Rt}$); (b) variation of normalized dent depth (d_d/t).

4.7 Conclusions

In this chapter, an extensive numerical investigation on both intact and dented metallic pipes is carried out. Numerical models have been developed and validated by test results, capable of predicting residual strength of dented pipe in terms of bending capacity and critical curvature. Through these numerical models, an investigation of influential parameters has been completed. Based on the performed work in this chapter, some conclusions can therefore be drawn:

(1) The occurrence of a dent damage accelerates the failure of pipe due to the rapid localization of the damaged region with an elastic-plastic failure mode.

(2) The material yield stress in the pipe longitudinal direction dominates the bending capacity of the structures. For a pipe with a considerable dent size, the effect of manufacturing induced initial imperfection has been shielded.

(3) With the decrease of D/t ratio of metallic pipes, the failure mode of pipes under bending gradually changes from an elastic buckling to an elastic-plastic failure.

(4) The ovalization in terms of the lateral displacement in the critical cross-section of dented pipe increases with the increase of dent depth.

The 4^{th} key question of this thesis in terms of the effects of dent parameters, including dent angle (θ_d), dent location, dent depth (d_d), dent length (l_d), and dent width (w_d), has been identified. The corresponding conclusions for each dent parameter are summarized as follows:

(5) A dent on the compression side of pipe surface has large negative effect on its residual strength. For a dent on the tensile side, a slight negative effect on residual bending moment exists, whereas the critical curvature increases a little due to the dent recovery.

(6) For the dent angle (θ_d), the larger the dent rotation angle is, the smaller the residual ultimate strength will be. A pipe with a hoop dent (90^o) on its compression side has the largest effect on residual strength.

(7) The dent length (l_d) and depth (d_d) have significant effects on the pipe strength, whereas the dent width (w_d) only slightly affects the strength.

(8) For the projected dent length (l'_d) (in 90^o), it significantly reduces the residual strength of dented metallic pipes, decreasing with the increase of its dimensionless length.

(9) The dent depth (d_d) significantly affects the residual strength of dented metallic pipes. With the increase of the dent depth, the strength decreases rapidly.

(10) The dent width (w_d) in pipe longitudinal direction has an insignificant effect on the pipe residual strength.

Furthermore, the effect of a dent on pipes subjected to pure bending has been quantified (the 5^{th} key question), accounting for the significant dent parameters d_d and l_d as listed above. Empirical formulas (Equation (4.8) and Equation (4.9)) for the predictions of residual strength are proposed. They could be utilized for practice purposes to estimate the residual bending strength of pipes after the suffering of dent damage.

In practice, the proposed equations can be used when a dent is produced due to a sudden accident such as the impact between fishing boat and pipes, and the dropping of foreign objects. Only a simple measurement of the damage length and depth is needed to estimate the reduction ratio of pipe strength under dominated bending moment. It should be noted that, the length of dent should be projected to the hoop direction of pipe if there is a rotational angle on the dent. The impact induced residual stress has not been accounted for in these equations. The application of these equations is limited to seamless metallic pipes with low diameter-to-thickness ratio (around 21).

Chapter 5

Quantification of metal loss effect on the residual strength of metallic pipes*

On the basis of the experimental investigation in Chapter 3, numerical investigation is conducted in this chapter on damaged seamless metallic pipelines with metal loss (diameter-to-thickness ratio D/t around 21) through nonlinear finite element method (FEM). Numerical models are developed and validated through test results by using the measured material properties and specimen geometry, capable of predicting the residual ultimate strength of pipes in terms of bending capacity (M_{cr}) and critical curvature (κ_{cr}). By changing the metal loss parameters, i.e. length (l_m), width (w_m) and depth (d_m), a series of numerical simulations are carried out.

Therefore, in this chapter, the effects of notch parameters are identified. The 4^{th} key question of this thesis in terms of metal loss and the 6^{th} key question on the quantification of the effect of metal loss have been answered.

The structure of this chapter is arranged as follows. Section 5.1 provides a general description of the developed finite element models accounting for metal loss, while Section 5.2 has validated the numerical model through test. Providing the bending stress in the entire pipe cross-section is uniform and pipe material is elastic-perfectly plastic, an analytical solution of ultimate bending moment of metallic pipes with metal loss in terms of a notch is derived in Section 5.3. Afterwards, Section 5.4 investigates the effect of each notch parameter including notch depth (d_m), notch length (l_m) and notch width (w_m). Based on the simulation data, empirical formulas are then developed in the function of notch width and loss area of notch in Section 5.5. In the end, conclusions of this chapter are drawn in Section 5.6.

*This chapter is based on the paper Jie Cai, Xiaoli Jiang, Gabriel Lodewijks, Zhiyong Pei and Weiguo Wu. Residual ultimate strength of damaged seamless metallic pipelines with metal loss. Marine Structures. 58: 242-253, 2018 [39].

5.1 Description of numerical models

The numerical models in this chapter have been developed in ABAQUS/Standard [1] through Python for the simulation of test specimens and the investigation of parameters' effects, as seen in Figure 5.1. The Python script for parameteric study in this chapter is presented in Appendix C. An elastic-plastic material with von Mises yield criterion and isotropic hardening is deployed. The material properties from the material tensile test and the fitted method, as described in Chapters 3 and 4, are used. The used material coupon ("L7") is cut from the longitudinal direction of specimen, with a yield stress of 378 MPa and an ultimate tensile stress of 542 MPa. A three dimensional element C3D8R is used for the sake of metal loss damage. A typical method for the introduce of initial imperfection is used due to the lack of test data, using the eigenvalue buckling mode from the same structure under the same loading type. It has been used in both engineering practice and research, such as DNV-RP-C208 [47], and Vasilikis et al [123]. Hence, the initial imperfection in terms of a wave-type is introduced for all models in the form of eigenvalue buckling mode. The imperfection amplitude is set to $3\%t$ (t is pipe thickness) based on the recommendation from [53] due to the lack of data in current test, as seen in Figure 5.2.

A simplified numerical model with metal loss is developed on the basis of test configuration in Chapter 3, accounting for the variation of notch size and angle. A simplify-supported boundary condition has been used and two referential nodes have been introduced to represent the loading location of specimen in test, exerting an equivalent forced-rotation through the reference points. It is admitted that discrepancy would be introduced by such a simplification. As described in Chapter 3, the local deformation in loading places is small enough due to the reinforcement from half-sleeve. Therefore, such effect is minor by using the simplified boundary. In addition, numerical comparisons in Chapter 4 between full test model and simplified model demonstrate that there is only a small discrepancy for strength prediction, less than 3% for residual bending moment.

5.1.1 Metal loss simplification

The shape of notch is simplified as a regular stretch body, based on the physical test with the notch depth (d_m) in the central pipe cross-section. The notch length (l_m) is the chord length of the remaining sector in the pipe cross-section with notch, as seen in Figure 5.3. There is a practical reason for this definition. In general, the on-site measurement of straight line is much easier and more accurate than the measurement of arc length after occurrence of damage. A notch is considered as 90 degree when its length is along the pipe hoop direction, while a notch is 0 degree when its length is along the pipe longitudinal direction. The mesh is largely refined around damaged region, with the minimum mesh size equal to 0.8 mm, i.e. less than 1.3% of one half-wave length ($\lambda_{cl} = 1.728\sqrt{Rt}$ [107]) of cylindrical shells. At least four layers of element in thickness direction are deployed to guarantee simulation accuracy.

5.2 Simulations of specimens with metal loss from tests

In this section, the residual strength and corresponding structural behavior of specimens with metal loss from test are simulated through the numerical models in previous section.

Simulation results have been compared with test results in terms of structural failure modes, bending moment-curvature diagrams, and strength capacity. A comparison of notch damage is shown in Figure 5.4.

Table 5.1: Results of specimens with metal loss damage (Dimension unit: mm; Notch angle is 90 degree).

S.N.	D	t	D/t	Notch ($l_m \times w_m \times d_m$)	Location	M_{cr}(Test) (kNm)	M_{cr}(FEA) (kNm)	κ_{cr}(Test) (1/m)	κ_{cr}(FEA) (1/m)
S3N3	166.89	7.90	21.13	$45 \times 10 \times 3$	C	92.89	93.04	0.268	0.303
S3N4	168.3	7.90	21.30	$45 \times 10 \times 3$	T	100.00	99.29	0.393	0.791

5.2.1 Reference values

For comparison of test results in this section, bending moment is normalized by plastic bending moment $M_y = 4R_a^2 t\sigma_y$, while curvature κ is normalized by the curvature-like expression $\kappa_0 = t/4R_a^2$. Only global curvature is selected for comparison between test and numerical simulation. The selected locations for calculation of global curvature in simulation are exactly the same with tests. Bending moment in simulation is the resultant of all node forces multiplying their corresponding force arms in the central cross-section of specimen.

5.2.2 Structural failure modes

The comparison results of structural failure modes of specimens between the numerical prediction and test are illustrated in Figure 5.5. Normally, as a result of the increase of structural deformation in the form of ovalization in pipe cross-sections, specimens fail due to the increasing of bending moment. Under a certain extent, such ovalization can be counterbalanced by material yielding and further material hardening so that the structure stays stable. When ovalization cannot be compensated for, the structure reaches its bending capacity with the largest ovalization in a specific pipe cross-section. For instance, the initiation of failure for intact specimen happens on the place far from the center of the specimen, as shown in Figure 5.5 (a), whereas the damaged specimen fails in the center of specimen due to the occurrence of damage, as seen in Figure 5.5 (b). Both failure mode and location have a good agreement with each other.

5.2.3 Moment-curvature diagrams

The comparison of bending moment-curvature diagrams between test and numerical predictions is presented in Figure 5.6. Specimen S3N3 has a notch with 90^o on its pipe compression side, while specimen S3N4 has a notch with 90^o on its tensile side. The occurrence of notch on the compression side of specimen has changed the variation tendency of bending moment-curvature diagrams, initiating a rapid failure of specimen and considerably reducing the critical bending curvature.

Table 5.1 lists all comparison results in terms of bending capacity (M_{cr}) and critical curvature (κ_{cr}). For the prediction result of M_{cr}, less than 1.0% discrepancy has been ob-

served for the damaged specimen. The discrepancy of κ_{cr} is about 13.1% for the damaged specimen S3N3 with notch on the compression side. These scatters may be introduced by factors such as the material properties, assumptions of friction coefficient and the measurement method for curvature. Detailed discussions have been presented in the experimental investigation part in Chapter 3.

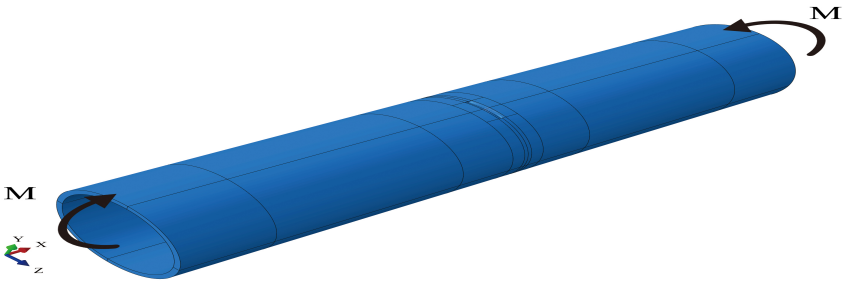

Figure 5.1: Simplified numerical model of pipe with metal loss.

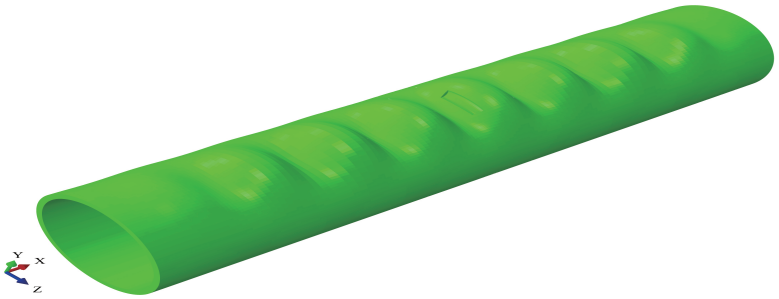

Figure 5.2: Intial imperfection in terms of wave-type on pipe surface (imperfection amplitude has been zooming in for the sake of clarity).

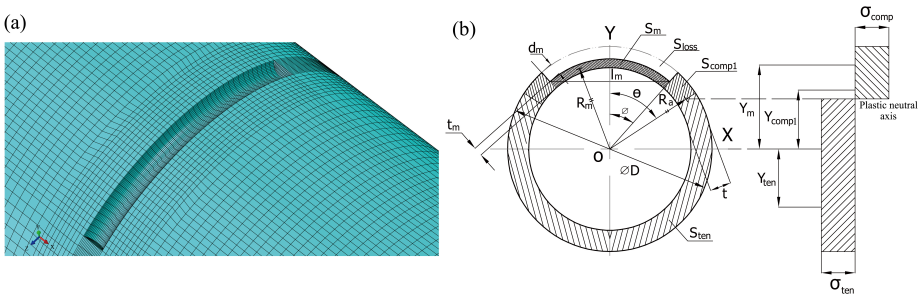

Figure 5.3: (a) schema of mesh distribution of notched region; (b) sketch of pipe cross-section with notch and notch parameters.

For specimen S3N4 with a notch on its tensile side, however, the prediction value is nearly double compared with test. One major reason is that the fracture failure in reality has not been accounted for in the simulation, which is out of the research domain of this research project. Further investigations on this scenario is carried out in Chapter 6. As a consequence, only metal loss on the compression side of pipes is further investigated in this chapter.

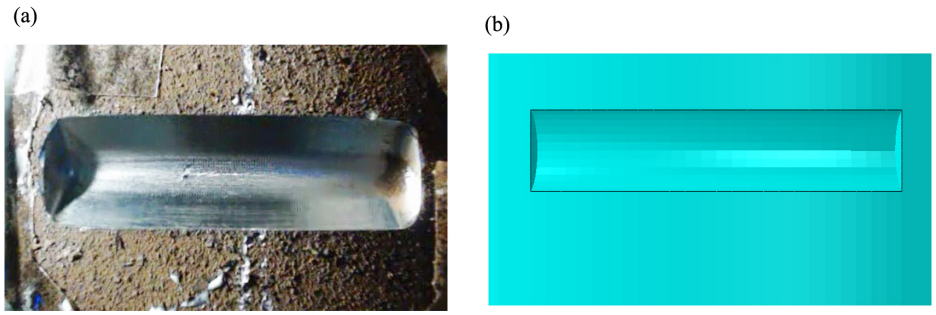

Figure 5.4: Notch damage in both test and numerical model: (a) artificial metal loss damage from test; (b) metal loss damage on numerical model.

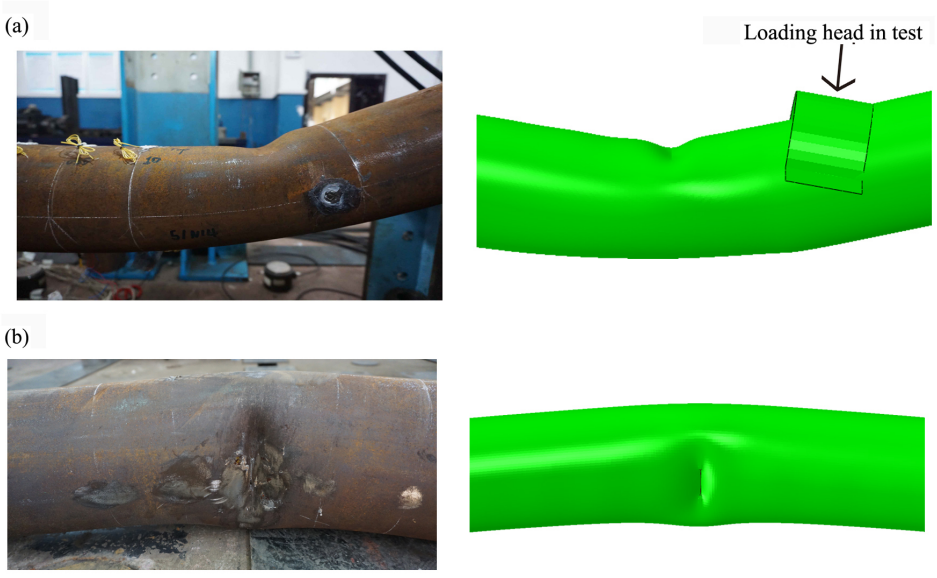

Figure 5.5: Representative failure mode of specimens:(a) specimen without damage (S1N4); (b) specimen with metal loss on its compression side (S3N3).

In addition, the failure procedure between simulation and test is similar with each other. Elastic-plastic failure is dominant, with residual ultimate strength M_{cr} exceeding plastic

bending moment M_y to some extent. M_{cr} is more than 1.12 times of M_y for the damaged specimen S3N3 based on predictions. Without the considering of fracture failure, specimen S3N4 has a much strong load carrying capacity during simulation. In test, fracture appears, which largely affects the strength of structure and the critical curvature. For the damaged specimen S3N4 with a notch on its tensile side, the failure procedure increases in a smooth way.

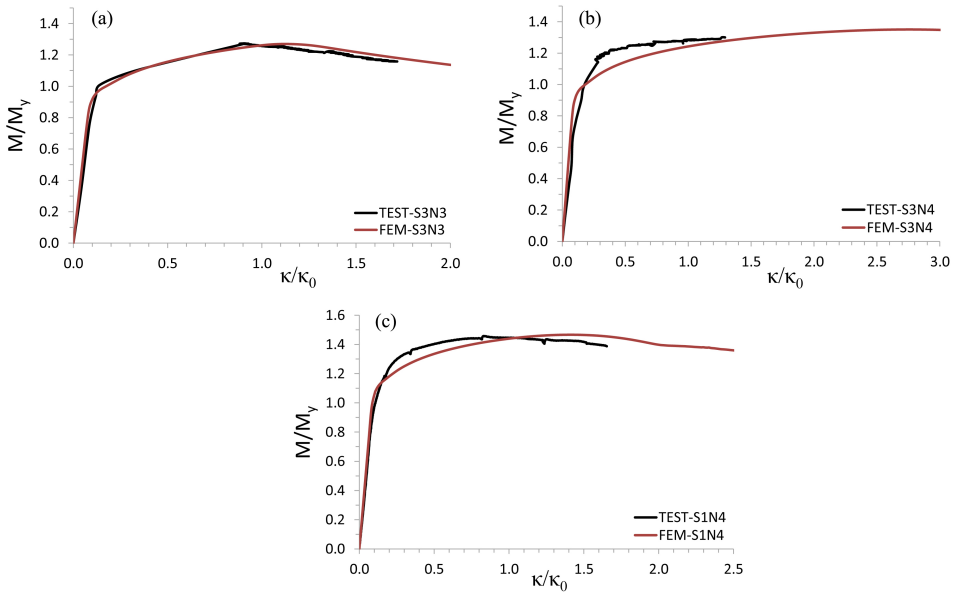

Figure 5.6: Comparison between numerical and test results in terms of bending moment-curvature diagram: (a) specimen S3N3 with 90^0 notch on its compression side; (b) specimen S3N4 with 90^0 notch on its tensile side; (c) specimen S1N4 without damage.

5.3 Analytical solutions

A simple derivation of metallic pipe with metal loss under bending moment is carried out in this section. A schema of the metal loss in pipe cross-section is shown in Figure 5.3 (b). Providing the bending stress in the entire pipe cross-section is uniform, the compression stress σ_{comp} and the tensile stress σ_{ten} are therefore equal to $-\sigma_y$ and σ_y, respectively, when the ultimate strength has reached.

The analytical solution of ultimate bending moment of pipe without a notch can be easily derived as $M_y = 4R_a^2 t\sigma_y$, as described in Chapter 2. When the metal loss is induced on pipe surface, a typical approach is to remove the corresponding area of the metal loss. Assumptions of elastic-perfectly plastic material, full plastic in the damaged cross-section and the metal loss on the compression side of pipes are also made.

The plastic neutral axis should be first obtained when residual strength has reached. Based on equilibrium condition, the true axial force F (zero for pure bending) can be ex-

pressed as:

$$F = S_m\sigma_{comp} + S_{comp1}\sigma_{comp} + S_{ten}\sigma_{ten} \tag{5.1}$$

Where S_m, S_{comp1}, and S_{ten} are the compression area of metal loss region, the compression area of region without metal loss, and the tensile area in pipe cross-section, respectively. They can be expressed as:

$$S_m = 2\int_0^{\phi} R_m t_m d\theta = 2R_m t_m \phi \tag{5.2}$$

$$S_{comp1} = 2(\theta - \phi)R_a t \tag{5.3}$$

$$S_{ten} = 2(\pi - \theta)R_a t \tag{5.4}$$

Where $R_m = R_a - \frac{d_m}{2}$ and $t_m = t - d_m$. Substituting Equations (5.2), (5.3) and (5.4) into Equation (5.1), the angle from bending plane to the plastic neutral axis (θ) can be obtained.

$$\theta = \frac{-F + 2R_a t\sigma_y(\pi + k_1\phi)}{4Rt\sigma_y} = \frac{(\pi + k_1\phi)}{2} \tag{5.5}$$

$$\phi = arcsin(\frac{l_m}{D - 2d_m}) \tag{5.6}$$

Where ϕ is the half angle of metal loss (in radians), expressed in Equation (5.6), k_1 is a constant related to notch depth, as expressed in Equation (5.7). Then we start to derive the residual bending moment (M_{cr}), which can be written as Equation (5.8).

$$k_1 = 1 - (1 - \frac{d_m}{2R_a})(1 - \frac{d_m}{t}) \tag{5.7}$$

$$M_{cr} = \sigma_{comp}(S_m Y_m + S_{comp1}Y_{comp1}) + \sigma_{ten}S_{ten}Y_{ten} \tag{5.8}$$

Where Y_m, Y_{comp1}, and Y_{ten} are force arms from bending axis to the mass center of respective area segment. They can be written as:

$$Y_m = \frac{\int_0^{\phi} R_m cos(\theta)\cdot t_m R_m d\theta}{R_m t_m \phi} = \frac{R_a sin(\phi)}{\phi}(1 - \frac{d_m}{2R_a}) \tag{5.9}$$

$$Y_{comp1} = R_a\frac{(sin(\theta) - sin(\phi))}{\theta - \phi} \tag{5.10}$$

$$Y_{ten} = R_a\frac{sin(\theta)}{\pi - \theta} \tag{5.11}$$

Substituting Equations (5.9), (5.10) and (5.11) into Equation (5.8), the residual bending moment can be re-written as Equation (5.12).

$$M_{cr} = 4R_a^2 t\sigma_y sin(\theta) - 2R_a^2 t\sigma_y k_2 sin(\phi) \tag{5.12}$$

Where k_2 is also a constant related to the depth of metal loss, expressed in Equation (5.13). In this equation, the so called "neighbor response" [130] induced by the finite dimension of metal loss (w_m) is not accounted for due to the assumption of infinite metal loss in the pipe longitudinal direction.

$$k_2 = 1 - (1 - \frac{d_m}{2R_a})^2 (1 - \frac{d_m}{t}) \tag{5.13}$$

Hence, the analytical solution for reduction ratio of bending moment is obtained:

$$\frac{M_{cr}}{M_y} = sin(\theta) - \frac{k_2 sin(\phi)}{2} \tag{5.14}$$

Table 5.2: Principal dimension of pipe model for numerical investigation

Pipe type	Diameter D(mm)	Thickness t(mm)	Length L_0(mm)	D/t	L_0/D
Seamless	166.89	7.9	800	21.1	4.79

Table 5.3: Residual ultimate strength of pipes with varying of notch length.

Capacity	d_m=3 mm, w_m=10 mm $\lambda_l = l_m/\sqrt{Rt}$											
	0.234	0.467	0.545	0.900	1.000	1.300	1.400	1.500	1.600	1.753	1.900	2.100
M_{cr}/M_i	0.999	0.992	0.988	0.969	0.963	0.947	0.942	0.936	0.931	0.921	0.915	0.905
κ_{cr}/κ_i	0.955	0.888	0.851	0.734	0.704	0.628	0.606	0.583	0.559	0.526	0.506	0.465
	2.400	2.600	2.800	3.000	3.200	3.400	3.800	4.000	4.200	4.400	4.600	4.800
M_{cr}/M_i	0.890	0.882	0.873	0.866	0.859	0.859	0.850	0.847	0.844	0.842	0.844	0.846
κ_{cr}/κ_i	0.417	0.393	0.369	0.353	0.337	0.338	0.313	0.303	0.295	0.295	0.295	0.296

5.4 Investigation of metal loss parameters

In this section, a series of numerical simulations are conducted based on the validated model in Section 5.2, changing the geometrical size of notch parameters. The principal dimension of pipes for investigation is listed in Table 5.2. The simulation results in terms of residual ultimate strength (M_{cr}) and critical curvature (κ_{cr}) are presented in Tables 5.3, 5.4 and 5.5, where the reference values of M_i and κ_i are described in Section 5.4.1. In these tables, the notch depth (d_m) is normalized by pipe thickness t, while l_m and w_m are normalized by $\sqrt{Rt}$, expressed as $\lambda_l = l_m/\sqrt{Rt}$ and $\lambda_w = w_m/\sqrt{Rt}$, respectively.

Practically, two criteria are used for the selection of notch size as described in the research scope in Chapter 1. On the one hand, tiny notch defects may produce stress concentration and undermine the fatigue life under cyclic loading in long term, which is out of the research domain of this thesis. On the other hand, extra large notch would introduce a rapid failure of structures in short time and serious leaking of gas and/or oil, which is also impractical to account for. Therefore, in this chapter, the selected size of metal loss is moderate, with notch depth (d_m/t) between 0.2 and 0.65 (65%t), notch length (λ_l) between 0.2 and 4.8 ($\sim$ 74%D). The selected notch width (λ_w) is between 0.3 and 1.4 ($\sim$ 22%D).

Table 5.4: Residual ultimate strength of pipes with varying of notch depth.

Capacity	l_m=45 mm, w_m=10 mm d_m/t											
	0.20	0.23	0.25	0.27	0.28	0.29	0.30	0.32	0.33	0.35	0.38	0.41
M_{cr}/M_i	0.980	0.964	0.964	0.960	0.956	0.952	0.947	0.939	0.939	0.931	0.921	0.915
κ_{cr}/κ_i	0.792	0.747	0.702	0.688	0.665	0.641	0.628	0.594	0.590	0.559	0.526	0.506
	0.43	0.44	0.46	0.48	0.51	0.53	0.56	0.57	0.58	0.59	0.61	0.63
M_{cr}/M_i	0.908	0.903	0.901	0.895	0.889	0.886	0.882	0.879	0.879	0.877	0.876	0.872
κ_{cr}/κ_i	0.494	0.478	0.481	0.466	0.463	0.457	0.460	0.453	0.465	0.465	0.466	0.462

Table 5.5: Residual ultimate strength of pipes with varying of notch width.

Capacity	d_m=3 mm, l_m=45 mm $\lambda_w = w_m/\sqrt{Rt}$											
	0.389	0.467	0.556	0.584	0.701	0.721	0.821	0.925	1.018	1.104	1.184	1.396
M_{cr}/M_i	0.921	0.914	0.913	0.907	0.911	0.909	0.915	0.904	0.901	0.901	0.900	0.903
κ_{cr}/κ_i	0.526	0.509	0.498	0.496	0.502	0.492	0.522	0.478	0.470	0.465	0.471	0.479

5.4.1 Reference values

The strength value M_i and κ_i from intact pipes are used as references in the following sections. Reference values M_i and κ_i from numerical results are 101.41 kNm and 0.624 $1/m$, respectively, obtained through the simulation of intact pipes with the same principal dimension subjected to bending moment, as described in Chapter 4. Meanwhile, reference values for test data are the intact results from specimen S1N4, as shown in Chapter 3.

5.4.2 Effects of metal loss parameters

In this section, the effects of metal loss in terms of notch depth (d_m) effect, length (l_m) effect and width (w_m) effect are investigated based on the developed numerical model (wave-type initial imperfection with amplitude of $3\%t$, central location, compression side, 90^o notch). The material anisotropy has not been taken into account. Due to possible fracture failure for pipe with notch on its tensile side, only a notch on the compression side is considered.

Figure 5.7 presents the normalized bending moment-curvature diagrams with the variation of notch parameters. Compared with intact pipes, notch damage has a considerable influence on pipe strength. Residual ultimate strength reaches at much lower critical curvature compared with intact pipe. The damaged structures fail rapidly with a fast losing of strength in post-buckling stage.

The effect of each specific parameter of a notch can be clearly seen in Figure 5.8. It presents the varying tendency of strength capacity with the changing of different notch parameters. The numerical results indicate that both notch depth and notch length in pipe hoop direction have significant effects on ultimate strength. The larger the d_m or l_m is, the less the bending capacity will be. For instance, a notch depth equal to half of the pipe thickness can reduce M_{cr} and κ_{cr} by more than 11% and 54%, respectively. In addition, a notch length equal to 2 times of $\sqrt{Rt}$ has reduced M_{cr} and κ_{cr} by nearly 10% and 54%, respectively. The increase of the notch width slightly reduces the pipe strength, presenting a linear tendency, as shown in Figure 5.7 (c) and Figure 5.8 (c). It is also observed that the range of reduction ratio is less than 2% for κ_{cr} and less than 5% for M_{cr} when λ_w increases

from 0.4 to 1.4.

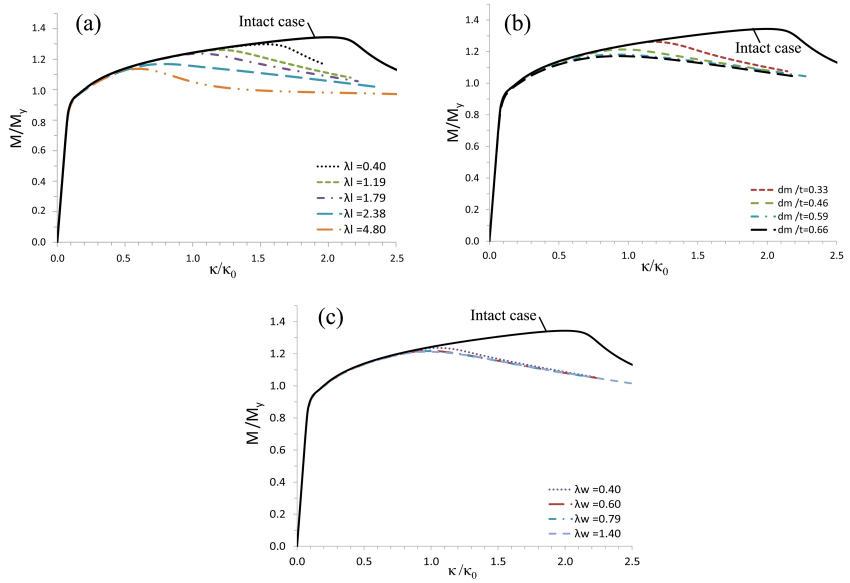

Figure 5.7: Normalized bending moment-curvature diagrams with varing of notch parameters: (a) diagrams with variation of normalized notch length (λ_l, w_m=10 mm, d_m=3 mm); (b) diagrams with variation of normalized notch depth (d_m/t, l_m=45 mm, w_m=10 mm); (c) diagrams with variation of normalized notch width (λ_w, l_m=45 mm, d_m=3 mm).

5.5 Empirical formulas for residual strength prediction

To date, it has been shown from previous research [78] that the loss of notch area dominates the residual ultimate strength of notched structures. Hence, it is reasonable to construct a type of empirical formula including the product of notch length l_m and notch depth d_m. In spite of the minor effect as found in Section 5.4, notch width (w_m) is accounted for to correct the "neighbor response" effect. With these regards, the formulas for both bending moment and critical curvature are constructed as follows:

$$\begin{aligned}\frac{M_{cr}}{M_i}(\frac{\kappa_{cr}}{\kappa_i}) &= 1 - f(\frac{S_{loss}}{S_0}, \lambda_w) \\ &= 1 - f(\lambda_l d_m/t, \lambda_w)\end{aligned} \tag{5.15}$$

Where M_i and κ_i are the ultimate bending moment and the critical curvature of intact pipe, respectively. A regression analysis on the FEM results is undertake to build up such relationship.

$$\frac{M_{cr}}{M_i} = 1 - a_1(\lambda_l \frac{d_m}{t})^{b_1}(\lambda_w)^{c_1} \tag{5.16}$$

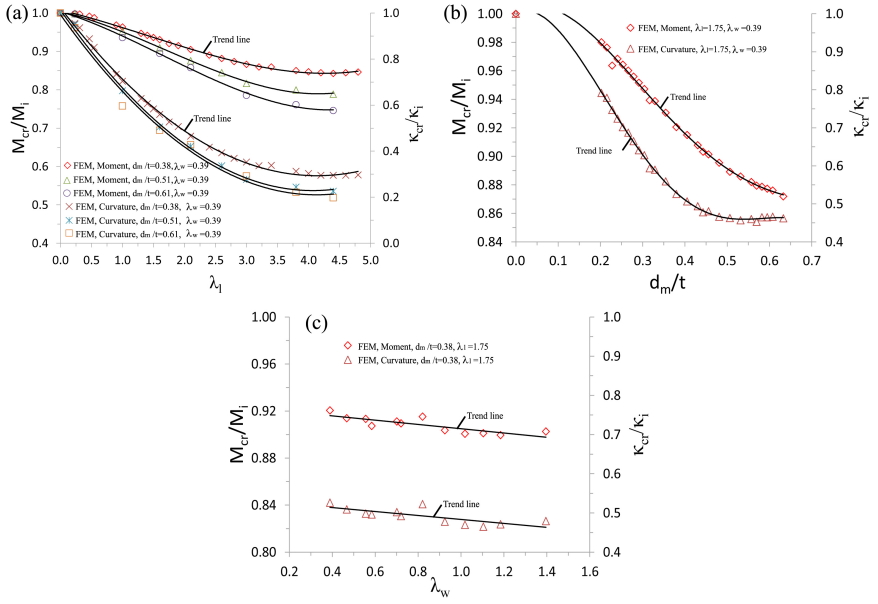

Figure 5.8: Variation tendencies of residual bending moment and critical curvature: (a) variation of normalized notch length (λ_l); (b) variation of normalized notch depth (d_m/t); (b) variation of normalized notch width (λ_w).

$$\frac{\kappa_{cr}}{\kappa_i} = 1 - a_2(\lambda_l \frac{d_m}{t})^{b_2}(\lambda_w)^{c_2} \tag{5.17}$$

Where a_1, b_1 and c_1 are 0.139, 0.91 and 0.253, respectively; a_2, b_2 and c_2 are 0.652, 0.557 and 0.205, respectively. The prediction results are compared with the test, analytical and simulation results, as shown in Figure 5.9. A satisfying comparison has been presented. Compared with the analytical solution, the formula of bending moment produces a lower prediction due to the accounting of notch width effect.

Likewise, the definition from [15] has been used to determine model uncertainty.

$$X = X_{true}/X_{predict} \tag{5.18}$$

Where X_{true} is the data from either experimental test or numerical simulation, and $X_{predict}$ is the prediction values due to proposed equations. It is also assumed that both X_{true} and $X_{predict}$ are from the same cases with the same material properties and geometry. Hence, the mean value (bias), standard error of X, and coefficient of variation (COV) are statistically calculated, as shown in Table 5.6. The comparison with test has not been conducted since only one valid test data from specimen is available.

It shows that the extent of variability for the prediction of M_{cr} is smaller than 1.5% in relation to the mean bias value. A relative large COV (22.42%) for the prediction of κ_{cr} is obtained. However, a conservative prediction is provided for most of the cases with k_{cr}/k_i between 0.2 and 0.7, as seen in Figure 5.9 (b).

Table 5.6: Model uncertainties of the proposed formulas.

X	Moment, Equation (5.16)		Curvature, Equation (5.17)	
	Mean (Bias)	COV	Mean (Bias)	COV
FEM	1.0012	0.013	1.024	0.2242

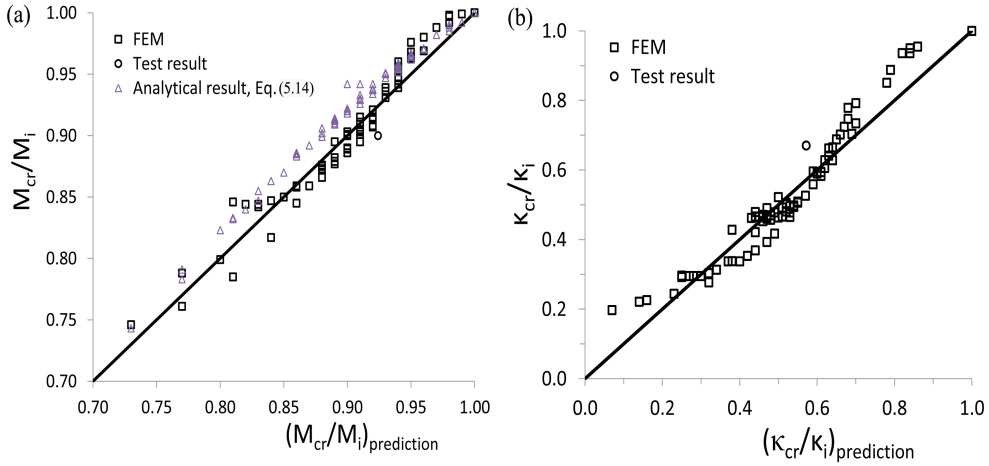

Figure 5.9: Comparison among prediction of proposed equations, experimental, numerical results and analytical results: (a) normalized residual ultimate moment (M_{cr}/M_i); (b) normalized critical curvature (κ_{cr}/κ_i).

Figure 5.10 shows the prediction results of notched metallic pipes with the changing of the loss area of metal loss. Notch width is fixed to 0.39 for all the compared cases. The FEM results are also presented in this figure. With the increase of loss area, both bending moment and curvature decrease considerably. Analysis of variance (ANOVA) shows that R squares of the fitted equations are 0.958 and 0.927, respectively, which reflects a high precision of prediction.

5.6 Conclusions

In this chapter, a numerical investigation on seamless pipes with low diameter-to-thickness ratio that suffered from metal loss damage has been preformed. A simplified numerical model accounting for structural damage has been developed, which can provide a fast modeling and calculation based on nonlinear FEM. The results of physical test from representative specimens have been numerically simulated and used for validation. Through the numerical models, the effect of notch and its specific parameters has been identified. The occurrence of notch damage on the compression side accelerates the failure of pipe due to the rapid localization of damaged region with an elastic-plastic failure mode.

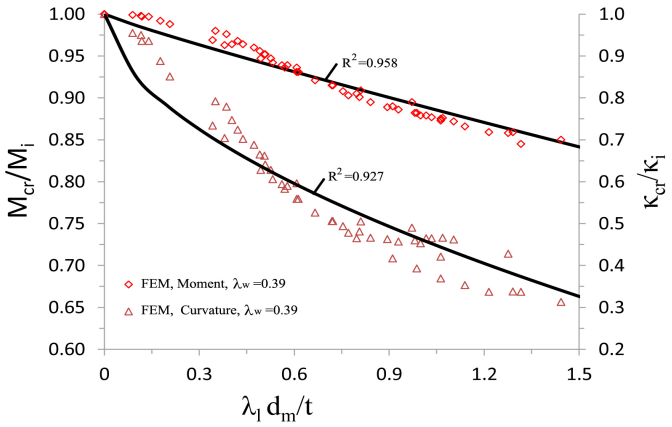

Figure 5.10: Prediction of damaged metallic pipes with changing of the loss area of a notch in the damaged pipe cross-section.

The 4^{th} key question of this thesis in terms of the effects of metal loss parameters, including notch depth (d_m), notch length (l_m), and notch width (w_m), has been identified. The larger the notch depth and/or the notch length is, the smaller the bending capacity will be. The increase of notch width slightly reduces pipe strength, presenting a linear tendency.

Moreover, the effect of metal loss on pipes subjected to pure bending has been quantified (the 6^{th} key question), expressed as a function of loss area of notch in terms of the production of notch depth and length. The effect of notch width is also accounted for in order to correct "neighbor response" effect. Empirical formulas (Equations (5.16) and (5.17)) for the predictions of residual strength are proposed for quantification.

These formulas could be utilized for practice purposes to estimate the residual ultimate strength of damaged pipes with metal loss on their compression side, and then facilitate the decision-making of pipe maintenance after mechanical interference. It should be noted that the proposed formulas in this chapter are only based on a certain type of metallic pipes with D/t around 21. Further validation is still needed to be done for their applicability in other relevant domains. Meanwhile, the impact induced residual stress from mechanical interference has not been accounted for in the proposed formulas.

Chapter 6

Studies of combined damage and fracture failure on the strength of metallic pipes*

In the former chapters, the effects of individual structural damage including a dent and the metal loss in terms of a notch induced by mechanical interference are quantified. As stated in Chapter 2, however, structural damage in terms of combinations thereof is more likely to happen in reality, and few relevant studies have been found on its effect on pipe residual strength. Obviously, the consequence of combined damage on metallic pipes cannot be simply estimated through linear superposition of the effect of individual damage due to factors such as geometrical nonlinearity of damage. A lack of consensus on how to account for the severity of the combined damage on metallic pipes under bending still exists. Another detrimental consequence is the fracture failure caused by structural damage on pipes under bending. For any types of damage on the tensile side of pipes under bending, possible fracture failure may be introduced. Its occurrence dominates the residual strength of pipes. Therefore, the aim of this chapter is to quantify the residual ultimate strength of seamless pipes with combined dent and metal damage subjected to bending. An initial exploration on the interaction effect between fracture failure and residual strength is also carried out based on case studies.

The structure of this chapter is arranged as follows. A brief description on the basis of fracture mechanism is presented in Section 6.1 in order to take into account the fracture failure in this chapter. Section 6.2 describes the simplifications of the combined dent and notch damage, as well as the damage with a crack. Numerical models accounting for different kinds of combined damage are developed and described respectively in Section 6.3. The XFEM (Extended Finite Element method) is used for the damaged models which may have a crack initiation and propagation. Section 6.4 presents the comparison results between simulation and test in terms of failure modes and moment-curvature diagrams for the spec-

*This chapter is partially based on the paper Jie Cai, Xiaoli Jiang, Gabriel Lodewijks, Zhiyong Pei, and Weiguo Wu. Residual ultimate strength of damaged seamless metallic pipelines with combined dent and metal loss. Marine Structures. 61:188-201, 2018 [37].

imens with combined dent and notch. A series of case studies are carried out for pipes with different types of damage in Section 6.5. In this section, an investigation of residual stress on pipes is performed. Meanwhile, the simulation results of pipes with combined damage are presented by changing the geometrical size of each type of damage. A qualitative study on pipes with a crack is also conducted. In Section 6.6, prediction formulas are developed, and the application domain is extended to different types of D/t based on simulation. In the end, conclusions of this chapter are drawn in Section 6.7.

6.1 The basis of fracture mechanism

A brief description of the fracture mechanism is presented in this section, which will facilitate the understanding of the study on the effect of the fracture failure on residual strength of pipes.

Fractures occur when the bonding of micro-structural elements within a material is broken in some way. In fracture mechanism, how the crack formed is not necessarily relevant. What is important is to assess how an existing discrete crack can affect the continued operating life or the structural strength of the containing body. The cracks can be propagating at a fairly steady rate, or remain stationary, waiting to fail if the stresses in their vicinity build up to critical levels, or exist with no danger to the integrity of the structure [97]. The conditions of operation, as well as the actual loading that the body is undergoing, are extremely important for the crack behavior on structures. Meanwhile, the effects of temperature, time, and material ductility all play an important role on the future of the given discrete crack. Therefore, fracture mechanics is required in order to evaluate fracture parameters under specific conditions.

Normally, a crack is assumed to exist somewhere in structures with a definable geometry. Depending on the complexity of geometries, the crack and surrounding material can be represented either as a 2D (two dimensional) problem or a 3D (three dimensional) problem. In a 2D problem, it is considered as a plane stress condition when the out-of-plane thickness is constant and small with a zero out-of-plane stress component. When the thickness is large enough and the out-of-plane strain component is zero, it is considered as a plane strain condition. In the 2D cases, the discrete crack ends in a tip, whereas it is a front or a profile in 3D problems. Once the fracture parameters on these places are evaluated, an indication of how likely the crack will affect the structures will be provided. The typical fracture parameters which are used to evaluate the stability of existing cracks include the stress intensity factor (K_I), the energy release rate (G), the J-integral (J) and the crack tip opening displacement (CTOD), etc [6, 28, 97]. In this chapter, however, these parameters have not been compared due to the lack of test data.

At a given load level, if the extent of the plastic zone surrounding the crack tip, or profile in 3D, is small, then it can be defined as a condition of linear elastic fracture mechanics (LEFM). The plasticity effects can be neglected under this condition. If on the other hand, the plastic zone is considerable, then elastic-plastic fracture mechanics (EPFM) condition is used. For the metallic pipes with a low D/t in this thesis, a considerable amount of plastic strain exists. Hence, their material behaves in a ductile manner in the condition of EPFM. Meanwhile, there are three basic fracture modes at a loaded crack tip, including Mode I, Mode II and Mode III, as seen in Figure 6.1. They represent the opening mode, shearing

mode and tearing mode respectively. In practice, fracture Mode I dominates. Therefore, in this thesis, only Mode I crack has been taken into account when pipes are subjected to pure bending.

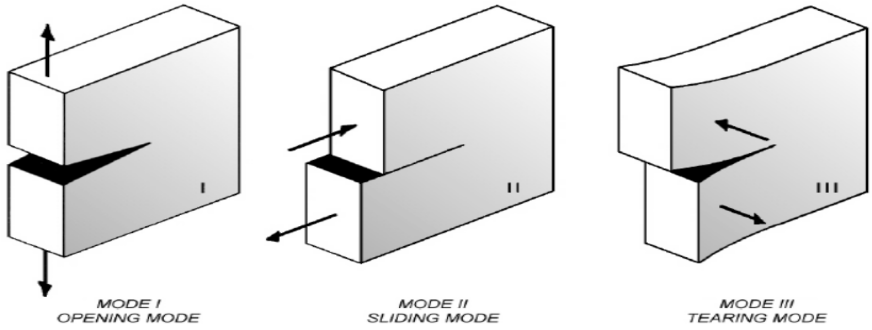

Figure 6.1: Fracture modes at the 3D crack tip [97].

6.2 Damage simplifications

The damage considered in this chapter includes a combined dent and notch damage on the pipe compression side, a combined notch and crack damage on the pipe tensile side, a notch on the pipe tensile side and a crack on the pipe tensile side. We do not take into account any crack damage on the compression side of pipes, which will not produce fracture failures.

6.2.1 Combined dent and notch

The configuration of a combination of a dent and a notch is based on the physical test, as seen in Figure 6.2. For the notch, the notch length (l_m) is the chord length of the remaining sector in the damaged pipe cross-section, while the notch depth (d_m) locates in the central axis of the damaged cross-section, as seen in Figure 6.3. There is a practical reason for this definition as well. In general, the on-site measurement of a straight line is much easier and more accurate than the measurement of an arc length after the occurrence of damage. Only a notch with rotation angle (θ_m) of 90^o is considered. Furthermore, the outer surface of the notch has been deformed due to the dent damage. Hence, it is assumed that such a dent induced deformation can seldom affect the notch, for instance, its depth and its regular shape. The definition of a dent is the same as the one in the former research on a dent in Chapter 4. Due to the largest effect of a dent with the rotation angle (θ_d) of 90^o, we only considered the dent with its length (l_d) in the pipe hoop direction in this study.

6.2.2 Damage with a crack

For any types of damage with a crack, they will be simplified, as illustrated in the sketches in Figure 6.4. In practice, a surface crack is usually simplified as a semi-circle shape or a semi-elliptical shape with the crack depth of c and half-crack length of a. In this thesis,

however, due to the workmanship for crack cutting in the test specimens in Chapter 3, the configuration of a crack on pipe surface is simplified as an arc-shape with equal crack depth. The crack depth is denoted as $c = d_c$, while the crack length is denoted as $a = l_c/2$, as seen in Figure 6.4. Only a crack in the hoop direction of the pipe surface ($\theta_c = 90^o$) on its tensile side is taken into account. It is supposed to produce a Mode I fracture failure under pure bending.

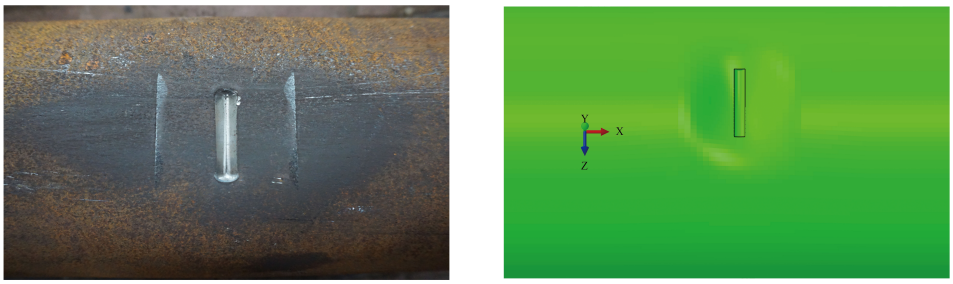

(Damage from test) (Damage from FEM)

Figure 6.2: Combined dent and metal loss damage from both test and numerical model.

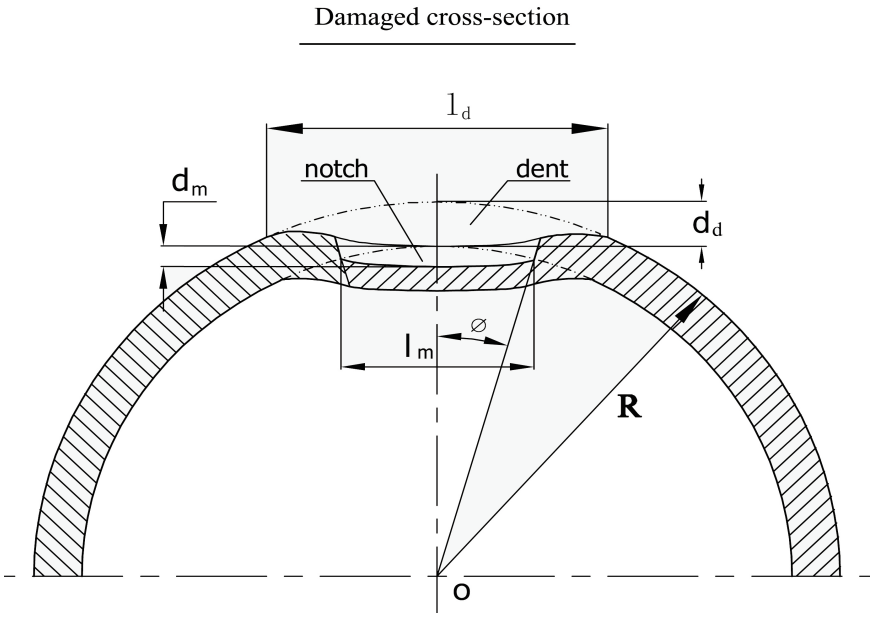

Figure 6.3: Sketch of a combined dent and notch damage on pipe surface (damaged cross-section).

6.3 Numerical models

For the cases that will not introduce fracture failure, the traditional FEM method will be used for modeling and calculation (Section 6.3.1). Due to the introduction of a crack and the possible fracture failure, the XFEM (Extended Finite Element Method) will be used for simulation of pipes with damage on their tensile side, which is presented in Section 6.3.2.

6.3.1 Model for combined dent and notch

The numerical model with an overall of 248000 elements, accounting for combined damage, have been developed in ABAQUS /Standard [1] through Python script, as seen in Figure 6.5. The isotropic hardening of the material and the von Mises yield criterion are used in the numerical simulation. Due to the data missing of large strain ($\sim \geq 0.1$) in tests, as described in Chapter 3, the detailed stress-strain relationship is fitted through the measured material properties. The fitting method has been described in Chapter 4. A three dimensional element C3D8R is used in the numerical model. According to the research of the influence of initial imperfection on damaged pipes in Chapter 4, initial imperfection has not been accounted for any more.

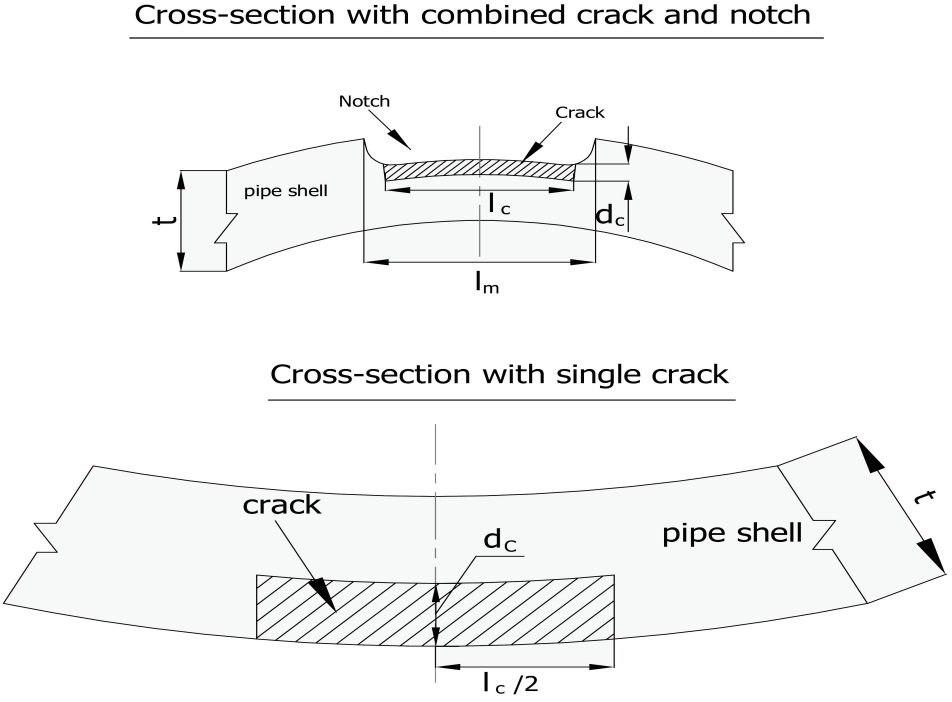

Figure 6.4: Sketches of a single crack, and a combined notch and crack.

A simplified model has been deployed, removing the contact segments between specimen and strips for the sake of simulation efficiency. Instead, a simplify-supported boundary condition has been used and two referential nodes have been introduced to represent the loading location of specimen in the test, exerting an equivalent forced-rotation through the reference points.

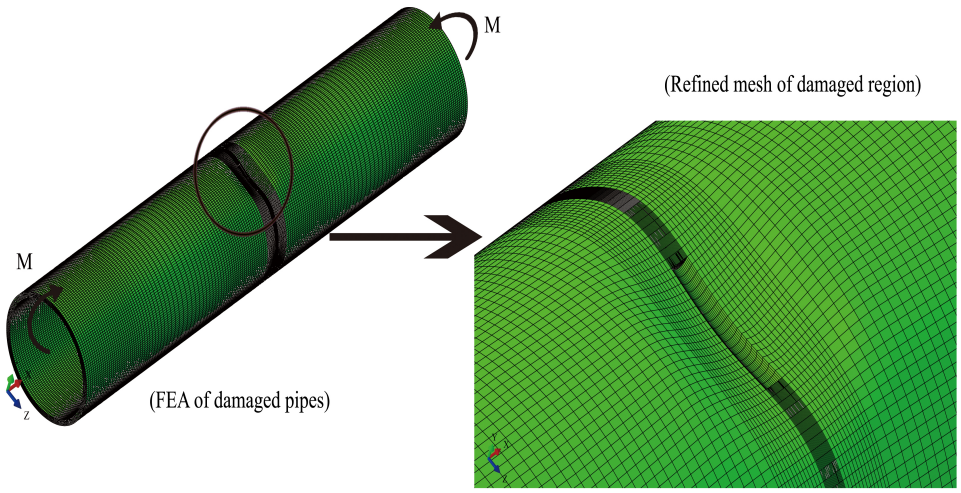

Figure 6.5: Schema of FEM model of pipes with combined damage.

A mesh sensitivity study is conducted for the numerical model. As seen in Figure 6.5, the general mesh size in pipe hoop direction is 3 *mm*, less than 7% of one half-wave length ($\lambda_{cl} = 1.728\sqrt{Rt}$ [107]), while the general mesh size in pipe longitudinal direction is from 4 *mm* ($9\%\lambda_{cl}$) to 9 *mm* ($20\%\lambda_{cl}$) with a double bias mesh strategy. Meanwhile, the mesh is largely refined in damaged region, with the maximum mesh size equal to 0.5 *mm*, i.e. less than 1.2% of one half-wave length (λ_{cl}) of cylindrical shells. The number of elements are only allowed to increase in places that cannot assign a specific mesh seeds. Six layers of elements in thickness direction are deployed to guarantee the simulation accuracy.

6.3.2 Model for damage with a crack

In this section, a brief comparison between the traditional fracture method and the XFEM is carried out due to the complexity of the crack modeling. Besides, the numerical models for damaged pipes through XFEM are presented.

Traditional fracture method

In traditional finite element method, cracks are often modeled as well-defined tips or profiles to obtain the K_I or J. The mesh should conform to the cracked geometry. The crack front should be explicitly defined with a specification of the virtual crack extension direction. The smaller the radial dimension of the elements from the crack tip, the better the calculations of stress, strain, and contour integral will be.

Meanwhile, a special collasped element for crack tip is required in order to obtain the singularity feature around the crack tip, as shown in Figure 6.6. This type of element has a modified shape function which reflects the $\sqrt{r}$ (r is the distance between crack tip and the points in the crack vicinity) displacement variation around the crack tip. A ring of the special crack element is usually used surrounding the crack tip, whist standard elements are used in other places. The angles of elements around the crack tip should be in the range of 10-22.5 degree for accurate simulation [1]. In practice, the crack tip singularity is realized by moving the midside nodes along the sides of crack tip elements. For instance, in the commercial software Abaqus, by moving the midside nodes of collapsed elements to the quarter positions (0.25) close to the tip, the $\frac{1}{\sqrt{r}}$ strain singularity for an elastic fracture mechanics application can be created.

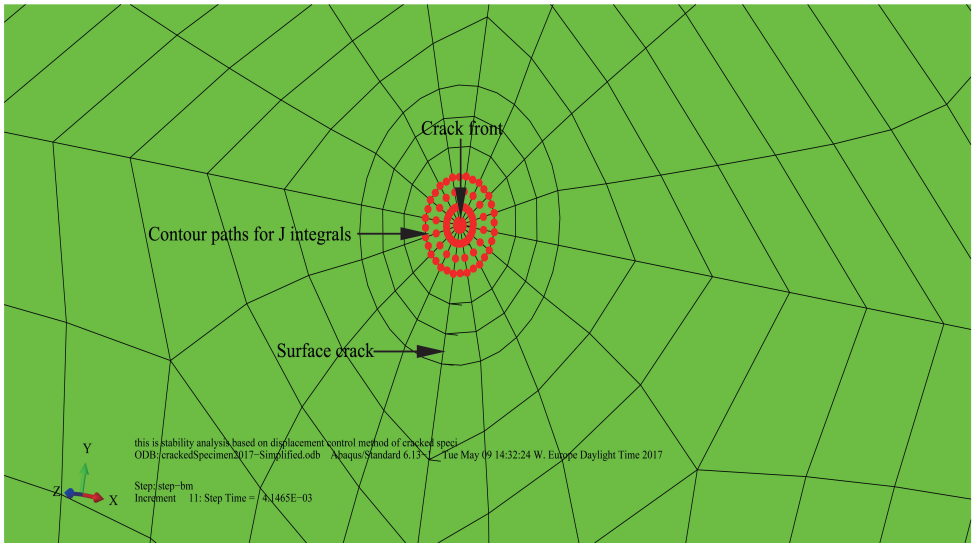

Figure 6.6: An image of crack front with special collapsed element in a pipe surface by the traditional fracture method.

Extended finite element method

As described in the previous section, a great effort is needed on the refined meshing of crack tip region. Modeling a growing crack is even more cumbersome due to the re-meshing of the crack geometry and the discontinuity when the crack is progressing. In order to circumvent these shortcomings, the extended finite element method (XFEM) was first introduced by Belytschko and Black [20] based on the concept of partition of unity by Melenk and Babuska [93].

XFEM is an extension of the traditional finite element method. The essential concept in XFEM is to add enrichment functions to the approximation which contains a discontinuous displacement field. Therefore, the presence of a crack is ensured by the special enriched functions in conjunction with additional degrees of freedom.

As a result, for an existing crack in structures, this method does not require the mesh to match the geometry of the discontinuities. As seen from the crack at the bottom of a

notch on a pipe surface in Figure 6.7, only the location of an existing crack is needed to be designated with an enriched region for the possible crack propagation. Meanwhile, it can be also used to perform contour integral evaluations for an arbitrary stationary surface crack. Both material and geometrical nonlinearity are allowed. Therefore, it is an attractive and effective way for the simulation of the interaction effect between a fracture and the residual strength of a damaged pipe.

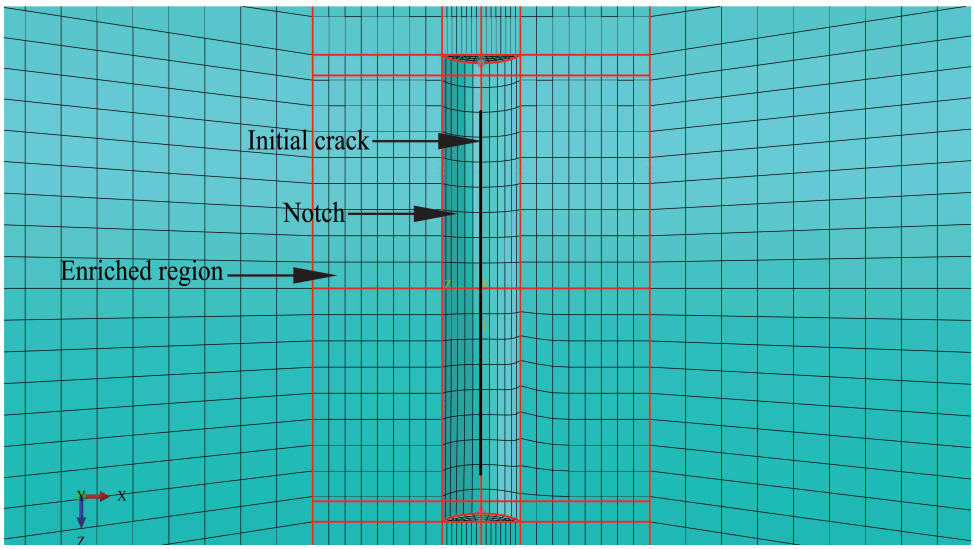

Figure 6.7: An image of a crack at the bottom of a notch on a pipe surface by the XFEM.

Additional damage modelings, including damage initiation criteria and damage evolution laws, are required for the simulation of degradation and eventual fracture failure of an enriched element by XFEM. Once the damage initiation criterion is met, damage will occur according to damage evolution laws. Typical crack initiation criteria are available in most of the commercial structural software, such as the maximum principal stress criterion, the maximum principal strain criterion, or the maximum nominal stress criterion. The crack propagation direction is normally orthogonal to the maximum principal stress/strain direction when the fracture criterion is satisfied. In this study, only the maximum principal stress criterion is used.

For possible crack propagation during simulation, the critical energy release rate G^* is estimated based on the method in [31]. Since it is impossible to directly measure the fracture toughness by testing, the estimation of K_{IC} may be obtained from the correlations with Charpy V-notch impact test. The material for impact test should be the same general microstructural type with the structure (e.g. weld metal, HAZ, parent material). Equation (6.1) describes the relationship between Charpy impact energy (measured on standard specimen with $10mm \times 10mm$, $2mm$ deep V-notched) and the fracture toughness values in terms of K_{IC}, where impact energy is from Charpy specimens. Meanwhile, to avoid the overestimation of fracture toughness at the service temperature, K_{IC} shall not exceed the value given by the following Equation (6.2) [31].

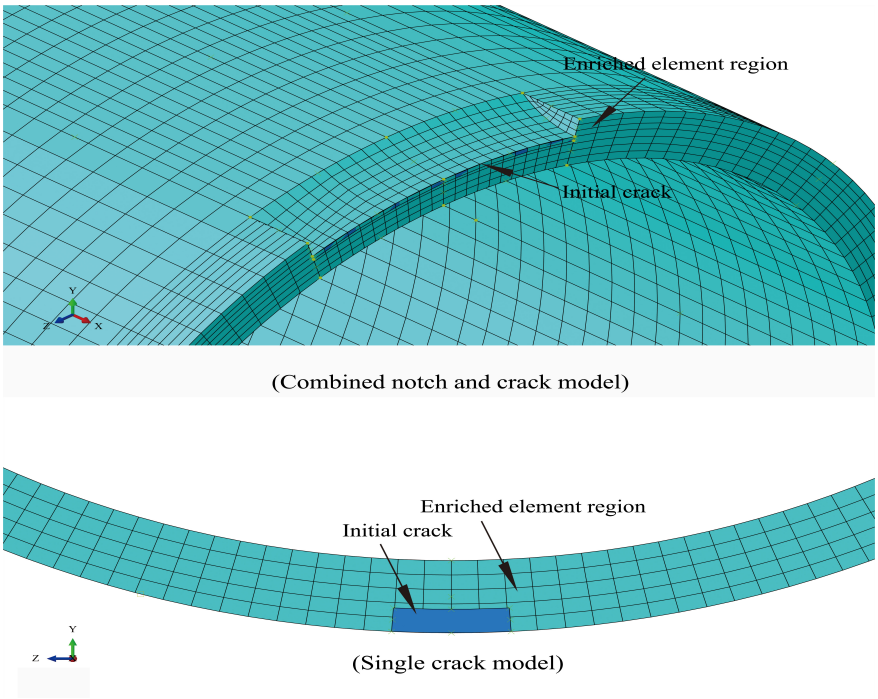

Figure 6.8: Schema of mesh distribution of cracked regions.

$$K_{IC} = [(12\sqrt{C_v} - 20)(\frac{25}{B})^{0.25}] + 20 \tag{6.1}$$

$$K_{IC} = 0.54C_v + 55 \tag{6.2}$$

Where K_{IC} is the estimation of the fracture toughness (in $MPa\sqrt{m}$), B is the thickness of the material (in mm), and C_v is the lower bound Charpy V-notch impact energy at the service temperature (in *joules*). The fracture toughness in energy (G^*) can be written as Equation (6.3) (in $Mjoules$):

$$G^* = \frac{(1-\nu^2)}{E} K_{IC}^2 \tag{6.3}$$

According to the material certificate of test specimens in Chapter 3, the material Charpy impact energy is 36 *joules*. When the nominal thickness of pipe specimens is 8 mm, for instance, the estimated fracture toughness K_{IC} and the corresponding critical energy release rate G^* are 74.44 $MPa\sqrt{m}$ and 0.0245 $MJoules$, which will be used in the following case studies of damaged pipes with a crack.

The modeling strategy is the same with the traditional FEM by the use of XFEM. Two types of numerical model with a crack are shown in Figure 6.8, including the pipe with a single crack and the pipe with a crack at the bottom of a notch. The three dimensional element C3D8R is used for the model. Since there is no need to refine the mesh in crack

front, the mesh distribution is the same as the model in the previous section. No extra refine of mesh around the crack region is required. The crack dimension and location are based on the physical test, while the crack shape is illustrated in Section 6.2.2. Through the XFEM, an enriched element region is designated in the vicinity of the crack. The newly introduced crack direction is orthogonal to the maximum principal stress direction as long as the fracture criterion has been satisfied.

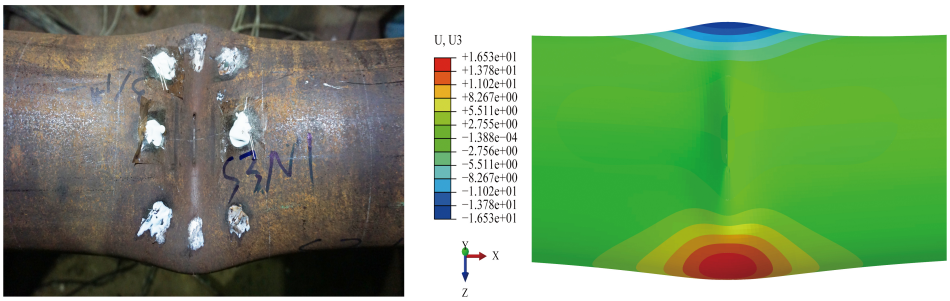

Failure mode in test Failure mode in FEM

Figure 6.9: Failure mode of specimen with combined damage.

6.4 Model validations

In this section, the structural behaviors of specimens with combined dent and notch from test are simulated through the developed model in the previous section. The material properties from the material tensile test in Chapter 3 are used, having a yield stress of 400 MPa, an ultimate tensile stress of 583 MPa and the maximum elongation of 22.6%. The test data have been compared with the simulation results in terms of structural failure modes, bending moment-curvature diagrams and strength capacity. Due to the lack of test data in specimens with a crack, comparisons with cracked specimens are not carried out.

For a comparison of the results, the bending moment (M) is normalized by the plastic bending moment ($M_y = 4R_a^2 t\sigma_y$), while the curvature (κ) is normalized by the curvature-like expression ($\kappa_0 = t/4R_a^2$). Only global curvature in the simulation is selected for comparison. The selected locations for the calculation of global curvature in the numerical simulation are the same as used for the tests. The bending moment in the simulation is the resultant of all node forces multiplied by their corresponding force arms in the central cross-section of specimens.

6.4.1 Comparison of simulation results

Both the structure failure mode and failure location have a good agreement with each other, as illustrated in Figure 6.9. Due to the occurrence of combined damage, it initiates the failure of the pipe specimen. The largest lateral displacement of the damaged pipe cross-section has not been compared due to a lack of data.

The comparisons of the bending moment-curvature diagrams between test and numerical results are shown in Figure 6.10. The corresponding geometry and results of the speci-

mens are listed in Tables 6.1 and 6.2, respectively. Both specimens (S5N1 and S5N2) have a combined dent and notch with 90^o on the pipe compression side, as shown in Figure 6.2. The occurrence of combined damage has induced a rapid failure of the specimens. Once the bending moment has reached the peak point, it decreases quickly with the further increase of curvature in almost a linear tendency until the termination of the test. The early scatter in the elastic domain of the curves indicates that there is a discrepancy of elastic modulus between the test and the simulation, where the default value for seamless steel is used as 2.06×10^5 *MPa* in this chapter.

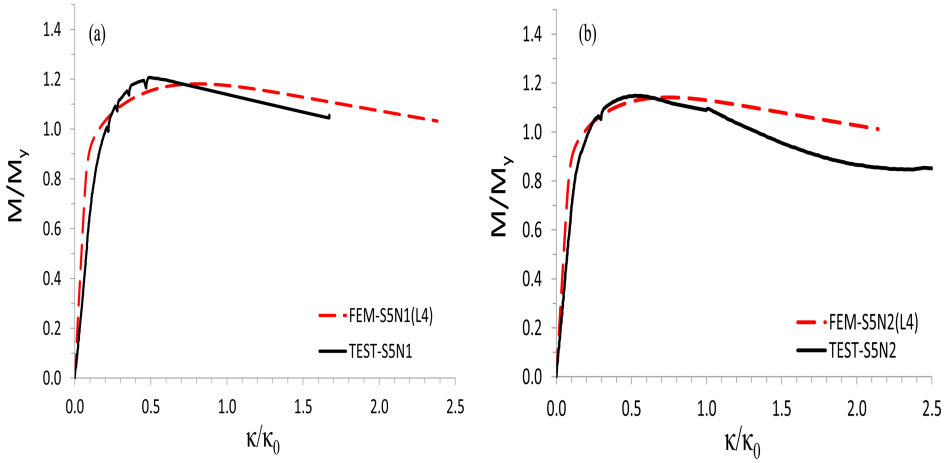

Figure 6.10: Comparison between numerical and test results in terms of bending moment-curvature diagram: (a) specimen S5N1; (b) specimen S5N2.

Table 6.1: Overview of specimens with combined damage (Dimension unit: mm; Compression side; Damage size: $l_{(i)} \times w_{(i)} \times d_{(i)}$).

S.N.	D	t	D/t	Crack	Dent	Notch
S5N1	168.25	8.33	20.20	$44 \times 0.31 \times 0.70$	$110 \times 80 \times 10$	$44 \times 9.5 \times 3.0$
S5N2	168.80	7.60	22.21	$44 \times 0.31 \times 0.70$	$110 \times 80 \times 10$	$44 \times 10 \times 3.0$

The comparison results in terms of critical bending moment (M_{cr}) and curvature (κ_{cr}) are listed in Table 6.2. It is observed that a good agreement in the critical bending moment has been reached, i.e., less than 2.2% discrepancy. The results of critical curvature from the simulation have overestimated the deformation capacity of specimens with a relative large scatter. This is likely attributed to the factors of the material properties and the measurement method for curvature in the test.

Table 6.2: Comparison results of damaged specimens.

S.N.	M_{cr}(Test) (kNm)	M_{cr}(FEA) (kNm)	κ_{cr}(Test) (1/m)	κ_{cr}(FEA) (1/m)	error-M (%)	error-κ (%)
S5N1	97.173	95.12	0.163	0.264	-2.11	61.96
S5N2	85.72	85.21	0.153	0.218	-0.59	42.48

6.5 Case studies

In this section, numerical simulations on damaged pipes are carried out based on the validated models. The effect of residual stress is investigated, assuming a linear distribution in the pipe hoop direction. Meanwhile, case studies on damaged pipes with fracture failure are carried out to investigate the interaction effect between fracture and residual strength.

6.5.1 Investigation of residual stress

Residual stress is the auto-balancing stress that is locked into material when it is free from external forces. Factors such as fabrication processes, pipe joining processes, thermal processing, welding, heat treatment, mechanical forming and long term service conditions are the most common sources of residual stresses [5, 104, 113]. They are presented in every manufacture component and assembled structures. It can be estimated through numerical modeling of forming processes, welding processes and impact scenarios or through experimental methods.

In this section, the distributions of residual stress on different types of pipes are first presented. Then, its effects on seamless pipes with/without damage are investigated. Assumptions of the stress distribution are made based on the real stress distribution of pipes caused by manufacture workmanship.

Distribution of residual stress

As illustrated in Figure 6.11, three different types of residual stress on pipes are found. For the spiral-welded pipe developed by the cold bending manufacture process [53, 123], it has a tensile residual stress on the inner surface and a compression stress on the outer surface in the pipe hoop direction. Due to the occurrence of weld seam, the stress component in hoop direction has several turning points between compression and tension along the pipe thickness. For seamless pipes produced by cold-drawing, residual stress presents a monotonical state. As shown in Figure 6.11(b) [104], the residual stress component in the hoop direction changes from compression on the inner surface to tension on the outer surface. The axial component changes from a strong compression on the inner surface to tension on the outer surface. The residual stress in the radial direction is small, varying from 0 on the inner surface to a slight compression on the outside of pipe.

Moreover, for seamless pipes produced by hot-rolling, the residual stress component in the hoop direction also presents a monotonical increase/decrease state, as shown in Figure 6.11 (c). In the test from [5] on a typical API X60 seamless steel pipe, it is measured

that there is a compression stress component in the hoop direction on the outside layer of seamless pipe, monotonical decreasing until the largest tensile stress on the inside layer of pipes. The maximum residual stress is approximately 10% of the material yield stress.

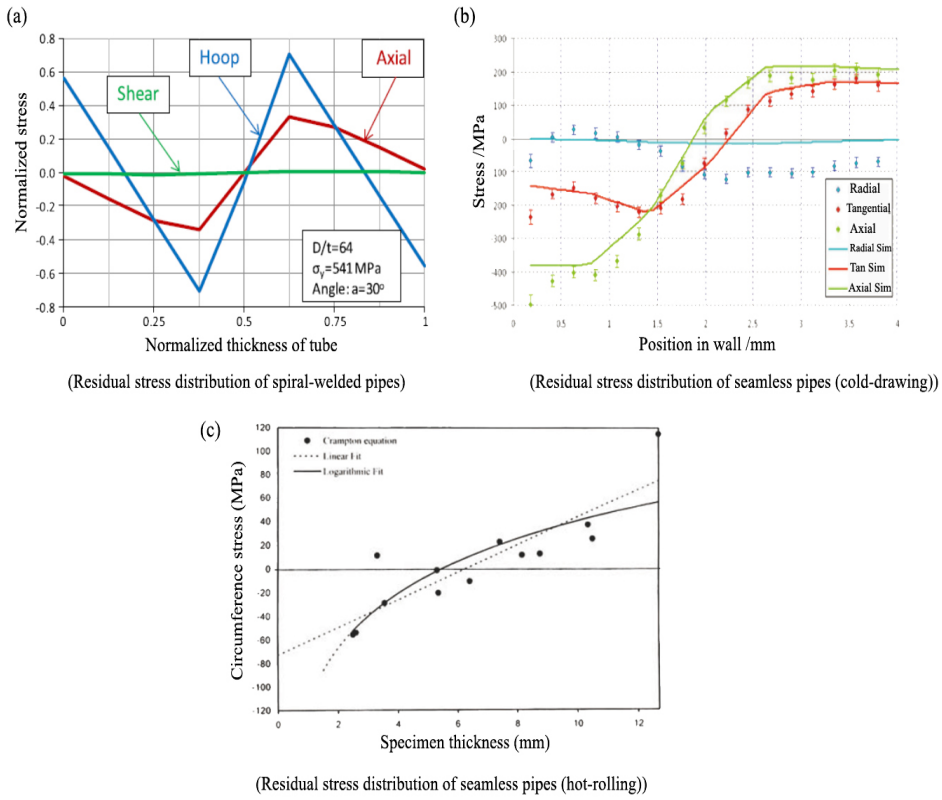

Figure 6.11: Typical residual stress distribution of different types of pipes: (a) spiral-welde pipes (image from [123]); (b) seamless pipes by cold-drawing (image from [104]); (c) seamless pipes by hot-rolling (image from [5]).

Effect of residual stress

As described in the previous section, the distribution and peak values of residual stress on pipes vary with their manufacture methods. When it comes to the distribution of residual stress induced by impact, it would be more complex due to factors such as specific impact location, angle, damage type, and energy level. Meanwhile, the lack of test data and relevant research on such distribution make it more difficult to quantify its effect on the pipe strength. Hence, assumptions of its distribution are first made in this section. An analysis of the effect of residual stress is then carried out on pipes with/without damage for comparisons.

Since the seamless pipes in this study is produced by hot-rolling, the residual stress is assumed only in the pipe hoop direction. The peak values of residual stress are assumed to be $\pm 10\%\sigma_y$ with a linear distribution, as shown in Figure 6.12, where the values of 0.0

and 1.0 correspond to the inner surface and the outer surface of the pipes respectively. The lowest compression residual stress ($-34.5MPa$) is on the outer surface of pipes, while the largest tensile stress ($34.5MPa$) exists on the inner surface of pipes. The local stress induced by impact is not considered. The type of existing damage in this section is intentionally separated for comparisons.

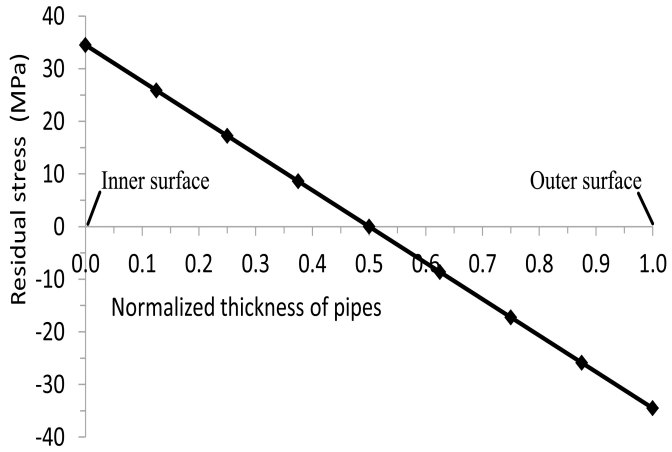

Figure 6.12: Distribution of residual stress in the pipe hoop direction across pipe thickness for the simulation.

Figure 6.13 illustrates the normalized residual strength in terms of M_{cr}/M_y and κ_{cr}/κ_y with respect to the wrinkling imperfection δ_i/t for an intact pipe. The range of the initial imperfection amplitude is between 0 and $0.2t$. If the results between the pipes without residual stress and the pipes with residual stress are compared then, it is found that the residual stress only slightly affects the pipe strength. With the increase of imperfection, the residual stress presents a small retardation effect on the strength capacity.

When structural damage occurs on the pipe surface, different phenomena appear. Figure 6.14 shows the effect of residual stress on pipes with a dent. The dent depth varies between $0.2t$ and $2t$ with a fixed dent width (60 *mm*) and a dent length (100 *mm*) in the pipe hoop direction. The numerical results demonstrate a large increase of strength capacity accounting for residual stress when the dent depth is smaller than the pipe thickness t. With the further increase of dent depth ($t < d_d \leq 2t$), such retardation effect is shielded due to the large damage effect. It is likely because of the fact that the occurrence of the compression residual stress on the pipe outer surface postpones its yielding and then the loss of bending stiffness. When there is only a notch on pipes, it is found that the residual stress can seldom affect pipe strength, as illustrated in Figure 6.15. No obvious differences have been observed based on the numerical results. The occurrence of a notch has completely shielded the effect of residual stress. In sum, the residual stress in the assumed distribution provides a positive effect on the pipe strength, especially for intact pipes with a large initial imperfection (δ_i no less than $0.2t$) and dented pipes with small dent depth ($d_d \leq t$). Due to the occurrence of large structural damage, the effect of residual stress is shielded and becomes insignificant.

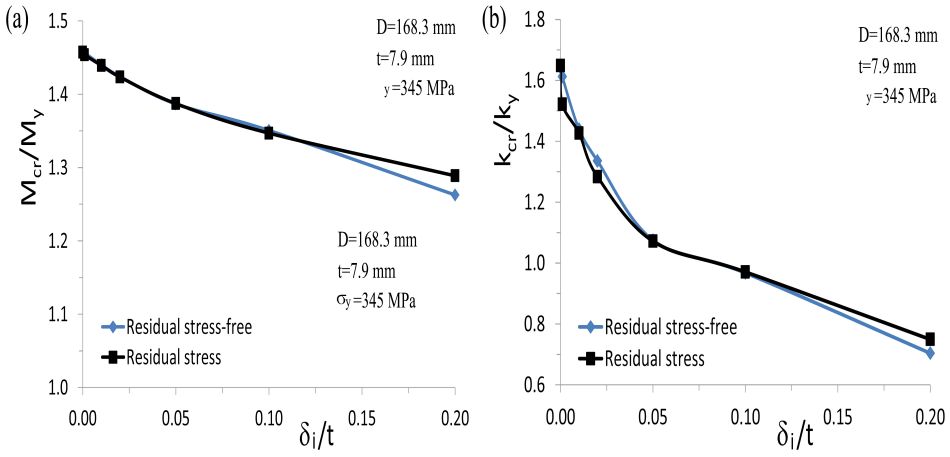

Figure 6.13: Normalized residual strength (M_{cr}/M_y, κ_{cr}/κ_y) with respect to wrinkling imperfection (δ_i/t) for an intact pipe; Effect of residual stress.

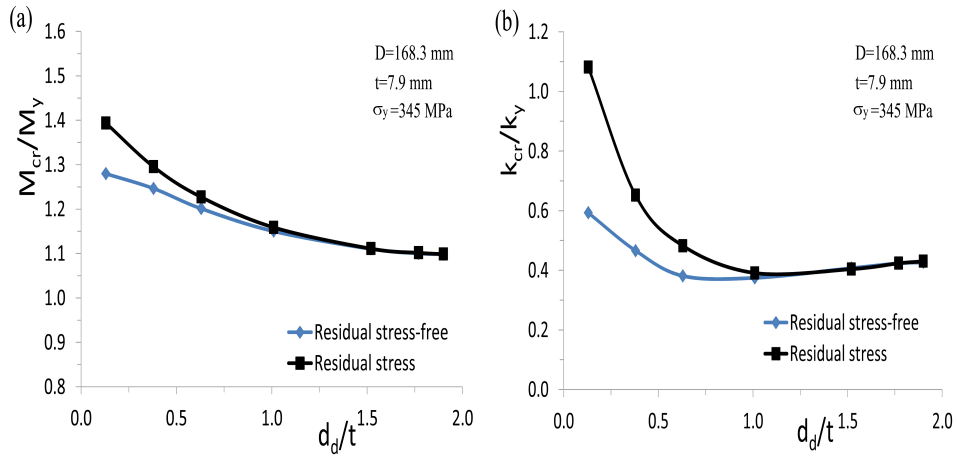

Figure 6.14: Normalized residual strength (M_{cr}/M_y, κ_{cr}/κ_y) with respect to dent depth (d_d/t) for a dented pipe; Effect of residual stress.

Table 6.3: Residual ultimate strength of pipes with varying of dent (G1, fixed notch).

Capacity	t=7.5 mm, l_m=44 mm, w_m=10 mm, d_m=1.5 mm, d_d/t											
G1	0.00	0.07	0.20	0.33	0.47	0.60	0.73	0.87	1.00	1.13	1.27	2.00
M_{cr}/M_i	0.980	0.955	0.916	0.886	0.862	0.844	0.830	0.820	0.811	0.804	0.798	0.778
κ_{cr}/κ_i	0.804	0.656	0.487	0.402	0.358	0.337	0.335	0.330	0.333	0.326	0.330	0.362

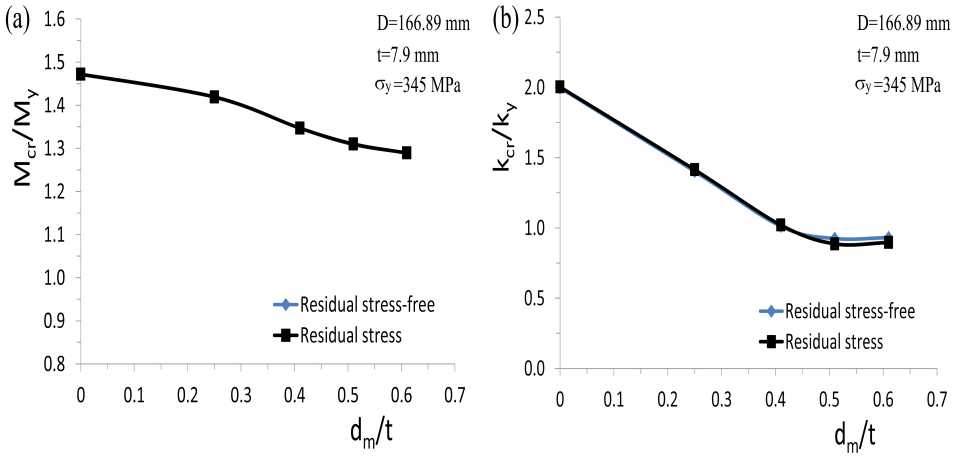

Figure 6.15: Normalized residual strength (M_{cr}/M_y,κ_{cr}/κ_y) with respect to notch depth (d_m/t) for a pipe with notch; Effect of residual stress.

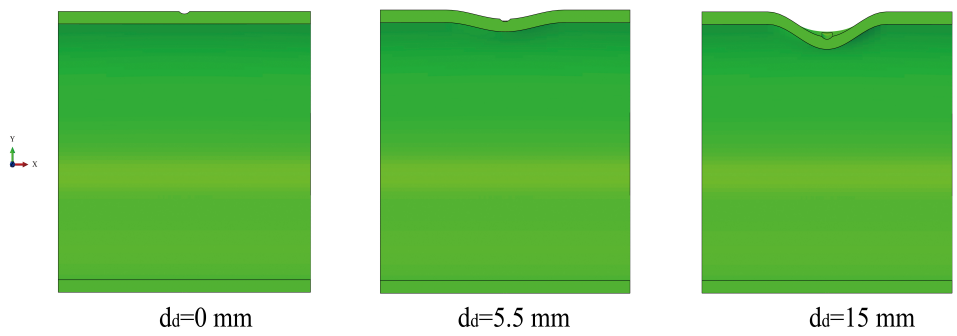

Figure 6.16: Images of varied dent depth with a fixed notch in combined damage.

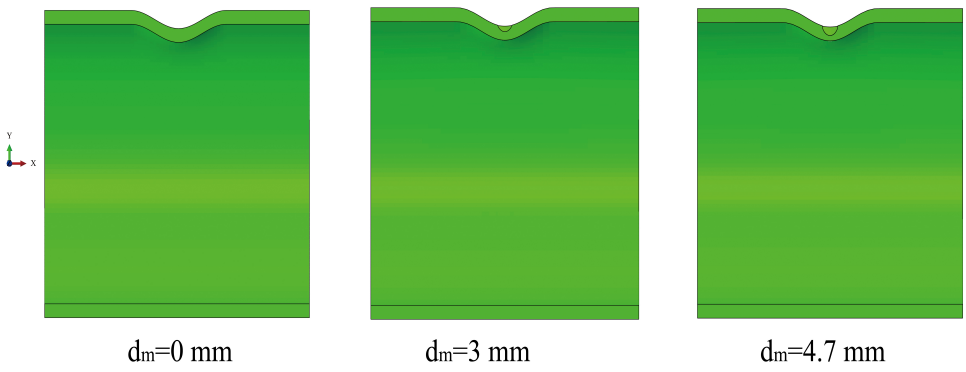

Figure 6.17: Images of varied notch depth with a fixed dent in combined damage.

Table 6.4: Residual ultimate strength of pipes with varying of dent (G2, fixed notch).

Capacity	t=7.6 mm, l_m=44 mm, w_m=10 mm, d_m=3.0 mm, d_d/t											
G2	0.00	0.07	0.20	0.33	0.46	0.59	0.72	0.86	0.99	1.12	1.25	1.97
M_{cr}/M_i	0.918	0.902	0.875	0.854	0.838	0.826	0.816	0.808	0.802	0.796	0.792	0.776
κ_{cr}/κ_i	0.522	0.461	0.397	0.370	0.345	0.342	0.337	0.340	0.344	0.345	0.349	0.368

Table 6.5: Residual ultimate strength of pipes with varying of dent (G3, fixed notch).

Capacity	t=7.6 mm, l_m=44 mm, w_m=10 mm, d_m=4.5 mm, d_d/t											
G3	0.00	0.07	0.20	0.33	0.46	0.59	0.72	0.86	0.99	1.12	1.25	1.97
M_{cr}/M_i	0.878	0.868	0.850	0.836	0.825	0.815	0.807	0.801	0.796	0.792	0.788	0.773
κ_{cr}/κ_i	0.465	0.440	0.408	0.383	0.378	0.371	0.364	0.368	0.358	0.361	0.363	0.380

Table 6.6: Residual ultimate strength of pipes with varying of notch (G4, fixed dent).

Capacity	t=7.6 mm, l_d=120 mm, w_d=60 mm, d_d=10 mm, d_m/t											
G4	0.00	0.20	0.24	0.28	0.32	0.36	0.39	0.43	0.47	0.51	0.55	0.62
M_{cr}/M_i	0.790	0.784	0.782	0.780	0.779	0.777	0.776	0.775	0.774	0.773	0.772	0.771
κ_{cr}/κ_i	0.326	0.335	0.330	0.342	0.342	0.344	0.344	0.344	0.344	0.356	0.356	0.358

Table 6.7: Residual ultimate strength of pipes with varying of notch (G5, fixed dent).

Capacity	t=7.6 mm, l_d=120 mm, w_d=60 mm, d_d=5 mm, d_m/t							
G5	0.00	0.20	0.28	0.36	0.43	0.51	0.59	0.62
M_{cr}/M_i	0.845	0.830	0.821	0.814	0.807	0.803	0.800	0.800
κ_{cr}/κ_i	0.329	0.329	0.322	0.328	0.341	0.343	0.357	0.357

6.5.2 Effect of combined dent and notch

In this section, by changing the geometrical size of damage, numerical simulations on damaged pipes are carried out. The geometrical dimensions of used pipes for investigation are listed in Tables 6.3 to 6.7 with the same outer diameter of 168.80 *mm*. The same material properties from the material tensile test in Chapter 3 are used, having a yield stress of 378 *MPa*, an ultimate tensile stress of 542 *MPa* and the maximum elongation of 24.6%. As discussed in the previous section, the residual stress has brought a little positive effect on the pipe strength capacity, and such effect is, for most of the time, shielded by the occurrence of large damage in damaged pipes. Hence, it has not been taken into account here, which represents a more severe situation.

In the following investigation, both the notch depth (d_m) and the dent depth (d_d) are normalized by the pipe thickness t. The simulation results in bending moment-curvature diagrams are normalized by M_y and κ_0, as described in Section 6.4. The results in terms of critical bending moment and critical curvature are normalized by their corresponding pipes without structural damage (M_i and κ_i). Therefore, reference values for G1 in simulation are 98.33 kNm and 0.567 $1/m$, while reference values for the other groups are 99.71 kNm and 0.579 $1/m$. The reference value for the test are 102.71 kNm and 0.401 $1/m$ based on specimen S1N4 in Chapter 3.

Two strategies are used for the following simulations and investigations in this section. The first one is to change the dent depth (d_d) whilst a moderate metal loss in terms of notch with a fixed dimension is preset, as shown in Figure 6.16. As shown in Tables 6.3 to 6.5, the normalized dent depth (d_d/t) varies between 0 and 2.0 under three different types of specific notch ($d_m/t = 0.2$, $d_m/t = 0.4$ and $d_m/t = 0.59$). Hence, they are categorized as groups $G1$, $G2$ and $G3$. The second one is to change the notch depth (d_m) whilst a moderate dent with a fixed dimension is preset, as shown in Figure 6.17. As shown in Tables 6.6 and 6.7, the normalized notch depth (d_m/t) varies between 0 and 0.62 under two different types of specific dent ($d_d/t = 1.32$ and $d_d/t = 0.66$). Hence, they are categorized as groups $G4$ and $G5$.

Figure 6.18 presents the normalized bending moment-curvature diagrams with the variation of dent depth in a combined damage. The "Intact-fixed-notch-G1" denotes the corresponding pipe case without any structural damage, while the "Dent-free" denotes the case with only notch damage. The following notations for a notch are the same. A single notch significantly decreases the pipe strength capacity. It is observed that, under all three sizes of notch, the occurrence of a dent further decreases the pipe strength largely. However, such further decrease is relative small with the increase of dent depth ($d_d/t = 0.07$ to $d_d/t = 2.0$).

Figure 6.19 shows the normalized bending moment-curvature diagrams with the variation of the notch depth in a combined damage. Compared with the fixed notch cases in Figure 6.18, an interesting phenomenon can be observed. Once a dent damage occurs on a pipe, further increase of the severity of notch in terms of notch depth (d_m/t from 0.20 to 0.62) only has slight effect on the residual pipe strength. Therefore, we can come to the conclusions that the combined damage has a more severe effect on the pipe residual strength compared to a single damage, and the dent damage plays a more dominant role on pipe residual strength in the combined dent and notch damage.

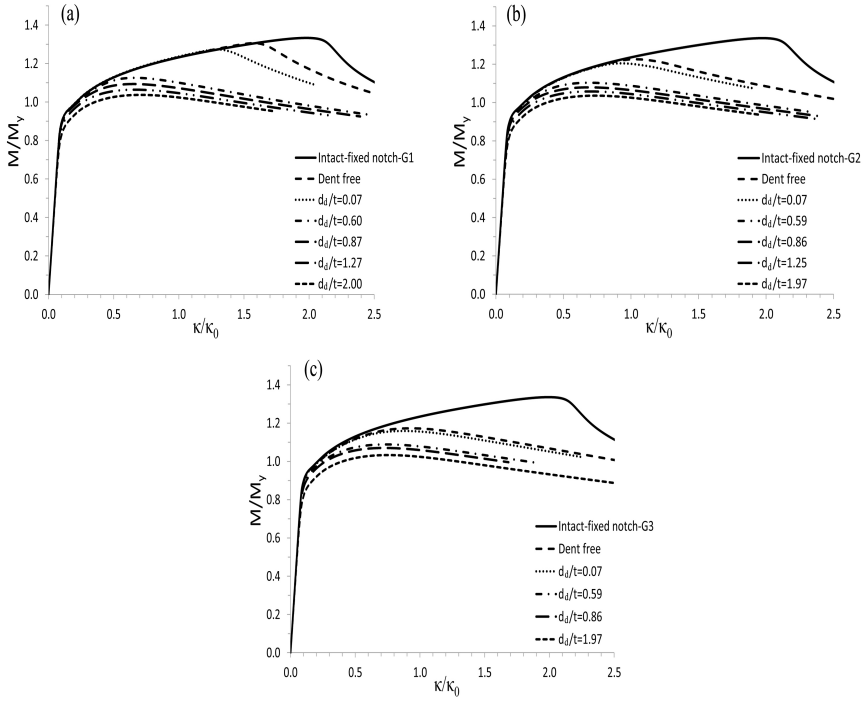

Figure 6.18: Normalized bending moment-curvature diagrams with varying of dent depth in a combined damage: (a) diagrams with fixed notch in G1 ($l_m = 44mm, w_m = 10mm, d_m = 1.5mm$); (b) diagrams with fixed notch in G2 ($l_m = 44mm, w_m = 10mm, d_m = 3.0mm$); (c) diagrams with fixed notch in G3 ($l_m = 44mm, w_m = 10mm, d_m = 4.5mm$).

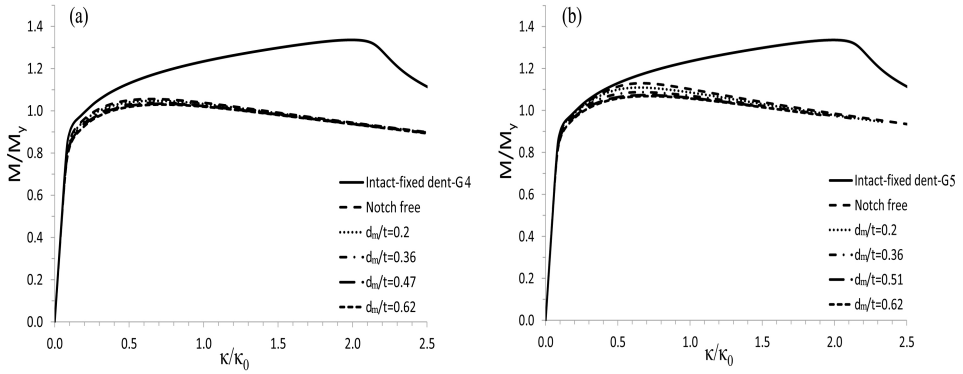

Figure 6.19: Normalized bending moment-curvature diagrams with varying of notch depth in a combined damage: (a) diagrams with fixed dent in G4 ($l_d = 120mm, w_d = 60mm, d_d = 10mm$); (b) diagrams with fixed dent in G5 ($l_d = 120mm, w_d = 60mm, d_d = 5mm$).

Table 6.8: Pipe specimens (in Chapter 3) with damage (a notch, and a crack) on the tensile side (dimension unit: mm; angle unit: degree).

S.N.	D	t	D/t	Damage $(l_{(i)} \times w_{(i)} \times d_{(i)})$	Damage angle	Location	M_{cr} (kNm)	κ_{cr} (1/m)
S3N4	168.30	7.90	21.30	$45 \times 10 \times 3$ (notch)	90	T	100.00	0.393
S4N8	168.20	7.66	21.96	$10.00 \times 0.22 \times 2.50$ (crack)	90	T	100.69	0.717

6.5.3 Interaction between fracture failure and residual strength

In the study of the previous section, no fracture criterion has been taken into account. However, we have to consider it when the damage is occurred on the tensile side of pipes. Hence, the effects between fracture failure and residual strength are qualitatively explored through numerical simulations in this section. All the types of damage that could produce fracture failure on seamless pipes are accounted for.

Simulation of a pipe with a single crack

A pipe with a single crack due to impact scenarios can occur, and fracture failure in Mode I may be initiated when structures are subjected to a large bending moment. In the simulation of a seamless pipe with a single crack, the maximum principal stress criterion for crack initiation is deployed. Four different levels of principal stress are used for comparisons, including $C1 = 378MPa$, $C2 = 478MPa$, $C3 = 800MPa$ and $C4 = 900MPa$. The used pipes (S4N8) for simulation are listed in Table 6.8 based on test measurements.

Table 6.9 lists the simulation results in terms of critical bending moment and curvature of pipes with single damage under different principal stress levels. If the results from case C4 are used as references, with the decrease of principal stress, the critical bending moment has a largest decrease by 36.10%, while the critical curvature has a maximum reduction value of 96.78%. Figure 6.20 shows the bending moment-curvature diagrams in different crack initiation level. Hence, from the standpoint of ultimate strength, the occurrence of crack initiation and the fracture failure have dominated the strength of structures. This conclusion is also demonstrated by the changing of failure modes. In Figure 6.21, two types of failure modes on the cracked pipes under pure bending are presented, including fracture failure and non-fracture failure. STATUSXFEM indicates the enriched elements with different crack status, lying between 0.0 and 1.0. For instance, if an element is completely cracked, the status of an enriched element is 1.0, while it is 0.0 if the element contains no crack.

Figure 6.22 illustrates the von Mises distribution of the cracked region of a pipe subjected to pure bending when the ultimate bending moment has reached. It is obvious that, from the standpoint of practice, leaking (such as oil/gas pipes) has occurred before the reach of ultimate strength. Under this circumstance, it is meaningless to further account for residual strength. Instead, it becomes the issues of when the fracture will happen and how long the structure will continue to carry load before crack initiation. Due to the lack of test data and the focus on ultimate strength in this thesis, only the qualitative comparisons have been discussed. The structure life and fracture failure should be further studied.

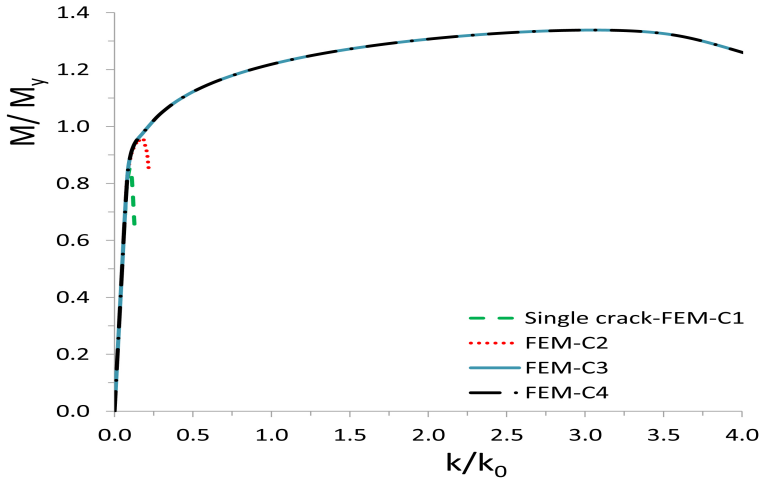

Figure 6.20: Bending moment-curvature diagram of cracked pipes with different levels of principal stress during crack initiation.

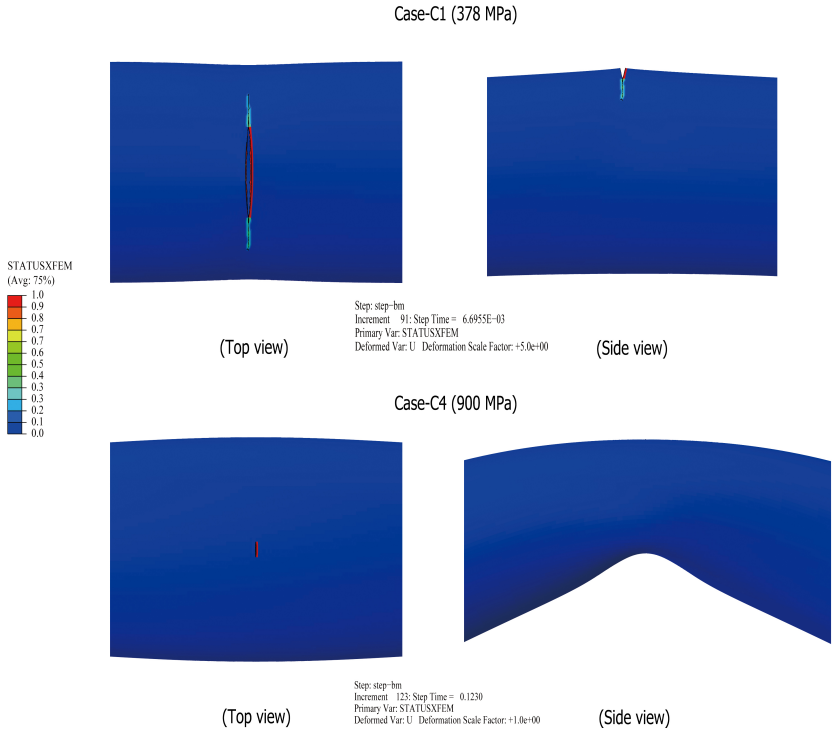

Figure 6.21: Change of failure modes of a pipe with intial single crack during crack propagation.

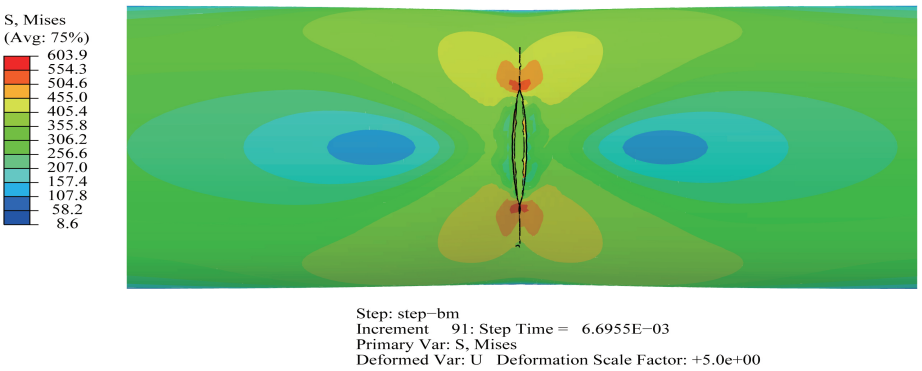

Figure 6.22: Mises distribution in the cracked region of a pipe with intial single crack at the maximum bending moment point.

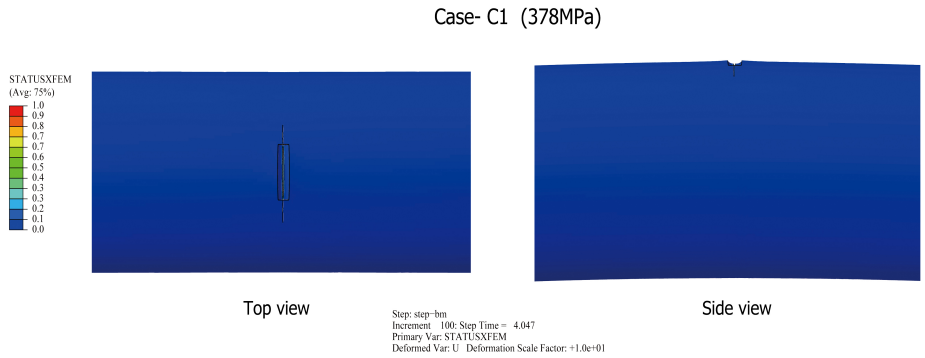

Figure 6.23: Fracture failure of a pipe with intial single notch at the maximum bending moment point.

Table 6.9: Simulation results of pipes in terms of critical bending moment and curvature.

Principal stress	M_{cr} (MPa)	κ_{cr} (1/m)	Dis-M %	Dis-κ %
C1 (378*MPa*)	63.84	0.029	-36.10	-96.78
C2 (478*MPa*)	71.37	0.053	-28.56	-94.12
C3 (800*MPa*)	99.90	0.902	0.00	0.11
C4 (900*MPa*)	99.90	0.901	0.00	0.00

Table 6.10: Pipe specimen with combined crack and notch on the tensile side (dimension unit: mm; damage size: $l_{(i)} \times w_{(i)} \times d_{(i)}$).

S.N.	D	t	D/t	Crack	Dent	Notch	Location	M_{cr} (kNm)	κ_{cr} (1/m)
S5N3	167.65	7.38	22.72	$45 \times 0.50 \times 0.70$	-	$45 \times 9.5 \times 3.0$	T	87.68	0.170

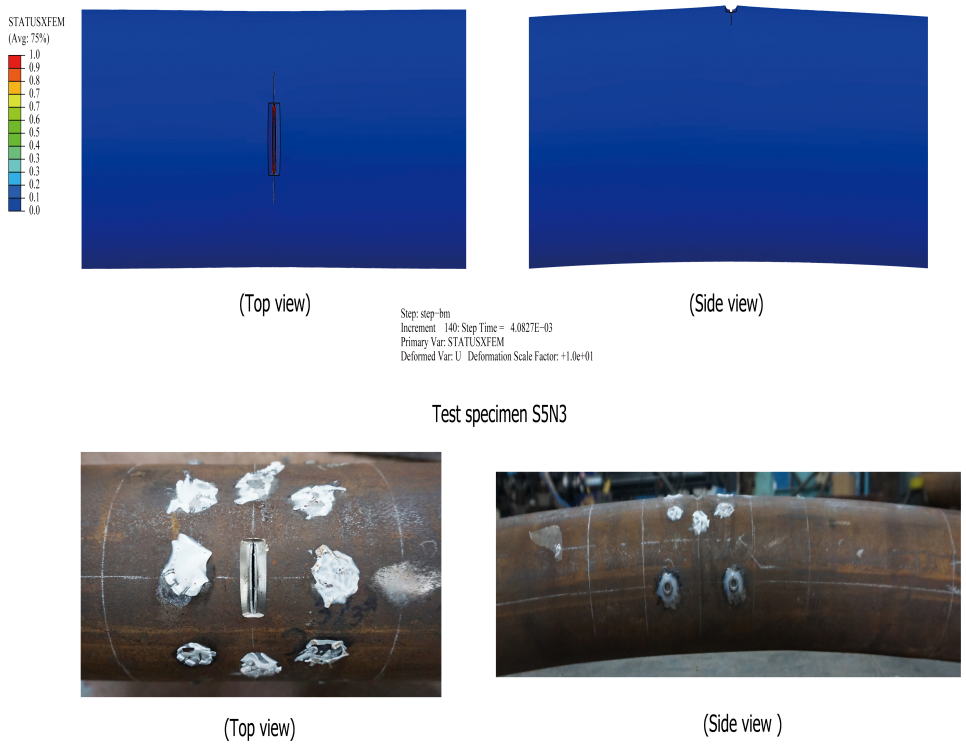

Figure 6.24: Fracture failure of a pipe with combined notch and crack at the maximum bending moment point.

Simulation of a pipe with a single notch

Another case that may produce fracture failure is the pipe with a single notch on its tensile side under bending. Through the developed numerical model in Chapter 5, it has been simulated. The enriched elements are put in the vicinity of the notch. The used pipe (S3N4) is listed in Table 6.8. Figure 6.23 presents the fracture initiation and the crack propagation direction of notched pipe subjected to pure bending. As seen from the side view, at a very small curvature (0.0239), the maximum bending moment has reached. Significant fracture failure also occurs before the reach of ultimate strength.

Table 6.11: Comparison results of pipes in terms of critical bending moment and curvature (by XFEM simulation).

S.N.	M_{cr} (MPa)	κ_{cr} (1/m)	Dis-M %	Dis-κ %
S4N8	63.84	0.029	0.00	0.00
S3N4	58.51	0.024	-8.35	-17.24
S5N3	47.39	0.020	-25.77	-31.03

Simulation of a pipe with combined crack and notch

The third type of damage that may produce fracture failure is the combined crack and notch, which is illustrated in Figure 6.7. The initial crack is put at the bottom of the notch, with the crack depth of 0.7 *mm* (as seen from specimen S5N3 in Table 6.10).

Figure 6.24 compares the failure modes of the pipe with combined crack and notch damage (S5N3) between simulations and tests. A similar failure mode has been observed from the test. Meanwhile, a more severe fracture occurs at the ultimate strength point compared with the case with a single notch (S3N4 in Figure 6.23).

We also carried out a comparison among all the cracked specimens, as seen in Figure 6.25 and Table 6.11. It is found that the pipe with combined notch and crack (S5N3) has the most severe effect on its residual strength, i.e. 25.77% lower in critical bending moment and 31.03% lower in critical curvature than the case with a single crack (S4N8). At a very low curvature, the residual strength has reached due to the occurrence of fracture failure. Such simulation results also conform to the observation in the test in Chapter 3.

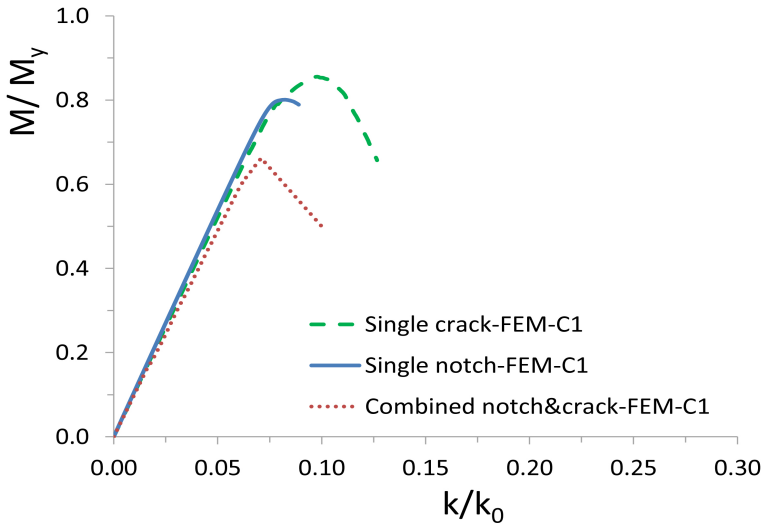

Figure 6.25: Comparison of bending moment-curvature diagrams among the three damage scenarios with a crack.

6.6 Proposed formulas

In this section, empirical formulas are proposed for pipes with a combined dent and notch damage based on the simulation results in Section 6.5.2. In the research in Chapters 4 and 5, empirical formulas are proposed for each type of structural damage respectively, taking into account their relevant critical damage parameters. For a pipe with a single plain dent in its central cross-section under bending moment (see Chapter 4), formulas are proposed and can be written as:

$$(\frac{M_{cr}}{M_i})_d = 1 - a_1(\frac{d_d}{t})^{b_1}(\lambda_l)^{c_1} \tag{4.8}$$

$$(\frac{\kappa_{cr}}{\kappa_i})_d = 1 - (a_2 + b_2\frac{t}{d_d})(\lambda_l)^{c_2} \tag{4.9}$$

Where a_1, b_1 and c_1 are 0.017, 0.696 and 1.48, respectively; a_2, b_2 and c_2 are 0.192, -0.026 and 0.955, respectively. Parameter λ_l here is the normalized dent length in the pipe hoop direction ($\lambda_l = l_d/\sqrt{Rt}$).

Meanwhile, For a pipe with a single notch (see Chapter 5) in its central cross-section under a bending moment, the empirical formulas can be written as:

$$(\frac{M_{cr}}{M_i})_m = 1 - a_3(\lambda_l\frac{d_m}{t})^{b_3}(\lambda_w)^{c_3} \tag{5.16}$$

$$(\frac{\kappa_{cr}}{\kappa_i})_m = 1 - a_4(\lambda_l\frac{d_m}{t})^{b_4}(\lambda_w)^{c_4} \tag{5.17}$$

Where a_3, b_3 and c_3 are 0.139, 0.91 and 0.253, respectively; a_4, b_4 and c_4 are 0.652, 0.557 and 0.205, respectively. Parameter λ_l here is the normalized notch length in the pipe hoop direction ($\lambda_l = l_m/\sqrt{Rt}$), while λ_w is the normalized notch width in the pipe longitudinal direction ($\lambda_w = w_m/\sqrt{Rt}$).

6.6.1 Residual strength prediction

For combined dent and notch damage, there may be a coupling effect between each damage, which is difficult to obtain directly. Therefore, in this thesis, we first construct the form of prediction formulas in the functions of individual damage, as seen in Equations (6.4) and (6.5). Where $(M_{cr}/M_i)_d$ and $(\kappa_{cr}/\kappa_i)_d$ are the reduction ratios due to a single dent, which can be calculated by Equations (4.8) and (4.9) respectively; $(M_{cr}/M_i)_m$ and $(\kappa_{cr}/\kappa_i)_m$ are the reduction ratios due to a single notch, which can be calculated by Equations (5.16) and (5.17) respectively. Through the corresponding numerical simulation results on pipes with combined damage (Tables 6.3 to 6.7), a regression analysis on the constructed formulas (Equations (6.4) and (6.5)) is carried out. As a result, the obtained coefficients a_5, b_5 and c_5 are 0.338, 0.566 and 0.016 respectively, and a_6, b_6, c_6, d_6, e_6 and f_6 are 0.251, 0.299, -0.653, -0.605, 0.828 and 0.647 respectively for the quadratic polynomial Equation (6.5).

$$(\frac{M_{cr}}{M_i})_{com} = a_5(\frac{M_{cr}}{M_i})_m + b_5(\frac{M_{cr}}{M_i})_d + c_5 \tag{6.4}$$

Table 6.12: Model uncertainties of the proposed formulas.

X	Moment, Equation (6.4)		Curvature, Equation (6.5)	
	Mean (Bias)	COV	Mean (Bias)	COV
FEM	1.0000	0.0128	1.0001	0.0333

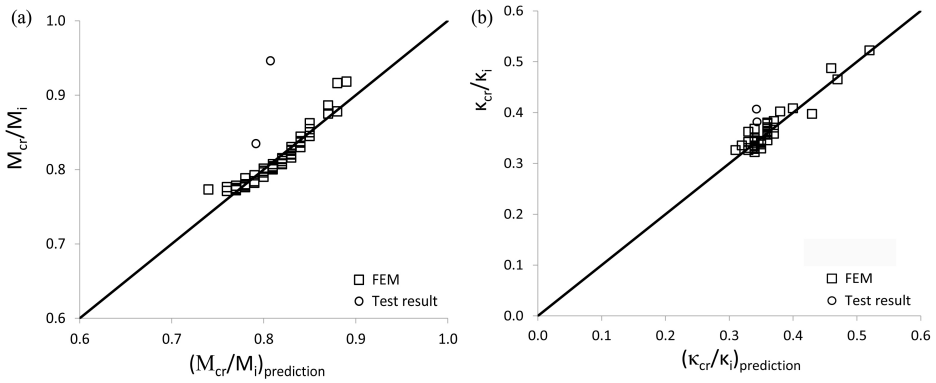

Figure 6.26: Comparison between prediction of proposed equations and experimental, numerical results and analytical results: (a) Normalized residual ultimate moment (M_{cr}/M_i); (b) Normalized critical curvature (κ_{cr}/κ_i).

$$(\frac{\kappa_{cr}}{\kappa_i})_{com} = a_6(\frac{\kappa_{cr}}{\kappa_i})_m^2 + b_6(\frac{\kappa_{cr}}{\kappa_i})_d^2 + c_6(\frac{\kappa_{cr}}{\kappa_i})_m + d_6(\frac{\kappa_{cr}}{\kappa_i})_d + e_6(\frac{\kappa_{cr}}{\kappa_i})_m(\frac{\kappa_{cr}}{\kappa_i})_d + f_6 \quad (6.5)$$

In order to determine the model uncertainty, we use the same method as in Chapters 4 and 5. The definition of X can be written as $X = X_{true}/X_{predict}$, where X_{true} is the data from either experimental test or numerical simulation, $X_{predict}$ is the prediction values based on proposed equations. Both X_{true} and $X_{predict}$ are assumed from the same cases with the same material properties and geometry. Table 6.12 shows the statistical results of X in terms of the mean value (bias) and coefficient of variation (COV, defined as the ratio of the standard deviation to the mean value of data). Due to the limited number of tests, comparison with test results has not been statistically carried out here. Results show that the extent of variability for the prediction of M_{cr} is within 1.28%, while the extent of variability for the prediction of κ_{cr} is within 3.33%. Furthermore, Figure 6.26 shows the results of the comparison between predictions, test and numerical simulations. An underestimation from the formulas has been obtained compared with the test results. Thus, these results show a satisfying agreement of the proposed formulas from the standpoint of engineering.

Figure 6.27 presents the prediction results of metallic pipes with combined damage with respect to the varying of different damage (d_d/t for dent, d_m/t for notch). Analysis of variance (ANOVA) shows that R square of the fitted formulas are 0.917 and 0.902 respectively, which demonstrated a high accuracy of the predictions from the proposed formulas.

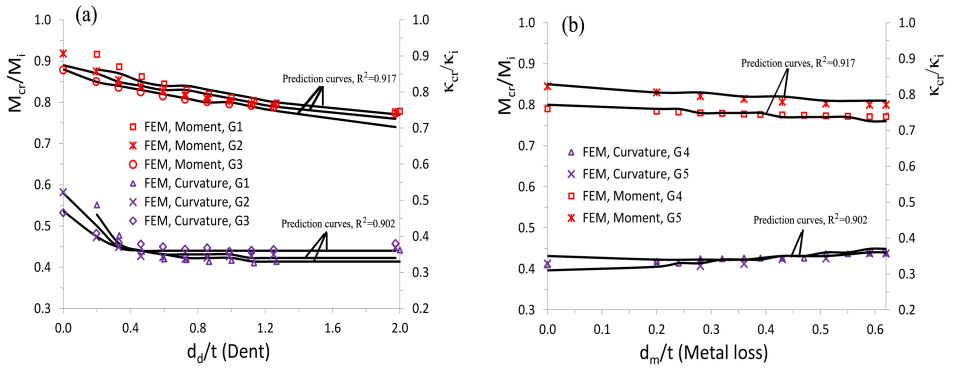

Figure 6.27: Prediction of damaged metallic pipes with respect to the varying of damage: (a) fixed notch with varying of dent; (b) fixed dent with varying of notch.

6.6.2 Expansion of the application domain of formulas

In practice, when mechanical interference happens, the proposed formulas in this section can be used to predict the residual ultimate strength of metallic pipes with combined damage under dominant bending. An on-site geometrical measurement should be first carried out for individual damage (a dent and/or a notch). By using the prediction formulas in Chapters 4 and 5, the specific effect of single type of damage can be first calculated. Substituting all these data into Equations (6.4) and (6.5), we can then find a final estimation of the effect of the combined damage.

As discussed above, the prediction formulas are proposed based on a specific type of pipe with D/t around 21. In order to expand their application domain, extra numerical simulations with varying of D/t (from 15 to 50) are carried out. Through a change of pipe thickness, different D/t ratios of pipes have been obtained (pipe diameter D is 168.8 mm). A combined damage with fixed dimension is introduced on the pipe surface, including the dent size of $l_d \times w_d \times d_d = 120 \times 60 \times t$ *mm* and the notch size of $l_m \times w_m \times d_m = 44 \times 10 \times 0.4t$ *mm*. Therefore, the simulation results from both the intact pipes and the damaged pipes with different D/t are listed in Tables 6.13 and 6.14. As demonstrated from the bending moment-curvature diagrams in three types of pipes in Figure 6.28, the failure modes of pipes begin to present differences in the case with $D/t = 29$. In the case with $D/t = 50$, rapid failure of structures occurs with an abrupt degradation. Hence, the change of failure mode may affect the reduction ratio of strength on damaged pipes with different D/t.

A further comparison of the predictions and the numerical results on pipes with different D/t ratios is shown in Figure 6.29. As can be seen in Figure 6.29 (a), the proposed formula can also provide a good prediction on critical moment for pipes with D/t from 15 to 50. A little bit underestimation of the strength is introduced in pipes with $D/t = 50$, with the maximum discrepancy of 5.7%. For the prediction of critical curvature, an underestimation is introduced for cases with D/t less than 25, which is on a safety zone. However, with the increase of D/t, an overestimation of the critical curvature is introduced, as can be seen in Figure 6.29 (b). The larger the D/t is, the larger the discrepancy from the prediction will be. In sum, accounting for the valid application domain of each damage parameter for pipes

with a single type of damage, we consider that the proposed formulas in this chapter can be also used for damaged pipes with D/t up to 30. In spite of such reasonable expansion, further tests are needed to confirm the validity of the formulas.

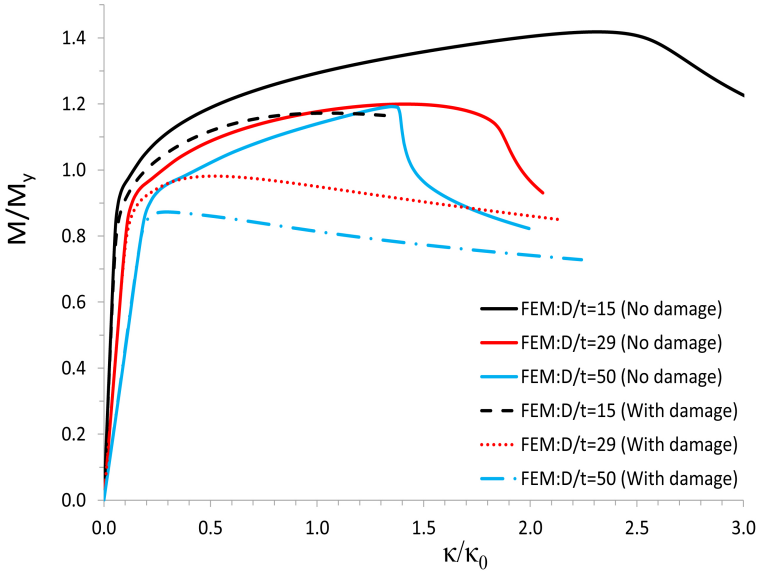

Figure 6.28: Normalized bending moment-curvature diagrams with varying of pipe diameter-to-thickness ratios (D/t is 15, 29 and 50 respectively).

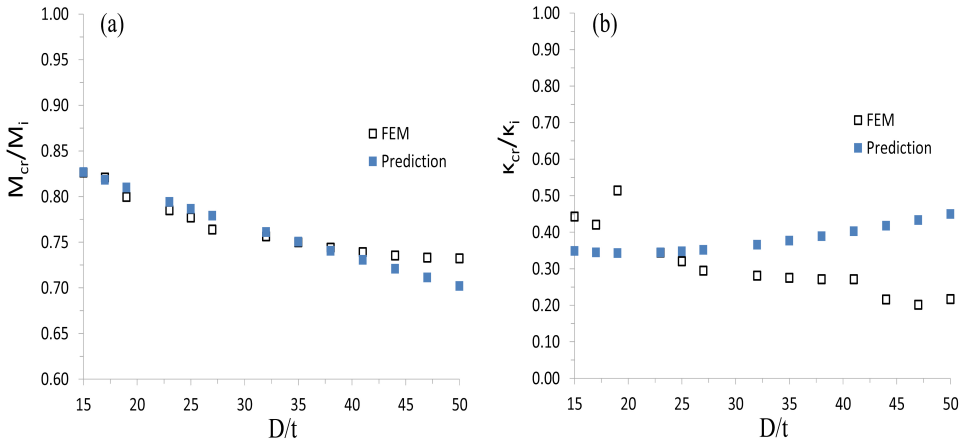

Figure 6.29: Comparison results between prediction and numerical results on pipes with varying of D/t: (a) normalized critical moment; (b) normalized critical curvature.

Table 6.13: Residual ultimate strength of intact pipes with varying of diameter-to-thickness ratios.

Capacity	D=168.8 mm, No imperfection, $\sigma_y = 378MPa$							
D/t	15	17	19	23	25	27	29	32
$M_i(MPa)$	149.73	131.78	117.38	96.11	87.94	80.99	70.09	67.6
$\kappa_i(1/m)$	1.048	0.866	0.733	0.529	0.484	0.435	0.306	0.331
D/t	35	38	41	44	47	50		
$M_i(MPa)$	61.25	56.03	51.66	47.85	44.46	41.62		
$\kappa_i(1/m)$	0.287	0.251	0.225	0.204	0.184	0.166		

Table 6.14: Residual ultimate strength of damaged pipes with varying of diameter-to-thickness ratios.

Capacity	$D = 168.8$ mm, l_d=120 mm, w_d=60 mm, $d_d = t$ mm l_m=44 mm, w_m=10 mm, $d_m = 0.4 \times t$ mm							
D/t	15	17	19	23	25	27	29	32
M_{cr}/M_i	0.826	0.821	0.800	0.785	0.777	0.764	0.818	0.765
κ_{cr}/κ_i	0.443	0.420	0.514	0.344	0.320	0.294	0.369	0.281
D/t	35	38	41	44	47	50		
M_{cr}/M_i	0.750	0.744	0.739	0.735	0.733	0.732		
κ_{cr}/κ_i	0.275	0.271	0.271	0.216	0.201	0.217		

6.7 Conclusions

As a consecutive study, this chapter has provided an extensive numerical investigation in seamless pipes with low diameter-to-thickness that suffered from combined dent and metal loss damage, and the damage that may produce fracture failure. A simplified numerical model accounting for combined structural damage has been developed based on nonlinear FEM. The effect of residual stress has been initially explored to consider the impact effect. The XFEM was used to predict the fracture failure in damaged pipes. The 7^{th} key question of this thesis in terms of the effect of the combined dent and metal loss damage has been identified. The 8^{th} key question of this thesis "What is the effect of existing cracks on the residual strength of metallic pipes?" has been explored. However, due to the lack of test data and the focus on ultimate strength in this thesis, the interaction between fracture and strength is only qualitatively compared. The detail of structure life and the quantification of crack effect should be further studied. The conclusions of this chapter are drawn as follows:

(1) The developed numerical model accounting for combined dent and notch damage is capable of providing an accurate prediction of the bending behavior in terms of critical bending moment and failure mode. The prediction of critical curvature over-estimates the deformation capacity of the test specimens.

(2) The residual stress in the assumed distribution in this chapter provides a positive effect on the pipe strength, especially for intact pipes with large initial imperfection (δ_i no less than $0.2t$) and dented pipes with small dent depth ($d_d \leq t$). Due to the

occurrence of large structural damage, the effect of residual stress is shielded and becomes insignificant. Further studies on residual stress are needed based on the real distribution from impact tests.

(3) The combined dent and notch damage has a more severe effect on the pipe residual strength compared with other types of damage (excluding the possible fracture failure). The dent damage plays a more dominant role on the pipe residual strength compared with the notch in combined damage.

(4) A cracked pipe with a high crack initiation stress is more prone to fail in a non-fracture failure mode. Once a fracture failure occurs, it dominates the residual strength of pipes under bending moment.

(5) Through a comparison between three types of damage (a single crack, a single notch and a combined notch and crack) that will induce fracture failure, it is found that the pipe with combined notch and crack has a more severe effect on the residual strength.

(6) Empirical formulas are proposed to predict the residual ultimate strength of metallic pipes with combined damage under a bending moment. These formulas could be utilized for practice purposes through a simple on-site measurement, which will facilitate the decision-making of pipe maintenance after mechanical interference. The application domain has been extended to damaged pipes with D/t up to 30 through further simulation. Further tests are still required in order to confirm the validity of such an expansion of the application domain.

Chapter 7

Conclusions

This chapter presents the final conclusions of the thesis, aiming to provide an effective prediction of the residual ultimate strength of damaged seamless metallic pipes subjected to bending, and to overcome some engineering limitations in current standards, such as DNV-OS-F101 [48]. All the research questions established in Chapter 1 have been answered. The findings in this thesis can be potentially integrated into engineering standards, and facilitate the decision-making of stakeholders after the occurrence of mechanical interference between pipes and foreign objects. The main conclusions of this research are presented in Section 7.1. In Section 7.2, recommendations for future research are presented.

7.1 Main conclusions

This Ph.D. project reported in this thesis, developed effective prediction models for residual ultimate strength of damaged metallic pipes under a bending moment. The main question of this research project proposed in **Chapter 1** is:

- To what extent does structural damage induced by mechanical interference affect the residual ultimate strength of seamless metallic pipelines subjected to a bending moment?

The main question is addressed by answering the corresponding key questions in the chapters of this thesis:

- What are the influential parameters that affect the structural behavior of metallic pipelines ?
- How do these influential parameters affect the structural behavior of pipelines?

According to the literature survey presented in **Chapter 2**, the influential parameters that may affect the structural behavior of metallic pipes have been found, including but not limited to the diameter-to-thickness ratios (D/t) of pipes, the initial imperfections, the material properties, the residual stresses, the test factors such as boundary conditions (friction effect), the manufacture methods of pipes, and the load types. Most of these parameters

were widely investigated by other researchers. However, their effects may vary with the variations of pipes, for instance, damaged or intact pipes, seamless or welded pipes, etc.

Hence, the effects of these influential parameters have been investigated and identified under the specific conditions in **Chapter 3**, **Chapter 4**, **Chapter 5** and **Chapter 6** in this thesis (seamless pipes by hot-rolling method; under bending).

D/t: D/t ratio governs the major failure modes of metallic pipes. For instance, the elastic-plastic failure generally occurs on pipes with D/t less than 20, while elastic buckling/instability happens on pipes with D/t large than 40. A combined failure mode would occur on the pipes with ratios between 20 and 40. For a seamless pipe with D/t between 20 and 50, the residual strength of damaged pipes decreases approximately in a linear way with the increase of D/t.

Initial imperfection: Appropriate initial imperfection for intact seamless pipes is required in order to obtain accurate simulation results. However, simulation results show that it can hardly affect the residual strength of pipes with damage due to the shielding effect of damage, such as a dent.

Material properties: The effect of material anisotropy in terms of different yield stress in pipe longitudinal and hoop directions is insignificant on the residual strength of seamless metallic pipes. The results obtained in this study imply that the yield stress in the pipe longitudinal direction dominates the pipe residual strength.

Residual stress: The distributions of initial residual stress in pipes vary with different manufacture methods, such as the hot-rolling or cold-drawing methods for seamless pipes, and the welding method. The impact induced residual stress is more complex due to factors such as impact locations, angles, damage types and energy levels. Hence, an investigation has been carried out on the effect of residual stress on seamless pipes, with the assumption of a specific linear distribution in pipe thickness along the pipe hoop direction. For intact pipes with different initial imperfections (amplitude from 0 to $0.2t$), it only slightly affects the pipe strength. For dented pipes with varying of dent depth, retardant effect on residual strength has been found (between 0 and t). With the increase of dent depth from t to $2t$, such retardation is shielded by the large damage effect. For seamless pipes with notch, it barely affects the residual strength based on simulation.

Boundary conditions: In a four point bending test, the designed boundary conditions affect the physical phenomena of pipe specimens and their prediction accuracy on strength. In this thesis, the effect of friction force that partially maintained the designed simply-supported boundary condition has been studied. Simulation results found that the larger the friction force was, the larger the equivalent axial compression force along the specimen would be. Within the normal engineering domain of the friction coefficients on steel surface (0.2 to 0.4), its effect on residual strength of pipes is small. Based on the simulation results and the laboratory observations, the friction coefficient has been therefore set to 0.26 for the simulations of test specimens in this thesis.

- What kind of structural damage normally occurs in metallic pipes due to mechanical interference?

Three basic types of structural damage exist on the surface of metallic pipes due to mechanical interference, including a dent, metal loss and a crack. In addition, their combinations thereof are more likely to happen because of the complexity of damage introduce environment.

- How do the different types of structural damage and the relevant damage parameters affect the structural behavior of pipelines?

In **Chapter 3**, a detailed design of a four point bending test on damaged pipes was carried out, trying to reveal their real physical phenomena. The test results have been carefully recorded, and discussed based on the observations from each specimen. A satisfying agreement has been achieved based on the comparisons between experiments, numerical simulations and some analytical solutions. In spite of the limited number of tests, fundamental results have been obtained, which provides a convincing basis for further answering these keys questions.

Results from **Chapter 3** and **Chapter 4** show that a dent on the compression side of the seamless metallic pipes (D/t around 21) has a large negative effect on their bending strength. For instance, a dent with the dent depth equal to 0.73 times of the pipe thickness can reduce the M_{cr} and κ_{cr} by more than 9% and 50% respectively. A dent with the dent length equal to 3.37 times of $\sqrt{Rt}$ can reduce the M_{cr} and κ_{cr} by more than 14% and 61% respectively. For a dent on the tensile side, a slight negative effect on the residual bending moment exists, whereas the critical curvature increases a little due to its recovery. As observed from the test for a dent on the tensile side, the reduction ratio of ultimate bending is only 1.11%, and the critical curvature has increased a little (7.5%). The occurrence of a dent damage accelerates the failure of pipe due to the rapid localization of the damaged region with an elastic-plastic failure mode.

A dent is simplified as a consinusoidal shape in the function of the dent angle (θ_d), the dent length (l_d), the dent depth (d_d) and the dent width (w_d). For the dent angle (θ_d), the larger the angle is, the smaller the residual ultimate strength will be. A pipe with a hoop dent (90^0) on its compression side has the largest effect on the residual strength of pipes. The projected dent length (angle in 90^0) reduces the residual strength of pipes significantly, decreasing with the increase of length. With the increase of the dent depth (d_d), the strength decreases rapidly. Furthermore, the dent width (w_d) in the pipe longitudinal direction has an insignificant effect on the pipe residual strength.

In **Chapter 5**, the metal loss in terms of a notch, which is expressed as the function of the notch depth (d_m), the notch length (l_m), and the notch width (w_m), is investigated. A considerable reduction of bending strength is induced by the metal loss on the compression side of pipes. For instance, a notch with the notch depth equal to half of the pipe thickness can reduce M_{cr} and κ_{cr} by more than 11% and 54% respectively. Fracture failure dominates the pipe behavior when the metal loss is on the tensile side of pipes. Research has found that the larger the notch depth (d_m) and/or the notch length (l_m) is, the smaller the bending capacity will be. The increase of notch width slightly reduces the pipe strength, presenting a linear tendency. For instance, it is observed that the reduction ratio is less than 2% for κ_{cr} and less than 5% for M_{cr} when λ_w increases from 0.4 to 1.4.

The combined dent and notch damage also has been studied in this project in **Chapter 6**. The simplifications of damage are the same as the previous descriptions for a single dent and a single notch. The most severe condition is considered with the dent in the pipe hoop direction. Simulation results show that the combined damage has a more severe effect on the pipe residual strength compared with other single types of damage. The dent in the combined damage plays a more dominant role on the pipe strength.

- To what extent does the dent damage affect the structure ultimate strength in terms of bending moment and critical curvature?

For the dent damage on pipes during operation stage after long-term use, as stated in DNV-OS-F101, the maximum accepted ratio of permanent dent depth to the pipe diameter caused by impact/mechanical interference is given by $H_p \leq 0.05\eta$, where H_p is the depth of dent, D is the outer diameter of pipes. The usage factor η depends on the impact frequency. In addition, it is also stated that, when allowing for permanent dents during operation, additional failure modes such as fatigue and collapse shall be taken into account. Any beneficial effect of internal over-pressure should not be included. However, the limitation of such general guidelines is that we cannot make any further predictions when a large dent caused by impact appears. For instance, when the dent depth is 6%D (or $1t$, and $2t$, etc. in this thesis), we do not know exactly what the residual strength of the damaged pipes is based on the standards. Under this circumstance, should we just simply abandon the damaged pipes as suggested by DNV-OS-F101? If so, it may be a waste of material. Alternatively, we can still start a FEM simulation for strength check as suggested from the standard. But it is always cumbersome and time-consuming.

Hence, based on the quantification of dent effect in this thesis, we will know exactly what the residual strength or the reduction ratio of the strength is when a specific dent appears, say a dent with the depth of 6%D, 7%D or even 10%D. The analytical solutions proposed for the dent can be used as a supplement of this standard for fast checking decision-making.

In order to further quantify the dent effect, a series of simulations have been carried out based on validated numerical models, accounting for the variation of different dent parameters. An empirical model has been proposed for the dent effect on the residual strength of seamless pipes in terms of bending moment and critical curvature (Equations (4.8) and (4.9) as follows). Hence, we can estimate exactly the reduction extent of a dent damage by knowing their specific geometrical dimensions.

$$(\frac{M_{cr}}{M_i})_d = 1 - a_1(\frac{d_d}{t})^{b_1}(\lambda_l)^{c_1} \tag{4.8}$$

$$(\frac{\kappa_{cr}}{\kappa_i})_d = 1 - (a_2 + b_2\frac{t}{d_d})(\lambda_l)^{c_2} \tag{4.9}$$

Where a_1, b_1 and c_1 are 0.017, 0.696 and 1.48, respectively; a_2, b_2 and c_2 are 0.192, -0.026 and 0.955, respectively. The suitable application domain of the normalized dent length ($\lambda_l = l_d/\sqrt{Rt}$, in pipe hoop direction) is between 0.8 and 5.2, while the range for normalized dent depth d_d/t is between 0.1 and 2.2. The normalized dent width λ_w should be in the range of 1.0 to 3.17.

- To what extent does metal loss damage affect the structure ultimate strength in terms of bending moment and critical curvature?

As explained in the former chapters for metal loss, there are some limitations based on the existing literature and the standards such as DNV-OS-F101 and DNV-RP-F101. It is summarized as follows:

(1). The metal loss caused by mechanical interference has not been taken into account, as stated in DNV-RP-F101;

(2). The so-called "neighbor effect" induced by the finite width of the notch is general ignored;

(3). Analytical solutions for damage pipes with scattered corrosion under external or internal pressure exist in standards. However, analytical solution of pipe with metal loss caused by mechanical interference under bending is rare.

Therefore, the research for metal loss caused by mechanical interference in this thesis has overcome the limitations as mentioned above. The empirical equations have been proposed in this thesis, as expressed in the following Equations (5.16) and (5.17).

$$(\frac{M_{cr}}{M_i})_m = 1 - a_3(\lambda_l \frac{d_m}{t})^{b_3}(\lambda_w)^{c_3} \tag{5.16}$$

$$(\frac{\kappa_{cr}}{\kappa_i})_m = 1 - a_4(\lambda_l \frac{d_m}{t})^{b_4}(\lambda_w)^{c_4} \tag{5.17}$$

Where a_3, b_3 and c_3 are 0.139, 0.91 and 0.253, respectively; a_4, b_4 and c_4 are 0.652, 0.557 and 0.205, respectively. Parameter λ_l here is the normalized notch length in pipe hoop direction ($\lambda_l = l_m/\sqrt{Rt}$, $\lambda_l \in [0.2, 4.8]$), while λ_w here is the normalized notch width in pipe longitudinal direction ($\lambda_w = w_m/\sqrt{Rt}$, $\lambda_l \in [0.3, 1.4]$). d_m/t is the normalized notch depth which is between 0.2 and 0.65.

- To what extent does the combined dent and metal loss affect the structure ultimate strength in terms of bending moment and critical curvature?

For the effect of combined dent and metal loss, no specific guidelines or even literature have been found so far. Therefore, the results in this part can be also used by the engineering practice. For combined dent and notch damage, there may be a coupling effect between each damage, which is difficult to obtain directly. Therefore, taking into account of the individual effect from each type of damage, empirical formulas have been proposed to quantify the effect of combined damage, as expressed in the following Equations (6.4) and (6.5).

$$(\frac{M_{cr}}{M_i})_{com} = a_5(\frac{M_{cr}}{M_i})_m + b_5(\frac{M_{cr}}{M_i})_d + c_5 \tag{6.4}$$

$$(\frac{\kappa_{cr}}{\kappa_i})_{com} = a_6(\frac{\kappa_{cr}}{\kappa_i})_m^2 + b_6(\frac{\kappa_{cr}}{\kappa_i})_d^2 + c_6(\frac{\kappa_{cr}}{\kappa_i})_m + d_6(\frac{\kappa_{cr}}{\kappa_i})_d + e_6(\frac{\kappa_{cr}}{\kappa_i})_m(\frac{\kappa_{cr}}{\kappa_i})_d + f_6 \tag{6.5}$$

Where the corresponding coefficients a_5, b_5 and c_5 are 0.338, 0.566 and 0.016 respectively; and a_6, b_6, c_6, d_6, e_6 and f_6 are 0.251, 0.299, -0.653, -0.605, 0.828 and 0.647 respectively for the quadratic polynomial Equation (6.5); $(M_{cr}/M_i)_m$ and $(\kappa_{cr}/\kappa_i)_m$ are the reduction ratios of residual strength due to a single notch, which can be calculated by Equations (5.16) and (5.17) respectively; $(M_{cr}/M_i)_d$ and $(\kappa_{cr}/\kappa_i)_d$ are the reduction ratios of residual strength due to a single dent, which can be calculated by Equations (4.8) and (4.9) respectively. The application of these two equations can be also expanded to the seamless pipes with the D/t ratios under 30.

- What is the effect of existing cracks on the residual strength of metallic pipes?

A qualitative investigation of the interaction effect between fracture failure and residual strength of metallic pipes has been conducted through XFEM. Three types of damage, which may produce fracture failures on structures, have been considered, including a single crack, a single notch on the tensile side of pipes and the combined crack and notch. Research found that a cracked pipe was more prone to fail in a non-fracture failure mode under a high crack initiation stress. Once a fracture failure occurs, it dominates the residual strength of pipes under bending moment. The combined notch and crack induces the fastest fracture failure on metallic pipes such that a lowest residual strength of pipes has been produced.

In practice, the proposed empirical formulas in this research could be effectively utilized to predict the residual ultimate strength under bending by a simple on-site measurement of structural damage. Therefore, the decision-making of pipe maintenance after mechanical interference can be facilitated. A flowchart is made for the detailed assessment procedure of residual strength of damaged pipes after possible mechanical interference, as seen in Figure 7.1. Once mechanical interference has happened, the basic inputs of pipes are required for assessments, such as pipe types, impact types and possible load conditions, as described in **Chapters 2** and **3**. Then the entire damage should be carefully checked to exclude the most severe conditions such as leaking, so that the feasibility of further damage estimation on pipes could be constructed. Therefore, we have clarified what kinds of structural damage have happened, and what is the initial severity of accident on the pipes. Afterwards, a detailed measurement of each type of damage is required. Reasonable simplifications of the damage are needed if possible, as recommended in **Chapter 4** for a dent, **Chapter 5** for metal loss in terms of a notch and **Chapter 6** for combined damage. If a crack occurs, further analysis and simulations are also needed to check the possible fracture failure. Meanwhile, experts' advice should be used as a supplement under this circumstance. Based on all the obtained information, the reduction ratios of the residual ultimate strength will be calculated by the proposed formulas (Equations (4.8) and (4.9) for a dent; Equations (5.16) and (5.17) for metal loss; Equations (6.4) and (6.5) for combined damage). A further estimation is still required through the existing standards such as DNV-OS-F101, to guarantee the satisfactory of the residual strength of damaged structures. Here, experts' advice is also important once the predicted reduction ratios are too large to maintain the safety of structures. Based on these assessments, the final reports about the damage effect are made. The final decision for how to deal with the damaged pipes is therefore made.

7.2 Recommendations for future research

The recommendations for future research are presented in this section in order to further improve these prediction models.

In this study, a comprehensive four-point bending test has been designed and carried out to determine the strength of damaged pipes. However, further studies on the test are necessary. Firstly, the measurement of the initial state of test specimens has not been taken, resulting in some assumptions in the stage of numerical modeling of intact specimens. It is recommended to design suitable facilities for the automatic measurement of initial imperfections in each direction of the specimens. Secondly, the local residual stress due to

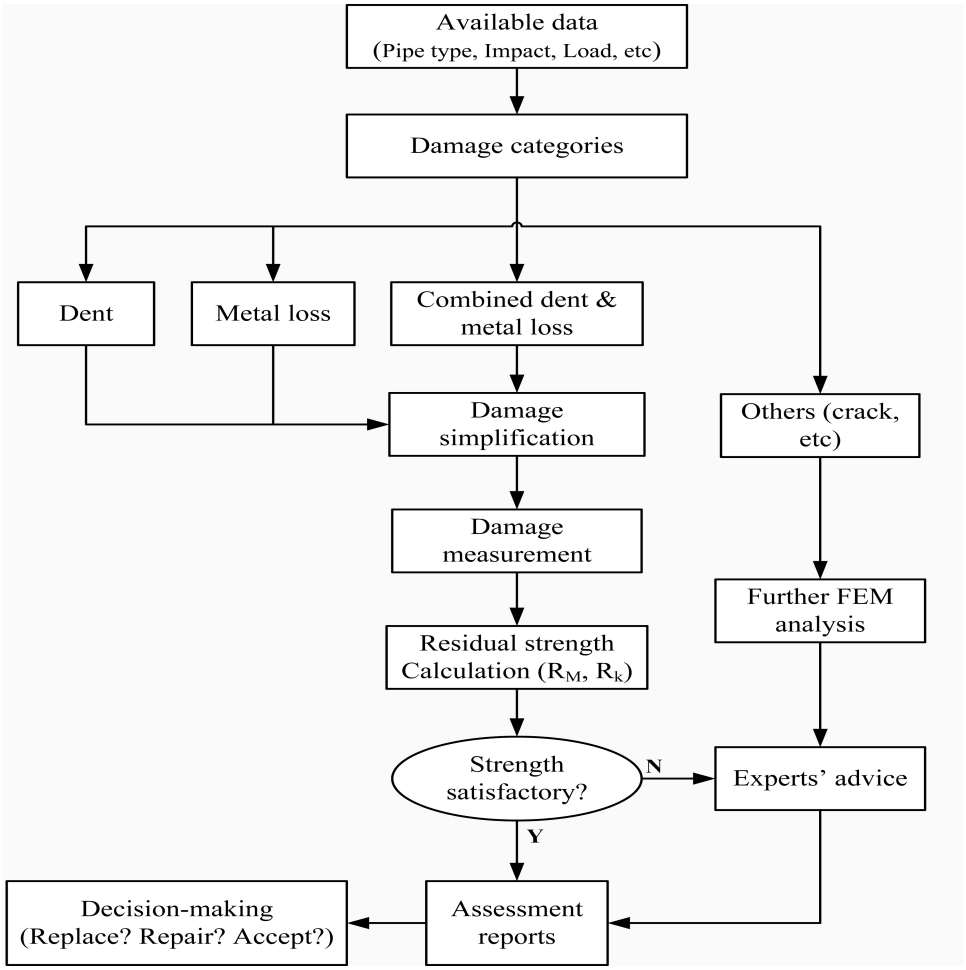

Figure 7.1: General procedure of residual strength assessment for damaged pipes based on research in this thesis.

mechanical interference has not been measured. Hence, assumptions of the distribution of residual stress have been also made for numerical study. It is recommended to measure the residual stress around the damaged region through traditional destructive BRSL method (Block Removal Splitting and Layering Method) or the non-destructive method such as the DIC optical method (Digital image correlation). Thirdly, for the strain measurements of the critical points on pipe specimens, quite a lot of data have been missed due to the using of discrete data recording method during loading. Hence, consecutive measurements for these data are recommended to improve the database. Fourthly, the designed overall length of specimens is not long enough, which has brought difficulties in both the test configurations and the test operations. Another consequence due to the length effect of specimens is that relative large system errors have been introduced because of the variation of bending arm and extra shear force. Thus, it is recommended to use the full pipe specimens with a length as long as possible (based on the specific laboratory conditions) for bending tests. Fifthly, the types of structural damage used in the tests are limited, which leads to assumptions and simplifications in the developed models. As we may known, all the additional inputs and possible updating of tests may result in further improvement of predictions for numerical models. Therefore, it is important to obtain the real state of damaged pipe structures for more accurate simulation results.

Only a specific type of seamless pipe with D/t around 21 has been used in the tests. Empirical formulas have been developed for the predictions of residual strength. An expansion of the application of the formulas has been conducted based on the simulations on damaged pipes with combined dent and notch with different D/t from 15 to 50. However, more experimental tests accounting for different D/t and different types of pipes (such as welded one) should be further carried out. Studies are needed to further update these developed formulas so that they can have more practical applications in engineering domain.

For the fracture failure, it is actually a different topic which is related to the initiation and propagation of cracks. Once the conditions for crack initiation and propagation have been satisfied, the structure will fail rapidly. Therefore, it is recommended to obtain detailed fracture parameters in a test so that we can build the relationship between crack failure and residual strength.

The research in this thesis focuses on the residual strength of pipes under bending moment. In reality, other dominated loading conditions exist with the variation of external factors such as pipe phases, pipe installation methods, and pipe applied environment. With the exploitation of energy into deep and/or ultra-deep water, the structural behavior of damaged pipes under external pressure is becoming more and more important. Hence, studies on the damaged pipes under external pressure are also recommended in the future research.

Bibliography

[1] Abaqus6.13. Abaqus: User's manual, 6.13, 2013.

[2] F. Abeele, B. Galvan, P. Ramos, and J. Muylle. Numerical simulation of the interference between trawl gear and offshore pipelines. In *The Sixth International Pipeline Technology Conference*. Lab.Soete and Tiratsoo Technical, 2013.

[3] ABS. Subsea pipeline systems and risers. *American Bureau of Shipping,2001*, 2001.

[4] C.R. Alexander and J.F. Kiefner. Effects of smooth and rock dents on liquid petroleum pipelines. In *1999 API Pipeline Conference, Dallas, Texas*, 1997.

[5] A. Amirat, K. Chaoui, Z. Azari, and G. Pluvinage. Residual stress analysis in seamless api x60 steel gas pipelines. *Sciences & Technologie B*, pages 7–10, 2004.

[6] T. L. Anderson. *Fracture mechanics: fundamentals and applications*. CRC press, 2017.

[7] T.L. Anderson and T.L. Anderson. *Fracture mechanics: fundamentals and applications*. CRC press, 2005.

[8] ANSI. *Manual for Determining the Remaining Strength of Corroded Pipelines: A Supplement to ASME B31 Code for Pressure Piping*. American Society of Mechanical Engineers, 1991.

[9] API. 5l: Specification for line pipe. *American Petroleum Institute, Washington, DC*, 2012.

[10] API579. *Fitness for Service, American Petroleum Institute, Washington, DC*, 2007.

[11] ASME B31G-2009. Manual for determining the remaining strength of corroded pipelines. ASME New York, NY, 2009.

[12] Q. Bai and Y. Bai. *Subsea pipeline design, analysis, and installation*. Gulf Professional Publishing, 2014.

[13] Y. Bai and Q. Bai. *Subsea pipeline integrity and risk management*. Gulf Professional Publishing, 2014.

[14] Y. Bai and S. Hauch. Analytical collapse capacity of corroded pipes. In *The Eighth International Offshore and Polar Engineering Conference*. International Society of Offshore and Polar Engineers, 1998.

[15] Y. Bai, R. T. Igland, and T. Moan. Ultimate limit states of pipes under tension and bending. *International Journal of Offshore and Polar Engineering,1994*, 4(04), 1994.

[16] Y. Bai, S. Hauch, and J.C. Jensen. Local buckling and plastic collapse of corroded pipes with yield anisotropy. In *The Ninth International Offshore and Polar Engineering Conference*. International Society of Offshore and Polar Engineers, 1999.

[17] L. M. Bartolini, A. Battistini, L. Marchionni, A. Parrella, M. Spinazzè, and L. Vitali. Pipe strength and deformation capacity: A novel FE tool for the numerical lab. In *ASME 2014* 33rd *International Conference on Ocean, Offshore and Arctic Engineering*, pages V06BT04A058–V06BT04A058. American Society of Mechanical Engineers, 2014.

[18] A. Barut, E. Madenci, V.O. Britt, and J.H. Starnes. Buckling of a thin, tension-loaded, composite plate with an inclined crack. *Engineering fracture mechanics*, 58 (3):233–248, 1997.

[19] M. Beller, C. Mattheck, and J. Zimmermann. Stress concentrations in pipelines due to the presence of dents. In *The First International Offshore and Polar Engineering Conference*. International Society of Offshore and Polar Engineers, 1991.

[20] T. Belytschko and T. Black. Elastic crack growth in finite elements with minimal remeshing. *International journal for numerical methods in engineering*, 45(5):601–620, 1999.

[21] A. Benjamin and E. Andrade. Predicting the failure pressure of pipelines containing nonuniform depth corrosion defects using the finite element method. In *ASME 2003* 22nd *International Conference on Offshore Mechanics and Arctic Engineering*, pages 557–564. American Society of Mechanical Engineers, 2003.

[22] W.J. Beranek. *Krachtswerking deel 0; Basiskennis*. TU Delft, Delft, 1997.

[23] J.H. Besten. *Fatigue resistance of welded joints in aluminum high-speed craft:A total stress concept*. PhD thesis, Delft University of Technology, 2015.

[24] C. Bisagni. Dynamic buckling of fiber composite shells under impulsive axial compression. *Thin-Walled Structures*, 43(3):499–514, 2005.

[25] O.H. Bjørnøy, O. Rengård, S. Fredheim, and P. Bruce. Residual strength of dented pipelines, DNV test results. In *The Tenth International Offshore and Polar Engineering Conference*. International Society of Offshore and Polar Engineers, 2000.

[26] A.V. Bogdan, I.V. Lokhman, S.M. Ageev, and I.V. Orynyak. The limit load calculations for pipelines with axial complex-shaped defects. *Strength of Materials*, 41: 45–51, 2009.

[27] BP. BP energy outlook 2030. *BP Statistical Review*, 2012.

[28] D. Broek. *Elementary engineering fracture mechanics*. Springer Science & Business Media, 2012.

[29] R. Bruschi, L. Bartolini, M. Spinazzè, E. Torselletti, and L. Vitali. A numerical lab to predict the strength capacity of offshore pipelines. In *ASME 2005* 24th *International Conference on Offshore Mechanics and Arctic Engineering*, pages 597–607. American Society of Mechanical Engineers, 2005.

[30] BS8010. Code of practice for pipelines, part 3: Pipelines subsea: Design, construction and installation. *British Standards Institution*, 1993.

[31] BSI. BS7910:guide on methods for assessing the acceptability of flaws in metallic structures. *British Standards Institution*, 2005.

[32] J. Cai, X.L. Jiang, and G. Lodewijks. Ultimate strength of damaged stiffened panels subjected to uniaxial compression loads accounting for impact induced residual stress and deformation. In *ASME 2015* 34th *International Conference on Offshore Mechanics and Arctic Engineering*. American Society of Mechanical Engineers, 2015.

[33] J. Cai, X.L. Jiang, and G. Lodewijks. Residual strength of metallic pipelines subject to combined loads accounting for impact induced damage. In *The 26th International Ocean and Polar Engineering Conference*. International Society of Offshore and Polar Engineers, 2016.

[34] J. Cai, X.L. Jiang, and G. Lodewijks. Residual ultimate strength of offshore metallic pipelines with structural damage–a literature review. *Ships and Offshore Structures*, pages 1–19, 2017.

[35] J. Cai, X.L. Jiang, G. Lodewijks, Z.Y. Pei, and L. Zhu. Experimental investigation of residual ultimate strength of damaged metallic pipelines. In *ASME 2017* 36th *International Conference on Offshore Mechanics and Arctic Engineering*. American Society of Mechanical Engineers, 2017.

[36] J. Cai, X.L. Jiang, and G. Lodewijks. Numerical investigation of residual ultimate strength of dented metallic pipes subjected to pure bending. *Ships and Offshore Structures*, 13(5):519–531, 2018.

[37] J. Cai, X.L. Jiang, G. Lodewijks, Z.Y Pei, and W.G. Wu. Residual ultimate strength of damaged seamless metallic pipelines with combined dent and metal loss. *Marine Structures*, 61:188–201, 2018.

[38] J. Cai, X.L. Jiang, G. Lodewijks, Z.Y. Pei, and W.G. Wu. Residual ultimate strength of seamless metallic pipelines under a bending moment - a numerical investigation. *Ocean Engineering*, 164:148–159, 2018.

[39] J. Cai, X.L. Jiang, G. Lodewijks, Z.Y. Pei, and W.G. Wu. Residual ultimate strength of damaged seamless metallic pipelines with metal loss. *Marine Structures*, 58:242–253, 2018.

[40] J. Cai, X.L Jiang, G. Lodewijks, Z.Y. Pei, and L. Zhu. Experimental investigation of residual ultimate strength of damaged metallic pipelines (accepted). *Journal of Offshore Mechanics and Arctic Engineering*, 2018.

[41] Y.F. Cheng. *Stress corrosion cracking of pipelines*. John Wiley & Sons, 2013.

[42] A. Cosham and P. Hopkins. The effect of dents in pipelines-guidance in the pipeline defect assessment manual. *International Journal of Pressure Vessels and Piping*, 81 (2):127–139, 2004.

[43] CSA. *Oil and gas pipeline systems*. Canadian Standards Association, 2011.

[44] C.A. Dimopoulos and C.J. Gantes. Comparison of stiffening types of the cutout in tubular wind turbine towers. *Journal of Constructional Steel Research*, 83:62–74, 2013.

[45] DNV. DNV-RP-F101 corroded pipelines. *Det Norske Veritas*, 2004.

[46] DNV. DNV-RP-F111 interference between trawl gear and pipelines. *Det Norske Veritas*, 2010.

[47] DNV. DNV-RP-C208: Determination of structural capacity by non-linear FE analysis methods. *Det Norske Veritas*, 2013.

[48] DNV. DNV-OS-F101 submarine pipeline systems. *Det Norske Veritas*, 2013.

[49] DNV DNV-RP-F108. Recommended practice dnv-rp-f108: fracture control for pipeline installation methods introducing cyclic plastic strain, 2006.

[50] L. H. Donnell. A new theory for the buckling of thin cylinders under axial compression and bending. *Trans. Asme*, 56(11):795–806, 1934.

[51] J.Y. Dyau and S. Kyriakides. On the localization of collapse in cylindrical shells under external pressure. *International journal of solids and structures*, 30(4):463–482, 1993.

[52] M.S. El Naschie. A branching solution for the local buckling of a circumferentially cracked cylindrical shell. *International Journal of Mechanical Sciences*, 16(10):689–697, 1974.

[53] S. Es, A.M. Gresnigt, D. Vasilikis, and S.A. Karamanos. Ultimate bending capacity of spiral–welded steel tubes–part i: Experiments. *Thin-Walled Structures*, 102:286–304, 2016.

[54] H.E. Estekanchi and A. Vafai. On the buckling of cylindrical shells with through cracks under axial load. *Thin-walled structures*, 35(4):255–274, 1999.

[55] European Committee for Standardization. *Eurocode 3: Design of Steel Structures--Part 1 –1: General Rules for Buildings*. Brussels,Belgium, latest edition, 2006.

[56] P. Fassina, F. Bolzoni, G. Fumagalli, L. Lazzari, L. Vergani, and A. Sciuccati. Influence of hydrogen and low temperature on mechanical behaviour of two pipeline steels. *Engineering Fracture Mechanics*, 81:43–55, 2012.

[57] Fluent. Fluent and Ansys User's guide 12.0, 2009.

[58] J.R. Fowler, C.R. Alexander, P.J. Kovach, and L.M. Connelly. Cyclic pressure fatigue life of pipelines with plain dents, dents with gouges, and dents with welds. Technical report, American Gas Association, Inc., Arlington, VA (United States); Stress Engineering Services, Inc., Houston, TX (United States), 1994.

[59] B. Fu and M.G. Kirkwood. Predicting failure pressure of internally corroded linepipe using the finite element method. Technical report, American Society of Mechanical Engineers, New York, NY (United States), 1995.

[60] O. Fyrileiv, O. Aamlid, A. Venås, and L. Collberg. Deepwater pipelines–status, challenges and future trends. *Proceedings of the Institution of Mechanical Engineers, Part M: Journal of Engineering for the Maritime Environment*, 227(4):381–395, 2013.

[61] GB/T 1591. *High strength low alloy structural steels (in Chinese)*. The Chinese National Standard, latest edition, 2008.

[62] GB/T 228.1. *Metallic materials-Tensile testing-Part1: Method of test at room temperature (in Chinese)*. The Chinese National Standard, latest edition, 2008.

[63] H. Ghaednia, J. Silva, S. Kenno, S. Das, R. Wang, and R. Kania. Pressure tests on 30–in. diameter X65 grade pipes with dent–crack defects. *Journal of Pipeline Engineering*, 12(1):61–67, 2013.

[64] H. Ghaednia, S. Das, R. Wang, and R. Kania. Effect of operating pressure and dent depth on burst strength of NPS30 linepipe with dent–crack defect. *Journal of Offshore Mechanics and Arctic Engineering*, 137(3), 2015.

[65] H. Ghaednia, S. Das, R. Wang, and R. Kania. Safe burst strength of a pipeline with dent–crack defect: Effect of crack depth and operating pressure. *Engineering Failure Analysis*, 55:288–299, 2015.

[66] T.G. Ghazijahani, H. Jiao, and D. Holloway. Experiments on dented steel tubes under bending. *Advances in Structural Engineering*, 18(11):1807–1817, 2015.

[67] B. Gorenc, R. Gorenc, B.E.and Tinyou, and A. Syam. *Steel designers' handbook*. UNSW Press, 2005.

[68] A.M. Gresnigt and R.J. Van Foeken. Local buckling of UOE and seamless steel pipes. In *The Eleventh International Offshore and Polar Engineering Conference*. International Society of Offshore and Polar Engineers, 2001.

[69] A.M. Gresnigt, R.J. Van Foeken, and S.L. Chen. Collapse of UOE manufactured steel pipes. In *The Tenth International Offshore and Polar Engineering Conference*. International Society of Offshore and Polar Engineers, 2000.

[70] A.M. Gresnigt, S.A. Karamanos, and K.P. Andreadakis. Lateral loading of internally pressurized steel pipes. *Journal of Pressure Vessel technology*, 129(4):630–638, 2007.

[71] F. Guarracino, A.C. Walker, and A. Giordano. Effects of boundary conditions on testing of pipes and finite element modelling. *International Journal of Pressure Vessels and Piping*, 86(2):196–206, 2009.

[72] B. Guo, S.H. Song, and A. Ghalambor. *Offshore pipelines: design, installation, and maintenance*. Gulf Professional Publishing, 2013.

[73] S. Hauch and Y. Bai. Bending moment capacity of groove corroded pipes. In *The Tenth International Offshore and Polar Engineering Conference*. International Society of Offshore and Polar Engineers, 2000.

[74] A. Hilberink. *Mechanical behaviour of lined pipe*. PhD thesis, Delft University of Technology, 2011.

[75] R. Hill. A theory of the yielding and plastic flow of anisotropic metals. *Proceedings of the Royal Society A*, 193, 1948.

[76] P. Hopkins, D.G. Jones, and A. Clyne. The significance of dents and defects in transmission pipelines. In *International Conference on Pipework Engineering and Operations, London*, pages 137–145, 1989.

[77] P. Hopkins, I. Corder, and P. Corbin. The resistance of gas transmission pipelines to mechanical damage. In *International Conference on Pipeline Reliability*, volume 2, 1992.

[78] X.L. Jiang and C. G. Soares. Ultimate capacity of rectangular plates with partial depth pits under uniaxial loads. *Marine Structures*, 26(1):27–41, 2012.

[79] T. Karman. The strength of thin plates in compression. *Trans. ASME*, 54(2):53–57, 1932.

[80] J. Kiefner, W. Maxey, R. Eiber, and A. Duffy. Failure stress levels of flaws in pressurized cylinders. In *Progress in flaw growth and fracture toughness testing*. ASTM International, 1973.

[81] D.W. Kim, M.H. Mohd, B.J. Lee, D.Y. Kim, J.K. Seo, B.J. Kim, and J.K. Paik. Investigation on the burst strength capacity of aging subsea gas pipeline. In *ASME 2013* 32$^{\text{nd}}$ *International Conference on Ocean, Offshore and Arctic Engineering*. American Society of Mechanical Engineers, 2013.

[82] W. Kim, Y. Kim, Y. Kho, and J. Choi. Full scale burst test and finite element analysis on corroded gas pipeline. In *2002* 4$^{\text{th}}$ *International Pipeline Conference*, pages 1501–1508. American Society of Mechanical Engineers, 2002.

[83] W.T. Koiter. The stability of elastic equilibrium. Technical report, Stanford University CA Dept of Aeronautics and Astronautics, 1970.

[84] S. Kyriakides and E. Corona. *Mechanics of offshore pipelines:Volume 1 buckling and collapse*, volume 1. Elsevier, 2007.

[85] E.R. Lancaster and S.C. Palmer. Burst pressures of pipes containing dents and gouges. *Proceedings of the Institution of Mechanical Engineers, Part E: Journal of Process Mechanical Engineering*, 210(1):19–27, 1996.

[86] E.R. Lancaster and S.C. Palmer. Strain concentrations in pressurized dented pipes. *Proceedings of the Institution of Mechanical Engineers, Part E: Journal of Process Mechanical Engineering*, 210(1):29–38, 1996.

[87] G. Lee, H. Pouraria, J.K. Seo, and J.K. Paik. Burst strength behaviour of an aging subsea gas pipeline elbow in different external and internal corrosion-damaged positions. *International Journal of Naval Architecture and Ocean Engineering*, 7(3): 435–451, 2015.

[88] E. Levold, L. Marchionni, L. Vitali, C. Molinari, A. Restelli, and I. F. Ozkan. Strength and deformation capacity of corroded pipe-laboratory tests and FEM analyses. In *The Twenty-third International Offshore and Polar Engineering Conference*. International Society of Offshore and Polar Engineers, 2013.

[89] E. Levold, A. Restelli, L. Marchionni, C. Molinari, and L. Vitali. Strength and deformation capacity of corroded pipes: The joint industry project. In *ASME 2013* 32nd *International Conference on Ocean, Offshore and Arctic Engineering*. American Society of Mechanical Engineers, 2013.

[90] J.F. Loureiro, T.A. Netto, and S.F. Estefen. On the effect of corrosion defects in the burst pressure of pipelines. In *Proceedings of the* 20th *International Conference on Offshore Mechanics and Arctic Engineering*, 2001.

[91] J.J. Lynch. The measurement of residual stresses. *American Society for Metals, Residual Stress Measurements, Cleveland, OH*, pages 42–96, 1952.

[92] K.A. Macdonald and A. Cosham. Best practice for the assessment of defects in pipelines–gouges and dents. *Engineering Failure Analysis*, 12(5):720–745, 2005.

[93] J. M. Melenk and I. Babuška. The partition of unity finite element method: basic theory and applications. *Computer methods in applied mechanics and engineering*, 139(1-4):289–314, 1996.

[94] I. Miraoui, M. Boujelbene, and M. Zaied. High-power laser cutting of steel plates: Heat affected zone analysis. *Advances in Materials Science and Engineering*, 2016, 2016.

[95] M.H. Mohd, D.W Kim, B. J. Lee, D.Y. Kim, J.K. Seo, and J.K. Paik. On the burst strength capacity of an aging subsea gas pipeline. *Journal of Offshore Mechanics and Arctic Engineering*, 136(4):041402, 2014.

[96] T.A. Netto, U.S. Ferraz, and A. Botto. Residual strength of corroded pipelines under external pressure: A simple assessment. In *2006 International Pipeline Conference*, pages 143–156. American Society of Mechanical Engineers, 2006.

[97] F. Nilsson. *Fracture Mechanics: From Theory to Applications*. Department of Solid Mechanics, Royal Institute of Technology, 1999.

[98] L.S. Ong, A.K. Soh, and J.H. Ong. Experimental and finite element investigation of a local dent on a pressurized pipe. *The Journal of Strain Analysis for Engineering Design*, 27(3):177–185, 1992.

[99] I.V. Orynyak, V Rozhonyuk, V, and L.S. Shlapak. Residual strength of pipelines with dents. *Materials Science*, 35:689–694, 1999.

[100] J.K. Paik. Ultimate strength of steel plates with a single circular hole under axial compressive loading along short edges. *Ships and Offshore Structures*, 2(4):355–360, 2007.

[101] L. Pakiding. Design criteria for high strength steel joints, 2007.

[102] T.D. Park and S. Kyriakides. On the collapse of dented cylinders under external pressure. *International Journal of Mechanical Sciences*, 38(5):557–578, 1996.

[103] PHMSA. Pipeline incident 20 year trend. Technical report, U.S.Department of Transportation, 2017.

[104] T. Pirling, A. Carradò, and H. Palkowski. Residual stress distribution in seamless tubes determined experimentally and by fem. *Procedia Engineering*, 10:3080–3085, 2011.

[105] G. Pluvinage. pipe-defect assessment based on the limit analysis,failure-assessment diagram,and subcritical crack. *Materials Science*, 42:127–139, 2006.

[106] V. Polenta, S.D. Garvey, D. Chronopoulos, A.C. Long, and H.P. Morvan. Optimal internal pressurisation of cylindrical shells for maximising their critical bending load. *Thin-walled Structures*, 87:133–138, 2015.

[107] B. Prabu, A.V. Raviprakash, and A. Venkatraman. Parametric study on buckling behaviour of dented short carbon steel cylindrical shell subjected to uniform axial compression. *Thin-Walled Structures*, 48(8):639–649, 2010.

[108] W. Ramberg and W.R. Osgood. Description of stress–strain curves by three parameters. 1943.

[109] A. Riks, C.C. Rankin, and F.A. Broan. The buckling of a central crack in a plate under tension. *Engineering Fracture Mechanics*, 26:1023–1042, 1992.

[110] E. Riks. The application of Newton's method to the problem of elastic stability. *Journal of Applied Mechanics*, 39(4):1060–1065, 1972.

[111] E. Riks. An incremental approach to the solution of snapping and buckling problems. *International Journal of Solids and Structures*, 15(7):529–551, 1979.

[112] O.L. Seng, C.Y. Wing, and G. Seet. The elastic analysis of a dent on pressurised pipe. *International Journal of Pressure Vessels and Piping*, 38(5):369–383, 1989.

[113] J.R. Shadley and E.F. Rybicki. Experimental method for determining through thickness residual hoop stresses in thin walled pipes and tubes without inside access. *Strain*, 26(1):7–14, 1990.

[114] J. Silva, H. Ghaednia, and S. Das. Fatigue life assessment for NPS30 steel pipe. In *2012* 9th *International Pipeline Conference*, pages 619–624. American Society of Mechanical Engineers, 2012.

[115] C.Y. Song, J.G. Teng, and J.M. Rotter. Imperfection sensitivity of thin elastic cylindrical shells subject to partial axial compression. *International Journal of Solids and Structures*, 41(24):7155–7180, 2004.

[116] J.H. Starnes and C.A. Rose. Buckling and stable tearing responses of unstiffened aluminum shells with long cracks. In *The 39th AIAA/ASME/ASCE/AHS/ASC Structures, Structural Dynamics and Materials Conference and Exhibit*, pages 20–23, 1998.

[117] J.H. Starnes and C.A. Rose. Nonlinear response of thin cylindrical shells with longitudinal cracks and subjected to internal pressure and axial compression loads. In *NASA Conference Publication*, pages 197–208. NASA, 1998.

[118] M. Stein. The influence of prebuckling deformations and stresses on the buckling of perfect cylinders. 1964.

[119] C. Tam, P. Raven, R. Robinson, T. Stensgaard, A.M. Al-Sharif, and R. Preston. Oman India pipeline:development of design methods for hydrostatic collapse in deep water. In *Offshore Pipeline Technology Conference*, pages 1–17. IBC Technical Services Limited, 1996.

[120] C. Thinvongpituk, S. Poonaya, S. Choksawadee, and M. Lee. The ovalisation of thin-walled circular tubes subjected to bending. In *Proceedings of the World Congress on Engineering*, volume 2, pages 2–4, 2008.

[121] S.P. Timoshenko and J.M. Gere. *Theory of elastic stability*. Courier Corporation, 2009.

[122] S.P. Timoshenko and S. Woinowsky-Krieger. *Theory of plates and shells*. McGraw-hill, 1959.

[123] D. Vasilikis, S.A. Karamanos, S. Es, and A.M. Gresnigt. Ultimate bending capacity of spiral–welded steel tubes–part ii: Predictions. *Thin-Walled Structures*, 2015.

[124] A. Vaziri and H.E. Estekanchi. Buckling of cracked cylindrical thin shells under combined internal pressure and axial compression. *Thin-Walled Structures*, 44(2): 141–151, 2006.

[125] L. Vitali, L. Bartolini, D. Askheim, R. Peek, and E. Levold. Hotpipe JI project: Experimental test and FE analyses. In *ASME 2005* 24th *International Conference on Offshore Mechanics and Arctic Engineering*, pages 715–729. American Society of Mechanical Engineers, 2005.

[126] H.M. Westergaard. *Theory of elasticity and plasticity*, volume 367. Harvard University Press Cambridge, 1952.

[127] G. Zecheru, P. Yukhymets, G. Draghici, and A. Dumitrescu. Methods for determining the remaining strength factor of pipelines with volumetric surface defects. *Revisia de Chimie*, 66(5):710–717, 2015.

[128] U. Zerbst, R.A. Ainsworth, H. T. Beier, H. Pisarski, Z.L. Zhang, K. Nikbin, T. Nitschke-Pagel, S. Münstermann, P. Kucharczyk, and D. Klingbeil. Review on fracture and crack propagation in weldments–a fracture mechanics perspective. *Engineering Fracture Mechanics*, 132:200–276, 2014.

[129] K. Zhao, L. Wang, Y. Chang, and J. Yan. Identification of post-necking stress-strain curve for sheet metals by inverse method. *Mechanics of Materials*, 92:107–118, 2016.

[130] M. Zheng, J.B. Li, and X. Shu. Modified expression for predicting the bending resistance of a locally corroded pipeline and its experimental verification. *Metals and Materials International*, 11:215–219, 2005.

[131] A. Zingoni. Liquid-containment shells of revolution: a review of recent studies on strength, stability and dynamics. *Thin-Walled Structures*, 87:102–114, 2015.

Appendices

These appendices contain the Python scripts for the fitting of material properties by using the method from Section 4.1.1 in Chapter 4, and the damage produce methods on the surface of pipes. For clarity reason, only the script for a dent and a notch is presented.

Appendix A : Python script for material stress-strain curve

```
__author__ = 'Jie Cai'
# -*- coding: utf-8 -*-
'''
Fitting method of material properties based on basic material parameters.
Default input parameters (yield stress, ultimate tensile stress, and the
maximum elongation based on the test in this thesis): 378 MPa 542 MPa
    0.246.
The units system is MPa,mm,N.
'''

import numpy as np
import matplotlib.pyplot as plt
from math import *
from scipy.optimize import fsolve
from openpyxl import Workbook
from openpyxl import load_workbook
from openpyxl.cell import get_column_letter
from openpyxl.writer.excel import ExcelWriter

# Input basic material parameters for calculation
xiegamaE,xiegamaU,elonM=[float(el) for el in input("Please input three
    basic material parameters: ").split()]
E,mv=2.1e5,0.3          # Young's modulus and Poission's ratio
ibxilongE=xiegamaE/E    # Calculate the  strain at yield point
ibxilongU=0.38*elonM    # Calculate the strain at ultimate point
ibxilongFail=elonM      # Calculate the failure strain at fracture point
betaM=0.7               # Material constant for downward phase
rfaM=0.38               # Material constant for downward phase
rfaS=xiegamaU*(1-betaM)/((ibxilongFail*(1-rfaM))**2)
j=8                     # Seriel number of sheet for storing data in Excel

# Create a new Excel file for data restoring
wb_materialnew=Workbook()
ew=ExcelWriter(workbook=wb_materialnew)
dest_filename="D:/academia/python_codes/material_created/
    materialFittingData3.xlsx"
```

```
ws_newsheet=wb_materialnew.create_sheet('j')
ws_newsheet.title= 'L'+str(j)
ws_newsheet.append({'A':'SN','B':'strainEng','C':'stressEng','D':'
    strainTrue','E':'stressTrue'})
ws_newsheet.append({'B':0,'C':0,'D':0,'E':0})
#  obatin the list of three basic known material points
strainEngBsc=[0,ibxilongE,ibxilongU,ibxilongFail]
stressEngBsc=[0,xiegamaE,xiegamaU,0.7*xiegamaU]
plt.plot(strainEngBsc,stressEngBsc,color="red",linewidth=2.5,linestyle="-",
    label="Engineering stress-strain curve")

# Calculate the material constant n based on Ramberg-Osgood equation
def materialParameter(n):
    return (ibxilongU-xiegamaU/E-0.002*(xiegamaU/xiegamaE)**n)
n=fsolve(materialParameter,10)

# Fit the engineering stress-strain curve (upward phase)
x1=np.linspace(ibxilongE+0.002,ibxilongU,num=40)
y1=[]
def ROequ(xiegama):
    return ibxilong-xiegama/E-0.002*((xiegama/xiegamaE)**n)
for ibxilong in x1:
    e=fsolve(ROequ,xiegamaU)
    y1.extend(e)
plt.plot(x1,y1,color="blue",linewidth=2.5,linestyle="--",label="Fitted
    engineering stress-strain curve")

# Calculate the true stress-strain curve (upward phase)
x11=[]
y11=[]
x1=x1.tolist()
x1=[0,ibxilongE]+x1
y1=[0,xiegamaE]+y1
for el in x1:
    ibxilongT=np.log(1+el)
    x11.append(ibxilongT)
i=-1
for ely in y1:
    i=i+1
    ibxilong=x11[i]
    xiegamaT=ely*(1+ibxilong)
    y11.append(xiegamaT)
plt.plot(x11,y11,color="black",linewidth=2.5,linestyle="-",label="True
    stress-strain curve")

# Fit the engineering stress-strain curve (downward phase).
x2=np.linspace(ibxilongU,ibxilongFail,num=40,endpoint=True)
y2=[]
for ibxilongD in x2:
    xiegamaD=xiegamaU-rfaS*(ibxilongD-ibxilongU)**2
    xiegama2=xiegamaD
    y2.append(xiegama2)
plt.plot(x2,y2,color="blue",linewidth=2.5,linestyle="--")

# Calculate the true stress-strain curve (downward phase)
x22=np.linspace(ibxilongU,ibxilongFail,num=40,endpoint=True)
y22=[]
x22=x22.tolist()
```

```
x2=x2.tolist()

def downWard(p):
    k,npp=p
    return (y11[-1]-k*x11[-1]**(npp),y11[-2]-k*x11[-2]**(npp))
k,npp=fsolve(downWard,(760,0.2))
print(k,npp)
for ibxilongT in x22:
    xiegamaT=k*ibxilongT**(npp)
    y22.append(xiegamaT)
x11.pop(0)  # remove the first data in elastic domain
y11.pop(0)  # remove the first data in elastic domain
x1.pop(0)
y1.pop(0)
StressT=y11+y22
StrainT=x11+x22
stressEng=y1+y2
strainEng=x1+x2
len1=len(StressT)
len2=len(stressEng)
print (len1,len2)

# Write data into file and plot
for i in range(0,len1):
    temp=strainEng[i]
    temp1=stressEng[i]
    temp2=StrainT[i]
    temp3=StressT[i]
    ws_newsheet.cell(row=i+3,column=2).value=temp
    ws_newsheet.cell(row=i+3,column=3).value=temp1
    ws_newsheet.cell(row=i+3,column=4).value=temp2
    ws_newsheet.cell(row=i+3,column=5).value=temp3
array=np.array(StrainT)
StrainPlastic=array-xiegamaE/E
StrainPlastic.tolist()
data1=list(zip(StressT,StrainPlastic))
data2=list(zip(StressT,StrainPlastic))
fileName1=" materialTrueStressPStrainStress"
fileName2=" materialTrueStressPStrainStrain"
outFile1=open(fileName1,"w")
outFile2=open(fileName2,"w")

for data in data1:
    temp=format(data[0],'.1f')
    outFile1.write(temp )
    outFile1.write("\n")

for data in data2:
    temp=format(data[1],'.3f')
    outFile2.write(temp )
    outFile2.write("\n")
outFile2.close()
outFile1.close()

print ("the true material data are: ",data1 )
plt.plot(x22,y22,color="black",linewidth=2.5,linestyle="-")
plt.legend(loc='lower right',fontsize=16)
plt.xlim(0,ibxilongFail+0.01)
```

```
146 plt.ylim(0,1.4*xiegamaU)
147 plt.xlabel('Strain(-)',fontsize=15)
148 plt.ylabel('Stress(MPa)',fontsize=15)
149 plt.show()
150 ew.save(filename=dest_filename)
```

Appendix B : Python script for a dent

```
__author__ = 'Jie Cai'
'''
The function is to produce a dent with the variation of dent length,
dent width, dent depth, and dent rotational angle on the surface of
pipes. The definition of dent parameters is explained in Figure 4.5 in
Chapter 4.
'''

from abaqus import *
from abaqusConstants import *
import testUtils
import regionToolset
# A developed library for selection by range
from selectByRange_Function import selectByRange
# A developed library for transforming list to sequence.
from listToseq_Function import listToseq
testUtils.setBackwardCompatibility()

def dentProduing(iDlength,iDwidth,iDdepth,iangle):
    iDlength=float(iDlength)
    iDwidth=float(iDwidth)
    iDdepth=float(iDdepth)
    iangle=float(iangle)      # The unit is degree.
    a=m.rootAssembly
    inst=a.instances['Part-1-1']     # The name of instance in the function
    n=a.instances['Part-1-1'].nodes[:]  # Define a meshNodeArray
    lab=[]

    # The profie (shape) of a dent is based on Equation (4.6) in Chapter 4.
    selectNode=selectByRange(inst,'NODE',(-1,iDlength/2),(0,1.1*iDiameter
    /2),(-iDwidth/2,iDwidth/2))
    region=listToseq(inst,'NODE',selectNode)
    leng=len(region)
    a.Set(nodes=region,name='selectNode')
    for node in selectNode:
        d_coor=node.coordinates
        label=node.label
        x0=d_coor[0]
        y0=d_coor[1]
        z0=d_coor[2]
        offset_lon=(abs(x0))
        offset_tra=z0
        dy2=iDdepth*(1+cos(2*pi*offset_lon/iDlength))*\
        (1+cos(2*offset_tra*pi/iDwidth))/4.0
        nodes=n[label-1:label]
        a.editNode(nodes=nodes,offset2=-dy2)
        lab.append(label)
        leng=leng-1
        a.Set(name='deformedNode',nodes=n.sequenceFromLabels(lab))
        print leng,label,offset_lon,offset_tra,dy2
```

Appendix C: Python script to produce a notch on pipe surface

```
__author__ = 'Jie Cai'
'''
This script is used for the production of a pipe with metal loss in terms
of a notch under a bending moment. A simplified model is used, as described
in Chapter 5.The notch parameters in terms of depth, length,and width is
varied. The rotational angle is 90 degree. The Units system is mm,Mpa,N.
'''

from abaqus import *
from abaqusConstants import *
import testUtils
# the developed material library
from material_libraryNotch import material_library
import displayGroupMdbToolset as dgm
testUtils.setBackwardCompatibility()


# Input all the parameters (pipe dimension and notch dimension, etc)
# iMvangle is the angle that defines the notch tip (from notch depth and
# notch width)
iDiameter,iThickness,iLength,iMlength,iMdepth,iMangle,iMvangle,iMwidth,
    materials,myModel,SN=166.8,7.60,2200,44,3,90,118,10,'Steel-Q345-testL8'
    ,'pipeWithMetalloss',2
iDiameter,iThickness,iLength,iMlength,iMdepth,iMangle,iMvangle,iMwidth=
    float(iDiameter),float(iThickness),float(iLength),float(iMlength),float
    (iMdepth),float(iMangle),float(iMvangle),float(iMwidth)
iLengthBm,iLengthArm,iLengthSleeve,iLengthStrip=400,300,200,100
sLon,sCir,sNotchHoop,sNotchLon,sNotchSlope=12,4,2.5,4,1.5
nVt,nNotchLon=4,4
SN=str(SN)
materials=str(materials)
iLengthBm=float(iLengthBm)
iLengthArm=float(iLengthArm)
iLengthStrip=float(iLengthStrip)
iLengthSleeve=float(iLengthSleeve)
sLon,sCir,sNotchHoop,sNotchLon,sNotchSlope=float(sLon),float(sCir),float(
    sNotchHoop),float(sNotchLon),float(sNotchSlope)
nVt=int(nVt)
iMvangle=float(iMvangle)
modelName=str(myModel)
m=mdb.Model(name=modelName)
myViewport=session.Viewport(name=modelName)
myViewport.makeCurrent()
myViewport.maximize()


# Create initial geometry parts
s1=m.Sketch(name='cylinder',sheetSize=iDiameter*2)
g1,v1=s1.geometry,s1.vertices
s1.setPrimaryObject(option=STANDALONE)
s1.CircleByCenterPerimeter(center=(0,0),point1=(iDiameter/2,0))
s1.CircleByCenterPerimeter(center=(0,0),point1=(iDiameter/2-iThickness,0))
p1=m.Part(name='cylinder',dimensionality=THREE_D,type=DEFORMABLE_BODY)
```

```
49 p1.BaseSolidExtrude(sketch=s1,depth=iLengthBm)  # A half-model
50 myViewport.setValues(displayedObject=p1)
51 vp=session.viewports[session.currentViewportName]    # Create a viewport
52 vp.setValues(displayedObject=p1)
53 vp.view.fitView()
54
55
56 # Define datum planes, and partition parts
57 d1=p1.DatumPlaneByPrincipalPlane(principalPlane=XYPLANE, offset=iDiameter
       /2)
58 d2=p1.DatumPlaneByPrincipalPlane(principalPlane=XZPLANE, offset=0.0)
59 d3=p1.DatumPlaneByPrincipalPlane(principalPlane=YZPLANE, offset=0.0)
60 d5=p1.DatumPlaneByPrincipalPlane(principalPlane=XYPLANE, offset=iLengthBm
       -100)
61 d9=p1.DatumPlaneByPrincipalPlane(principalPlane=XYPLANE,offset=iMlength*cos
       (iMangle*pi/180.0)+2*iMwidth*sin(iMangle*pi/180.0))
62
63 myDatum=p1.datums
64 for num in range(0,5):
65     myCell=p1.cells
66     p1.PartitionCellByDatumPlane(datumPlane=myDatum[num+2],cells=myCell)
67 myDatum=p1.datums
68 s3=m.ConstrainedSketch(name='notchPath',sheetSize=200.0) # create a notch
69 s2=m.ConstrainedSketch(name='V-notch1',sheetSize=200.0)
70 g2=s2.geometry
71 s2.setPrimaryObject(option=STANDALONE)
72 R=iDiameter/2
73 s2.ArcByCenterEnds(center=(0,iMwidth/2), point1=(iMwidth/2,iMwidth/2),
       point2=(-iMwidth/2,iMwidth/2), direction=CLOCKWISE)
74 s2.Line(point1=(iMwidth/2,iMwidth/2),point2=(-iMwidth/2,iMwidth/2))
75 p2=m.Part(name='v-notch',dimensionality=THREE_D,type=DEFORMABLE_BODY)
76 s2.rotate(centerPoint=(0.0,0.0),angle=90,objectList=(g2[2],g2[3]))
77 r=iDiameter/2-iMdepth
78 theta=asin(iMlength/(2*r))
79 h=r-r*cos(theta)
80 x=r-h
81 s3.ArcByCenterEnds(center=(iMlength/2,-x),point1=(0,0),point2=(iMlength,0),
       direction=CLOCKWISE)
82 p2.BaseSolidSweep(sketch=s2,path=s3)
83 e2=p2.edges
84 p4=m.Part(name='cutShell',dimensionality=THREE_D,type=DEFORMABLE_BODY)
85 s4=m.ConstrainedSketch(name='cutShell',sheetSize=200.0)
86 g4=s4.geometry
87 s5=m.ConstrainedSketch(name='cutShell-path',sheetSize=200.0)
88 s4.ArcByCenterEnds(center=(iMwidth/2, 0.0), point1=(iMwidth/2,iMwidth/2),
       point2=(iMwidth/2,-iMwidth/2), direction=COUNTERCLOCKWISE)
89 s5.CircleByCenterPerimeter(center=(0,0),point1=(r,0))
90 p4.BaseShellSweep(sketch=s4,path=s5)
91
92
93 # Create independent instances
94 a=m.rootAssembly
95 myViewport.setValues(displayedObject=a)
96 a.Instance(name='cylinder-1',part=p1,dependent=OFF)
97 cylinderInstance=a.instances['cylinder-1']
98 a.Instance(name='v-notch-1',part=p2,dependent=OFF)
99 vnotchInstance=a.instances['v-notch-1']
100
```

```
a.Instance(name='cutShell-1',part=p4,dependent=OFF)
a.translate(instanceList=('v-notch-1',),vector=(-iMlength/2,0,0))
a.translate(instanceList=('v-notch-1',),vector=(0,r-h,0))
a.rotate(instanceList=('v-notch-1',), axisPoint=(0.0,1,0), axisDirection
    =(0.0,-1,0), angle=90-iMangle)
a.InstanceFromBooleanCut(name='cylinderWithMetalloss',instanceToBeCut=
    cylinderInstance, cuttingInstances=(a.instances['cutShell-1'],),
    originalInstances=DELETE)
cylinderInstance=a.instances['cylinderWithMetalloss-1']
a.InstanceFromBooleanCut(name='cylinderWithMetalloss1',instanceToBeCut=
    cylinderInstance,cuttingInstances=(vnotchInstance,), originalInstances
    =DELETE)

p3=m.parts['cylinderWithMetalloss1']
a.Instance(name='cylinderWithMetalloss1-1',part=p3,dependent=OFF)
a.Instance(name='cylinderWithMetalloss1-2',part=p3,dependent=OFF)
cylinderWithMetallossInstance=a.instances['cylinderWithMetalloss1-1']
myCell,myEdge=a.instances['cylinderWithMetalloss1-1'].cells,a.instances['
    cylinderWithMetalloss1-1'].edges
# Partition the notched regions for further mesh
c=a.instances['cylinderWithMetalloss1-1'].cells
f=a.instances['cylinderWithMetalloss1-1'].faces
e1 = a.instances['cylinderWithMetalloss1-1'].edges
c2=a.instances['cylinderWithMetalloss1-2'].cells
f2=a.instances['cylinderWithMetalloss1-2'].faces
e22 = a.instances['cylinderWithMetalloss1-2'].edges
chord_length=R-sqrt(R**2-iMlength**2/4)
thetaCut=atan(iMlength/(R-iMdepth-chord_length)/2)

notchedCell_1 =c.findAt(((R*sin(pi/10),R*cos(pi/10),30),))
face_cut1=f.getByBoundingBox(xMin=0.1*iMlength,xMax=iMlength)
a.Set(cells=notchedCell_1, name='notchedCell_1')
a.Set(faces=face_cut1,name='face_cut1')
a.PartitionCellByExtendFace(extendFace=face_cut1[0], cells=notchedCell_1)
notchedCell_2 =c.findAt(((-R*sin(pi/10),R*cos(pi/10),30),))
face_cut2=f.getByBoundingBox(xMax=-0.1*iMlength,xMin=-iMlength)
a.Set(cells=notchedCell_2, name='notchedCell_2')
a.Set(faces=face_cut2,name='face_cut2')
a.PartitionCellByExtendFace(extendFace=face_cut2[0], cells=notchedCell_2)
notchedCell_2 =c2.findAt(((R*sin(pi/10),R*cos(pi/10),30),))
face_cut2=f2.getByBoundingBox(xMin=0.1*iMlength,xMax=iMlength)
a.PartitionCellByExtendFace(extendFace=face_cut2[0], cells=notchedCell_2)
notchedCell_2 =c2.findAt(((-R*sin(pi/10),R*cos(pi/10),30),))
face_cut2=f2.getByBoundingBox(xMax=-0.1*iMlength,xMin=-iMlength)
a.PartitionCellByExtendFace(extendFace=face_cut2[0], cells=notchedCell_2)


# Creat mesh. X coordiante is in the pipe longitudinal direction
a.rotate(instanceList=('cylinderWithMetalloss1-1',),axisPoint=(0,0,0),
    axisDirection=(0,1,0),angle=90.0)
a.rotate(instanceList=('cylinderWithMetalloss1-2',),axisPoint=(0,0,0),
    axisDirection=(0,1,0),angle=-90)
a.InstanceFromBooleanMerge(name='cylinderWithMetalloss1-all', instances=(a.
    instances['cylinderWithMetalloss1-1'], a.instances['
    cylinderWithMetalloss1-2'],), keepIntersections=ON, originalInstances=
    DELETE,domain=GEOMETRY)
p8=m.parts['cylinderWithMetalloss1-all']
a.Instance(name='cylinderWithMetalloss1-all-1',part=p8,dependent=OFF)
```

```
148 c=a.instances['cylinderWithMetalloss1-all-1'].cells
149 f=a.instances['cylinderWithMetalloss1-all-1'].faces
150 e1 = a.instances['cylinderWithMetalloss1-all-1'].edges
151
152 l_longbiasCenter=e1.findAt(((iDiameter/2+1,iDiameter/2,0),),((iDiameter
        /2+1,-iDiameter/2,0),), ((iDiameter/2+1,0,iDiameter/2),),((iDiameter
        /2+1,0,-iDiameter/2),))
153 l_longbiasCenter_1=e1.findAt(((iDiameter/2+1,(iDiameter-2*iThickness)/2,0)
        ,),((iDiameter/2+1,-(iDiameter-2*iThickness)/2,0),),((iDiameter/2+1,0,(
        iDiameter-2*iThickness)/2),),((iDiameter/2+1,0,-(iDiameter-2*iThickness
        )/2),))
154 l_longInnerCenter=e1.findAt(((iDiameter/2-1,(iDiameter-2*iThickness)/2,0),)
        ,((iDiameter/2-1,-iDiameter/2,0),),((iDiameter/2-1,0,(iDiameter-2*
        iThickness)/2),),((iDiameter/2-1,0,-iDiameter/2),))
155 l_longInnerCenter_1=e1.findAt(((iDiameter/2-1,-(iDiameter-2*iThickness)
        /2,0),),((iDiameter/2-1,iDiameter/2,0),),((iDiameter/2-1,0,iDiameter/2)
        ,),((iDiameter/2-1,0,-(iDiameter-2*iThickness)/2),))
156 l_longBM1=e1.findAt(((iLengthBm-1,iDiameter/2,0),),((iLengthBm-1,-iDiameter
        /2,0),),((iLengthBm-1,0,iDiameter/2),),((iLengthBm-1,0,-iDiameter/2),)
        ,((iLengthBm-1,R-iMdepth,0),))
157 l_longBM1_1=e1.findAt(((iLengthBm-1,(iDiameter-2*iThickness)/2,0),),((
        iLengthBm-1,-(iDiameter-2*iThickness)/2,0),),((iLengthBm-1,0,(iDiameter
        -2*iThickness)/2),),((iLengthBm-1,0,-(iDiameter-2*iThickness)/2),))
158 l_longCenter=e1.findAt(((1,-iDiameter/2,0),),((1,0,iDiameter/2),),((1,0,-
        iDiameter/2),))
159 l_longCenter_1=e1.findAt(((1,-(iDiameter-2*iThickness)/2,0),),((1,0,(
        iDiameter-2*iThickness)/2),),((1,0,-(iDiameter-2*iThickness)/2),))
160 l_longbiasCenterL=e1.findAt(((-iDiameter/2-1,iDiameter/2,0),),((-iDiameter
        /2-1,-iDiameter/2,0),),((-iDiameter/2-1,0,iDiameter/2),),((-iDiameter
        /2-1,0,-iDiameter/2),))
161
162 l_longbiasCenterL_1=e1.findAt(((-iDiameter/2-1,(iDiameter-2*iThickness)
        /2,0),),((-iDiameter/2-1,-(iDiameter-2*iThickness)/2,0),),((-iDiameter
        /2-1,0,(iDiameter-2*iThickness)/2),),((-iDiameter/2-1,0,-(iDiameter-2*
        iThickness)/2),))
163 l_longInnerCenterL=e1.findAt(((-iDiameter/2+1,(iDiameter-2*iThickness)/2,0)
        ,),((-iDiameter/2+1,-iDiameter/2,0),),((-iDiameter/2+1,0,(iDiameter-2*
        iThickness)/2),),((-iDiameter/2+1,0,-iDiameter/2),))
164 l_longInnerCenterL_1=e1.findAt(((-iDiameter/2+1,-(iDiameter-2*iThickness)
        /2,0),),((-iDiameter/2+1,iDiameter/2,0),),((-iDiameter/2+1,0,iDiameter
        /2),),((-iDiameter/2+1,0,-(iDiameter-2*iThickness)/2),))
165 l_longBML1=e1.findAt(((-iLengthBm+1,iDiameter/2,0),),((-iLengthBm+1,-
        iDiameter/2,0),),((-iLengthBm+1,0,iDiameter/2),),((-iLengthBm+1,0,-
        iDiameter/2),),((-iLengthBm+1,R-iMdepth,0),))
166 l_longBML1_1=e1.findAt(((-iLengthBm+1,(iDiameter-2*iThickness)/2,0),),((-
        iLengthBm+1,-(iDiameter-2*iThickness)/2,0),), ((-iLengthBm+1,0,(
        iDiameter-2*iThickness)/2),),((-iLengthBm+1,0,-(iDiameter-2*iThickness)
        /2),))
167 l_longCenterL=e1.findAt(((-1,-iDiameter/2,0),),((-1,0,iDiameter/2),)
        ,((-1,0,-iDiameter/2),))
168 l_longCenterL_1=e1.findAt(((-1,-(iDiameter-2*iThickness)/2,0),),((-1,0,(
        iDiameter-2*iThickness)/2),),((-1,0,-(iDiameter-2*iThickness)/2),))
169
170 e1=a.instances['cylinderWithMetalloss1-all-1'].edges
171 edge_notchLong1=e1.getByBoundingBox(zMax=-1,zMin=-iMlength,yMin=0,yMax=R-
        iMdepth-chord_length-1)
172 edge_notchLong2=e1.getByBoundingBox(zMin=1,zMax=iMlength,yMin=0,yMax=R-
        iMdepth-chord_length-1)
```

```
edge_notchLong3=e1.findAt(((iMwidth+1,R-iThickness,0),))
a.Set(name='edge_notchLongBot',edges=edge_notchLong1+edge_notchLong2+
    edge_notchLong3)
edge_notchLongL3=e1.findAt(((-iMwidth-1,R-iThickness,0),))
a.Set(name='edge_notchLongBotL',edges=edge_notchLongL3)
edge_notchLong4=e1.getByBoundingBox(zMax=-1,zMin=-iMlength,yMin=R-iMdepth-
    chord_length,xMin=1)
edge_notchLong5=e1.getByBoundingBox(zMin=1,zMax=iMlength,yMin=R-iMdepth-
    chord_length,xMin=1)
edge_notchLong6=e1.findAt(((iMwidth+5,R,0),))
a.Set(name='edge_notchLongTop',edges=edge_notchLong4+edge_notchLong5+
    edge_notchLong6)
edge_notchLong7=e1.getByBoundingBox(zMax=-1,zMin=-iMlength,yMin=R-iMdepth-
    chord_length,xMin=0,xMax=iMwidth/2+1)
edge_notchLong8=e1.getByBoundingBox(zMin=1,zMax=iMlength,yMin=R-iMdepth-
    chord_length,xMin=0,xMax=iMwidth/2+1)
a.Set(name='edge_notchLongTop1',edges=edge_notchLong7+edge_notchLong8)
edge_notchLongL4=e1.getByBoundingBox(zMax=-1,zMin=-iMlength,yMin=R-iMdepth-
    chord_length,xMax=-1)
edge_notchLongL5=e1.getByBoundingBox(zMin=1,zMax=iMlength,yMin=R-iMdepth-
    chord_length,xMax=-1)
edge_notchLongL6=e1.findAt(((-iMwidth-5,R,0),))
a.Set(name='edge_notchLongTopL',edges=edge_notchLongL4+edge_notchLongL5+
    edge_notchLongL6)
edge_notchLongL7=e1.getByBoundingBox(zMax=-1,zMin=-iMlength,yMin=R-iMdepth-
    chord_length,xMax=0,xMin=-iMwidth/2-1)
edge_notchLongL8=e1.getByBoundingBox(zMin=1,zMax=iMlength,yMin=R-iMdepth-
    chord_length,xMax=0,xMin=-iMwidth/2-1)
a.Set(name='edge_notchLongTopL1',edges=edge_notchLongL7+edge_notchLongL8)


# Define the vertical edges in the notched regions.
edge_notchVt=e1.getByBoundingBox(yMin=0,yMax=R-iMdepth-chord_length+1,zMax
    =-1,zMin=-iMlength,xMin=-1,xMax=1)
edge_notchVt1=e1.getByBoundingBox(yMin=0,yMax=R-iMdepth-chord_length+1,zMin
    =1,zMax=iMlength,xMin=-1,xMax=1)
d_offset=iMlength*cos(iMangle*pi/180.0)+2*iMwidth*sin(iMangle*pi/180.0)
edge_notchVt2=e1.getByBoundingBox(yMin=0,zMax=-1,zMin=-iMlength,xMin=
    d_offset-1,xMax=d_offset+1)
edge_notchVt3=e1.getByBoundingBox(yMin=0,zMin=1,zMax=iMlength,xMin=d_offset
    -1,xMax=d_offset+1)
edge_notchVt4=e1.findAt(((0,R-iThickness+1,0),))
edge_notchVt5=e1.findAt(((d_offset,R-iThickness+1,0),))
a.Set(name='edge_notchVt',edges=edge_notchVt+edge_notchVt1+edge_notchVt2+
    edge_notchVt3+edge_notchVt4+edge_notchVt5)
d_offset=iMlength*cos(iMangle*pi/180.0)+2*iMwidth*sin(iMangle*pi/180.0)
edge_notchVtL2=e1.getByBoundingBox(yMin=0,zMax=-1,zMin=-iMlength,xMax=-
    d_offset+1,xMin=-d_offset-1)
edge_notchVtL3=e1.getByBoundingBox(yMin=0,zMin=1,zMax=iMlength,xMax=-
    d_offset+1,xMin=-d_offset-1)
edge_notchVtL5=e1.findAt(((-d_offset,R-iThickness+1,0),))
a.Set(name='edge_notchVtL',edges=edge_notchVtL2+edge_notchVtL3+
    edge_notchVtL5)


# Define the hoop edges in the notched regions
edge_notchHoop=e1.findAt(((0,(R-iThickness)*cos(0.01),(R-iThickness)*sin
    (0.01)),),((0,(R-iThickness)*cos(0.01),-(R-iThickness)*sin(0.01)),),((
```

```
    d_offset,(R-iThickness)*cos(0.01),(R-iThickness)*sin(0.01)),),((
    d_offset,(R)*cos(0.01),(R)*sin(0.01)),),((d_offset,(R)*cos(0.01),-(R)*
    sin(0.01)),),((0,(R-iMdepth)*cos(0.01),(R-iMdepth)*sin(0.01)),),((0,(R-
    iMdepth)*cos(0.01),-(R-iMdepth)*sin(0.01)),),((d_offset,(R-iThickness)*
    cos(0.01),-(R-iThickness)*sin(0.01)),))
a.Set(name='edge_notchHoop',edges=edge_notchHoop)
edge_notchHoopL=e1.findAt(((0,(R-iThickness)*cos(0.01),(R-iThickness)*sin
    (0.01)),),((0,(R-iThickness)*cos(0.01),-(R-iThickness)*sin(0.01)),),((-
    d_offset,(R-iThickness)*cos(0.01),(R-iThickness)*sin(0.01)),),((-
    d_offset,(R)*cos(0.01),(R)*sin(0.01)),),((-d_offset,(R)*cos(0.01),-(R)*
    sin(0.01)),),((0,(R-iMdepth)*cos(0.01),(R-iMdepth)*sin(0.01)),),((0,(R-
    iMdepth)*cos(0.01),-(R-iMdepth)*sin(0.01)),),((-d_offset,(R-iThickness)
    *cos(0.01),-(R-iThickness)*sin(0.01)),))
a.Set(name='edge_notchHoopL',edges=edge_notchHoopL)


# Define the non-vertical edge around the notch
edge_notchSlope=e1.getByBoundingBox(zMin=-1,zMax=1,xMin=-1,xMax=d_offset-1,
    yMin=R-iMdepth-chord_length-1,yMax=R+1)
a.Set(name='edge_notchSlope',edges=edge_notchSlope)
edge_notchSlopeL=e1.getByBoundingBox(zMin=-1,zMax=1,xMax=1,xMin=-d_offset
    +1,yMin=R-iMdepth-chord_length-1,yMax=R+1)
a.Set(name='edge_notchSlope',edges=edge_notchSlopeL)
a.seedEdgeBySize(edges=edge_notchHoop+edge_notchHoopL, size=sNotchHoop,
    constraint=FINER)
a.seedEdgeByNumber(edges=edge_notchLong1+edge_notchLong2+edge_notchLong3+
    edge_notchLongL3,number=3*nNotchLon,constraint=FINER)
a.seedEdgeByNumber(edges=edge_notchLong4+edge_notchLong5+edge_notchLong6+
    edge_notchLongL4+edge_notchLongL5+edge_notchLongL6,number=2*nNotchLon,
    constraint=FINER)
a.seedEdgeByNumber(edges=edge_notchLong7+edge_notchLong8+edge_notchLongL7+
    edge_notchLongL8,number=2*nNotchLon,constraint=FINER)
a.seedEdgeBySize(edges=edge_notchSlope+edge_notchSlopeL,size=sNotchSlope,
    constraint=FINER)
a.seedEdgeByNumber(edges=edge_notchVt+edge_notchVt1+edge_notchVt2+
    edge_notchVt3+edge_notchVt4+edge_notchVt5+edge_notchVtL2+edge_notchVtL3
    +edge_notchVtL5,number=nVt,constraint=FINER)
a.seedEdgeBySize(edges=l_longCenter+l_longCenter_1,size=sNotchLon,
    deviationFactor=0.1,constraint=FINER)
a.seedEdgeBySize(edges=l_longCenterL+l_longCenterL_1,size=sNotchLon,
    deviationFactor=0.1,constraint=FINER)
a.seedEdgeByBias(biasMethod=SINGLE,end1Edges=l_longInnerCenter_1, end2Edges
    =l_longInnerCenter,minSize=sNotchLon,maxSize=sLon/3,constraint=FINER)
a.seedEdgeByBias(biasMethod=DOUBLE,endEdges=l_longbiasCenter+
    l_longbiasCenter_1, minSize=sLon/3,maxSize=3*sLon/4, constraint=FINER)
a.seedEdgeByBias(biasMethod=SINGLE,end1Edges=l_longInnerCenterL_1,
    end2Edges=l_longInnerCenterL,minSize=sNotchLon,maxSize=sLon/3,
    constraint=FINER)
a.seedEdgeByBias(biasMethod=DOUBLE,endEdges=l_longbiasCenterL+
    l_longbiasCenterL_1, minSize=sLon/3,maxSize=3*sLon/4, constraint=FINER)
a.seedEdgeBySize(edges=l_longBM1_1+l_longBM1,size=sLon/3,constraint=FINER)
a.seedEdgeBySize(edges=l_longBML1_1+l_longBML1,size=sLon/3,constraint=FINER
    )
a.Set(edges=l_longbiasCenter+l_longbiasCenter_1,name='l_longbiasCenter')
a.Set(edges=l_longCenter+l_longCenter_1,name='l_longCenter')
a.Set(edges=l_longBM1_1+l_longBM1,name='l_longBM1')
a.Set(edges=l_longInnerCenter+l_longInnerCenter_1,name='l_longInnerCenter')
a.Set(edges=l_longbiasCenterL+l_longbiasCenterL_1,name='l_longbiasCenterL')
```

```
240 a.Set(edges=l_longCenterL+l_longCenterL_1,name='l_longCenterL')
241 a.Set(edges=l_longBML1_1+l_longBML1,name='l_longBML1')
242 a.Set(edges=l_longInnerCenterL+l_longInnerCenterL_1,name='
        l_longInnerCenterL')
243
244 l_cir=e1.findAt(((0,iDiameter*sqrt(2)/4,iDiameter*sqrt(2)/4),),((0,
        iDiameter*sqrt(2)/4,-iDiameter*sqrt(2)/4),),((0,-iDiameter*sqrt(2)/4,
        iDiameter*sqrt(2)/4),),((0,-iDiameter*sqrt(2)/4,-iDiameter*sqrt(2)/4),)
        ,((iLength/2,iDiameter*sqrt(2)/4,iDiameter*sqrt(2)/4),),((iLength/2,
        iDiameter*sqrt(2)/4,-iDiameter*sqrt(2)/4),),((iLength/2,-iDiameter*sqrt
        (2)/4,iDiameter*sqrt(2)/4),),((iLength/2,-iDiameter*sqrt(2)/4,-
        iDiameter*sqrt(2)/4),),((iLengthBm,iDiameter*sqrt(2)/4,iDiameter*sqrt
        (2)/4),),((iLengthBm,iDiameter*sqrt(2)/4,-iDiameter*sqrt(2)/4),),((
        iLengthBm,-iDiameter*sqrt(2)/4,iDiameter*sqrt(2)/4),),((iLengthBm,-
        iDiameter*sqrt(2)/4,-iDiameter*sqrt(2)/4),))
245 l_cir_1=e1.findAt(((0,(iDiameter-2*iThickness)*sqrt(2)/4,(iDiameter-2*
        iThickness)*sqrt(2)/4),),((0,(iDiameter-2*iThickness)*sqrt(2)/4,-(
        iDiameter-2*iThickness)*sqrt(2)/4),),((0,-(iDiameter-2*iThickness)*sqrt
        (2)/4,(iDiameter-2*iThickness)*sqrt(2)/4),),((0,-(iDiameter-2*
        iThickness)*sqrt(2)/4,-(iDiameter-2*iThickness)*sqrt(2)/4),),((iLength
        /2,(iDiameter-2*iThickness)*sqrt(2)/4,(iDiameter-2*iThickness)*sqrt(2)
        /4),),((iLength/2,(iDiameter-2*iThickness)*sqrt(2)/4,-(iDiameter-2*
        iThickness)*sqrt(2)/4),),((iLength/2,-(iDiameter-2*iThickness)*sqrt(2)
        /4,(iDiameter-2*iThickness)*sqrt(2)/4),),((iLength/2,-(iDiameter-2*
        iThickness)*sqrt(2)/4,-(iDiameter-2*iThickness)*sqrt(2)/4),),((
        iLengthBm,(iDiameter-2*iThickness)*sqrt(2)/4,(iDiameter-2*iThickness)*
        sqrt(2)/4),),((iLengthBm,(iDiameter-2*iThickness)*sqrt(2)/4,-(iDiameter
        -2*iThickness)*sqrt(2)/4),),((iLengthBm,-(iDiameter-2*iThickness)*sqrt
        (2)/4,(iDiameter-2*iThickness)*sqrt(2)/4),),((iLengthBm,-(iDiameter-2*
        iThickness)*sqrt(2)/4,-(iDiameter-2*iThickness)*sqrt(2)/4),))
246 l_cir_2=e1.findAt(((iDiameter/2,iDiameter*sqrt(2)/4,iDiameter*sqrt(2)/4),)
        ,((iDiameter/2,iDiameter*sqrt(2)/4,-iDiameter*sqrt(2)/4),),((iDiameter
        /2,-iDiameter*sqrt(2)/4,iDiameter*sqrt(2)/4),),((iDiameter/2,-iDiameter
        *sqrt(2)/4,-iDiameter*sqrt(2)/4),), ((iLengthBm+iLengthSleeve+
        iLengthArm,iDiameter*sqrt(2)/4,iDiameter*sqrt(2)/4),),((iLengthBm+
        iLengthSleeve+iLengthArm,iDiameter*sqrt(2)/4,-iDiameter*sqrt(2)/4),),
        ((iLengthBm+iLengthSleeve+iLengthArm,-iDiameter*sqrt(2)/4,iDiameter*
        sqrt(2)/4),),((iLengthBm+iLengthSleeve+iLengthArm,-iDiameter*sqrt(2)
        /4,-iDiameter*sqrt(2)/4),))
247 l_cir_3=e1.findAt(((iDiameter/2,(R-iThickness)*sqrt(2)/2,(R-iThickness)*
        sqrt(2)/2),),((iDiameter/2,(R-iThickness)*sqrt(2)/2,-(R-iThickness)*
        sqrt(2)/2),), ((iDiameter/2,-(R-iThickness)*sqrt(2)/2,(R-iThickness)*
        sqrt(2)/2),),((iDiameter/2,-(R-iThickness)*sqrt(2)/2,-(R-iThickness)*
        sqrt(2)/2),),((iLengthBm+iLengthSleeve+iLengthArm,(R-iThickness)*sqrt
        (2)/2,(R-iThickness)*sqrt(2)/2),),((iLengthBm+iLengthSleeve+iLengthArm
        ,(R-iThickness)*sqrt(2)/2,-(R-iThickness)*sqrt(2)/2),),((iLengthBm+
        iLengthSleeve+iLengthArm,-(R-iThickness)*sqrt(2)/2,(R-iThickness)*sqrt
        (2)/2),),((iLengthBm+iLengthSleeve+iLengthArm,-(R-iThickness)*sqrt(2)
        /2,-(R-iThickness)*sqrt(2)/2),))
248 l_vt=e1.findAt(((0,0,(iDiameter-2*iThickness)/2+1),),((0,0,-(iDiameter-2*
        iThickness)/2-1),),((0,-(iDiameter-2*iThickness)/2-1,0),),((iLength
        /2,0,(iDiameter-2*iThickness)/2+1),),((iLength/2,0,-(iDiameter-2*
        iThickness)/2-1),),((iLength/2,-(iDiameter-2*iThickness)/2-1,0),),((
        iLength/2,(iDiameter-2*iThickness)/2+1,0),),((iDiameter/2,0,(iDiameter
        -2*iThickness)/2+1),),((iDiameter/2,0,-(iDiameter-2*iThickness)/2-1),)
        ,((iDiameter/2,-(iDiameter-2*iThickness)/2-1,0),),((iDiameter/2,(
        iDiameter-2*iThickness)/2+1,0),))
249 l_vt_1=e1.findAt(((iLengthBm-100,0,(iDiameter-2*iThickness)/2+1),),((
```

```
    iLengthBm-100,0,-(iDiameter-2*iThickness)/2-1),),((iLengthBm-100,-(
    iDiameter-2*iThickness)/2-1,0),),((iLengthBm-100,(iDiameter-2*
    iThickness)/2+1,0),),((iLengthBm+iLengthSleeve,0,(iDiameter-2*
    iThickness)/2+1),),((iLengthBm+iLengthSleeve,0,-(iDiameter-2*iThickness
    )/2-1),),((iLengthBm+iLengthSleeve,-(iDiameter-2*iThickness)/2-1,0),)
    ,((iLengthBm+iLengthSleeve,(iDiameter-2*iThickness)/2+1,0),))
250 l_cirL=e1.findAt(((0,iDiameter*sqrt(2)/4,iDiameter*sqrt(2)/4),),((0,
    iDiameter*sqrt(2)/4,-iDiameter*sqrt(2)/4),),((0,-iDiameter*sqrt(2)/4,
    iDiameter*sqrt(2)/4),),((0,-iDiameter*sqrt(2)/4,-iDiameter*sqrt(2)/4),)
    ,((-iLength/2,iDiameter*sqrt(2)/4,iDiameter*sqrt(2)/4),),((-iLength/2,
    iDiameter*sqrt(2)/4,-iDiameter*sqrt(2)/4),),((-iLength/2,-iDiameter*
    sqrt(2)/4,iDiameter*sqrt(2)/4),),((-iLength/2,-iDiameter*sqrt(2)/4,-
    iDiameter*sqrt(2)/4),),((-iLengthBm,iDiameter*sqrt(2)/4,iDiameter*sqrt
    (2)/4),),((-iLengthBm,iDiameter*sqrt(2)/4,-iDiameter*sqrt(2)/4),),((-
    iLengthBm,-iDiameter*sqrt(2)/4,iDiameter*sqrt(2)/4),),((-iLengthBm,-
    iDiameter*sqrt(2)/4,-iDiameter*sqrt(2)/4),))
251 l_cirL_1=e1.findAt(((0,(iDiameter-2*iThickness)*sqrt(2)/4,(iDiameter-2*
    iThickness)*sqrt(2)/4),),((0,(iDiameter-2*iThickness)*sqrt(2)/4,-(
    iDiameter-2*iThickness)*sqrt(2)/4),),((0,-(iDiameter-2*iThickness)*sqrt
    (2)/4,(iDiameter-2*iThickness)*sqrt(2)/4),),((0,-(iDiameter-2*
    iThickness)*sqrt(2)/4,-(iDiameter-2*iThickness)*sqrt(2)/4),),((-iLength
    /2,(iDiameter-2*iThickness)*sqrt(2)/4,(iDiameter-2*iThickness)*sqrt(2)
    /4),),((-iLength/2,(iDiameter-2*iThickness)*sqrt(2)/4,-(iDiameter-2*
    iThickness)*sqrt(2)/4),),((-iLength/2,-(iDiameter-2*iThickness)*sqrt(2)
    /4,(iDiameter-2*iThickness)*sqrt(2)/4),),((-iLength/2,-(iDiameter-2*
    iThickness)*sqrt(2)/4,-(iDiameter-2*iThickness)*sqrt(2)/4),),((-
    iLengthBm,(iDiameter-2*iThickness)*sqrt(2)/4,(iDiameter-2*iThickness)*
    sqrt(2)/4),),((-iLengthBm,(iDiameter-2*iThickness)*sqrt(2)/4,-(
    iDiameter-2*iThickness)*sqrt(2)/4),),((-iLengthBm,-(iDiameter-2*
    iThickness)*sqrt(2)/4,(iDiameter-2*iThickness)*sqrt(2)/4),),((-
    iLengthBm,-(iDiameter-2*iThickness)*sqrt(2)/4,-(iDiameter-2*iThickness)
    *sqrt(2)/4),))
252 l_cirL_2=e1.findAt(((-iDiameter/2,iDiameter*sqrt(2)/4,iDiameter*sqrt(2)/4)
    ,),((-iDiameter/2,iDiameter*sqrt(2)/4,-iDiameter*sqrt(2)/4),),((-
    iDiameter/2,-iDiameter*sqrt(2)/4,iDiameter*sqrt(2)/4),),((-iDiameter
    /2,-iDiameter*sqrt(2)/4,-iDiameter*sqrt(2)/4),), ((-iLengthBm-
    iLengthSleeve-iLengthArm,iDiameter*sqrt(2)/4,iDiameter*sqrt(2)/4),),((-
    iLengthBm-iLengthSleeve-iLengthArm,iDiameter*sqrt(2)/4,-iDiameter*sqrt
    (2)/4),),((-iLengthBm-iLengthSleeve-iLengthArm,-iDiameter*sqrt(2)/4,
    iDiameter*sqrt(2)/4),),((-iLengthBm-iLengthSleeve-iLengthArm,-iDiameter
    *sqrt(2)/4,-iDiameter*sqrt(2)/4),))
253 l_cirL_3=e1.findAt(((-iDiameter/2,(R-iThickness)*sqrt(2)/2,(R-iThickness)*
    sqrt(2)/2),),((-iDiameter/2,(R-iThickness)*sqrt(2)/2,-(R-iThickness)*
    sqrt(2)/2),),((-iDiameter/2,-(R-iThickness)*sqrt(2)/2,(R-iThickness)*
    sqrt(2)/2),),((-iDiameter/2,-(R-iThickness)*sqrt(2)/2,-(R-iThickness)*
    sqrt(2)/2),),((-iLengthBm-iLengthSleeve-iLengthArm,(R-iThickness)*sqrt
    (2)/2,(R-iThickness)*sqrt(2)/2),),((-iLengthBm-iLengthSleeve-iLengthArm
    ,(R-iThickness)*sqrt(2)/2,-(R-iThickness)*sqrt(2)/2),), ((-iLengthBm-
    iLengthSleeve-iLengthArm,-(R-iThickness)*sqrt(2)/2,(R-iThickness)*sqrt
    (2)/2),), ((-iLengthBm-iLengthSleeve-iLengthArm,-(R-iThickness)*sqrt(2)
    /2,-(R-iThickness)*sqrt(2)/2),))
254 l_vtL=e1.findAt(((0,0,(iDiameter-2*iThickness)/2+1),),((0,0,-(iDiameter-2*
    iThickness)/2-1),),((0,-(iDiameter-2*iThickness)/2-1,0),),((-iLength
    /2,0,(iDiameter-2*iThickness)/2+1),),((-iLength/2,0,-(iDiameter-2*
    iThickness)/2-1),),((-iLength/2,-(iDiameter-2*iThickness)/2-1,0),),((-
    iLength/2,(iDiameter-2*iThickness)/2+1,0),),((-iDiameter/2,0,(iDiameter
    -2*iThickness)/2+1),),((-iDiameter/2,0,-(iDiameter-2*iThickness)/2-1),)
    ,((-iDiameter/2,-(iDiameter-2*iThickness)/2-1,0),), ((-iDiameter/2,(
```

```
    iDiameter-2*iThickness)/2+1,0),))
l_vtL_1=e1.findAt(((-iLengthBm+100,0,(iDiameter-2*iThickness)/2+1),),((-
    iLengthBm+100,0,-(iDiameter-2*iThickness)/2-1),),((-iLengthBm+100,-(
    iDiameter-2*iThickness)/2-1,0),),((-iLengthBm+100,(iDiameter-2*
    iThickness)/2+1,0),), ((-iLengthBm-iLengthSleeve,0,(iDiameter-2*
    iThickness)/2+1),),((-iLengthBm-iLengthSleeve,0,-(iDiameter-2*
    iThickness)/2-1),),((-iLengthBm-iLengthSleeve,-(iDiameter-2*iThickness)
    /2-1,0),),((-iLengthBm-iLengthSleeve,(iDiameter-2*iThickness)/2+1,0),),))
a.seedEdgeByNumber(edges=l_vt+l_vt_1+l_vtL+l_vtL_1,number=nVt,constraint=
    FINER)
a.seedEdgeBySize(edges=l_cir+l_cir_1+l_cir_2+l_cir_3+l_cirL+l_cirL_1+
    l_cirL_2+l_cirL_3,size=sCir,deviationFactor=0.1,constraint=FINER)
e_notchFace_L=e1.getByBoundingBox(zMin=1,zMax=iMlength,xMin=-1,xMax=iMwidth
    ,yMin=R-iMdepth-chord_length-1,yMax=100)
a.Set(name='e_notchFace_L',edges=e_notchFace_L)
e_notchFace_R=e1.getByBoundingBox(zMin=-iMlength,zMax=-1,xMin=-1,xMax=
    iMwidth,yMin=R-iMdepth-chord_length-1,yMax=100)
a.Set(name='e_notchFace_R',edges=e_notchFace_R)
a.Set(edges=l_cir+l_cir_1+l_cir_2+l_cir_3,name='l_cir')
a.Set(edges=l_vt+l_vt_1,name='l_vt')
notchedCell_L1= c.findAt(((0,-R*sin(pi/3),R*cos(pi/3)),))
notchedCell_R1= c.findAt(((0,-R*sin(pi/3),-R*cos(pi/3)),))
a.Set(name='notchedCell_L1',cells=notchedCell_L1)
a.Set(name='notchedCell_R1',cells=notchedCell_R1)
partInstances =(a.instances['cylinderWithMetalloss1-all-1'], )
a.generateMesh(regions=partInstances)


#  Define the material property
material_library(myModel)
m.HomogeneousSolidSection(name='Section-pipe',material=materials,thickness=
    None)
myCell=p8.cells[:]
region=(None,None,myCell,None)
p8.SectionAssignment(region=region,sectionName='Section-pipe',offset=0.0,
    offsetType=MIDDLE_SURFACE)


# Define the analysis step
m.StaticStep(name='step-bm',previous='Initial',nlgeom=ON,initialInc=0.001,
    minInc=1e-09,maxInc=0.001,maxNumInc=1000)
m.FieldOutputRequest(name='F1',createStepName='step-bm',variables=('RF','SF
    ','E','RM','NFORC'))
node=a.instances['cylinderWithMetalloss1-all-1'].nodes
nodeleft_pipeEnd30=node.getByBoundingCylinder((iLengthBm-30,0,iDiameter
    /2+1),(iLengthBm-30,0,iDiameter/2-iThickness-1),2)
noderight_pipeEnd30=node.getByBoundingCylinder((iLengthBm-30,0,-iDiameter
    /2-1),(iLengthBm-30,0,-iDiameter/2+iThickness+1),2)
a.Set(name='nodeleft_pipeEnd30',nodes=nodeleft_pipeEnd30)
a.Set(name='noderight_pipeEnd30',nodes=noderight_pipeEnd30)
nodeleft_pipeCenter=node.getByBoundingCylinder((0,0,iDiameter/2+1),(0,0,
    iDiameter/2-iThickness-1),0.5)
noderight_pipeCenter=node.getByBoundingCylinder((0,0,-iDiameter/2-1),(0,0,-
    iDiameter/2+1+iThickness),0.5)
a.Set(name='nodeleft_pipeCenter',nodes=nodeleft_pipeCenter)
a.Set(name='noderight_pipeCenter',nodes=noderight_pipeCenter)
nodeTop_pipe0D=node.getByBoundingCylinder((0,iDiameter/2+1,0),(0,iDiameter
    /2-1-iThickness,0),0.5)
```

```
nodeBottom_pipe0D=node.getByBoundingCylinder((0,-iDiameter/2-1,0),(0,-iDiameter/2+1+iThickness,0),0.5)
a.Set(name='nodeTop_pipe0D',nodes=nodeTop_pipe0D)
a.Set(name='nodeBottom_pipe0D',nodes=nodeBottom_pipe0D)
nodeTop_pipe05D=node.getByBoundingCylinder((iDiameter/2,iDiameter/2+1,0),(iDiameter/2,iDiameter/2-1-iThickness,0),0.5)
nodeBottom_pipe05D=node.getByBoundingCylinder((iDiameter/2,-iDiameter/2+1,0),(iDiameter/2,-iDiameter/2+1+iThickness,0),0.5)
a.Set(name='nodeTop_pipe05D',nodes=nodeTop_pipe05D)
a.Set(name='nodeBottom_pipe05D',nodes=nodeBottom_pipe05D)
nodeTop_pipe1D=node.getByBoundingCylinder((iDiameter,iDiameter/2+1,0),(iDiameter,iDiameter/2-1-iThickness,0),3)
nodeBottom_pipe1D=node.getByBoundingCylinder((iDiameter,-iDiameter/2+1,0),(iDiameter,-iDiameter/2+1+iThickness,0),3)
a.Set(name='nodeTop_pipe1D',nodes=nodeTop_pipe1D)
a.Set(name='nodeBottom_pipe1D',nodes=nodeBottom_pipe1D)
nodeTop_pipeEnd_50=node.getByBoundingCylinder((iLengthBm-50,iDiameter/2+1,0),(iLengthBm-50,iDiameter/2-1-iThickness,0),2)
nodeBottom_pipeEnd_50=node.getByBoundingCylinder((iLengthBm-50,-iDiameter/2+1,0),(iLengthBm-50,-iDiameter/2+1+iThickness,0),2)
a.Set(name='nodeTop_pipeEnd_50',nodes=nodeTop_pipeEnd_50)
a.Set(name='nodeBottom_pipeEnd_50',nodes=nodeBottom_pipeEnd_50)
node_0D=node.getByBoundingCylinder((0,-iDiameter/2-0.5,0),(0,-iDiameter/2+0.5,0),0.5)
node_1D=node.getByBoundingCylinder((iDiameter,-iDiameter/2-1,0),(iDiameter,-iDiameter/2+1,0),sCir)
node_End50=node.getByBoundingCylinder((iLengthBm-50,-iDiameter/2-1,0),(iLengthBm-50,-iDiameter/2+1,0),2)
a.Set(name='node_0D',nodes=node_0D)
a.Set(name='node_1D',nodes=node_1D)
a.Set(name='node_End50',nodes=node_End50)
elem=a.instances['cylinderWithMetalloss1-all-1'].elements
elem_0Dall=elem.getByBoundingBox(xMin=-0.5,xMax=3)
a.Set(name='elem_0Dall',elements=elem_0Dall)
node_0Dall=node.getByBoundingBox(xMin=-0.5,xMax=0.5)
a.Set(name='node_0Dall',nodes=node_0Dall)
elem=a.instances['cylinderWithMetalloss1-all-1'].elements
elem_End50all=elem.getByBoundingBox(xMin=-50+iLengthBm-sCir,xMax=iLengthBm-50+1.2*sCir)
a.Set(name='elem_End50all',elements=elem_End50all)
node_End50all=node.getByBoundingBox(xMin=iLengthBm-50-0.8*sCir,xMax=iLengthBm-50)
a.Set(name='node_End50all',nodes=node_End50all)
elem=a.instances['cylinderWithMetalloss1-all-1'].elements
elem_05Dall=elem.getByBoundingBox(xMin=iDiameter/2.0-sNotchLon,xMax=iDiameter/2.0+1.5*sNotchLon)
a.Set(name='elem_05Dall',elements=elem_05Dall)
node_05Dall=node.getByBoundingBox(xMin=iDiameter/2.0-sNotchHoop,xMax=iDiameter/2.0+sNotchHoop)
a.Set(name='node_05Dall',nodes=node_05Dall)
region=a.sets['nodeleft_pipeEnd30']
m.HistoryOutputRequest(name='nodeleft_pipeEnd30',createStepName='step-bm',variables=('U3',),region=region)
region=a.sets['noderight_pipeEnd30']
m.HistoryOutputRequest(name='noderight_pipeEnd30',createStepName='step-bm',variables=('U3',),region=region)
region=a.sets['nodeleft_pipeCenter']
m.HistoryOutputRequest(name='nodeleft_pipeCenter',createStepName='step-bm',
```

```
    variables=('U3',),region=region)
region=a.sets['noderight_pipeCenter']
m.HistoryOutputRequest(name='noderight_pipeCenter',createStepName='step-bm'
    ,variables=('U3',),region=region)
region=a.sets['node_0D']
m.HistoryOutputRequest(name='node_0D',createStepName='step-bm',variables=('
    U2',),region=region)
region=a.sets['node_1D']
m.HistoryOutputRequest(name='node_1D',createStepName='step-bm',variables=('
    U2',),region=region)
region=a.sets['node_End50']
m.HistoryOutputRequest(name='node_End50',createStepName='step-bm',variables
    =('U2',),region=region)


# Define the interaction relationship: coupling
f1=a.instances['cylinderWithMetalloss1-all-1'].faces
refPoint1=a.ReferencePoint(point=a.instances['cylinderWithMetalloss1-all-1'
    ].InterestingPoint(edge=e1.findAt(coordinates=(-iLengthBm,-iDiameter*
    sqrt(2)/4,-iDiameter*sqrt(2)/4)),rule=CENTER))
refPoint2=a.ReferencePoint(point=a.instances['cylinderWithMetalloss1-all-1'
    ].InterestingPoint(edge=e1.findAt(coordinates=(iLengthBm,-iDiameter*
    sqrt(2)/4,-iDiameter*sqrt(2)/4)),rule=CENTER))
v1=a.referencePoints
d10=a.DatumCsysByThreePoints(name='cylCoord',coordSysType=CYLINDRICAL,
    origin=(0,iDiameter/2,0),point1=(0,-iDiameter/2,0),point2=(0,0,
    iDiameter/2))
datum=a.datums[d10.id]
faceBottom=f1.getByBoundingBox(xMin=-iLengthBm-1,xMax=-iLengthBm)
a.Set(name='faceBottom',faces=faceBottom)
region=a.Surface(side1Faces=faceBottom, name='faceBottom')
region1=a.Set(name='refPointBottom',referencePoints=(v1[refPoint1.id],))
m.Coupling(name='C-Bottom',controlPoint=region1,surface=region,couplingType
    =KINEMATIC,
            localCsys=datum,influenceRadius=WHOLE_SURFACE, u1=ON,u2=ON,u3=
    ON,ur1=ON, ur2=ON, ur3=ON)
faceEnd=f1.getByBoundingBox(xMin=iLengthBm,xMax=iLengthBm+1)
a.Set(name='faceEnd',faces=faceEnd)
region=a.Surface(side1Faces=faceEnd, name='faceEnd')
region1=a.Set(name='refPointEnd',referencePoints=(v1[refPoint2.id],))
m.Coupling(name='C-end',controlPoint=region1,surface=region,couplingType=
    KINEMATIC,localCsys=datum,influenceRadius=WHOLE_SURFACE, u1=ON,u2=ON,u3
    =ON,ur1=ON, ur2=ON, ur3=ON)


# Define the loading and BC conditions
vp.assemblyDisplay.setValues(loads=ON,bcs=ON)
region = a.sets['refPointEnd']
m.DisplacementBC(name='Loading',createStepName='step-bm',region=region,u1=
    SET,u2=SET,u3=SET,ur1=SET,ur2=SET,ur3=2.0,localCsys=None)
region = a.sets['refPointBottom']
m.DisplacementBC(name='support',createStepName='step-bm',region=region,u1=
    UNSET,u2=SET,u3=SET, ur1=SET,ur2=SET,ur3=-2.0,localCsys=None)


# Define a job for calculation
print 'The residual ultimate strength analysis for notched pipe starts'
jobName='NotchedSpecimen-lm%.2s'%(SN)
```

```
376 mdb.Job(name=jobName, model=modelName, description='this is stability
    analysis based on displacement control method of notched specimen',
    numCpus=8, numDomains=8)
```

Glossary

List of symbols and notations

Below follows a list of the most frequently used symbols and notations in this thesis.

Greek

α_m	material constant for material curve fitting, $\alpha_m = 0.333$ [-]
α_s	material constant for material curve fitting, $\alpha_s = \frac{\sigma_u(1-\beta_m)}{e_u^2(1-\alpha_m)^2}$ [-]
β_m	material constant for material curve fitting, $\beta_m = 0.6$ [-]
γ_{xy}	shear strain [-]
δ	ovalisation [-]
δ_0	initial ovalisation [-]
δ_i	amplitude of wrinkling initial imperfection [mm]
δ_{max}	maximum ovalisation [-]
ε_c	critical strain under pure bending [-]
$\varepsilon_{true}, \varepsilon_{true1}$	true strain [-]
ε_0	referential strain [-]
ε_{11}	strain component in pipe axial direction [-]
ε_{22}	strain component in pipe hoop direction [-]
ε_{eng}	engineering strain [-]
ε_x	strain component in x direction [-]
ε_y	strain component in y direction [-]

η_c	correction factor based on dent locations and safety class etc [-]
θ	angle from bending plane to the plastic neutral axis [rad]
θ_d	rotational angle of dent [deg]
$\theta_{(i)}$	damage rotational angle, 'i' represents the type of damage [deg]
θ_m	rotational angle of metal loss [deg]
θ_{arc}	tangential angle of a given arc [rad]
κ	pipe global curvature [1/m]
κ_0	reference curvature [1/m]
κ_1, κ_2	pipe local curvature [1/m]
κ_i	critical curvature of intact pipes [1/m]
κ_{cr}	critical curvature of damaged pipes [1/m]
λ_d	dimensionless length of dent [-]
λ_l	normalised damage length; damage type could be a dent, a notch or a crack [-]
λ_w	normalised damage width; damage type could be a dent, a notch or a crack [-]
λ_{cl}	critical half-wave length [mm]
ν	Poisson's ratio [-]
σ_{11}	stress component in pipe axial direction [MPa]
σ_{22}	stress component in pipe hoop direction [MPa]
$\overline{\sigma}$	flow stress of material [MPa]
σ_l	membrane stress in pipe longitudinal direction [MPa]
σ_h	ultimate stress in hoop direction [MPa]
σ_u	ultimate tensile stress [MPa]
σ_y	yield stress [MPa]
σ_θ	membrane stress in pipe hoop direction [MPa]
σ_{cb}, σ_{cr}	bursting stress of pipe [MPa]

σ_{hy}	yield stress in pipe hoop direction [MPa]
σ_{cbe}	elastic buckling stress under pure bending [MPa]
σ_{comp}	compression stress [MPa]
σ_{ten}	tensile stress [MPa]
σ_{eng}	engineering stress [MPa]
σ_{long}	ultimate stress in longitudinal direction [MPa]
$\sigma_{true}, \sigma_{true1}$	true stress [MPa]
ϕ	half angle of metal loss [rad]
ω	shell deflection [mm]
ω_0	pre-buckling deformation along radial direction [mm]
ω_1	buckling deformation along radial direction [mm]
ω_d	dent depth variation [mm]

Latin

a	half crack length [mm]
$a1, a2$	real bending arm [mm]
a_i	correction parameters for damage effect, 'i' represents the types of damage, $i = 1;2;3;4;5$ [-]
a_{ii}	correction parameters, $i = 1;2;3;4$ [-]
A_e	area of pipe cross-section under external pressure [mm^2]
A_i	area of pipe cross-section under internal pressure [mm^2]
A_m	pipe buckling parameter [-]
b_i	correction parameters for damage effect, 'i' represents the types of damage, $i = 1;2;3;4;5$ [-]
B	thickness of material specimen [mm]
c	crack depth [mm]

c_i	correction parameters for damage effect, 'i' represents the types of damage, $i = 1;2;3;4;5$ [-]
c_{ii}	correction parameters proposed from tests, $i = 1;2$ [-]
C_v	lower boundary Charpy V-notch impact energy at service temperature [J]
d_6	correction parameter for the combined damage effect [-]
d_c	crack depth [mm]
d_d	dent depth [mm]
d_m	metal loss depth [mm]
d_r	relative vertical displacement between measured points [mm]
$d_{(i)}$	damage depth, 'i' represents different types of damage
D	pipe outer diameter [mm]
D_0	original pipe diameter before slitting [mm]
D_1	final pipe diameter after slitting [mm]
D_{ave}	pipe average outer diameter [mm]
D_{max}	pipe maximum outer diameter [mm]
D_{min}	pipe minimum outer diameter [mm]
e_6	correction parameter for combined damage effect [-]
e_u	the maximum elongation [-]
E	Young's modulus [MPa]
E'	plane strain Young's modulus [MPa]
f_6	correction parameter for damage effect [-]
F	true axial force [N]
G	energy release rate [J]
G^*	critical energy release rate [MJ]
h	remaining pipe wall thickness due to metal loss [mm]
J	J integral [J]

k_1, k_2	constants related to notch depth [-]
K	stress intensity factor [$MPam^{1/2}$]
K_1	material constant [-]
K_I	stress intensity factor in Mode I [$MPam^{1/2}$]
K_{IC}	critical stress intensity factor in Mode I [$MPam^{1/2}$]
l_c	crack length [mm]
l_d	dent length [mm]
l_m	notch length [mm]
l'_d	dent length projected in pipe hoop direction [mm]
$l_{(i)}$	damage length, 'i' represents the type of damage
l_{curv}	chord length [mm]
L	full length of pipe [mm]
L_0	pipe length under pure bending [mm]
$L1, L_{AB}$	half length of pipe under pure bending [mm]
$L2, L4$	length of loading/support strip [mm]
$L3$	original bending arm [mm]
$L5$	side length of pipe [mm]
L_{CD}	arc length of pipe cross-section [mm]
m	the number of half-wave along cylindrical shell axis when buckling [-]
M, M_1, M_2	bending moment [kNm]
M_c	critical bending moment of intact pipe [kNm]
M_{cr}	residual bending moment [kNm]
M_f	bulging parameter [-]
M_i	ultimate bending moment of intact pipe [kNm]
M_y	plastic bending moment [kNm]
M_{yh}	ultimate bending moment accounting for material hardening [kNm]

M_{ym}	residual strength of pipe with metal loss [kNm]
M_{ref}	reference value of ultimate bending moment from analytical methods [kNm]
M_{test}	ultimate bending moment from test [kNm]
$n, n1$	material constant [-]
N_x	unit internal force in x direction [N/m]
N_y	unit internal force in y direction [N/m]
N_{xy}	unit shear internal force in xy plane [N/m]
N_{x0}, N_{y0}, N_{xy0}	unit force at pre-buckling in x, y, and z direction respectively [N/m]
N_{x1}, N_{y1}, N_{xy1}	unit force at buckling in x, y, and z direction respectively [N/m]
P_1, P_2	vertical force [kN]
P_{11}, P_{22}	force component [kN]
p_i	pipe internal pressure [MPa]
p_e	pipe external pressure [MPa]
P_b	critical bursting pressure of pipes [MPa]
P_{ce}	external buckling pressure of pipes [MPa]
P_{ee}	elastic external buckling pressure of pipes [MPa]
P_{ye}	external pressure at material yielding [MPa]
q	external force exerted on shell element [N/m]
Q	correction factor of metal loss [-]
r	distance between crack tip and the points in crack tip vicinity [mm]
R	pipe outer radius [mm]
R_a	pipe average radius [mm]
R_m	reduced pipe average pipe due to notch [mm]
R^2	coefficient of determination [-]
S_m	compression area with metal loss in pipe cross-section [mm^2]
S_{ten}	tensile area of pipe cross-section [mm^2]

S_{comp1}	compression area without metal loss in pipe cross-section [mm^2]
S_{loss}	metal loss area in pipe cross-section [mm^2]
S_{eff}	effective axial force [N]
$U_{lateral}$	the maximum lateral displacement of pipe [mm]
t	pipe thickness [mm]
t_m	reduced pipe thickness due to notch [mm]
T_c	ultimate tension force subjected to uniaxial tension [N]
T_{ya}	plastic axial force [N]
u, v	deformation along x and y direction respectively [m]
u_0, v_0	pre-buckling deformation along x and y direction respectively [m]
u_1, v_1	buckling deformation along x and y direction respectively [m]
w_c	crack width [mm]
w_d	dent width [mm]
w_m	notch width [mm]
$w_{(i)}$	damage width, 'i' represents the type of damage
X	model uncertainty parameters [-]
X_1	parameter in analytical formula for bending moment [-]
X_{true}	true values from test or simulation [-]
$X_{predict}$	prediction values [-]
y_{comp}	force arm for the compression segment in pipe cross-section [mm]
y_{tems}	force arm for the tensile segment in pipe cross-section [mm]
Y_m	force arm of the segment S_m [mm]
Y_{ten}	force arm of the segment S_{ten} [mm]
Y_{comp1}	force arm of the segment S_{comp1} [mm]

List of abbreviations

The following abbreviations are used in this thesis:

API	American Petroleum Institute
ASME	American Society of Mechanical Engineers
ANOVA	Analysis Of Variance
BRSL	Block Removal Splitting and Layering Method
CDF	Crack Driving Force
COV	Coefficient Of Variation
CTOD	Crack Tip Opening Displacement
DIC	Digital Image Correlation
DNV	Det Norske Veritas
EPFM	Elastic-Plastic Fracture Mechanics
FAD	Failure Assessment Diagram
FEA	Finite Element Analysis
FEM	Finite Element Method
HAZ	Heat Affected Zone
LEFM	Linear Elastic Fracture Mechanics
LVDT	Linear Variable Differential Transformer
PDAM	Pipeline Defect Assessment Manual
PEEQ	Equivalent Plastic Strain
PHMSA	Pipeline and Hazardous Materials Safety Administration
UOE	U-ing, O-ing, and Expanding process
XFEM	Extended Finite Element Method

List of standards and design guidelines

The following standards and design guidelines are used in this thesis:

ABS (2001)	Subsea pipeline systems and risers
API 5L	Specification for line pipe
API 579-1/ASME FFS-1	Fitness for service
ASME B31G	Manual for determining the remaining strength of corroded pipelines
BS 7910	Guide on methods for assessing the acceptability of flaws in metallic structures
BS 8010-3	Code of practice for pipelines: Pipelines subsea: Design, construction and installation
DNV-OS-F101	Submarine pipeline systems
DNV-RP-F101	Corroded pipelines
DNV-RP-F111	Interference between trawl gear and pipelines
DNV-RP-C208	Determination of structural capacity by non-linear FE analysis methods
DNV-RP-F108	Fracture control for pipeline installation methods introducing cyclic plastic strain

EUROCODE 3	Design of steel structures:Part 1-1: General rules for buildings
GB/T 1591	High strength low alloy structural steels (in Chinese)
GB/T 228.1	Metallic materials- Tensile testing-Part 1: Method of test at room temperature (in Chinese)

Samenvatting

Onderwerp van dit proefschrift is de invloed van structurele beschadigingen aan naadloze metalen pijpen op de sterkte van de pijp. Onder structurele beschadiging wordt hier de schade verstaan die ontstaat door een externe mechanische oorzaak en die aanzienlijke invloed heeft op de sterkte en de stabiliteit van de pijp. Er is niet alleen schade aan het oppervlak van de pijp; belangrijker is dat pijp mogelijk niet meer voldoet aan de functionele eisen.

Doel van dit onderzoek is de ontwikkeling van een effectief model voor het voorspellen van de reststerkte van een beschadigde pijp bij buiging. Om de reststerkte goed te kunnen voorspellen moeten de types structurele schade worden gecategoriseerd en vereenvoudigd. Bij de verdere kwantificering van de effecten worden drie typerende soorten schade onderscheiden: een deuk, materiaalverlies door een kerf, en een combinatie van een deuk en een kerf. De breuk die kan worden veroorzaakt door een beschadiging aan de spanningszijde van de pijp, wanneer de beschadigde pijp wordt gebogen, wordt kwalitatief onderzocht. De gevolgen van pijpbreuk kunnen ernstig zijn.

Aan het begin van dit onderzoek wordt een specifieke definitie van de reststerkte gebruikt, gebaseerd op de theorie van de sterkte van cilindrische oppervlakken. Afhankelijk van de verhouding tussen de diameter D van de pijp en de dikte t van de wand wordt de reststerkte bepaald door de stabiliteit van de constructie, of door de sterkte in relatie tot de plasticiteit van het materiaal. Eerst wordt aan de hand van de literatuur ingegaan op de kenmerken van alle types beschadigingen aan pijpen: de oorzaken, de bestaande methoden voor het schatten van de sterkte, de mogelijke gevolgen en de methoden voor proefopzet. Voor het verdere onderzoek van de effecten van beschadigingen op de sterkte van metalen pijpen is in Hoofdstuk 2 in een literatuuronderzoek nagegaan welke de factoren zijn die invloed hebben en welke methoden er zijn voor het bepalen van de sterkte van pijpen onder verschillende belastingen. Hiermee kan vervolgens het experiment worden opgezet en uitgevoerd voor de bepaling van de reststerkte van beschadigde pijpen.

In Hoofdstuk 3 hebben we een fundamenteel experimenteel onderzoek gedaan aan beschadigde pijpen. Pijpen met geschikt gekozen beschadigingen zijn onderworpen aan een vierpunts buigproef. Op grond van de waargenomen verschijnselen hebben we de effecten van beschadigingen aan metalen pijpen onder buiging in beeld gebracht. De verkregen testdata geven ook een goede basis voor het volgende kwantitatieve onderzoek.

Met behulp van de Finite Element Method is de juistheid nagegaan van de waargenomen constructieve eigenschappen van de testitems. Er zijn numerieke modellen voor de constructieve schade ontwikkeld. Deze modellen zijn gevalideerd met behulp van de resultaten van de tests. In de modellen zijn alle types beschadigingen opgenomen, in termen van

de bijbehorende kritische parameters.

In Hoofdstuk 4 is de invloed van alle parameters uit Hoofdstuk 2 verklaard met behulp van een parametrisch onderzoek. We weten daardoor hoe deze parameters in verder numeriek onderzoek in rekening moeten worden gebracht. Bijvoorbeeld: hoewel er bij constructieve analyse meestal eisen worden gesteld aan initile fouten, is de invloed daarvan op een beschadigde pijp klein en verwaarloosbaar ten opzichte van het effect van de beschadiging bij buiging. De invloed van een deuk is onderzocht. De deukparameters zoals deukhoek (θ_d), diepte (d_d), lengte (l_d) en breedte (w_d) zijn onderzocht met behulp van simulaties. Met behulp van statistische methodes zijn empirische formules, functies van de deukparameters, opgesteld, gebaseerd op de resultaten van een aantal numerieke simulaties. Daarmee is antwoord gegeven op de onderzoekvraag: hoe benvloedt deukschade de sterkte van metalen pijpen in termen van buigmoment en kritische kromming.

Vervolgens is in Hoofdstuk 5 van dit proefschrift onderzocht wat het verband is tussen de schade ten gevolge van een kerf en de sterkte van een pijp. Eerst is het kerfmodel vereenvoudigd ten behoeve van numerieke simulaties. Er zijn analytische oplossingen voor pijpen met kerfschade afgeleid, aannemend dat de kerf oneindig breed is. Met de gevalideerde modellen zijn simulaties uitgevoerd van de effecten van de parameters van het materiaalverlies (diepte (d_m), lengte (l_m) en breedte (w_m)). Met de resultaten van de simulaties zijn formules opgesteld voor de sterkte en de kritische kromming als functie van de kerfparameters. Daarmee is antwoord gegeven op de onderzoekvraag: hoe benvloedt het materiaalverlies de reststerkte van metalen pijpen bij buiging.

In de werkelijkheid zal een beschadiging meestal bestaan uit een deuk n een kerf. Het is niet duidelijk hoe deuk en kerf elkaar benvloeden. Daarom is in Hoofdstuk 6 onderzoek gedaan naar de effecten van een gecombineerde beschadiging. Daaruit blijkt dat bij een combinatie van beschadigingen de deuk de belangrijkste invloed heeft op de sterkte van de pijp. Een combinatie van beschadigingen heeft meer invloed op de sterkte dan andere types schade (afgezien van breuk). Er zijn ook case studies gedaan bij beschadigde pijpen waarin mogelijk breuk optreedt. Vergelijking van de resultaten laat zien dat bij een combinatie van beschadigingen eerder breuk optreedt. Door een beschadiging ontstaat in een pijp extra spanning. Omdat we niet genoeg testgegevens hebben om de spanningsverdeling te bepalen, hebben we slechts een basisonderzoek gedaan naar de invloed van deze spanning op de sterkte van de pijp; daarbij is een hypothetische spanningsverdeling gebruikt. Er is een verband vastgesteld. Aan het eind van dit hoofdstuk worden modellen gepresenteerd voor het voorspellen van de sterkte van een pijp met een combinatie-beschadiging bij buiging en de in de Hoofdstukken 4 en 5 gepresenteerde formules voor enkelvoudige beschadigingen. Deze formules zijn toepasbaar gemaakt voor D/t tot 30. Er zijn meer experimenten nodig om de geldigheid van deze uitbreiding van het toepassingsdomein te bevestigen.

De belangrijkste bijdrage van dit onderzoek is de kwantificering van de residuele sterkte van beschadigde pijpen onder buiging. Het onderzoek dat in dit proefschrift wordt gepresenteerd geeft een fundamenteel inzicht in de constructieve gevolgen van een beschadiging en methodes om de kwaliteit van beschadigde pijpen te schatten. Met behulp van de in dit proefschrift gepresenteerde modellen kan een effectieve schatting worden gemaakt van de residuele sterkte van een pijp na een beschadiging. Het is daardoor voor constructeurs makkelijker om te bepalen hoe om te gaan met een beschadigde pijp.

Summary

This thesis deals with the structural damage and its corresponding effect on the residual ultimate strength of seamless metallic pipes. The structural damage is here characterized as the type of damage produced by external mechanical interference, considerably undermining the strength and/or stability of the pipes. Not only the aesthetic appearances of the pipes are affected by the occurrence of damage, but most importantly the pipes' functional demands are jeopardized.

This research project aims to develop an effective prediction model to predict the residual ultimate strength of damaged metallic pipes subjected to a bending moment. To be able to effectively predict the residual strength, the types of structural damage need to be first categorized and simplified. Three typical types of damage are deployed for the further quantification of the effects, including a dent, metal loss in terms of a notch, and a combined dent and notch on the compression side of pipes. Meanwhile, the damage in terms of a crack, a notch and the combined notch and crack on the tensile side of pipes is qualitatively investigated. Once it occurs, the fracture failure of pipes is likely to happen, which may introduce a detrimental consequence.

We have started this research with a specific definition of the residual ultimate strength (load carrying capacity) based on the classical strength theory of cylindrical shells. Depending on the ratios of pipes' diameter D to wall thickness t, the residual ultimate strength of structures is determined by either structures' stability or the strength related to material plasticity. Specifically, we first focus on the features of each type of structural damage on pipelines based on literature review, including the causes of damage, the existing estimation methods for pipe strength with damage, the possible consequences of damage, and the design and manufacture methods of damage in laboratories. To prepare for the further investigation of damage effects on the strength of metallic pipes, the possible influential parameters are explored, and the methods of strength evaluation on pipes subjected to different loads are studied through a literature survey in Chapter 2 of this thesis. This facilitates the following experimental design, conduction and the identification of residual strength of damaged pipes.

In Chapter 3, we have carried out a fundamental experimental investigation on damaged pipes. A four-point bending test is conducted on the damaged specimens with properly introduced structural damage. Through the test observations, we have conceptualized the effects of the damage on the metallic pipes under bending. The obtained test data also provide a solid foundation for the further research on quantification.

The Finite Element Method has been used in order to confirm the observations of the structural behavior of damaged specimens from the tests. Numerical models with the cor-

responding structural damage have been developed, and then been validated through the test results. Each type of structural damage in terms of their critical parameters has been integrated into the numerical models for the following comparisons.

In Chapter 4, the effect of each influential parameter raised in Chapter 2 has been clarified through a parametric study. Therefore, we know how to take into account these influential parameters in further numerical investigations. For instance, in spite of the necessary requirements of the initial imperfection in most of structural analysis, its effect in damaged pipes is small and can be neglected under a bending moment due to the shielding effect of damage. The effect of dent damage has been clarified. The dent parameters such as dent angle (θ_d), depth (d_d), length (l_d) and width (w_d), are studied through simulations respectively. Empirical formulas based on the results from a series of numerical simulations are proposed through statistical methods, in the functions of dent parameters. Hence, we have answered the key research question: to what extent the dent damage affects the residual strength of metallic pipes in terms of bending moment and critical curvature.

Subsequently, in Chapter 5 of this thesis, we have established the relations between another typical type of damage - metal loss in terms of a notch - and the residual strength of pipes. We first simplify the notch model, which is suitable for numerical simulations. The analytical solutions of damaged pipes with a notch are derived, with the assumption that the notch width is infinitely large. Simulations on the effects of the metal loss parameters including depth (d_m), length (l_m), and width (w_m), are carried out based on the validated models. Through the simulation results, empirical models in the functions of the notch parameters and the volume loss due to the notch have been proposed for both strength and curvature predictions. Therefore, we have answered the key research question: to what extent the metal loss damage will affect the residual strength of metallic pipes under a bending moment.

In reality, the combined dent and notch damage is more prone to happen after mechanical interference. The interaction relations between a dent and a notch is not clear. Hence, we have carried out another investigation on the combined damage in Chapter 6. It shows that the dent damage plays a more dominant role on the pipe residual strength compared with the notch in the combined damage. The combined dent and notch damage has a more severe effect on the pipe residual strength compared with other types of damage (excluding the possible fracture failure). Case studies on the damaged pipes that may induce fracture failure have been also carried out. The comparison results show that the pipe with combined notch and crack has a faster fracture failure. The residual stress produced by impact exists in pipes. Since we have not obtained enough test data for the distribution of such residual stress, we have only conducted an initial exploration on its effect of pipe residual strength based on an assumed distribution. Positive effect has been obtained. In the end of this chapter, predictions models are proposed to predict the residual strength of pipes with combined damage under a bending moment through simulations and the proposed formulas for single damage in Chapters 4 and 5 respectively. The application domain of these formulas has been extended to pipes with D/t up to 30. However, we still need more tests to confirm the validity of such an expansion of application domain.

The main contribution of this research lies in the quantification of the residual ultimate strength of damaged pipes under a bending moment. With the study in this thesis, the expert knowledge is provided for the structural response of metallic pipes suffering from damage, and for the assessment methods for the performance of damaged pipes. By using

the proposed models in this thesis, we can effectively estimate the reduction ratios of pipe residual strength. The structural engineers are therefore be facilitated to deal with damaged pipes when some damage occurs after mechanical interference.

Curriculum vitae

Jie Cai was born in Yiyang, Hunan Province, P. R. China. In 2003, he went to Harbin Engineering University, Harbin, to study at the faculty of Shipbuilding Engineering. In 2007, he obtained his Bachelor's degree in Naval Architecture with a GPA ranking among the top 8%. After graduation, he continued his Master study in Ocean Engineering in Shanghai Jiao Tong University, Shanghai, where he carried out an investigation on the vortex induced vibration (VIV) characteristics of a flexible deep-sea riser with high aspect ratio under a uniform current profile. He deployed a novel method to simulate the complex three-dimensional fluid-structure interaction phenomenon, and obtained meaningful results. This project belonged to a National 863 Project in the group of Prof. You, Yunxiang. In 2010, he obtained his Master's degree in Ocean Engineering.

During his Master's period, he did his internship (7 months) in China Classification Society, Guangzhou branch, where he served as an assistant engineer in the plan approval center, and also an assistant surveyor in the shipyard of Guangzhou International Company.

Since March 2010 after obtaining his Master's degree, Jie has been employed by the institute of China Ship Development and Design Center in Wuhan. He worked as a ship structure engineer, specializing in the structural design, scantling calculation, FEM simulation and engineering of submarines' structures. Due to the work, he has had a very close cooperation with the shipyards/dockyards, device institutes/ factories and military bases in China. Among which, he involved in the trouble-shooting, inspection of structural constructions in shipyards, on-site devices and structural experiments, and escape and rescue systems. In 2013, he was officially appointed as one of the project managers in the division of structural center.

In 2014, he left this institute and started his Ph.D. research at the section of Ship Hydromechanics and Structures with Prof. M.L. Kaminski in the department of Maritime and Transport Technology in Delft University of Technology, the Netherlands. Four months later in February 2015, he moved to the section of Transport Engineering and Logistics, and continued his research project under the supervision of Prof. G. Lodewijks. His research interests include ultimate strength, structural analysis, data analysis, and hydrodynamic analysis of offshore platforms and wind turbines, etc. The results of his Ph.D. research on the residual ultimate strength of damaged seamless metallic pipes are presented in this thesis.

List of my publications

1. **Jie Cai**, Xiaoli Jiang, Gabriel Lodewijks, Zhiyong Pei, and Weiguo Wu. 2018. *Residual ultimate strength of damaged seamless metallic pipelines with metal loss*. Marine Structures. 58:242-253. DOI: https://doi.org/10.1016/j.marstruc.2017.11.011.

2. **Jie Cai**, Xiaoli Jiang, and Gabriel Lodewijks. 2018. *Numerical investigation of residual ultimate strength of dented metallic pipes subjected to pure bending*. Ships and Offshore Structures. DOI: https://doi.org/10.1080/17445302.2018.1430200.

3. **Jie Cai**, Xiaoli Jiang, and Gabriel Lodewijks. 2017. *Residual ultimate strength of offshore metallic pipelines with structural damage - a literature review*. Ships and Offshore Structures. 1-19. DOI: https://doi.org/ 10.1080/17445302.2017.1308214.

4. **Jie Cai**, Xiaoli Jiang, Gabriel Lodewijks, Zhiyong Pei, and Weiguo Wu. 2018. *Residual ultimate strength of seamless metallic pipelines under a bending moment - a numerical investigation*. Ocean Engineering.164:148-159. https://doi.org/10.1016/j.oceaneng.2018.06.044.

5. **Jie Cai**, Xiaoli Jiang, Gabriel Lodewijks, Zhiyong Pei, and Weiguo Wu. 2018. *Residual ultimate strength of damaged seamless metallic pipelines with combined dent and metal loss*. Marine Structures. 61:188-201. https://doi.org/10.1016/j.marstruc.2018.05.006.

6. **Jie Cai**, Xiaoli Jiang, Gabriel Lodewijks, Zhiyong Pei, and Ling Zhu. 2018. *Experimental investigation of residual ultimate strength of damaged metallic pipelines (Accepted)*. Journal of Offshore Mechanics and Arctic Engineering.

7. **Jie Cai**, Yunxiang You, Wei Li, Zhongmin, Yan Qu. 2010. *The VIV characteristics of deep-sea risers with high aspect ratio in a uniform current profile (in Chinese)*. Chinese Journal of Hydrodynamics. 25(1): 50-61. DOI:10.3969/j.issn.1000-4874.2010-01.008.

8. **Jie Cai**, Xiaoli Jiang, Gabriel Lodewijks, Zhiyong Pei, and Ling Zhu. June 2017. *Experimental investigation of residual ultimate strength of damaged metallic pipelines*. In: ASME 2017 36th International Conference on Offshore Mechanics and Arctic Engineering. American Society of Mechanical Engineers. Trondheim, Norway.

9. **Jie Cai**, Xiaoli Jiang, and Gabriel Lodewijks. June 2016. *Residual strength of metallic pipelines subjected to combined loads accounting for impact induced damage*. In: 26th International Offshore and Polar Engineering Conference. International Society of Offshore and Polar Engineers. Rhodes, Greece.

10. **Jie Cai**, Xiaoli Jiang, and Gabriel Lodewijks. June 2015. *Ultimate strength of damaged stiffened panels subjected to uniaxial compressive loads accounting for impact induced residual stress and deformation*. In: ASME 2015 34th International Conference on Offshore Mechanics and Arctic Engineering. American Society of Mechanical Engineers. St.John's, Canada.

11. Matteo Schiaretti, **Jie Cai**, Xiaoli Jiang, Shengming Zhang and Dingena Schott. *A numerical comparison between Extended Finite Element Method (XFEM) and Finite Element Method (FEM) for the prediction of stress intensity factor (SIF)*. (Corresponding author, Under review for Ocean Engineering) 2018.

TRAIL Thesis Series

The following list contains the most recent dissertations in the TRAIL Thesis Series. For a complete overview of more than 200 titles see the TRAIL website: www.rsTRAIL.nl.

The TRAIL Thesis Series is a series of the Netherlands TRAIL Research School on transport, infrastructure and logistics.

Cai, J., *Residual Ultimate Strength of Seamless Metallic Pipelines with Structural Damage*, T2018/5, September 2018, TRAIL Thesis Series, the Netherlands

Ghaemi, N., *Short-turning Trains during Full Blockages in Railway Disruption Management*, T2018/4, July 2018, TRAIL Thesis Series, the Netherlands

Gun, van der J.P.T., *Multimodal Transportation Simulation for Emergencies using the Link Transmission Model*, T2018/3, May 2018, TRAIL Thesis Series, the Netherlands

Van Riessen, B., *Optimal Transportation Plans and Portfolios for Synchromodal Container Networks*, T2018/2, March 2018, TRAIL Thesis Series, the Netherlands

Saeedi, H., *Network-Level Analysis of the Market and Performance of Intermodal Freight Transport*, T2018/1, March 2018, TRAIL Thesis Series, the Netherlands

Ypsilantis, P., *The Design, Planning and Execution of Sustainable Intermodal Port-hinterland Transport Networks*, T2017/14, December 2017, TRAIL Thesis Series, the Netherlands

Han, Y, *Fast Model Predictive Control Approaches for Road Traffic Control*, T2017/13, December 2017, TRAIL Thesis Series, the Netherlands

Wang, P., *Train Trajectory Optimization Methods for Energy-Efficient Railway Operations*, T2017/12, December 2017, TRAIL Thesis Series, the Netherlands

Weg, G.S. van de, *Efficient Algorithms for Network-wide Road Traffic Control*, T2017/11, October 2017, TRAIL Thesis Series, the Netherlands

He, D., *Energy Saving for Belt Conveyors by Speed Control*, T2017/10, July 2017, TRAIL Thesis Series, the Netherlands

Beŝinović, N., *Integrated Capacity Assessment and Timetabling Models for Dense Railway Networks*, T2017/9, July 2017, TRAIL Thesis Series, the Netherlands

Chen, G., *Surface Wear Reduction of Bulk Solids Handling Equipment Using Bionic Design*, T2017/8, June 2017, TRAIL Thesis Series, the Netherlands

Kurapati, S., *Situation Awareness for Socio Technical Systems: A simulation gaming study in intermodal transport operations*, T2017/7, June 2017, TRAIL Thesis Series, the Nether-

lands

Jamshidnejad, A., *Efficient Predictive Model-Based and Fuzzy Control for Green Urban Mobility*, T2017/6, June 2017, TRAIL Thesis Series, the Netherlands

Araghi, Y., *Consumer Heterogeneity, Transport and the Environment*, T2017/5, May 2017, TRAIL Thesis Series, the Netherlands

Kasraian Moghaddam, D., *Transport Networks, Land Use and Travel Behaviour: A long term investigation*, T2017/4, May 2017, TRAIL Thesis Series, the Netherlands

Smits, E.-S., *Strategic Network Modelling for Passenger Transport Pricing*, T2017/3, May 2017, TRAIL Thesis Series, the Netherlands

Tasseron, G., *Bottom-Up Information Provision in Urban Parking: An in-depth analysis of impacts on parking dynamics*, T2017/2, March 2017, TRAIL Thesis Series, the Netherlands

Halim, R.A., *Strategic Modeling of Global Container Transport Networks: Exploring the future of port-hinterland and maritime container transport networks*, T2017/1, March 2017, TRAIL Thesis Series, the Netherlands

Olde Keizer, M.C.A., *Condition-Based Maintenance for Complex Systems: Coordinating maintenance and logistics planning for the process industries*, T2016/26, December 2016, TRAIL Thesis Series, the Netherlands

Zheng, H., *Coordination of Waterborn AGVs*, T2016/25, December 2016, TRAIL Thesis Series, the Netherlands

Yuan, K., *Capacity Drop on Freeways: Traffic dynamics, theory and Modeling*, T2016/24, December 2016, TRAIL Thesis Series, the Netherlands

Li, S., *Coordinated Planning of Inland Vessels for Large Seaports*, T2016/23, December 2016, TRAIL Thesis Series, the Netherlands

Berg, M. van den, *The Influence of Herding on Departure Choice in Case of Evacuation: Design and analysis of a serious gaming experimental set-up*, T2016/22, December 2016, TRAIL Thesis Series, the Netherlands

Luo, R., *Multi-Agent Control of urban Transportation Networks and of Hybrid Systems with Limited Information Sharing*, T2016/21, November 2016, TRAIL Thesis Series, the Netherlands

Campanella, M., *Microscopic Modelling of Walking Behavior*, T2016/20, November 2016, TRAIL Thesis Series, the Netherlands

Horst, M. van der, *Coordination in Hinterland Chains: An institutional analysis of port-related transport*, T2016/19, November 2016, TRAIL Thesis Series, the Netherlands

Beukenkamp, W., *Securing Safety: Resilience time as a hidden critical factor*, T2016/18, October 2016, TRAIL Thesis Series, the Netherlands

Mingardo, G., *Articles on Parking Policy*, T2016/17, October 2016, TRAIL Thesis Series, the Netherlands